X-ray absorption studies of metalloporphyrin molecules on surfaces: Electronic interactions, magnetic coupling, and chemical switches

Im Fachbereich Physik
der Freien Universität Berlin
eingereichte Dissertation von

Christian Felix Hermanns

aus München

Juni 2013

1st referee	Prof. Dr. Wolfgang Kuch Freie Universität Berlin
2nd referee	Prof. Dr. José Ignacio Pascual CIC nanoGUNE Consolider
3rd referee	Prof. Dr. Michael Farle Universität Duisburg-Essen
Submission of thesis:	28th of June 2013
Day of disputation:	25th of September 2013

Abstract

This thesis is about the electronic and magnetic properties of Co and Fe octaethylporphyrin (CoOEP/FeOEP) molecules adsorbed in the submonolayer regime on nonmagnetic and ferromagnetic (FM) surfaces. Of interest are the impact of adsorbate–surface interactions on the electronic and magnetic properties of the molecules and their magnetic interaction with substrates. Also a reversible control of these interactions by a coordination of the small molecules carbon monoxide (CO) and nitric oxide (NO) to the adsorbed prophyrins is subject of this work. X-ray absorption spectrosopy (XAS) as well as the X-ray magnetic circular dichroism (XMCD) effect in the angle-, temperature-, and field-dependent absorption of soft X-rays are the tools applied to perform these studies.

First the electronic structure of CoOEP in bulk is discussed. Then an introduction to the applicability of the measurement techniques by studying CoOEP on highly ordered pyrolytic graphite (HOPG) and Cu(100) is given. The molecules lie almost flat on HOPG and Van der Waals forces dominate the adsorbate-substrate interaction, such that the molecular electronic structure survives upon adsorption. In contrast, for CoOEP on Cu(100), the spatial charge distribution of the unpaired electron at the Co site is modified and primarily located inside the porphyrine plane and not perpendicular to it as for pure CoOEP. An approach to gain control over the alignment of the Co magnetic moments without applying a magnetic field is presented by placing CoOEP on bare and oxygen-covered Ni surfaces. In both cases an FM exchange interaction between Ni and Co spins aligns the latter against their thermal fluctuations, while the adsorbate-surface interaction modifies the Co electronic structure. For CoOEP on Ni, a Co magnetization is present already at room temperature (RT), whereas for CoOEP on O/Ni this is only the case at 30 K, reflecting a weaker magnetic coupling strength for this system.

A strategy to preserve the molecular properties and at the same time to achieve a substrate-induced spin polarization is developed by putting CoOEP on graphene-passivated Ni surfaces. An indirect antiferromagnetic exchange coupling between the Ni and Co magnetic moments, which is magnetically anisotropic, across the graphene leads to a Co magnetization at 130 K. Despite the hybridization of Co $3d$ with molecular states, the Co spin m_S and orbital m_L^{xy} moments are of the same order of magnitude for an in-plane (IP) Co magnetization. The Co m_L^{xy} is recreated by spin–orbit coupling (SOC).

For a control of the magnetization of Co and Fe ions inside CoOEP and FeOEP at finite temperatures, magnetically coupled to a substrate magnetization, small molecules are attached to the porphyrins and subsequently thermally removed. So the coordination of CO to CoOEP on graphene/Ni allows to reversibly control the crystal field of the Co ion, which determines, together with the SOC, the size of m_L^{xy}. For CO-CoOEP, m_L^{xy} is reduced by $(77\pm6)\%$ compared to CoOEP. In contrast, the adsorption of NO on CoOEP molecules on O/Ni partially oxidizes the Co ions, changes the Co spin moment, and leads to a reduction of the Co magnetization by about a factor of two at 30 K. The adsorption of NO to FeOEP molecules, antiferromagnetically coupled to the magnetization of an oxygen-covered Co surface, reduces the corresponding magnetic coupling strength and hence the Fe magnetization by approximately 50% at 120 K.

Kurzfassung

Diese Doktoarbeit handelt von den elektronischen und magnetischen Eigenschaften von Kobalt- und Eisen-Octaethylporphyrinen (CoOEP/FeOEP), die auf ferro- (FM) und unmagnetischen Substraten als Submonolagen adsorbiert sind. Von Interesse ist der Einfluss der Adsorbat-Oberflächen-Wechselwirkung auf die elektronischen und magnetischen Eigenschaften der Moleküle und ihre magnetische Wechselwirkung mit dem Substrat. Die reversible Kontrolle dieser Wechselwirkungen durch die Koordination von kleinen Molekülen wie Kohlenstoffmonoxid (CO) und Stickstoffmonoxid (NO) an die Porphyrine ist ebenso Thema der Arbeit. Die Röntgenabsorptionsspektroskopie sowie der magnetische zirkulare Röntgendichroismus in winkelaufgelösten, feld- und temperaturabhängigen Absorptionsmessungen werden für die Untersuchungen benutzt.

Zuerst wird die elektronische Struktur von CoOEP-Volumenproben vorgestellt. Danach werden die Messtechniken anhand von Untersuchungen von CoOEP auf Kupfer(100)- und Graphitoberflächen eingeführt. Die Moleküle liegen nahezu flach auf dem Graphit und Van-der-Waals-Kräfte dominieren die Adsorbat-Substrat-Wechselwirkung, ohne die molekulare elektronische Struktur zu ändern. Dagegen ist die räumliche Ladungsverteilung der ungepaarten Co-Elektronen für CoOEP auf Cu(100) verändert und liegt primär in der Molekülebene und nicht senkrecht dazu wie bei isoliertem CoOEP. Durch das Aufbringen von CoOEP auf un- und sauerstoffbedeckte Ni-Oberflächen wird eine Möglichkeit präsentiert die magnetischen Co-Momente ohne Anlegen eines Magnetfeldes auszurichten. Auf beiden Substraten stabilisiert eine FM-Austauschwechselwirkung die Co-Spins gegen thermische Fluktuationen, wobei die Adsorbat-Substrat-Wechselwirkung die elektronische Struktur des Co ändert. Eine messbare Co-Magnetisierung (M_{Co}) liegt für CoOEP auf Ni bereits bei Raumtemperatur vor, auf O/Ni erst unterhalb von 30 K. Dies spiegelt eine geringere magnetische Kopplungsstärke für das letztere System wider.

Die Erhaltung der molekularen Eigenschaften und einer gleichzeitigen substratinduzierten Spinpolarisation wird durch das Aufbringen von CoOEP auf eine graphenpassivierte Ni-Oberfläche ermöglicht. Eine indirekte und anisotrope antiferromagnetische (AFM) Austauschkopplung zwischen den Ni- und Co-Spins durch das Graphen hindurch führt zu einem endlichen M_{Co} bei 130 K. Trotz der Hybridisierung der Co $3d$ Zuständen mit molekularen Zuständen weisen die Spin- (m_S) und Bahnmomente (m_L^{xy}) der Co-Ionen die gleiche Größenordnung auf, wenn M_{Co} entlang der Molekülebene ausgerichtet ist. Dies liegt am Einfluss der Spin-Bahn-Kopplung (SBK) auf den elektronischen Grundzustand der Co-Ionen.

Um die Fe- und Co-Magnetisierung von CoOEP- und FeOEP-Molekülen, die magnetisch zu einem Substrat koppeln, bei endlichen Temperaturen zu kontrollieren, werden NO und CO an die Porphyrine gebunden und anschließend wieder thermisch desorbiert. Die Koordination von CO an CoOEP/Graphen/Ni ermöglicht es das Kristallfeld der Co-Ionen, das zusammen mit der SBK die Größe von m_L^{xy} bestimmt, reversibel zu ändern. Nach der CO-Aufnahme ist m_L^{xy} um $(77 \pm 6)\%$ kleiner. Die Adsorption von NO auf CoOEP/O/Ni hingegen führt zu einer partiellen Oxidation sowie zu einer Veränderung des Spinmoments der Co-Ionen und zu einer Reduktion von M_{Co} um circa 50% bei 30 K. Die Adsorption von NO auf FeOEP-Molekülen, die AFM zu einem sauerstoffbedeckten Co-Film koppeln, mindert die zugehörige Kopplungsstärke und somit die Fe-Magnetisierung um etwa 50% bei 120 K.

Contents

Introduction

This doctoral thesis is about the electronic and magnetic properties of paramagnetic metalloporphyrin (MP) molecules adsorbed on nonmagnetic and ferromagnetic (FM) surfaces. Magnetic porphyrin–substrate interactions as well as the reversible control of the magnetization of the molecular central metal (M) ions in such exchange-coupled systems by the attachment and detachment of small molecules like nitric oxide (NO) or carbon monoxide (CO) are of interest. Fig. 1 depicts this. The work can be classified as fundamental research in the field of chemical surface physics. It aims to design magnetic structures on the nanoscale that can be useful for a future molecular spin electronics.

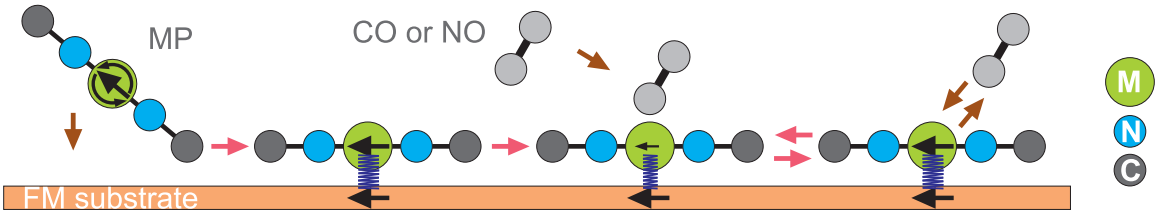

Figure 1: Schematic display of the key objectives of this work: Stabilization of molecular spins on FM surfaces and their reversible manipulation by chemical stimuli. Green, blue, and dark grey balls represent metal, nitrogen, and, carbon atoms, respectively.

Magnetism has fascinated humanity for many centuries. The phenomenon of materials that attract or repell each other was first written down by Thales, the Greek, already at around 600 B.C. He described the power of loadstone, also called magnetite, to attract iron. Also old Chinese literature is full of references to loadstone [1] and it is assumed that the first direction pointers were built during the Qin dynasty more than 2000 years ago. That the operation of the compass relies on the fact that the earth itself is a huge magnet was realized by Gilbert in the 16th century. Covering magnetism in all potential matters goes beyond the scope of this introduction. In modern physics, we distinguish between two different contributions to the magnetic moment, which is a property defined by the torque experienced in a magnetic field. The first is the intrinsic magnetism of elementary particles, like the spin magnetic moment in the case of an electron. The second is the motion of electric charges, which is associated to the orbital magnetic moment for electrons [2].

We encounter magnetism in our daily life in the context of various state-of-the-art technologies. To name only a few of them, magnets are incorporated in modern wind turbine generators, maglevs, or products of the information technology like computer hard discs. The elusive development of the latter after World War Two ended in the steady miniaturization of integrated functional units and led to new forefront research areas on this issue. One of them is spin engineering, which is dedicated to the manipulation and control of quantum spin systems in order to design new devices. Spin presents an appealing degree of freedom to be put into use, as the energy scale regarding its typical dynamics is several orders of magnitude smaller than the one being relevant for manipulating the electron charge in normal transistors. **Spintronics**, also known as magneto-

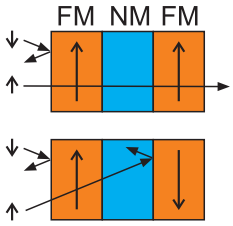

Figure 2: Schematic sketch of a spin valve. See text for explanation.

electronics, is the most developed area of spin engineering. This term describes the architecture of solid-state devices, which allow spin-dependent electron transport [3]. Here, studies address the issue of detecting, manipulating and injecting spins in the solid state environment. Doubtless the most prominent effect in this research field is the so-called giant magnetoresistance (GMR), which was observed in the 1980s [4, 5]. It is based on the modification of electrical resistance in a device, also called spin valve, constructed out of two FM layers separated by a non-magnetic conductive material as shown in fig. 2. Thereby the conductivity is high (upper picture of fig. 2) or low (lower picture of fig. 2) for parallel or antiparallel magnetizations of the two FM layers. The relative alignment between the direction of the spin of the electron and the magnetization of an FM layer determines the possibility that the electron passes through this layer as depicted in fig. 2. The GMR effect was used from 1997 on in commercial hard disc drives to read out the magnetic polarization of tiny magnetic fields presenting bits. Also magnetoresistive random-access memory uses the concept of the spin valve for data storage instead of the electron charge, as conventional RAM chip technologies do.

Research in the field of **molecular electronics**, which is another emerging technology, aims to design electronic devices by using organic molecules. The basic principle here is to substitute inorganic conductors like copper or silicon by molecular building blocks. The endless possibilities of chemical synthesis to engineer molecules, for instance with different end groups, gives outstanding chances to adapt their electronic properties to the needs of a desired device. A further advantage is a cheaper production process given the potential possibility to create functional units by inkjet printing instead of working e.g. in ultra high vacuum and including expensive high-temperature solid-state growth and patterning techniques, as it is the case for microelectronics based on silicon. In particular, molecular-scale electronics focuses on the realization of electronic components built by single molecules or nanoscale collections of single molecules [6]. The underlying idea is to shrink the dimension of components of an electrical circuit. In contrast, the notion "molecular materials" refers to bulk applications of conductive or semiconductive molecules [7].

The field of research referred to as "**molecular spintronics**" goes one step further and presents a combination of spintronics and molecular electronics. Here spin-polarized currents flow through molecules, which is advantageous as opposed to a flow through inorganic materials mainly because of two aspects. First, the intrinsic molecular properties, and here in particular small hyperfine and spin-orbit interactions, have to be mentioned. In standard semiconductors like Gallium arsenide, spin–orbit coupling (SOC) is one main interaction being responsible for reducing spin coherence, thus preventing long spin diffusion times. In contrast, for organic molecules containing elements with a low atomic number such as carbon or nitrogen, the spin-orbit constant is smaller and so the spin-lifetime is rather long. In general, the hyperfine intercation, which couples the nuclear and electron spins, is a source of electron spin decoherence as well, since the random flipping of the former can also flip the latter. The most abundant isotopic form of carbon is ^{12}C with a nuclear spin S_{N}=0, which hence is not hyperfine active. π-conjugated organic molecules, which are mainly used for spin-transport, have the distinctive feature of being composed of carbon atoms, where the transport takes place to a great extent across molecular states situated at the carbon atoms. This fact, together with the typical delocalization of the π states, leads to a

rather weak hyperfine interaction in organic materials. The use of molecules as transport medium for spins might be also smart considering their spin injection properties. The well-known conductivity mismatch between a metallic FM spin injector and a semiconducting layer [8] can be overcome by a spin-injection from a ferromagnet into organic molecules, as demonstrated for multilayers of copper-phthalocyanine (CuPc) molecules in contact with an FM material [9]. In that case a spin injection efficiency of 85-90 % was reported. In this context also the concept of an organic spin valve has to be mentioned, in which the conducting material between the two FM layers is made out of an organic semiconductor. The first such spin valve reported, which used the small π-conjugated molecule 8-hydroxy-quinoline aluminum (Alq_3), showed a magnetoresistance of 40% [10]. Two profound review articles from S. Sanvito *et al.* [11, 12] are dedicated to molecular spintronics and its up-to-date developments and can be recommended to the readership.

In general, organic chemistry deals with all possible compounds which are formed by carbon. However, there are exceptions concerning this differentiation to anorganic chemistry. The rudimental forms of carbon represent such exceptional cases, among which graphene, the omnipresent material of high current interest in the scientific community, is expected to push the realization of spin electronics forward, too. **Graphene** is a two-dimensional arrangement of sp^2-hybridized carbon atoms forming a regular hexagonal grid, as displayed in fig. 3, and possessing a delocalized π electronic system. The above-mentioned advantages of π-conjugated molecules built up by carbon atoms with respect to their suitability as transport medium for electron spins are also met by graphene [13, 14]. Together with high charge carrier mobility, provided by the specific band structure of graphene, it presents a tantalizing material for new spintronic concepts. So electronic spin transport as well as spin precession in single graphene layers at room temperature have been already observed over micrometre-scale distances [15].

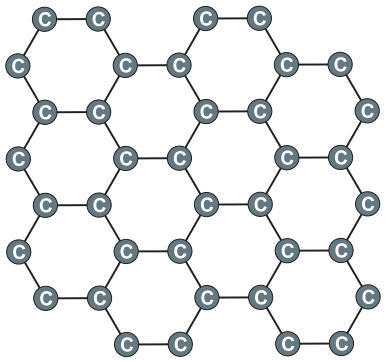

Figure 3: Schematic sketch of graphene. Grey balls represent carbon atoms.

Referring again to molecules and considering also magnetic ones, which thus possess a total net spin, expands the research area of molecular spintronics. In this context the possibility to **control the spin state** in such molecules may lead to routes for the establishment of new concepts in molecular spintronics. The switching by light, temperature, or pressure between paramagnetic and diamagnetic states is known to be feasible for an entire class of molecules, named spin-crossover (SCO) compounds [16]. These molecules comprise conventionally a single transition metal ion, which has six ligands and undergoes an entropy-triggered low-spin to high-spin transition or vice versa. This goes hand in hand with a geometrical reconstruction of the ligands being coordinated to the metal ion, but not at standard conditions of temperature and pressure. Only a short while ago a Ni complex, being composed out of a Ni porphyrin with an azopyridine molecule in its periphery linked to the porphinato ligand by benzene, received much attention, too, as it presents a bistable molecular spin switch even at room temperature. Electromagnetic radiation induces a reversible configurational change of the photochromic ligand which allows to alter the coordination of

the Ni ion between four- and fivefold and thus to switch between a diamagnetic and paramagnetic state [17].

All in all, organic materials appear to be a multifaceted and unequaled playing field for developing novel spintronics concepts and/or for upgrading existing ones. However, a **better comprehension of the interaction at an interface between FM electrodes and organic molecules**, in particular regarding spin-related processes and magnetic exchange coupling mechanisms, is still mandatory. From this point of view, a short summary on the most important experimental results published within the last years about organic molecules, mainly adsorbed in the submonolayer regime on FM surfaces, is presented in the following. Different experimental techniques such as scanning tunneling microscopy (STM), and especially spin-polarized scanning tunneling microscopy (SPSTM), spin-polarized ultraviolet photoelectron spectroscopy (SPUPS), spin-polarized metastable de-excitation spectroscopy (SPMDS), and X-ray magnetic circular dichroism (XMCD) have been applied to perform such studies. In particular, the investigations discussed deal with planar molecular building blocks like MP molecules, as also studied in the framework of this thesis, and metallophthalocyanine (MPc) molecules, which are chemically similar to them. These molecules are built up by a metal ion enclosed by a planar tetradentate dianonic ligand, leaving two further axial coordination sites opposite to each other. Before discussing the interaction between organic adsorbates and FM substrates, some recent results about these paramagnetic molecules adsorbed on non-magnetic surfaces have to be mentioned in the context of magnetism as well, underlining the extensive research activity within this field. These findings were obtained from STM studies, especially from elastic and inelastic scanning tunneling spectroscopy.

Regardless whether the substrate is magnetic or not, a **control of charge and spin of single molecules at an interface** is desirable. By changing the transition metal M (M= Fe, Co, Ni, and Cu), being coordinated by a planar phthalocyanine (Pc) ligand and a Ag(100) surface as additional axial ligand, not only the amount of charge on the central metal site can be tuned, but also the charge transfer and the hybridization mechanism with the surface, as well as the charge reorganization upon adsorption [18]. In these systems also the formation of coupled metal-ligand spin states was observed, induced by the presence of the metallic substrate [19]. Furthermore, the molecule–substrate coupling at the interface may affect the magnetic anisotropy. It has been shown for iron-phthalocyanine (FePc) adsorbed on an oxygen-covered Cu(110) surface that the anisotropy is changed from easy plane of the bulk to easy axis [20]. There might be also an exchange interaction between the localized spins of magnetic impurities and the conduction electrons in a host metal, as has been observed for individual manganese-phthalocyanine (MnPc) compounds adsorbed on top of Pb islands. Controllable differences of the Kondo effect, which emerges from this interaction, induced by thickness-dependent quantum-well states allow for controlling the spin–electron interaction through quantum size effects, i.e., the precise thickness control of thin Pb islands [21]. Moreover, for MnPc on a Pb(111) surface magnetic and superconducting interactions, Kondo screening and superconducting pair-breaking interactions, exist in parallel and rival in affecting the ground state of the localized magnetic Mn moments [22].

Coming back to the study of organic FM interfaces, **SPSTM**, which combines atomic-scale image resolution with sensitivity to spin orientation, can be regarded as

an ideal tool to investigate how spins are transferred from a magnetic surface to a single organic molecule. So it was shown that for non-magnetic organic molecules on top of an FM Fe contact, the spin orientation of current flowing across such a construction can be filtered or reversed, with respect to the substrate magnetization direction. This effect even depends on the place of the tunneling current within the molecular compound [23, 24]. Thereby chemical bond formation between the substrate and cobalt-phthalocyanine (CoPc), Pc, benzene, pentamethylcyclopentadiene, and cyclooctatetraene molecules is crucial for tuning the spin direction of the conducting electrons. Similar measurements for CoPc adsorbed on Co nanoislands allowed to resolve the unquenched Co spin within single molecules, which are in this case coupled parallel to the magnetization of the islands by an FM interaction partly carried by the organic ligands [25]. A different magnetic interaction, an RKKY-type exchange coupling, was found for MnPc molecules on Fe-supported Pb islands. By a combination of inelastic spin-flip electron tunneling with SPSTM, this interplay of the Mn ions with the Fe beneath the Pb layers via conduction electrons was revealed [26].

Analysing in more depth a potential ohmic-like contact of a direct organic-ferromagnetic interface, the appearance of a so called **hybrid interface state** (HIS), energetically located at the Fermi level and not completely filled, becomes important [27]. When it is present, carrier injection and transport can be established at such hybrid organic-ferromagnetic interfaces with only a few millivolts bias voltage and without the aid of thermal energy. The HIS acts as an electronic state which facilitates the electron hopping, as no injection barrier has to be overcome. However, the energy level alignment at the interface is just one issue. Within a direct contact system also the HIS may become spin polarized, which, on the other hand, should influence the spin injection characteristics. An HIS may be created through covalent bonding between the metal surface and some specific atoms from organic molecules, including the formation of a different molecular structure. Alternatively, whole π-conjugated orbitals of the molecule may interact with the metal orbitals, which leads to hybridization.

Besides SPSTM, **SPUPS** is also an adequate tool to study the spin polarization of valence levels at an organic-ferromagnetic metal interface. Different metallophthalocyanine (MPc) molecules in direct contact with Fe or Co substrates have been studied with this technique. A formation of spin-polarized HISs is found for CoPc adsorbed on Fe/Mo(110) [28] and for FePc, CoPc, and CuPc on a Co(100) surface [29, 30], which goes along with a chemisorption of the molecules. By comparing the results for the different MPc compounds on the Co substrate, the CuPc/Co interface shows the strongest spin polarization at the Fermi level. Exchanging the central metal ion allows for tuning the degree of spin polarization of the HIS, which provides the possibility to alter the spin injection efficiency and so the spin injection characteristics.

At the beginning of the last decade another experimental technique called **SPMDS** showed spin polarization in molecular orbitals of one monolayer (ML) CuPc deposited on an Fe(100) substrate [31], while the magnetic polarity was identical for the adsorbate and the FM substrate. The experimental technique SPMDS is based on the spin-polarized analysis of an electron energy spectrum which is created by de-excitation of a metastable atom close to a substrate. To the best knowledge, the mentioned investigation was the first regarding magnetism of such hybrid organic-ferromagnetic interfaces. Adsorption of oxygen on Fe before the molecule deposition was found to cause a clear difference in the spin polarization of the CuPc orbitals. An extension of

this study by using Pc and different MPc molecules (M=Mn, Fe, Cu, and Mg) showed clear differences for the measurement results regarding the spin polarization, which reflects in this context the importance of the choice of the metal ion [32].

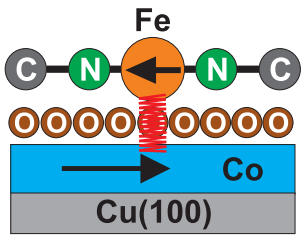

Figure 4: Schematic side view of FeOEP on O/Co/Cu(100). Green, orange, grey, and brown balls represent nitrogen, iron, carbon, and oxygen atoms, respectively.

Some years later also the use of the well-established **experimental XMCD technique** has been started to study interfaces of organic adsorbates and FM surfaces in order to gain insight into the spin polarization which in turn influences the spin injection within such potential segments of an organic spin valve. Pioneering work in this field was done by Scheybal and coworkers [33], who used the unique feature of this technique to resolve the magnetization of manganese-tetraphenylporphyrin chloride (MnTPPCl) molecules adsorbed on a Co substrate. They found an exchange coupling between the magnetization of the substrate and the Mn spins, while no explicite mechanism was provided to explain this experimental result. However, a direct coupling between Co and Mn $3d$ states was questioned due to the large distance between the Mn ions and the Co surface. Just a few years later, for a similar system, iron-octaethylporphyrin (FeOEP) adsorbed on thin Co films, also an FM coupling between the substrate magnetization and central metal ions of the porphyrins was reported. Here density functional theory (DFT) calculations clarified that a 90°-ferromagnetic superexchange interaction through the N ligands is responsible for the coupling [34]. A short time later, it was found that the introduction of half a layer of atomic oxygen between the Fe porphyrins and the magnetic thin film reverses the sign of the magnetic coupling and induces an antiparallel alignment of the Fe and substrate spins. In this case, the coupling mechanism is a 180°-antiferromagnetic (AFM) superexchange mediated by oxygen atoms, according to DFT+U calculations [35], as depicted in fig. 4. Also a magnetic polarization of π-conjugated orbitals within organic molecules as well as fullerenes, molecular compounds made out of carbon atoms, in contact with a FM substrate through hybridization and exchange coupling was found. In the former case, this was discovered by XMCD measurements at the N K edge for Alq_3 molecules on an Fe film [36] and in the latter, by an XMCD study at the C K edge for buckminsterfullerenes (C_{60}) adsorbed on an Fe(001) surface [37]. Moreover, XMCD investigations of single-molecule magnets (SMMs) on FM surfaces were carried out. SMMs like bis-phthalocyaninato-terbium ($TbPc_2$) are molecular compounds that show a magnetic hysteresis of totally molecular origin below a certain temperature. It was found that upon adsorption of $TbPc_2$ on FM surfaces a strongly anisotropic coupling between the substrate and the Tb magnetization boosts the magnetic remanence compared to the bulk phase [38]. Also real-space images of $TbPc_2$ spin-split molecular orbitals on top of FM nanostructures have been reported [39] and even exchange bias of $TbPc_2$ molecules to an AFM substrate.

In addition, the **reversible control at an interface**, being intended for potential spintronics devices, **of magnetic molecular properties by external stimuli** is desirable but, at the same time, a challenging task. The concept of a chemical switch provides a possible approach to this. For instance, the spins of adsorbed cobalt-tetraphenylporphyrin (CoTPP) molecules, being magnetically coupled to the

magnetization of an FM substrate, can be switched off and on by NO. The small molecule acts as an additional axial ligand to the porphyrin and changes the Co spin state from S=1/2 to S=0 , while its thermal desorption recovers the pristine state [40]. Even the magnetic properties of a self-assembled two-dimensional electron spin array of altering Fe–Mn–Fe spins can be reversibly manipulated by coordination and desorption of ammonia (NH_3). Chessboard-like assembled perfluorinated FePc and MnPc molecules, on a c(2x2) oxygen-reconstructed Co(100) surface, are used to engineer the spin array by supramolecular chemistry. The spins of both types of central metal ions are antiferromagnetically aligned to the magnetic moments of the substrate before NH_3 binds to the transition metal ions. After the attachment of NH_3, the Fe spins are quenched, but the ones at the Mn site remain coupled to the Co magnetization in an antiparallel fashion [41].

In addition, noteworthy experimental results about the **manipulation of properties of magnetic nanostructures on noble metal surfaces** have been published, which also mark a step forward towards future molecular-spintronic concepts. So a chemical stimulus has been employed to control the magnetic anisotropy in two-dimensinal high-spin Fe arrays at non-magnetic interfaces. The axial coordination of molecular oxygen to Fe atoms, forming together with terephthalate acid molecules a metal-organic network on a Cu surface, changes the orientation of the easy magnetization axis from in-plane to out-of-plane [42]. Alternatively to chemical strategies, a current-induced switching of the spin state of individual molecules on a Cu(100) surface, covered by a thin CuN insulating layer, could be demonstrated. The molecular compound in this case is an iron-based SCO molecule and the combined spin and conduction switching functionality of the system presents a way to store information in a single molecule [43].

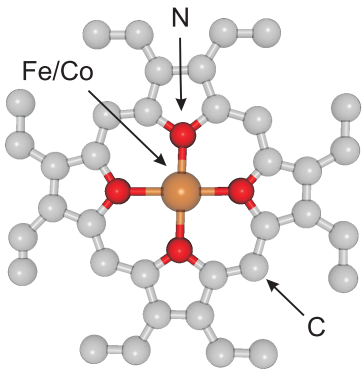

Figure 5: Schematic sketch of a FeOEP or CoOEP molecule, respectively. Grey, orange, and red balls represent carbon, nitrogen, and iron or cobalt atoms, respectively. Hydrogen atoms have been omitted.

After having spanned a wide range from fundamental basics about magnetism to molecular spintronics, now the **scientific question of the work presented here** including a description of links to existing works as discussed before, will be illustrated. This doctoral thesis is about molecular compounds with uncompensated spin moments adsorbed on non-magnetic and bare, oxygen-, and graphene-covered FM surfaces. The work targets the hybridization and the magnetic exchange coupling within such hybrid systems. It further highlights pathways for a reversible control of the electronic and magnetic properties at such organic–ferromagnetic interfaces by external chemical stimuli. Investigations of ensembles of cobalt-octaethylporphyrin (CoOEP) and FeOEP molecules (see fig. 5) in direct contact with a substrate are presented. All samples are prepared in-situ in ultra high vacuum by molecular beam epitaxy.

The experimental technique of choice is X-ray absorption spectrosopy (XAS), which provides high surface sensitivity combined with element specificity. It allows measurements of low effective coverages down to about a thirtieth of a monolayer of Co and Fe atoms and independent investigations of the electronic structure of different con-

stituents within a sample. In addition, by probing the unoccupied density of states, it offers chemical sensivity. At the same time, the use of XMCD provides information about the spin and orbital magnetic moments of a certain element. Thus the much stronger substrate magnetizations can be studied separately from the adsorbate magnetic moments. This feature is used in this thesis to verify the existence of exchange coupling between adsorbates and substrates without having to apply external magnetic fields. Further angle- and field-dependent XMCD measurements are presented, which supply information about the anisotropy of the spin density and the orbital moment as well as about saturated magnetic moments. Temperature-dependent XMCD studies are used to obtain the size of exchange fields, i.e., the coupling strengths in antiferromagnetically coupled systems. In addition, X-ray absorption (XA) measurements carried out with linearly polarized light are performed, which provide information about the molecular adsorption geometry and the anisotropy of the charge density within the $3d$ shell.

Investigations of submonolayers of CoOEP are presented in section 3.3 on FM and different non-magnetic surfaces, while the issue of the molecular adsorption geometry is addressed. Chemisorbed and physisorbed states of the molecules and in particular how the adsorbate-substrate interaction influences the electronic structure of the central metal ion are matters of the study. Thereby the Co oxidation and spin states and the electron density rearrangement within its $3d$ shell upon adsorption are in the focus of interest. Regarding the adsorption on the magnetic surface, attention is paid to a potential substrate-induced magnetic order inside the porphyrin molecules. In section 3.4 CoOEP molecules adsorbed on a graphene-protected Ni surface are studied. Thereby the focus is, on the one hand, on a potential magnetic coupling mediated by the π electron system of the graphene layer between the Ni magnetization and the molecules and, on the other hand, on the extent of electronic interaction between the substrate and the molecules. Further, the angle-dependent size of the orbital magnetic moment as well as of the intra-atomic spin dipole moment of the Co ions are analysed in detail. These investigations join all the studies listed before about different MPc and MP molecules on metal surfaces and try to complement them specifically through the search of new magnetic coupling mechanisms and unquenched orbital magnetic moments within such systems.

The target in section 3.5 is to reversibly control the electronic and magnetic properties of the central metal ions of MP molecules at such organic-ferromagnetic interfaces by an external stimulus. This is carried out by a chemical switch, the attachment and subsequent thermal detachment of small gas molecules to the active center of the porphyrin molecules. The effect of NO adsorption on CoOEP and FeOEP on oxygen-covered magnetic thin films and of CO adsorption on CoOEP on graphene/Ni as well as the potential desorption of the small molecules are investigated. These studies are dedicated to the search of new routes for the manipulation of exchange-coupled magnetic moments inside paramagnetic molecules on FM surfaces at finite temperatures. The influence of adsorbate-induced changes on the amount of electronic charge and thus on the spin magnetic moment, on the magnetic coupling strength between the porphyrins and the substrate, and on the orbital magnetic moment are studied. The basic idea is to control aligned magnetic moments of adsorbed molecules. In the mentioned investigations this was achieved by spin state changes.

1 Core level spectroscopy and magnetic properties of transition metal atoms

1.1 Introduction

At the beginning, this section describes the interaction of X rays with matter and, in paticular, the excitation of core hole electrons. A theoretical description is provided where the final state of the absorption process is either presented by a valence electron wavefunction or by a core hole together with an escaping electron. These two physical processes describe the basic concept behind the X-ray spectroscopy methods used in this thesis, respectively: near-edge X-ray absorption fine-structure (NEXAFS) spectroscopy and X-ray photoelectron spectroscopy (XPS). Especially angular- and polarization-dependent effects at the K and $L_{2,3}$ XA edges are discussed and how they can be applied for determining the adsorption geometry of organic molecules on substrates as well as for analysing the electronic properties of transition metal atoms on surfaces. Next, the XMCD effect, the different absorption of left and right circularly polarized light in magnetically ordered systems, is explained and how this can be used by means of the sum rules to determine quantitatively magnetic moments.

Also the requisite knowledge about the electronic and magnetic properties of the studied transition metal ions is provided. Approaches for the description of their interaction with ligands in molecular compounds are introduced. Further the potential appearance of orbital magnetic moments in magnetic nanostructures is discussed together with the corresponding consequence for the magnetic anisotropy. Finally, the magnetic coupling mechanisms which are of importance in the context of this work are presented.

1.2 X-ray spectroscopy

Experimental techniques applied in the framework of this thesis use X-ray excitation in order to analyse the sytems under study. Different kind of interactions between X rays and matter may occur depending on the energy of the former, as graphically shown in Fig. 6 by presenting the cross section as a function of the photon energy for a copper sample. Among them is the Compton scattering, which has its highest cross section at energies between 10 and 1000 keV. It refers to the inelastic scattering of photons with quasi-free valence electrons, where the energy of the photons is partly transferred to the electrons. Electron-positron pairs are created at photon energies higher than approximately 10^7 eV. This is not possible for the energy range considered in this work, from 280 to 880 eV. Here, Thomson scattering, which presents the low-energy limit of Compton scattering, where the photon energy before and after the interaction is identical, plays a role. However, the photoelectric absorption dominates the interaction of matter with photons below about 10^4 eV. All these interactions lead to an exponential decay of the X-ray intensity I_0 when X-rays traverse matter. Every substance possesses a characteristic length λ_x at which the intensity attenuation is given by the factor $1/e$. So after a damping over the distance z, the X-ray intensity is:

$$I(z) = I_0 e^{-\mu_x z}. \tag{1}$$

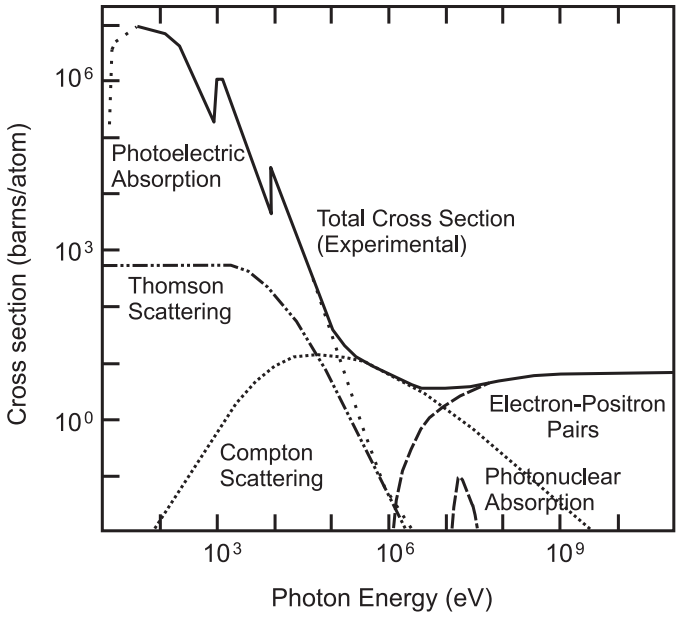

Figure 6: Cross sections of the photoelectric absorption, the Thomson effect, the Compton scattering, the photonuclear absorption, and the creation of electron-positron pairs for Cu as a function of the photon energy. After [44].

Thereby μ_x is the linear X-ray absorption coefficient, which is linked to λ_x by $\mu_x = 1/\lambda_x$. The cross section of a particular interaction between X rays and matter is given by the quotient of the corresponding absorption coefficient and the density of atoms n. The cross section of the photoelectric absorption $\sigma(E)$ which is here of interest shows absorption edges at element-dependent distinctive energies, which reflect the excitation of core electrons. These edges are labeled as K, L_1, L_2, L_3, etc. and correspond to electron excitations from the $1s$, $2s$, $2p_{1/2}$, $2p_{3/2}$, etc. levels, respectively. In the following $\sigma(E)$ is called absorption cross section.

$\sigma(E)$ can be discussed within a simple one-electron picture. The excitation of a core electron with energy E_i to the continuum or a bound state by a photon of energy $E_p = \hbar\omega$ takes place. In a quantum-mechanical description, this can be seen as a transition from an initial state $|i\rangle$ to a final state $|f\rangle$ with energy $E_f = E_i + \hbar\omega$ and density $\rho(E_f)$. The transition probability per unit time T_{if}, which can be calculated by means of the Fermi's golden rule, together with the incident photon flux density I_x determines $\sigma(E)$:

$$\sigma(E) = \frac{T_{if}}{I_x}, \quad T_{if} = \frac{2\pi}{\hbar} |\langle f| H |i\rangle|^2 \rho(E_f). \tag{2}$$

The perturbation Hamiltonian can be assigned to the time-dependent electromagnetic field with the vector potential $\vec{A}(\vec{r},t)$, the presence of which induces the transition:

$$H = -\frac{e}{2m_e c}\vec{A}(\vec{r},t)\vec{p} \;\text{ with }\; \vec{A}(\vec{r},t) = A_0\vec{\varepsilon}e^{i(\vec{k}\vec{r}-\omega)t} \approx A_0\vec{\varepsilon}e^{-i\omega t}. \tag{3}$$

Here $\vec{k}$ and $\vec{\varepsilon}$ are the wave and the unit photon polarization vector, respectively. In the last step the dipole approximation is assumed, which implies that $\vec{k}\vec{r} \ll 1$, as

it is the case for excitations of core electrons. Finally, with $I_x = A_0^2\omega/(8\pi\hbar c)$ the absorption cross section is:

$$\sigma(E_p) = \frac{4\pi^2 e^2}{c\hbar} E_p |\vec{\varepsilon}\langle f|\,\vec{r}\,|i\rangle\,|^2 \rho(E_f). \tag{4}$$

The final state may be below or above the ionization potential. In sections 1.4 and 1.5 the reader is introduced to the experimental techniques NEXAFS and XMCD spectroscopy, in which the former is the case, and in section 1.6 to XPS, where the latter holds true.

1.3 Transition matrix element

Starting point for a further analysis of the absorption cross section in the case of the photoelectric effect is the evaluation of the matrix element in equation 4. For that, both the initial and final state have to be described. For the studies within this work the initial state is given by a core electron wavefunction. In the case of an excitation into a state in the vicinity of an absorption edge, the final state consists of valence electron wavefunctions. This physical process constitutes the theoretical basics behind the NEXAFS spectroscopy. The final state is further characterized by a core hole, which affects all the other electrons. The interaction between the electrons of the shell into which an electron is exciteted as well as the chemical environment of the atom in general play a role, too. All in all the correct description of the final states presents a problem. In order to give a didactic evaluation of the matrix element, a description of the final state by the ground state of the system is chosen. This is done in a one-electron picture and by using atomic orbitals of the form:

$$|n, l, m_l, s, m_s\rangle = R_{n,l}(r) Y_{l,m_l}\,|s, m_s\rangle\,. \tag{5}$$

Here, n presents the principal, l the angular, and s the spin quantum number. The matrix elements factor into angular, spin, and radial contributions:

$$\langle n'l', m_l', s, m_s'|\,\vec{r}\,|n, l, m_l, s, m_s\rangle = \underbrace{\delta_{m_s' m_s}}_{spin}\underbrace{\langle n', l'|\,r\,|n, l\rangle}_{radial}\underbrace{\langle l', m_l'|\,\vec{r}\,|l, m_l\rangle}_{angular}. \tag{6}$$

As the dipole operator does not affect the spin, both s and m_s do not change during a transition. The nature of the absorption edge determines the quantum numbers n, n', l, and l', while the radial part is important concerning the strength of the transition. The latter provides an element-specific excitation since the initial state is strongly localized at the core. In the case of excitations into final states which lie below the ionization potential this also makes the transition sensitive to the valence shell properties. In that case, the absorption cross section can be broken down to:

$$\sigma(E_p) = GR|\vec{\varepsilon}\langle l', m_l'|\,\vec{r}\,|l, m_l\rangle\,|^2 \text{ with } G = (\frac{4\pi^2 e^2}{\hbar c})E_p \text{ and } R = |\,\langle n', l'|\,r\,|n, l\rangle\,|^2. \tag{7}$$

R presents the squared radial part and G includes besides physical constants the energy E_p of the photon. The relative orientation between the unit photon polarization vector ϵ and the transition matrix element influences the strength of the transition. In

an experiment using photons with a well-defined polarization vector this phenomenon can be utilized in order to reveal the orientation of atomic or molecular orbitals, as will be discussed in sections 1.4.1 and 1.4.2.

Only transitions for which the quantum numbers of the initial and final state are in a certain relation are possible, as summarized by the dipole selection rules:

$$\Delta s = 0 \quad \Delta m_s = 0 \quad \Delta l = \pm 1 \quad \Delta m_l = \pm 1, 0. \tag{8}$$

Hence, as the angular quantum number changes by ± 1, excitations from an s initial state just can take place into p and s orbitals. The excitation of an electron from a p initial state only occurs into d and s orbitals. $\Delta s = 0$ means that no spin-flip of the electron can happen during the transition. For excitations from spin–orbit split levels such as the $2p_{3/2}$ and $2p_{1/2}$ states, the total angular momentum and its corresponding quantum number j are of importance, too:

$$\Delta j = 0, \pm 1 \quad \Delta s = 0 \quad \Delta l = \pm 1 \quad \Delta m_j = \pm 1, 0. \tag{9}$$

Having discussed so far dipole transitions into unoccupied final states, an excitation of core shell electrons into the continuum is also possible. In this case, the final state is represented by a core hole at the site of the created ion and an outgoing electron. During the process, energy has to be conserved. The XPS is based on this physical effect. The reader will be introduced to this after having discussed in detail the experimental techniques NEXAFS and XMCD spectroscopy.

1.4 Near edge x-ray absorption fine structure

The study of the NEXAFS, also called X-ray absorption near-edge structure (XANES), is a type of XA spectroscopy. Photoelectrons are excited from core states to the unoccupied states above the Fermi level and below the ionization threshold. A NEXAFS spectrum is obtained by varying the energy of the photons in an energy range of some electron volts close to an absorption edge. The spectrum presents the unoccupied density of states as a function of energy, which may originate from valence states in the case of solids or from atomic or molecular orbitals in the case of molecules. The spatial distribution of the unoccupied density of states is further closely located at the site of the elements at which a core electron is excited. So this technique provides element-selective information about the chemical state and the coordination environment. For this reason it has become a widely used tool among physicists and chemists to study surfaces and adsorbates on substrates. The low penetration depth of X rays of 20 nm at the Fe, Co, and Ni $L_{2,3}$ edges on the one hand and the short escape depth of photoelectrons in bulk material of the corresponding elements, on the other hand, makes NEXAFS measurements highly surface sensitive. By measuring these electrons as a means to perform XA study, 63% of the signal at the Fe, Co, and Ni $L_{2,3}$ edges originates from about the first two 2 nm of the sample [2]. Moreover, the high sensitivity of the XA process itsely allows to measure effective coverages of a thirtieth of a ML of Co and Fe on copper and nickel surfaces at resonable measurement conditions, as done within this work.

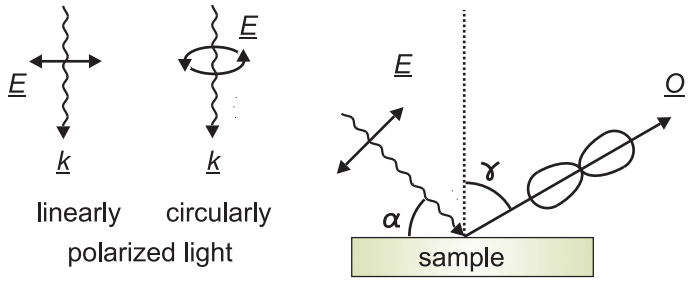

Figure 7: Left side: Schematic drawings of linearly and circularly polarized light, where the wave vector $\vec{k}$ and the polarization $\vec{E}$ are displayed. Right side: Sketch of the measurement geometry of an XA experiment performed with p-linearly polarized light at an incidence angle α between the surface plane and the wave vector $\vec{k}$. In addition, a p orbital, whose symmetry axis forms an angle γ with the surface normal, is shown. The orbital vector $\vec{O}$ is defined by the symmetry axis of the orbital.

1.4.1 Polarization and angle dependence at the $L_{2,3}$ edges

In the framework of this thesis linearly as well as circularly polarized light, both illustrated in Fig. 7, is used. Circularly polarized light presents a linear combination of two sources of linearly polarized X rays, where the corresponding $\vec{\epsilon}$ vectors are rotated by 90° to each other. In the following the photon polarization vector $\vec{E}$ instead of $\vec{\epsilon}$ is used for the description of the polarization of the X rays. Circularly polarized light may have positive or negative helicity, also referred to as right and left circularly polarized light. This depends on whether the photon spin is parallel or antiparallel to the wavevector $\vec{k}$. Both types of X rays are used in order to induce dipole transitions from the $2p$ core to $3d$ valence states of the transition metals Fe, Co, and Ni. As these kinds of excitations have a higher cross-section by more than a factor of 20 compared to $2p \rightarrow 4s$ transitions [45], the latter are negligible. Angle-dependent measurements are performed at an incidence angle of α between the surface plane and the $\vec{k}$ vector of the light, as depicted in Fig. 7, too. For all experiments performed with linearly polarized light in this work the $\vec{E}$ vector lies within the plane defined by the $\vec{k}$ vector of the incident beam and the surface normal. For that reason it is said that the measurements are carried out with p-linearly polarized light.

In a configuration picture the initial state of the transition is described by a $2p^6$ $3d^N$ electronic structure and the final state by $2p^5$ $3d^{N+1}$. Here, the $2p$ core state in the ground state is spherically symmetric, just as the two individual spin–orbit components $2p_{3/2}$ and $2p_{1/2}$, too. However, this is not necessarily the case for the $3d$ shell, which may carry an anisotropic hole density. A possible reason for this can be a chemical interaction which leads to the formation of strong directional bonds. Thus, the strength of the transition, obtained from the integration of the absorption cross section (eq. 7), and correspondingly the detected XA intensity depends on the orientation between the $\vec{E}$ vector of the light and the position of the final state orbital in space. It is zero when $\vec{E}$ lies in the nodal plane of the orbital and reaches its maximum in the case of a parallel alignment of $\vec{E}$ and the orbital.

The term dichroism is used to describe the phenomenon of a polarization-dependent absorption of light. In particular, X-ray natural linear dichroism (XNLD) refers to this

observation by using linearly polarized light, where the $\vec{E}$ vector acts as the so-called search light for the direction of the minimum and maximum number of unoccupied valence states.

Compared to isolated transition metal atoms, the electrons of the $3d$ shell of the Fe and Co ions studied here are subject of a crystal field (CF). For reasons of comprehensibility it can be assumed that the latter has a fourfold symmetry along the surface normal. This leads to the formation of the d_{z^2}, $d_{x^2-y^2}$, d_{xy}, and $d_{yz,xz}$ orbitals, which can be described in a cartesian coordinate system, as will be discussed in section 1.7. The states belonging to theses orbitals may present the final states of the absorption process in a one-electron picture. By varying the angle α, angle-dependent XA measurements can be performed and the orientation between the $\vec{E}$ vector and the probed $3d$ orbitals is changed. An alternative description of the orientation-dependent matrix element in eq. 7 can be useful. The angle-dependent strength of a transition from a $2p$ into an individual d_i state can be linked to the quadrupole moment Q^i_β of the anisotropic charge distribution of the probed d_i orbital. Q^i_β can be calculated by $\langle d_i | \, Q_{\beta\beta} \, | d_i \rangle$, whereby $Q_{\beta\beta}$ is the value of the quadrupole moment tensor for a certain dircetion β.

So the angle-dependent intensity of a transition induced by linearly as well as by helicity-averaged circularly polarized light is proportional to the sum of Q^i_β and the number of holes N_i per d_i orbital [2, 46]:

$$I_\beta^{\leftrightarrow/\circlearrowright\circlearrowleft} = \underbrace{\frac{2}{15} GR}_{C} N_i (1 + \frac{7}{B} Q^i_\beta). \tag{10}$$

For linearly ($\leftrightarrow$) and helicity-averaged circularly ($\circlearrowright\circlearrowleft$) polarized light B is –4 and 8, respectively, where in the first case $\vec{E} || \beta$ and in the second one $\vec{k} || \beta$. In table 1 the intensities of transitions into individual d_i orbitals are shown for the high symmetry cases with $\beta = x, y,$ and z and under the assumption of one hole per d_i orbital. Q^i_β can be either calculated [2] or directly obtained from literature [46], while in both cases hydrogen-wavefunctions are used.

polarization	axis	d_{xz}	d_{yz}	d_{z^2}	$d_{x^2-y^2}$	d_{xy}
$I_\beta^{\leftrightarrow}/C$	x	1.5	0	0.5	1.5	0
	y	0	1.5	0.5	1.5	1.5
	z	1.5	1.5	2	0	0
$I_\beta^{\circlearrowright\circlearrowleft}/C$	x	0.75	1.5	1.25	0.75	0.75
	y	1.5	0.75	1.25	0.75	0.75
	z	0.75	0.75	0.5	1.5	1.5

Table 1: Intensities of transitions into individual d_i orbitals in units of C for the high-symmetry cases with $\beta = x, y,$ and z assuming one hole per d_i orbital. The excitations are induced with linearly as well as helicity-averaged circularly polarized light.

1.4.2 Angle dependence at the K edge

Within this thesis also XA measurements at the N and C K XA edges are presented. Here, the electrons are excited from a $1s$ core state, which possesses an isotropic charge distribution. Correspondingly, the final state is represented by a $2p$ orbital due to the dipole selection rules. However, since organic molecules are studied, the $2p$ states form so-called molecular orbitals with orbitals of neighboring atoms. Hence, the final state is not inevitably of absolute p character. Instead π^* and σ^* antibonding molecular orbitals are tested. They are the counterparts of π and σ bonding molecular orbitals which are established by covalent bonds between N and C atoms, where atomic orbitals of $2s$ and $2p$ symmetry contribute. Thus, so-called π^* and σ^* resonances in K-shell excitation spectra are detected. In organic molecules, single or double bonds may be formed. In the first case a σ^* orbital lies parallel to the bond axis and in the second case additionally a π^* orbital is orientated perpendicularly to the interatomic axis. As only the final states have an anisotropic charge distribution, the XNLD effect can be used to investigate their orientation in space.

Fig. 7 shows a side view of the measurement geometry of an XA experiment performed with p-linearly polarized light at an incidence angle α between the surface plane and the wave vector $\vec{k}$. Also a p orbital whose symmetry axis forms an angle γ with the surface normal is shown. The strength of a transition from a $1s$ core state into this p orbital is defined by the scalar product of the polarization vector $\vec{E}$ of the light and the orbital vector $\vec{O}$, given by the symmetry axis of the orbital. Therefore the azimuthal orientation of the orbital vector, its component lying inside the surface plane, is also important for the strength of the transition. In an XA study, an ensemble of adsorbed molecules, to which the probed p orbitals may belong, is investigated. Assuming that all molecules and hence the corresponding p orbitals are equally oriented with respect to the surface besides a random azimuthal orientation, the dependence of the component of the vector $\vec{O}$ lying inside the surface plane on the intensity of the transition vanishes and the latter is [47]:

$$I(\alpha, \gamma) = A(\cos^2\alpha \, \cos^2\gamma + \frac{1}{2}\sin^2\alpha \, \sin^2\gamma). \tag{11}$$

Here a degree of linear polarization of 100% is assumed and A stands for the angle-integrated cross section. The azimuthal angular dependence on the transition intensity also cancels out in case that the probed ensemble of orbitals has a threefold or higher symmetry along the surface normal. An experimentally obtained angle-dependent intensity of an XA peak can be fitted to eq. 11 and the angle γ, the orientation of the molecule with respect to the surface normal, is obtained as fitting parameter.

1.5 The x-ray magnetic circular dichroism effect

In section 1.4.1 the term natural linear dichroism was introduced, which refers to the polarization-dependent absorption of linearly polarized X rays due to the spatial anisotropy of the probed hole density. In contrast, the expression XMCD describes the different absorption of left and right circularly polarized light because of spin alignment within a sample. This effect is measured in this work at the Fe, Co, and Ni $L_{2,3}$ edges. The idea is to induce an absorption process which is spin-dependent. Then,

the objective of the study is to obtain a quantity which provides information about the imbalance of spin-down and spin-up holes within the valence shell by comparing the intensity of transitions initiated by left and right circularly polarized light. In section 1.5.1 a simple model, which describes such a physical process, is discussed. By evaluating the XMCD difference signals at the $L_{2,3}$ absorption edges, an element-selective determination of the magnetic moments due to the separation in energy of characteristic X ray absorption edges can be obtained. The reader is introduced to this in section 1.5.2. This powerful approach even enables a separate determination of the spin and orbital magnetic moments.

1.5.1 Two step model

It is convenient to divide the absorption process of circularaly polarized light at the $L_{2,3}$ edges of transition metals into two steps. This allows to gain deeper insight into the XMCD effect. At a fist stage, a photon which carries either a positive ($+\hbar$) or a negative ($-\hbar$) photon spin is absorbed and conservation of angular momentum must be ensured. Hence, angular momentum is transfered to the produced photoelectrons. As the electric field of the photons does not interfere directly with the spin of the electrons, the photoelectrons take up the angular momentum at a first view as orbital angular momentum. However, the excitation of a photoelectron occurs from a spin-orbit split level, the $2p_{3/2}$ or the $2p_{1/2}$ level. This means that part of the photons angular momentum is transfered to the spin, which leads to a spin polarization of the excited electrons. As the $2p_{3/2}$ and $2p_{1/2}$ levels have inversed SOC, e.g., a parallel and antiparallel alignment of the spin and orbital moment, respectively, the spin polarization is just the opposite for excitations at the L_3 and the L_2 edges. Analogously, a different polarization of the photons induces an oppositely polarized electron current.

In the second step, the final $3d$ states act as a sensor of the spin and orbital momentum of the photoelectrons. For this, a different spin-up and spin-down occupation of the valence shell is required, leading to a net magnetic spin moment. This may be either the case in paramagnetic systems, where no spontaneous magnetic order is present, by the application of an external magnetic field, or in magnetically coupled systems at sufficiently low temperatures. However, this effect is only maximum in the case of a completely aligned magnetic spin moment, as then the different occupation of the two spin channels is maximum. A parallel alignment of the spin quantization axis of the final states and of the photoelectrons, the latter being identical to the one of the photon spins, is necessary for optimum detection. In case that the empty $3d$ state possesses an orbital magnetic moment itself, it can also work as a detector for the orbital angular momentum of the photoelectron.

In the following a detailed analysis of the XMCD effect at the $L_{2,3}$ edges is provided, assuming several simplifications of the physical process in order to enable the presentation in a feasible manner. A one-electron picture is applied and wave functions of the hydrogen atom are used to calculate the transition matrix element in eq. 7. Additionally, d orbitals in cubic symmetry and exchange as well as spin–orbit split p orbitals as final and initial states of the transition are considered, respectively. The z axis is chosen to be the spin quantization axis, which is parallel to the $\vec{k}$ vector of the light, and the spin-up ($m_S = -1/2$) and spin-down ($m_S = +1/2$) channels are completely and incompletely occupied, respectively. The photons are further 100%

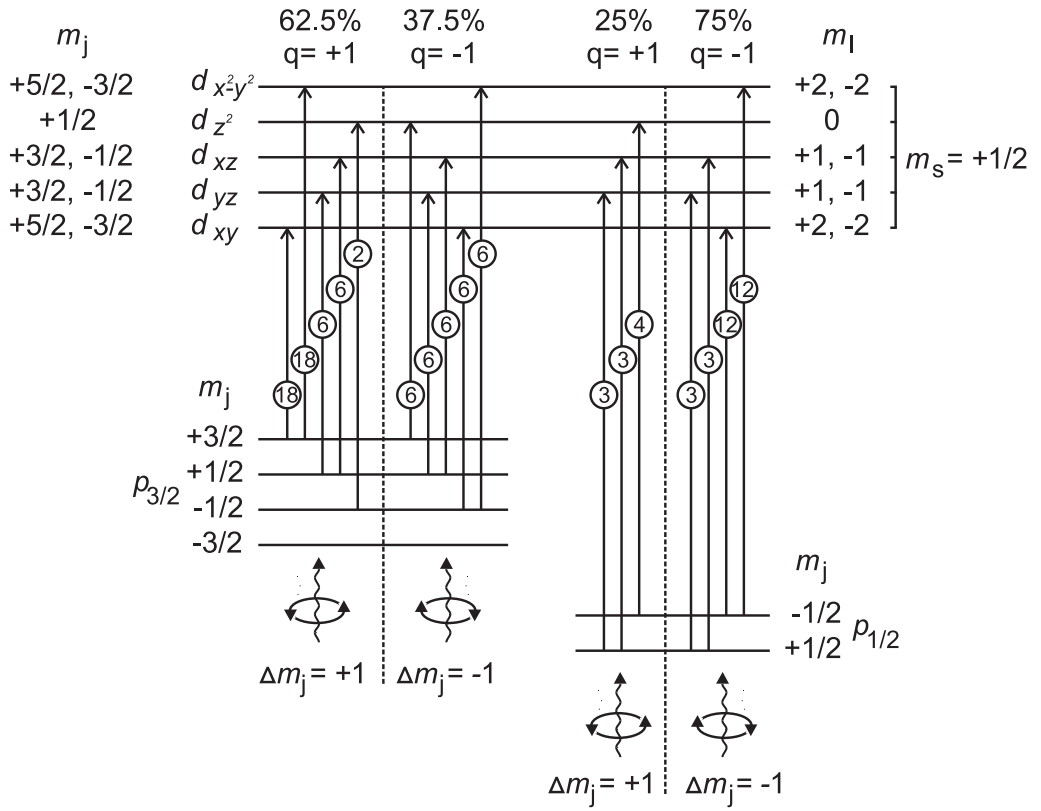

Figure 8: Polarization dependent transition intensities from exchange and spin–orbit split $2p$ states into $3d$ orbitals in cubic symmetry, where all spin-up states are occupied. The quantum numbers m_j, m_l, and m_S of the empty spin-down states are shown. A full description of all assumptions concerning the absorption process can be found in the text. There detailed explanations about the transitions are avalaible, too. A dichroic signal of opposite sign for excitations from the $2p_{3/2}$ and $2p_{1/2}$ states is found. After [2, 48].

spin polarized and a potential orbital moment of the d electrons due to spin–orbit coupling is not taken into account. The resulting intensities of transitions from the $p_{3/2}$ and $p_{1/2}$ levels with the respective quantum number m_j into the individual d orbitals are shown in Fig. 8. They are given in units of $\frac{1}{90}GR$. Only spin-down electrons can be excited, since no spin-flip of the electron can happen during the transition. So the quantum number m_l of the $3d$ states, also shown in Fig. 8, is of importance. The quantum number m_j, the sum of m_l and m_S, changes by +1 or –1 for a transition induced by X rays with positive ($q = +1$) or negative ($q = -1$) angular momentum (in units of $\hbar$), respectively. By summing up, the respective fraction of the total intensity for the absorption of X rays with positive or negative angular momentum is 62.5% and 37.5% from the $2p_{3/2}$ state or 25% and 75% from the $2p_{1/2}$ state, respectively. The two times higher occupation of the $2p_{3/2}$ compared to the $2p_{1/2}$ state leads in total to a dichroic intensity difference of the same size at the L_3 and L_2 edges, however, of opposite sign. This result can be easily extended to the more usual case where the two spin channels are partly filled. Only the sign of q has to be exchanged and for both of them the same excitation percentages are found like the ones shown in Fig. 8. This means that the dichroism signal of the two channels is of opposite sign.

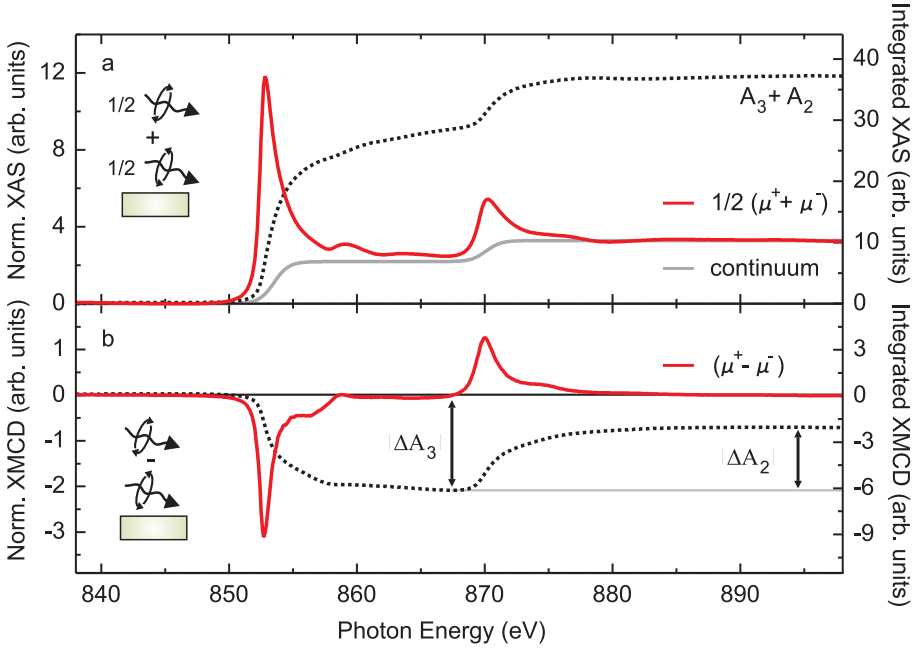

Figure 9: Visualization of the application of the sum rules. Upper panel: XA spectrum of approximately 26 ML Ni on W(110) at the Ni $L_{2,3}$ edges (red line) obtained by averaging signals for positive (μ^+) and negative (μ^-) helicity, measured at 30 K and 20° grazing incidence. In addition, the integration of the spectrum (dashed black line) after subtracting the contribution of the continuum (grey line) is shown. Lower panel: Corresponding XMCD intensity difference (red line) shown together with the integral over the signal (dashed black line). The grey line is an auxiliary line.

1.5.2 Sum rules

A link between the different absorption intensities for left and right circularly polarized X rays and the magnetic moments provide the so-called sum rules. They allow a quantitive evaluation of the measured XAS and XMCD spectra like for instance the ones shown in Fig. 9. There is a respective sum rule for the determination of the spin [49] and the orbital [50] magnetic moment. Their validation was experimentally checked for measurements at the Fe and Co $L_{2,3}$ edges [51].

Fig.9 (a) displays a helicity-averaged XA ($1/2(\mu^+ + \mu^-)$) spectrum (red line) recorded at the $L_{2,3}$ edges of a Ni film with a thickness of approximately 26 ML, grown on W(110). This spectrum is also referred to as white line. The spectra are measured at 30 K and at 20° grazing incidence, which means that there is an angle α of 20° between the surface plane and the $\vec{k}$ vector of the incoming X rays. Panel (b) shows the corresponding XMCD spectrum (red line), which represents the difference between the signals for positive (μ^+) and negative (μ^-) helicity of the incoming circularly polarized light. The peaks with maxima at 852.8 eV and 870.1 eV present the L_3 and L_2 edges, respectively. In panel (a) a continuum (grey line) is shown. It refers to transitions into states above the ionization threshold and is composed of two Fermi functions positioned at energies in the middle of the L_2 and L_3 edges with a relative height of 1:2, since the occupation of the $p_{3/2}$ state is just twice the one of the $p_{1/2}$

state.

The XMCD and XAS signals can be quantitatively analysed by integrating the corresponding signals over the L_3 and L_2 edges. As only the transitions into the $3d$ states are of interest, the continuum is subtracted:

$$\Delta A_j = \int_{L_j} (\mu^+ - \mu^-)\mathrm{d}E,\ A_j = \int_{L_j} (1/2(\mu^+ + \mu^-) - \mu_{continuum})\mathrm{d}E,\ j = 2, 3. \quad (12)$$

The so-called charge sum rule states that the integrated intensity of the XA signal is proportional to the total number of holes N_h in the $3d$ shell of the ground state. Also the measurement geometry and the spatial distribution of the probed hole density can have an influence on the white line intensity [46]:

$$[A_3 + A_2]_\beta = C(N_h + N_Q^\beta) = C\sum_i N_i(1 + \frac{7}{B}Q_\beta^i). \quad (13)$$

Here, N_Q^β is the anisotropy of the charge density within the $3d$ shell to which the individual unoccupied d_i orbitals contribute. This interpretation of N_Q^β is in line with eq. 10 just as the definitions of the variables β, C, N_i, B, and Q_β^i. As the quadrupole moment Q_β^i has a disappearing trace, an average of the absorption intensity obtained from three measurements along orthogonal directions yields the isotropic white line intensity. This means that $N_Q^\beta = 0$. Alternatively, N_Q^β vanishes at a certain direction of β for systems with higher than twofold symmetry or with random azimuthal orientations along the z axis, which is here the surface normal. This direction can be expressed with the help of the detection angle α, which is defined as the angle between the surface plane and the $\vec{k}$ vector of the used light, as displayed in Fig. 7. So a single measurement at the so-called magic angle of $\alpha = 54.7°$ for p-linearly polarized light and of $\alpha = 35.3°$ for helicity-averaged circularly polarized light yields the isotropic white line.

The spin sum rule links the integrated XMCD signals of the L_3 and the L_2 edges to the spin magnetic moment m_S and the anisotopy of the spin density expressed by the term $-7m_T(\beta)$:

$$[\Delta A_3 - 2\Delta A_2]_\beta = -\frac{C}{\mu_B}(m_S - 7m_T(\beta)) = -\frac{C}{\mu_B}\sum_i m_S^i(1 + \frac{7}{2}Q_\beta^i). \quad (14)$$

The corresponding correlation presented in eq. 14 is only valid for a sample magnetically saturated along the $\vec{k}$ vector of the X rays. $7m_T(\beta)$ is the so-called intra-atomic spin dipole moment. $m_T(\beta)$ is given by $\langle T_\beta \rangle \mu_B/\hbar$ [52], where $\langle T_\beta \rangle$ is the expectation value of the intra-atomic magnetic dipole operator and $T_\beta = \sum_\delta Q_{\beta\delta}S_\delta$. So there is a link between the charge and the spin density, expressed by the quadruple operator $Q_{\beta\delta}$ and the spin component S_δ of T, respectively. Advantageously, for the Co and Fe $3d$ transition metals studied within this thesis the energetic contribution to the total energy of the SOC is with 66 meV much smaller than the one of the ligand field with 1–2 eV [53]. Due to this reason the spin density nearly follows the atomic charge density and the term $-7m_T(\beta)$ can be rewritten as $(7/2)\sum_i Q_\beta^i m_S^i$ in the framework of a one-electron model. Here m_S^i is the projected spin moment of an individual d_i-orbital and Q_β^i the corresponding quadrupole moment of the d_i orbital.

polarization	axis	d_{xz}	d_{yz}	d_{z^2}	$d_{x^2-y^2}$	d_{xy}
$I_\beta^{\circlearrowright} - {}^{\circlearrowleft}/(\frac{Cm_S^i}{\mu_B})$	x	0	3	2	0	0
	y	3	0	2	0	0
	z	0	0	-1	3	3

Table 2: XMCD intensities of transitions into individual d_i orbitals of cubic symmetry in units of $\frac{Cm_S^i}{\mu_B}$ for the high-symmetry cases with $\beta = x, y,$ and z. Thereby a magnetic saturation of the magnetic moments m_i along β as well as one hole per d_i is assumed.

In order to eliminate the contribution of $7m_T(\beta)$ in eq. 14, an average over three measurements carried out along orthagonal directions is necessary. However, this is again only possible for systems with higher than twofold symmetry or with random azimuthal orientations along the z axis. There exists also the possibility to set $7m_T(\beta)$ to zero in a single measurement. This is the case for a detection angle α of 35.3°.

In analogy to the calculated transition strength of excitations for electrons from $2p$ levels into individual d_i orbitals of cubic symmetry in section 1.4.1, table 2 displays XMCD intensities for these excitations for the high-symmetry cases with $\beta = x$, y, and z [46]. Thereby one hole per d_i orbital as well as magnetic saturation of the magnetic moments m_i along β are assumed, and $\vec{k}||\beta$.

The orbital sum rule relates the sum of the integrated XMCD signals of the L_3 and the L_2 edges to the orbital moment m_L for measurements along a given direction β of the $\vec{k}$ vector, as expressed in eq. 15. m_L is an anisotropic quantity for the systems studied here, as dicussed in section 1.8. So $m_L(\beta)$ can be determined under the condition of magnetic saturation along the measurement direction.

$$[\Delta A_3 + \Delta A_2]_\beta = -\frac{3C}{2\mu_B} m_L(\beta) \tag{15}$$

The electron yield detection applied in this thesis to measure the absorption cross section does not provide it in absolute terms. Nevertheless, for the purpose of using the spin and orbital sum rule, the implementation of the charge sum rule to the evaluation offers a possibility. Replacing C in eqs. 14 and 15 with the help of eq. 13 leads to:

$$m_S - 7m_T(\alpha) = \frac{N_h \mu_B}{P cos(\theta)} \frac{[\Delta A_3 - 2\Delta A_2]_\alpha}{[A_3 + A_2]_{\beta^{iso}}} \text{ and} \tag{16}$$

$$m_L(\alpha) = -\frac{2}{3} \frac{N_h \mu_B}{P cos(\theta)} \frac{[\Delta A_3 + \Delta A_2]_\alpha}{[A_3 + A_2]_{\beta^{iso}}}. \tag{17}$$

The direction β is replaced by the detection angle α and β^{iso} referes to a measurement geometry at which the isotropic white line intensity is obtained. Instead of using $[A_3 + A_2]_{\beta^{iso}}$ in the numerator, it may be approximated by $[A_3 + A_2]_\alpha$ in the case that the isotropic white line intensity is not known. If both quantities are known, $[A_3 + A_2]_\alpha$ can be included within the error estimation of $m_S - 7m_T(\alpha)$ and $m_L(\alpha)$. Eqs. 16 and 17 further show that the number of holes N_h within the $3d$ shell enters as an input parameter for the evaluation of the sum rules. It has thus to be known or otherwise estimated. Also the degree of polarization P of the circularly polarized X

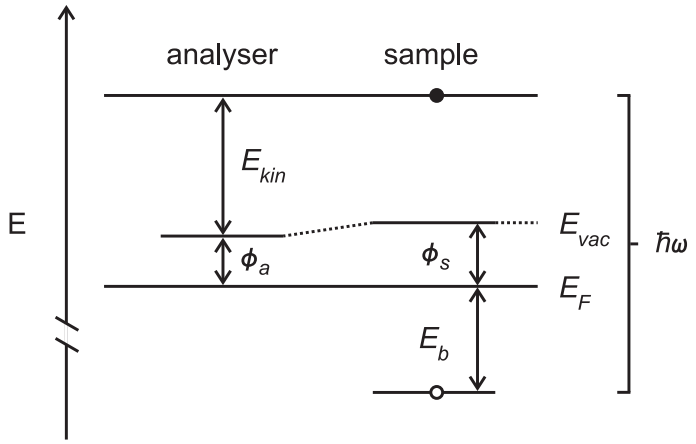

Figure 10: Schematic energy diagram of XPS measurements, including the sample and the analyser. The work functions of both the analyser ϕ_a and the sample ϕ_s as well as the binding energy E_b of the core electron and the kinetic energy E_{kin} of the photoelectron are sketched. The vacuum level E_{vac}, the photon energy $\hbar\omega$, and the common Fermi level E_F of the analyser and the sample are also shown.

rays appears in the two equations as well as the angle θ between the magnetization of the sample and the $\vec{k}$ vector of the incident X rays. This is because a noncollinearity of the latter leads to a measurement of the projection of the magnetic moments onto $\vec{k}$.

1.6 X-ray photoelectron spectroscopy

X-ray photoelectron spectra are measured at constant photon energies, in contrast to XA spectra, and the intensity of photoelectrons is recorded as a function of their kinetic energy with the help of a hemispherical mirror analyzer. XPS tests the occupied density of states, since the final state of the photoelectric effect is represented by an electron in the continuum, which escapes from the sample, and a core hole, as discussed in section 1.3. Hence, it is a complementary technique to XAS, which probes the unoccupied density of states. The analysis of XPS intensities allows to investigate the elemental composition of a system in a quantitative way. This is the case since XPS peaks at typical binding energies can be assigned to certain elements and at the same time present only the density of states at the atoms of a specific element as the core levels are extremely localized. Also low-energy secondary and Auger electrons can contribute to an XPS spectrum, the identification of which is possible by their energetic position.

Fig. 10 displays a scheme of an XPS measurement process. First photons with an energy of $\hbar\omega$ excite electrons of a core shell. As the created photoelectrons have enough energy in order to overcome the ionization threshold, they can escape from the sample, still possessing a characteristic kinetic energy E_{kin}. Now an analyser comes into play, which is electrically in contact with the sample so that their Fermi levels are aligned in energy. It detects the electron intensity at certain kinetic energies. By scanning the energy, an XPS spectrum is recorded. As it follows from the schematic

sketch in Fig. 10, it is possible to determine the binding energy E_b of the excited core electrons, as energy conservation must be fulfilled:

$$E_b = \hbar\omega - E_{kin} - \phi_a. \tag{18}$$

Here, fortunately only the known work function ϕ_a of the spectrometer appears in the equation. The work function is the minimum energy a photoelectron needs at $T = 0$ K in order to leave the sample.

The binding energy of the initial state of a certain atom is influenced by the surrounding charge density. The effective potential seen by the electrons depends thus also on the valency of the element under investigation. This is labeled as initial state effect. It can induce chemical shifts in compounds, which result in binding energies different compared to the pure element by some eV. So the measurement of the energy distribution provides insight into the chemical states of a particular element within the sample.

Further it has to be considered that once the electron has left its original state, the created core hole induces a rearrangement of the other electrons, which leads to its screening. The form of this process depends on the properties of the electrons within the valence shell and is also referred to as final state effect. This effect can also influence the value of E_b.

The transition of electrons from an energetically well-defined initial state into the vacuum induced by a photon of fixed energy does not lead to photoelectrons with a certain kinetic energy. There is a broadening of the electron intensity versus E_{kin}, with the shape of a Lorentz function being more pronounced for longer lifetimes of the created core hole. In addition, the detection of the electrons once more smears out the spectral profile in energy, which can be described by a Gauss function. Overall, the spectra experimentally obtained are fitted by a Voigt function, which is a convolution of a Lorentz and a Gauss function. Before doing so, a so-called Shirley background is subtracted from the raw data, which removes spectral features originating from inelastic scattering events. Before leaving the sample a part of the photoelectrons looses energy by interacting for instance with phonons or plasmons, such that there is an asymmetric broadening at lower kinetic energies of the XPS signal. Moreover, during the photoelectric effect a characteristic energy loss may induce the excitation of a second electron. Thereby a fraction of the original photoelectron energy allows to excite an additional electron into an unbound (shake-off) or unoccupied (shake-up) state, which again produces spectral features at higher binding energies.

In this work p-linearly polarized synchrotron light is used to obtain XPS spectra. X rays with $\vec{k}$ vectors forming an angle of 45° with the surface plane excite the sample, and the kinetic energy of photoelectrons emitted along the surface normal is measured. Data analysis is performed with the help of the *Casa XPS* software.

1.7 Crystal and ligand field theory

Both the crystal and the ligand field theory (CFT/LFT) present useful tools to describe the electronic structure of $3d$ electrons of first row transition metal atoms inside chemical complexes like the metalloporphyrins studied here. The theories aim to describe the chemical bonding between the ligands and the metal atom. The basic idea of the crystal field theory is to assign positive point charges to ligands [54], the electric

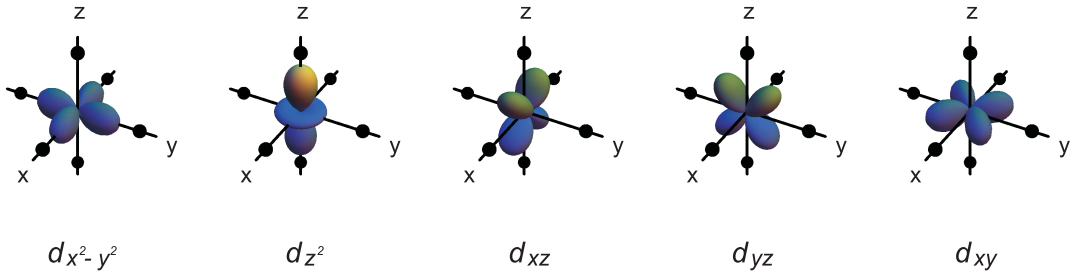

Figure 11: Graphic depiction of the spatial probability distribution of electrons within $3d$ orbitals in a crystal field of octahedral symmetry, obtained from the square of the sum of the respective spherical harmonics. Point charges are indicated by balls situated on the coordination axes at equal distances to the center of the atom.

field of which, the so-called CF, is interacting with the metal ions [55]. Starting from a quantum mechanical description of isolated atoms, wavefunctions may be ascribed to the electrons. The electrons contributing to the interaction with ligands are in the outer shell, here the $3d$ shell. For reasons of simplicity the corresponding wavefunctions can be given by hydrogen-wavefunctions assuming a one-electron approach.

A crystal field induces the formation of $3d$ orbitals which are linear combinations of wavefunction with pure $3d$ character. Their resulting spatial probability distributions for a CF with octahedral symmetry are displayed in a cartesian coordinate system in Fig. 11. According to crystal field theory, the $3d$ orbitals transform as $d_{3\mathrm{r}^2-\mathrm{z}^2}$, $d_{\mathrm{x}^2-\mathrm{y}^2}$, d_{xy}, and $d_{\mathrm{yz,xz}}$ in such an environment. In the following $d_{3z^2-r^2}$ will be called d_z^2. Fig. 11 also shows the point charges on the coordinate axes at equal distances to the center of the atom. Their presence lifts the energetic degeneration of the $3d$ states. So the metal atom in the center is subject to a crystal field with octahedral symmetry (O_h). The d orbitals that point more toward the spatial positions of the point charges are higher in energy because of electrostatic repulsion effects. This is the case for the d_{z^2} and the $d_{\mathrm{x}^2-\mathrm{y}^2}$ orbitals. So a threefold ($t_{2\mathrm{g}}$) and a twofold (e_{g}) degenerate state are formed. The d_{xy} and $d_{\mathrm{yz,xz}}$ orbitals belong to the first and the d_{z^2} and $d_{\mathrm{x}^2-\mathrm{y}^2}$ orbitals to the second. A schematic energy level diagram of the $3d$ states is shown in Fig. 12. There also the case of a weakly and a strongly tetragonally distorted crystal field with a D_{4h} symmetry is considered.

An increase of the distances between the center and the point charge on the z axis of the coordinate system splits both the e_{g} and the $t_{2\mathrm{g}}$ states into substates. Thus the $d_{\mathrm{x}^2-\mathrm{y}^2}$, d_{z^2}, $d_{\mathrm{yz,xz}}$, and d_{xy} orbitals form the new $b_{1\mathrm{g}}$, $a_{1\mathrm{g}}$, $b_{2\mathrm{g}}$, and e_{g} states, respectively. The orbitals belonging to the respective states may also be labeled according to the names of these states. The relative lowering and raising in energy of the out-of-plane (d_{z^2} and $d_{\mathrm{yz,xz}}$) and in-plane ($d_{\mathrm{x}^2-\mathrm{y}^2}$ and d_{xy}) d orbitals, respectively, may even lead to a crossing in energy of the $b_{1\mathrm{g}}$ and $a_{1\mathrm{g}}$ states in the case of a strong tetragonal distortion of the crystal field. Metalloporphyrin molecules in bulk (section 3.2) or adsorbed on low-reactive surfaces (sections 3.3.1 and 3.4) contain metal atoms which are constrained by a crystal field with a virtually square planar symmetry. It presents the special case where the charges on the z axis are completely absent.

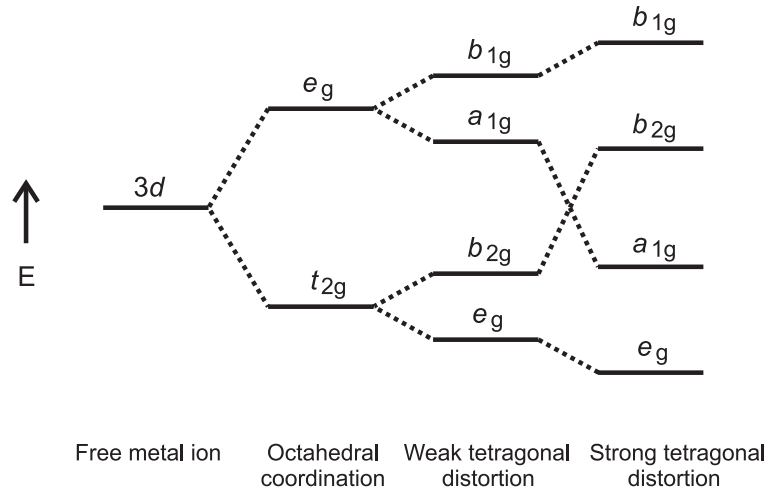

Figure 12: Schematic energy-level diagram of the $3d$ states in a crystal field with octahedral (e_g and t_{2g}) and with a weakly as well as a strongly tetragonally distorted symmetry (b_{1g}, b_{2g}, a_{1g}, and e_g). According to [56].

For MP molecules in direct contact with a reactive surface (sections 3.3.2, 3.3.3, and 3.5), the crystal field acting on the central metal ions has a tetragonally acentric distorted shape (C_{4v}). For the investigated nitrosyl complexes adsorbed on strongly interacting substrates (sections 3.5.2 and 3.5.3), the CF has rather an octahedral shape, however, still being somewhat tetragonally acentric distorted. The energy levels in a tetragonal complex are set by the entire electrostatic potential along the z axis, regardless of whether this potential is uniformly located below or above the molecular plane [57]. Hence, the energy splitting of the $3d$ orbitals in the latter case is qualitatively similar as for a crystal field with D_{4h} symmetry. For the sake of completeness it has to be mentioned that the contribution of the crystal field and the electron-electron interaction neglected here to the energetic splitting of the $3d$ orbitals are of comparable size (0–2 eV) for Fe and Co ions [53].

In contrast to the CFT which assumes a purely electrostatic interaction between ligands and transition metal atoms, the LFT describes the ligands by orbitals which interact with the $3d$ orbitals. So new molecular orbitals are created. As a consequence, charge transfer from and to the metal atoms may be present depending on whether the coordination bond is more of covalent or ionic character. This is in contrast to the crystal field theory (CFT). By means of DFT calculations, the energy splitting of the newly formed molecular orbitals can be obtained [58, 59]. A distinction is made between so-called σ and π interactions between orbitals of the transition metal and the ligand. In σ interactions there exists an axial orbital overlap, and in π interactions the orbital overlap appears laterally. Fig. 13 shows exemplarily such interactions between the antibonding π^* orbital of a NO molecule and $3d$ transition metal orbitals, which are the relevant ones within metal nitrosyl complexes formed by MPs. An NO molecule possesses eleven electrons and, in order to obtain closed shells, it may either donate or accept one electron depending on the nature of the metal and its valency. In the case of a donation, a ligand–to–metal π bonding occurs which combines antibonding π^* with $d_{yz,xz}$ orbitals, as shown in Fig. 13 (a). The reception of an electron by the NO is established by a metal–to–ligand σ bonding between the antibonding π and d_{z^2}

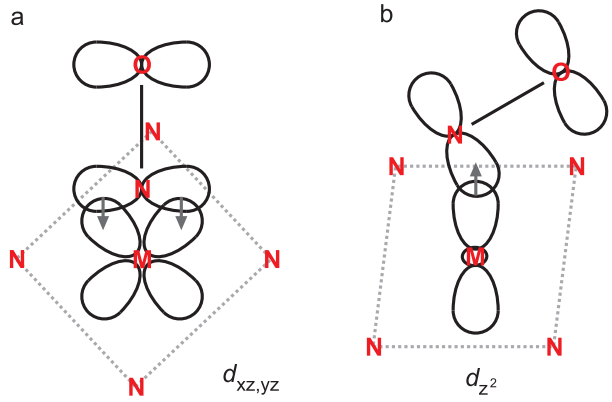

Figure 13: Schematic sketches of a π (a) as well as σ (b) intercation between the antibonding π^* orbital of NO and the $d_{yz,xz}$ and d_{z^2} transition metal orbitals of a MP molecule, respectively. N, O, and M stands for nitrogen, oxygen, and transition metal atoms, respectively. Also the four nitrogen atoms of the porphyrinato ligand are shown. Arrows indicate the charge transfer.

orbitals, as displayed in Fig. 13 (b). A bonding geometry with an angle of 180° or 120° is formed by the transition metal atom and the NO molecule, respectively. These two scenarios represent border cases, and also bonding geometries between 180° and 120° are possible, so that a mixture of both interactions is present depending on whether the NO molecule partially oxidizes or reduces the transition metal [60–63].

1.8 Spin-orbit coupling and anisotropic orbital magnetic moment

In the last section the energetic contribution of the SOC to the description of the $3d$ electronic structure was neglected. It is very small compared to crystal field and intra-shell interactions and more than an order of magnitude for $3d$ transition metals where it amounts to about 50 meV. For a free atom within a semiclassical model the SOC can be seen as a simple coupling of the spin magnetic moment to the orbital moment, which is related to the motion of the electronic charge of the electron around the atomic nucleus. Seeing the latter within a coordinate system with the zero point at the electron site, the atomic nucleus creates a magnetic field at the electron in which its spin can be differently oriented. So the magnetic dipole moment from the orbital motion of the charge interacts with the spin moment of the electron. For less than half-filled shells the spin and orbital moments align antiparallel to each other due to the negative charge of the electron. However, in the case of a more than half-filled $3d$ shell, as it is the case for the Fe and Co ions studied here, this is just opposite. An explanation provides the interpretation of a more than half-filled shell as a completely filled one carrying positively charged holes.

Chemical bonding induces the formation of new $3d$ orbitals as discussed in the context of the crystal field theory. The orbiting electrons can be interpreted as a standing wave, since the orbit of the electron is broken up by the formation of orbitals. Hence, the $d_{x^2-y^2}$, d_{z^2}, $d_{yz,xz}$, and d_{xy} orbitals have zero orbital moment. However, in the above deduction of the $3d$ orbitals in cubic symmetry the SOC has not been considered. It breaks time-reversal symmetry. This means that the overall motion of the orbiting electron is more pronounced in one direction than in the opposite one.

Thus a net orbital current around the atomic nucleus exists and so an orbital moment is present. The new $3d$ states which belong to the corresponding $3d$ orbitals can be obtained by treating the rather small spin-orbit interaction in the framework of the so-called perturbation theory [64]. So a combination of different $3d$ states, formed within a crystal field with cubic symmetry at a first approximation, builds the new eigenstates, which have anisotropic orbital momenta. The absolute size of SOC-induced orbital moments can be discussed in the framework of the perturbation theory. For reasons of simplicity this can be done by following the one-electron approach [52]. Thereby a large magnetic exchange splitting is assumed and an occupation of all spin-down states $|n\rangle$, while all the spin-up states $|m\rangle$ are empty. Finally the anisotropic orbital magnetic moment, as the first order perturbation expression, amounts to:

$$m_{L,n}^{\beta} = \frac{\mu_B \xi}{\hbar^2} \sum_m \frac{|\langle n| L_\beta |m\rangle|^2}{\Delta_{mn}} \tag{19}$$

along the different axes x, y, and z, as labeled by β. The resulting size of the orbital magnetic moment of a state $|n\rangle$ depends on the energetic separation $\Delta_{mn} = E_m - E_n$ between the mixing states of zero order and is bigger when the states are closer in energy. The total orbital magnetic moment is obtained by the sum over all unoccupied states $|m\rangle$. ξ, μ_B, and L_β are the SOC constant, the Bohr magneton, and the angular momentum operator acting along the different axes x, y, and, z, respectively. The results of the latter by acting on the zero order states can be found somewhere else [65]. Tabel 3 gives an overview over the resulting SOC-induced magnetic orbital momenta

zero order state	d orbital	m_L^z/μ_B	m_L^y/μ_B	m_L^x/μ_B
$\|5\rangle$	d_{xz}	$-\xi/\Delta_{54}$	$-\xi/\Delta_{51}-3\xi/\Delta_{52}$	$-\xi/\Delta_{53}$
$\|4\rangle$	d_{yz}	ξ/Δ_{54}	$-\xi/\Delta_{43}$	$-\xi/\Delta_{41}-3\xi/\Delta_{42}$
$\|3\rangle$	d_{xy}	$-4\xi/\Delta_{31}$	ξ/Δ_{43}	ξ/Δ_{53}
$\|2\rangle$	d_{z^2}	0	$3\xi/\Delta_{52}$	$3\xi/\Delta_{42}$
$\|1\rangle$	$d_{x^2-y^2}$	$4\xi/\Delta_{31}$	ξ/Δ_{51}	ξ/Δ_{41}

Table 3: SOC-induced orbital magnetic moments of a state $|n\rangle$ along the x, y, and z axes. Their size is calculated by means of a one-electron approach and the application of the perturbation theory. See text for details.

of a state $|n\rangle$ along the different axes. For completely filled spin-down and empty spin-up states the total resulting orbital magnetic moment is zero and the anisotopy vanishes. Only in the case of partially filled spin-up states the m_L^z may be unequal zero, as it is the case for the Co ions studied within this work. For the sake of completeness it has to be mentioned that for the assumed symmetry the d_{yz} and d_{xz} states are fully degenerate and form an orbital denoted as d_π. This d orbital possesses a non-zero first-order orbital moment along the z axis in the case that it carries three electrons and one hole [66].

The anisotopy of the orbital moment has important consequences on physical properties and in particular on the so-called magnetocrystalline anisotropy (MCA). The latter describes an energy which is necessary in order to change the orientation of the magnetic moments from the so-called easy axis to the so-called hard axis. The Bruno model states that the MCA is proportinal to the difference between the orbital

moments along the easy and hard magnetization directions [67] in transition metal monolayers. It also says that the orbital moment is bigger in size for its alignment parallel to the easy magnetization direction. Thereby a large magnetic exchange splitting is assumed. The physical concept behind this statement is the following: The crystal field defines the orbital motion of the unpaired electrons and locks the orbital moment into a preferential direction. A dipolar interaction between the electron's own orbital motion and its intrinsic spin forms the link between the orbital and spin system. In the following a uniaxial anisotropy is assumed. This implies that the x and y axes are equivalent and consequently m_L^x and m_L^y are identical. Consequently there is no energetically preferential alignment of the magnetic moments within the plane defined by the x and y axes. One may define: $m_L^{\perp} = m_L^z$ and $m_L^{\parallel} = m_L^x = m_L^y$. Thus, the MCA is [68]:

$$\Delta E = -\frac{G}{H}\,\frac{\xi}{4\mu_B}(m_L^{\perp} - m_L^{\parallel}). \tag{20}$$

The factor G/H is related to the details of the band structure. Originally Bruno derived this model for thin magnetic films on the basis of perturbation theory. However, its application to molecular compounds containing isolated transition metal ions is reasonable, since the MCA has also been deduced by using atomic $3d$ wave functions for its derivation, which leads to $G/H = 1$ [69].

1.9 Magnetic coupling

Material that contains atoms with unpaired electrons can magnetically order. This means that the electron spins get aligned without an external magnetic field. The magnetic dipole–dipole–interaction between the spins of neighbor atoms is in most materials too weak and leads only to long-range order at very low temperatures. More relevant for the arrangement of the magnetic order is the so-called exchange interaction, which is a quantum mechanical effect. This may be of direct nature, which requires an overlap of the electron wavefunction of neighbor atoms. Two electron model presents an adequate framework for discussing the inter-atomic exchange interaction [2]. Here, two electrons each belonging to one hydrogen atom interact with each other, following the Heitler-London calculation [70]. In this case new wavefunctions are formed, which present linear combinations of the atomic orbitals. This reflects the bonding between the neighbor atoms. The overlap in space enables the electrons to hop onto the neighboring atom. The total wavefunction of the system must be antisymmetric under exchange of the electrons, as electrons are fermions, and can be broken down into the product of the spatial and the spin parts. If the electrons occupy the same orbital, their spins must be antiparallel due to the Pauli principle, which prohibits the double occupancy of a quantum state. The spatial part of the wavefunction thus has to be symmetric and the spin part antisymmetric. The Coulomb energy of the system depends on the distance between the two electrons and may be lowered by the occupation of an energetically higher-lying orbital by one of the electrons. Since this implies an antisymmetric spatial wave function, the spin function is symmetric, i.e., the spins are aligned parallel. This corresponds to a ferromagnetic state, while the antiparallel aligned spins correspond to an antiferromagnetic state. For the H_2 molecule the spins of the electrons are of opposite sign in the electronic ground state. The discussed model links the formation of a covalent chemical bond, as

it may be present between atoms in a molecule or in the case of an interaction between an adsorbate and a substrate, to the spin alignment of the electrons contributing to the formation of the bond.

The Heisenberg model builds on the Heitler-London calculation for H_2 [71]. The part of the Hamiltonian describing the exchange interaction is as follows [2]:

$$H_{exch} = As_1s_2 \text{ with } A = -2J_{1,2}. \tag{21}$$

Thereby $J_{1,2}$ is the exchange integral which corresponds to the coupling of the spins s_1 and s_2 each belonging to electrons of two different atoms with respective spatial wavefunctions ψ_1 and ψ_2:

$$J_{1,2} = \int\int \psi_1(\mathbf{r}_1)\psi_2(\mathbf{r}_2)\frac{e^2}{4\pi\epsilon_0 r_{1,2}}\psi_1^*(\mathbf{r}_2)\psi_2^*(\mathbf{r}_1)d\mathbf{r}_1 d\mathbf{r}_2. \tag{22}$$

A positive value of $J_{1,2}$ means that the spins point into the same direction and a negative one that they are antiparallel aligned. The exchange integral decreases with increasing distance $r_{1,2}$ between the electrons.

There is another approach for treating the exchange interaction which is for instance useful for the description of the magnetic order in transition metal oxides. Instead of including spin operators into the Hamiltonian, the so-called Hubbard model analyses the contribution of two competing energies, that determine the magnetic ground state. One is the electrostatic Coulomb energy between electrons and the other one is the hopping energy of electrons to a neighbor atom. For the H_2 molecule the relevant part of the Hamiltonian H_{Hub} for the Coulomb and exchange interactions is written as [72]:

$$H_{Hub} = -t\sum_{\sigma=\downarrow,\uparrow}(c_{1\sigma}^\dagger c_{2\sigma} + c_{2\sigma}^\dagger c_{1\sigma}) + U(n_{1\uparrow}n_{1\downarrow} + n_{2\uparrow}n_{2\downarrow}) \text{ with } t > 0 \text{ and } U \geq 0. \tag{23}$$

The operators $c_{i\sigma}^\dagger$ and $c_{i\sigma}$ generate and annihilate an electron with spin σ on atom i, respectively. Hence, the first term in equation 23 can be interpreted as electron hopping from atom to atom, where $+t$ is proportional to the hopping energy and $-t$ to the kinetic energy of the electrons. Thereby the spin does not change. Since $-t$ appears in equation 23, a higher hopping energy and a lower kinetic energy of the electrons, respectively, minimize the total energy of the electrons due to their delocalization. The operator $n_{i\sigma}$ can be written as $c_{i\sigma}^\dagger c_{i\sigma}$ and correspondingly counts for a given spin σ the occupation on atom i. So the second term in eq. 23 can be interpreted as the Coulomb interaction U between electrons situated on the same atom with antiparallel aligned spins. The presence of two electrons on one atom costs a repulsion energy U and keeps the electrons apart. A balancing between this contribution to the total energy and the hopping energy defines the magnetic ground state. In H_2 the spins of the two electrons are antiferromagnetically aligned, which can be seen in the framework of this model as follows: For oppositely aligned spins hopping is allowed, although the Coulomb repulsion has to be overcome, while for a parallel spin alignment this is not possible, as two electrons with the identical spin on one atom can not exist. The two sketches on the left hand side of Fig. 14 represent this graphically, where the upper one displays the case for an opposite orientation

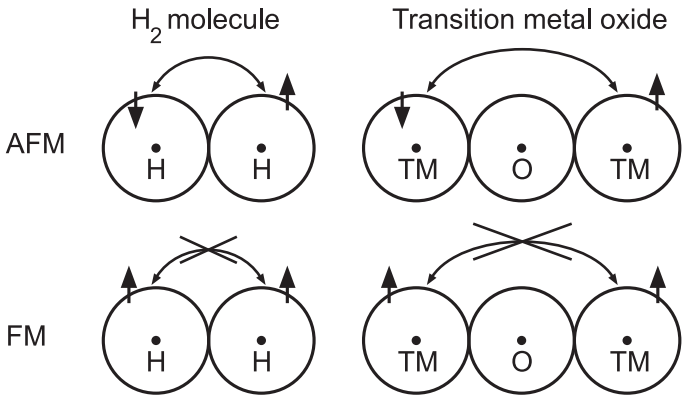

Figure 14: Schematic sketches for the explanation of the direct exchange and indirect superexchange interaction in the framework of the Hubbard model between hydrogen atoms of an H_2 molecule and between transition metal atoms separated by an oxygen atom, respectively. The upper sketches display the antiferromagnetic ground states where electron transfer is possible. See text for details. Figure according to [2].

of the electron spins and the lower one for a parallel spin alignment. The unlimited hopping state offers new degrees of freedom and the electrons can lower their kinetic energy.

Even if there is no direct electron wave function overlap between atoms with magnetic moments, a magnetic interaction between their spins can exist. This is called indirect exchange interaction. Here, an intermediary wavefunction overlaps simultaneously with the respective wavefunctions of two other magnetic atoms. There are different forms of this type of exchange interaction. The Hubbard model is a useful tool to discuss these physical phenomena. One of them is the superexchange coupling. It is known to occur for instance in transition metal oxides like NiO or CoO, where unpaired $3d$ electrons of the transition metals form bonds with the $2p$ valence electrons of the oxygen atoms, which tend to attract two electrons. Assuming the easiest case with one unpaired electron per transition metal atom and a diamagnetic oxygen atom which is twice negatively charged, there are four electrons, each one with a spin, which can be located and oriented in a different manner on the three atoms. As a result of the electronegativity of oxygen, it is reasonable to assume that it has a full shell and correspondingly an unchanged spin configuration. This allows to treat the problem with the same Hubbard formalism as the one applied to the H_2 molecule. Hence, the total energy is the lowest for an antiferromagnetic coupling of the spins situated on the transition metal atoms. The possible electron transfer is displayed in Fig. 14 by the two sketches on the right hand side. Also in a more detailed theoretical treatment which includes the occupation of the oxygen atom by only one electron and which can be found somewhere else in literature [2] the magnetic ground state is found to be the same.

In general, the coupling strength of the superexchange interaction depends on the magnitude of the magnetic moments on the metal atoms, the degree of hybridization between metal and non-metal states as well as the bond angle formed by the metal and non-metal atoms. There are the Kanamori-Goodenough rules which predict the sign of the superexchange coupling [73–75]. They take into account the total number

of $3d$ electrons within the $3d$ shell and the kind of $3d$ orbitals that are formed by the crystal field and that contribute to the bond formation as well as their geometrical orientation with respect to each other. The magnetic moments of metal ions forming a linear arrangement with a non-magnetic ligand in between couple in an antiferromagnetic fashion if the lobes of the orbitals at the metal side, which carry the unpaired electrons, would have a reasonable overlap integral in space by bringing the metals closer to each other. This is referred as to "180° superexchange". In the case that two magnetic metal ions and a non-magnetic ligand form an angle of 90°, the superexchange interaction is in most of these cases ferromagnetic. This is labeled as "90° superexchange".

Another form of indirect exchange interaction is the double exchange [76]. It is, for instance, present in magnetite, Fe_3O_4, and influences its magnetic ground state. This material will serve in the following as example in order to explain the mechanism of double exchange in the framework of the Hubbard model. The spinel magnetite contains Fe ions with 5 and 6 electrons in the $3d$ shell. These two types of Fe atoms with a valency of +3 and +2 are separated by oxygen atoms that are diamagnetic, as they are twice negatively charged. The crystal field that acts on the Fe ions is so small that their $3d$ states are occupied according to Hund's rule. A concurrent transfer of two electrons takes place, which minimizes the kinetic energy of the system. From the intermediate oxygen atom an electron hops to the Fe atom with a +3 valency and is replaced by an electron from the Fe atom in an oxidation state of +2. As spin-flips are forbiddden in the electron hopping procedure, an identical magnetic structure of the two Fe atom types beside the additional electron is energetically of advantage. Thus, five electron spins on each Fe atom point in the same direction, respectively, which may be the up direction, and the spin of the additional sixth electron is oppositely aligned. So only a spin down electron is transferred through the oxygen from one Fe ion to the next one due to the Pauli principle and the electron is delocalized, which minimizes the total energy. As a result the Fe magnetic moments couple across the diamagnetic atom ferromagnetically to each other. For the sake of completeness, it has to be mentioned that the electronic and magnetic structure of Fe_3O_4 is much more complex than the one presented here for didactical reasons. So it possesses for instance phase transitions, three inequivalent types of Fe atoms, and both superexchange as well as double exchange interactions are simultaneously present inducing a ferrimagnetic ground state.

2 Experimental details

2.1 Introduction

All XAS studies presented in this work were performed at the synchrotron radiation source BESSY II in Berlin. The measurements were either carried out with a group-owned ultra-high vacuum (UHV) chamber serving as an end station at the bending magnet beamline PM-3 as well as at the undulator beamline UE56/2-PGM1 or with the help of the high-field end station at the undulator beamline UE46-PGM1. Synchrotron radiation facilities provide X rays with tunable energies, as required for the investigations realized, while at the same time the X rays possess a high brilliance. The latter quantity defines the quality of an X-ray beam [77]:

$$\text{Brilliance} = \frac{\text{photons/second}}{(\text{mrad})^2(\text{mm}^2 \text{ source area})(0.1\% \text{ bandwidth})}. \tag{24}$$

The intensity, the number of photons per second, contributes to this quantity as well as the collimation of the beam which describes its divergence. The latter is normally given in milli-radian. Also the size of the source area, usually specified in mm^2, is of importance, as it quantifies the possibility to focus the X-ray beam. The spectral distribution may possess peaks at specific energies or might be almost smooth and, hence, plays a role as well. So the brilliance is defined for an energy range with a bandwidth of 0.1% about the selected energy.

First this section introduces the reader to the nature of synchrotron radiation combined with historical aspects regarding this topic. After this the functionality of modern synchrotron light sources is explained and how the thickness as well as energy calibration was carried out for the work presented here. Also the way of how to measure the absorption cross section is discussed and finally the sample preparation and characterization is in the focus.

2.2 Synchrotron radiation

The term synchrotron refers to a type of cyclic particle accelerator. A sketch of a top view on such a facility is displayed in the middle of Fig. 15 (a). It can be used to accelerate charged particles like protons or electrons to a relativistic velocity and its concept has been already designed in 1945 [78]. The particles are kept at a fixed orbit by bending magnets. In this case it follows for a relativistic particle from the equilibrium of the Lorentz and centrifugal forces [79]:

$$R = \frac{E_S}{ecB}. \tag{25}$$

This means that the ratio the of the particle energy E_S and the applied magnetic field B has to be constant, since the turning radius R is given by the design of the synchrotron. So E_S and B have to be synchronously increased, which explains the name of this kind of particle accelerator. E_S is enhanced by applying a voltage along an acceleration distance, which has in the case of BESSY II a value of 1.7 GV. At the beginning synchrotrons were only used among high energy physicists.

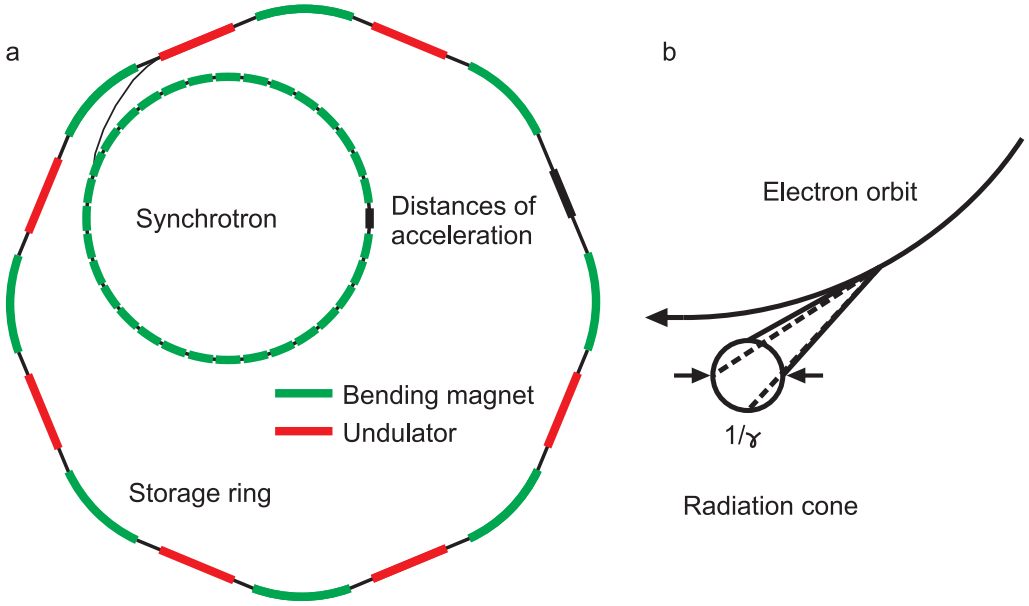

Figure 15: (a) Schematic drawing of a third-generation synchrotron radiation facility. Banding magnets and undulators are displayed in green and red colour, respectively. A synchrotron is used to accelerate the electrons, which are kept afterwards in a storage ring. Several installations and optical components are omitted. (b) Trajectory of a relativistic electron shown together with its radiation cone having an aperture angle of $1/\gamma$, according to [77].

Each accelerated and charged particle emits energy in form of a electromagnetic wave. As the bending magnets change the velocity vector of the orbiting particles in a synchrotron, the particles eject tangentially electromagnetic radiation. Experimentally this kind of radiation, which is induced by the perpendicular deflection of particles from their direction of motion, was first found by operating a 70-MeV synchrotron in the 1940s [80] and therefore called synchrotron radiation. This phenomenon was already predicted to occur at the end of the 19th century [81]. For particles that move with relativistic speed the radiated power is proportional to E_S^4 and inversely proportinal to the rest mass to the power of four [79]:

$$P \propto \frac{E_S^4}{m_0^4 R^2}. \tag{26}$$

As electrons have a mass that is around 1741 times smaller than the one of a proton, synchrotron radiation only plays an important role for the former. The radiation is emitted in form of a cone with an aperture angle of $1/\gamma$, as graphically shown in Fig. 15 (b). Thereby γ is the so called Lorentz factor, which is the electron energy in units of the rest mass energy [77]. The emitted X rays, which lie within the plane of the electron orbit, are completely linearly polarized. By contrast, the emitted photons outside of the orbit plane are circularly polarized. Thereby the degree of circular polarization increases with the size of the aperture angle, however, the photon intensity also falls off.

2.3 Synchrotron light sources

A state-of-the-art synchrotron light source is a combination of a storage ring and a particle accelerator, which in the case of BESSY II is a synchrotron. The accelerated electrons are transferred to the storage ring as displayed in Fig. 15 (a). The latter is under UHV and stores electron pockets, which emit X rays as magnets keep them on a fixed trajectory. So the electrons in a storage ring lose energy due to the ejection of electromagnetic radiation, which needs to be compensated by at least one acceleration distance within the ring. The measurements presented in this work have been performed in the multi-bunch mode of BESSY II, which is the standard operation mode. This means that there are several hundred electron pockets which are temporally separated by nanoseconds and which produce a maximum electron current of 300 mA. As permanently a part of the electrons collides with residual gas molecules, the ring current decreases up to a value of 150 mA and new injections are necessary after usually eight hours. As a consequence the intensity of the provided synchroton radiation is time-dependent. Nevertheless, the concept of merging a particle accelerator and a storage ring in order to create synchrotron radiation outclasses the use of a synchrotron for this purpose, as in the first case the electrons produce on average a constant high intensity of synchrotron radiation and not only at their maximum speed at the end of the acceleration process. Moreover, in a pure synchrotron due to permanently changing electron velocities, the radiated power and so the characteristics of the synchrotron radiation change. Also the fixed track of the electrons in a storage ring has the advantage that the appearance of the synchrotron radiation around the facility is locally constant, which is important in the case of fixed measuring stations.

BESSY II belongs to the so-called 3^{rd} generation of synchrotron light sources. Its storage ring is equipped with bending magnets and straight insertion devices like undulators, as shown in Fig. 15. The 1^{st} generation sources were primarily used for high-energy physics and only besides as a source for X rays. Only the 2^{nd} generation of synchrotron light sources, to which BESSY I belonged, is exclusively designed for the generation of X rays and bending magnets are installed within the storage ring. Electrons which pass through them produce a spectral photon density, which can be calculated according to Schwinger [82]. It increases with the electron energy E_S and the ring current I_{ring}. The spectral photon density as a function of the photon energy can be separated into two parts by the so-called critical energy, which is inversely proportional to the turning radius of the magnet. Above this energy the spectral photon density quickly drops off. The standard bending magnets at BESSY II as installed at the PM-3 beamline have a critical energy of 2.5 keV, whereby the turning radius R is 4.35 m [83]. So from 20 to 1900 eV the PM-3 beamline provides X rays for the users.

The undulators installed at the UE56/2-PGM1 and the UE46-PGM1 at BESSY II consist of permanent magnets which build up four different rows, as shown in Fig. 16. They lie below and above the trajectory of the electrons and can be shifted with respect to each other. The magnets within a row are ordered with respect to their polarity with a periodicity of λ_u. Within the so established magnetic field the electrons which travel along the undulator are periodically deflected. This direction is in the following defined as z axis. In case that the four rows are situated laterally on the same level just as in Fig. 16, the electrons pass through the device on a sinus-shaped

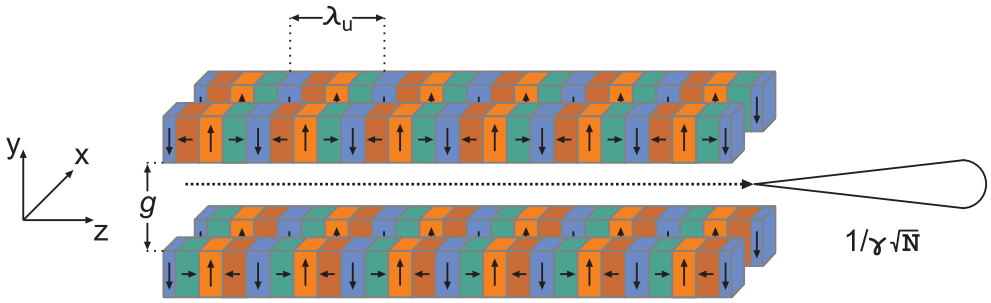

Figure 16: Schematic sketch of an Apple-II-type undulator. Four rows of permanent magnets each with a periodicity of λ_u are shown. Also the gap g, the periodicity λ_u, and the aperture angle $1/\gamma\sqrt{N}$ of the radiation cone from the undulator are displayed, according to [77].

trajectory lying in the xz plane. This is refered to as linear mode. The magnetic field $\tilde{B}$ acting along the straight in the middle of the undulator, which is displayed by a dotted line in Fig. 16, increases by dreasing the gap g between the upper and lower rows. The important parameter K [77] is defined as $0.934\lambda_u[\text{cm}]\tilde{B}[\text{T}]$. In the case of undulators, $K \leq 1$ applies, which implies small amplitude oscillations. The X rays of a certain wavelength emitted at earlier and later times in the undulator superimpose in a constructive manner. Mathematically the coherence condition for this is [79]:

$$\lambda_w = \frac{\lambda_u}{2\gamma^2}(1 + \frac{K^2}{2} + \gamma^2\phi_u). \tag{27}$$

Here, λ_w is the wavelength of the emitted photons and ϕ_u is the angle between the undulator axis in z direction and an observation point. The intensity of the light with λ_w is proportional to the square of the number N of magnetic periods of the undulator. So the X-ray intensity is higher than the one of N bending magnets due to the constructive interference. Further the radiation cone is compressed by a factor of around $1/\sqrt{N}$ compared to the natural opening angle of synchrotron radiation [77].

In order to produce circularly polarized light, the magnets need to be moved with respect to each other [84]. By a lateral shift of a quarter period in the same direction of two out of the four rows, which lie diagonally to each other, one being located above and one below the electron trajectory, the electrons pass on an almost circular spiral along the z axis through the undulator. Depending on which diagonal pair of rows is moved, either left or right circularly polarized light is ejected by the electrons.

In order to provide the desired X rays at the measuring station, a beamline under UHV connects the storage ring with the experiment. There are key components installed in a standard beamline. The first one is a mirror system just after the bending magnet or the undulator that parallelizes the beam path of the photons. The so prepared X rays enter into a monochromator which isolates the ones with a desired wavelength from the other ones. Finally these monochromatic photons pass through an exit slit and enter into the measurement chamber. Circularly polarized light with 90% degree of polarization at the UE46-PGM1 and with 85% at the PM-3 as well as at the UE56/2-PGM1 were used. At the latter beamline the linearly polarized photons had a degree of polarization of 99% and at the PM-3 of 95%. For the dipole and the two undulator beamlines the photon flux density was in the range of about

10^{12} and 10^{13} photons s^{-1} cm^{-2}, respectively. Moreover, the spot size of the X rays on the sample was ∼0.25 mm^2 at the bending magnet beamline and ∼0.5 mm^2 at the two undulator beamlines. The time for measuring an XA spectrum was about two to three minutes depending on the absorption edge and the beamline. Usually the noise signal was about 0.5 tenths of a percent of the measurement signal.

2.4 Thickness and energy calibration

Calibration of the photon energy at the Co, Ni, and Fe $L_{2,3}$ edges was performed with the help of XA measurements of Co films on a Cu(100) crystal setting the position of the CoL_3 edge to 778.5 eV [85, 86]. Additionally, NEXAFS measurements of gaseous N_2 setting the position of the first N π^* peak to 400.88 eV [87] were used to calibrate the photon energy at the N and C K edges except for the data presented in section 3.5.3. Identical XA and XMCD results, concerning the line-shape and results of the sum-rule analysis, were obtained for measurements of the systems under study carried out during different beamtimes. Data were recorded with an energy resolution of 300 meV at the Co, Ni, and Fe $L_{2,3}$ edges except the ones shown in Figs. 42 and 43, which were collected with an energy resolution of 150 meV, just as the ones obtained from measurements at the N and C K edges.

The thickness of the transition metal films, grown on Cu(100), was calibrated by means of the edge jump measured at 879.4 eV in the case of the Ni films and at 810.0 eV for the oxygen-covered Co films. Therefore a correlation between the edge jump in percentage of the pre-edge intensity and the coverage of the metals in ML was used, which had been obtained by experimental works of other or former group members of the AG Kuch [88]. The necessary knowledge had been gained by medium energy electron diffraction studies combined with XA measurements of the same physical systems. So an edge jump of 315% and 208% corresponds to a Ni film with a thickness of 12 ML and 8 ML, which is grown on a clean and a pre-oxidized Cu(100) surface, respectively. An edge jump of 145% is equivalent to a film thickness of 5 ML for the system O/Co/Cu(100). The thickness of the Ni films prepared on a W(110) single crystal was calibrated with the help of this knowledge. In this case the sample preparation was performed with the very same Ni evaporation rate, measured by the drain current of the sample and the flux monitor of the evaporator, the same pressure and the same power applied for the electron-beam evaporation.

The porphyrin coverage was calibrated from the signal–to–background ratio at the Co and Fe $L_{2,3}$ and N K XA edges, as a reliable determination of the edge jump was not possible due to an already too big bending of the XA spectra. Thereby again reference measurements with a known signal–to–background ratio in relation to the coverage were used, which had been performed by other persons of the AG Kuch and which provide a consistent parameter set for organic coverages, mainly azobenzene and porphyrin molecules, on various substrates. These works involve XAS measurements of the c(2×2) superstructure of oxygen on Co/Cu(100) (0.5 ML) [88], of molecules with a known C–to–O ratio [89], as well as STM measurements of FeOEP on Cu(001) performed at the ID08 beamline at the european synchrotron radiation facility on the very same samples that had been also measured by XAS [90]. The estimated systematic error of this coverage calibration is about 20%, which includes the uncertainty of the packing within the molecular layer.

2.5 Detection of the photoabsorption cross section

The physical quantity which has to be detected for XA and XMCD measurements is the photoabsorption cross section in the vicinity of an absorption edge. In the framework of this thesis molecules adsorbed on substrates with a thickness of a few millimeter are studied. A detailed description of the physical processes involved within the absorption process clarifies how to experimentally obtain the desired information. The creation of a core hole due to the absorption of light is followed by its decay after a lifetime of the order of 10^{-15} s [91]. The recombination of the core hole with an electron from a higher energy level leads to the relaxation of the atom excited state. This goes hand in hand with a release of energy in form of an ejected fluorescence photon or the emission of a so-called Auger electron with a characteristic kinetic energy [91]. The incoming X rays penetrate into the sample and within this process they are attenuated depending on their mean free path. The thereby created Auger electrons are mainly scattered depending on which depth inside the sample they are emitted. This generates cascades of so-called secondary electrons of lower energy. All electrons which have enough kinetic energy in order to pass the surface potential barrier can leave the grounded sample to which for this reason an electron current flows. The direct detection of the fluorescence photons or of the Auger electrons, but also the measurement of the sample drain current, provide means to experimentally access the absorption cross section.

The study of the Auger electrons which have not lost energy due to inelastic interactions allows to perform investigations with high surface sensitivity. In contrast, the detection of fluorescence photons enables the possibilty to carry out XA studies which provide information about bulk properties. This is because the generated photons can cross more layers without interacting with the sample as discussed in section 1.4. In order to carry out XA measurements in an externally applied magnetic field, the so-called total electron yield (TEY) mode presents a feasible approach. Thereby all electrons which escape from the sample are recorded by measuring the current $I_{sample/substrate}$ between the electric ground potential and the isolated sample, as graphically displayed in Figs. 17 and 18. This proceeding also allows in a simple manner to vary the measurement geometry, i.e. the detection angle α. At more grazing incidence of the X rays, their effective mean free path perpendicular to the suface decreases. As a consequence, the TEY signal increases by a factor of $\sin(\alpha)$ [92]. This is true as long as the signal does not saturate. For the study of molecules on substrates with a coverage in the submonolayer regime and at the most a grazing detection angle of 20° this holds true.

Since the TEY signal of the sample I_{sample} also carries information about the substrate, it has to be normalized to the signal of the corresponding spectrum of the clean substrate $I_{substrate}$. Further all spectra, before and after depositing the molecules, are either normalized to the drain current of a freshly evaporated gold grid $I_{reference}$ upstream to the experiment at the PM-3 and at the UE56/2-PGM1 or to the total electron yield $I_{reference}$ from the last refocussing mirror of the beamline at the UE46-PGM1. It is necessary to take these reference signals $I_{reference}^{sample}$ and $I_{reference}^{substrate}$ into account, as there are time-dependent X-ray intensity variations due to the inconstancy of the X-ray beam and the changing transmission function of the beamline. To take into consideration these two reference signals also ensures that their contri-

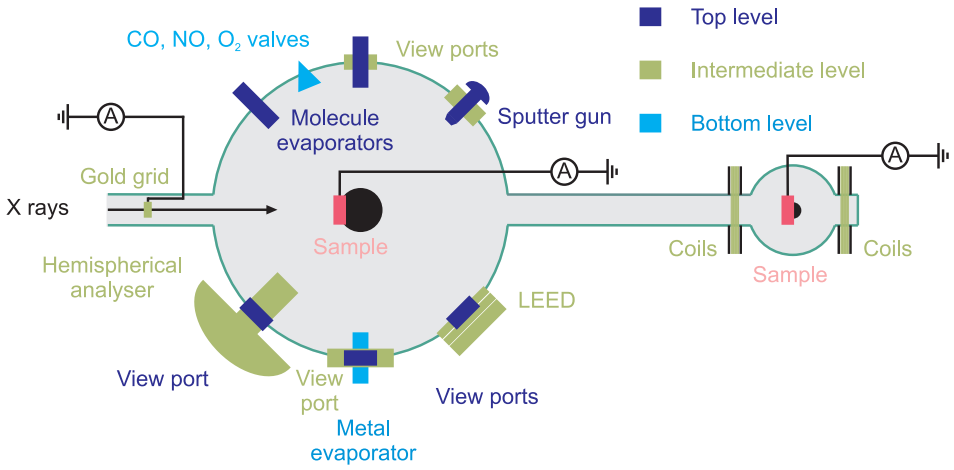

Figure 17: Schematic drawing of the UHV chamber used in this thesis. The most important devices regarding the sampe preparation and characterization are included. There are three main levels of operation. See text for detailed information about the mounted devices.

butions can be separated from the one of the adsorbate. A simple formula describes how to obtain the desired cross section of the adsorbate:

$$I = \frac{I_{sample}/I_{reference}^{sample}}{I_{substrate}/I_{reference}^{substrate}}. \tag{28}$$

All presented XA signals within this work have been obtained by treating the raw data by this procedure. Furthermore the such obtained XA spectra are normalized to one in the pre-edge region. From the spectra displayed in Fig. 9 additionally a subtrahend of one is removed. X-ray provoked damage of the porphyrins has been ruled out from the comparison of spectra recorded immediately after sample preparation and at later times.

2.6 Sample preparation and characterisation

Fig. 17 shows a schematic sketch of the group-own chamber used within the framework of this thesis in order to prepare, characterize, and measure samples. The chamber was installed as end station at the UE56/2-PGM1 and PM-3 beamlines. It has a base pressure of 2×10^{-10} mbar and provides different working levels as displayed. In the upper level home-made molecule evaporatores, which contain a tantalum Knudsen cell and which were already existing at the beginning of the PhD work, are mounted. By means of these evaporators CoOEP and iron-octaethylporphyrin chloride (FeOEP-Cl) molecules were evaporated by sublimating molecular powder at 485 K. They are equipped with a quartz microbalance in order to calibrate the evaporation rate. Further a sputter gun is available, which was used to clean a Cu(001) single crystal with cycles of Ar^+ sputtering at 1.0 keV and annealing to 900 K. On the bottom level different leak valves are mounted for the purpose of injecting CO, NO, or oxygen gas into the chamber. There, also the commercial four-pocket metal

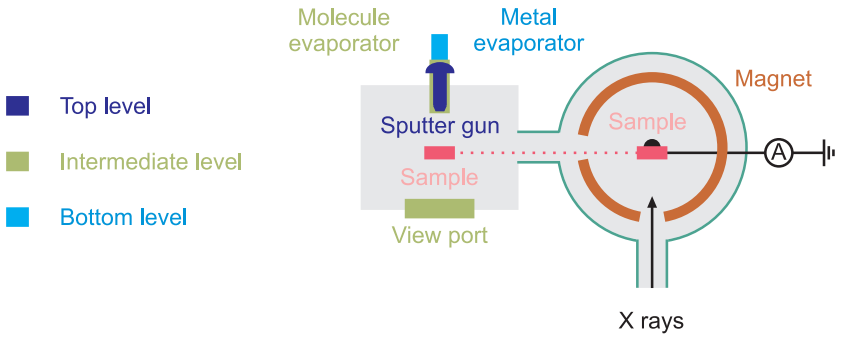

Figure 18: Schematic drawing of the high-field end station at the UE46-PGM1 and the experimental station for the sample preparation. The most important devices regarding the sampe preparation are included. They are mounted on three different levels. See text for detailed information about the installed devices and the measurement conditions.

evaporator EBE-4 of the specs company[1] is installed. It is used to prepare epitaxial Ni and Co films on pre-oxidized Cu(100) single crystals as well as Ni films on clean W(110) and Cu(100) surfaces at room temperature (RT) by electron-beam evaporation. The oxidized Cu(100) substrate was prepared by dosing 1200 Langmuir (1L = 10^{-6} mbar s) of O_2 at a substrate temperature of 500 K after the finishing annealing process, following the recipe described in ref. [93]. The W(110) surface was cleaned in a separate UHV side chamber by flash heating under 6×10^{-10} mbar oxygen to 1600 K for 15 min, followed by five flashes to 2300 K for 10 s each.

On the height of the intermediate level X rays enter the chamber and all experiments are performed. To this end two manipulators are available. On one of them all steps of the sample characterisation and preparation are performed. It is equipped with a cryostate which allows to cool the sample with liquid nitrogen down to around 120 K. On the second manipulator, displayed on the right side of Fig. 17, XMCD measurements can be carried out. Home-made coils produce a magnetic field of up to around 50 mT at the sample and allow to magnetize the sample at the measurement position. A cryostate makes it possible to lower the temperature down to 30 K. Also the entrance slit of the concentric hemispherical analyser Phoibos 100 of the specs company lies on this level. It is used as XPS analyser.

On the intermediate level a low energy electron diffraction (LEED) data acquisition system is further mounted. It was applied in order to check the surface quality of the prepared substrates before depositing molecules. Fig. 19 (a) displays schematically the arrangement in space of the last two metal layers of a clean Cu(100) surface and of a Ni film, grown on a Cu(100) substrate. In both cases a four-fold symmetry is present, as Cu has a face-centered cubic (fcc) crystal structure and Ni films adopt a pseudomorphic growth on Cu(100). In panel (b) the finishing metal layer and the second one from the top of a Ni or Co film grown on an pre-oxidized Cu(100) surface are presented. During the surfactant growth of the film the oxygen flots on top and finally forms a c(2×2) superstructure which corresponds to half a layer of atomic oxygen [93, 94]. Exemplarily the LEED image of a clean Cu(100) surface, recorded with electrons of an energy of 172.8 eV, is shown in Fig. 19 (c). The observed spots

[1] http://www.specs.de

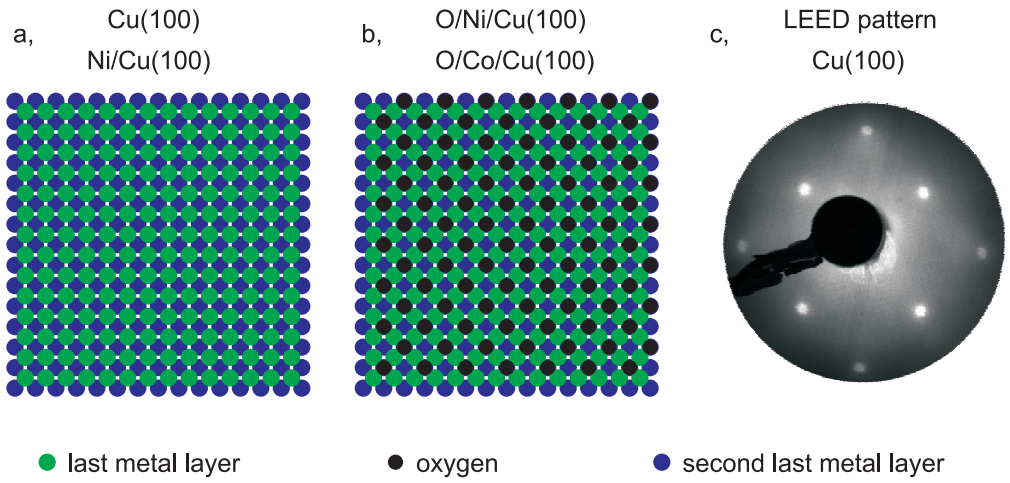

Figure 19: Schematic drawings of the location of atoms within the last two metal layers for a Cu(100)(a), Ni/Cu(100)(a), O/Ni/Cu(100)(b), and a O/Co/Cu(100)(b) surface. In panel (c) a LEED image of a Cu(100) substrate taken with an electron energy of 172.8 eV is shown.

are first-order spots and reflect the four-fold symmetry of this substrate.

The measurements at the UE46-PGM1 beamline were performed at the pre-installed high-field end station shown in Fig. 18. It is connected to an experimental station for the sample preparation. The high-field end station and the preparation chamber have a pressure of 1.0×10^{-10} and of 1.0×10^{-9} mbar, respectively. Magnetic films and molecules were evaporated by means of the same evaporators as in the group-owned chamber, which were mounted here at the bottom and intermediate level of the preparation chamber. Also a sputter gun is installed at the top level. A superconducting coil cooled with liquid helium and installed around the measurement position allows to record XA spectra down to a temperature of T = 4.5 K in an external magnetic field of up to 5.9 T, applied along the X-ray incidence direction.

Also graphene-protected Ni films, grown on a W(110) surface, are used as substrate within this work. Tungsten in bulk has a body-centered cubic (bcc) crystal structure so that a well-ordered Ni(111) surface is formed by evaporating 20 ML of Ni or more on W(110). On top of the Ni film a continuous and ordered graphene overlayer was produced via cracking of propylene gas (C_3H_6) at a partial pressure of 10^{-6} mbar for 10 min at a substrate temperature of 650 K, followed by annealing to 750 K for 10 min. [95]. A self-limiting monolayer growth process takes place and ensures the formation of one layer of graphene [96]. In literature six possible adsorbtion geometries of graphene on Ni/W(110) are discussed [97–101], which are shown in Fig. 20. These are denoted as the top-hcp (a), top-fcc (b), hcp-fcc (c), bridge-top (d), bridge-fcc (e), and bridge-hcp (f) geometry, respectively. Atoms from the two sublattices of graphene, labeled by the numbers 1 and 2 in Fig. 20 of each panel, are differently situated with respect to the different Ni layers. For the top-hcp configuration the C atoms of one sublattice are on top of the finishing-layer Ni and the C atoms of the other sublattice are situated above the second layer Ni atoms. For the top-fcc and the hcp-fcc configurations the atoms of the two sublattices are located above the Ni atoms in the 1^{st} and 3^{rd} or the 2^{nd} and 3^{rd} layers from top of the Ni(111) surface,

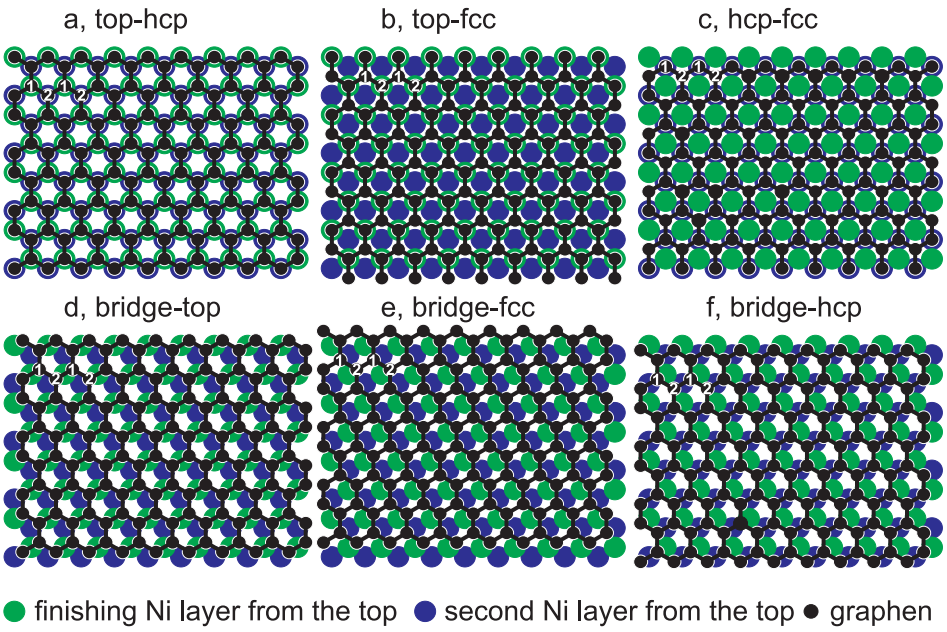

Figure 20: Different adsorption geometries for graphene on Ni(111): top-hcp (a), top-fcc (b), hcp-fcc (c), bridge-top (d), bridge-fcc (e), and bridge-hcp (f) configuration. See text for details.

respectively. In the bridge-top, bridge-fcc, and bridge-hcp adsorption geometry a top, second, and third layer Ni atom is exactly under the bridge build by two neighboring C atoms, respectively.

Figure 21: LEED image at 91.1 eV electron energy of a graphene layer on Ni/W(110).

Fig. 21 displays a LEED image of graphene on Ni/W(110) recorded at an electron energy of 91.1 eV. As expected from the small lattice mismatch of only 1.3% between the Ni atoms and C atoms [95], the latter form a p(1×1) overstructure on the Ni surface and no additional spots besides the ones of the Ni surface are present. The LEED pattern also reflects the hexagonal structure of the surface. From these observations no conclusions can be drawn regarding the absorption geometry of graphene on Ni/W(110). However, it can be stated that DFT calculations favored the bridge-top configuration [98, 102].

The highly ordered pyrolytic graphite (HOPG) substrates which were used in the framework of this thesis are SPI-1 high-grade materials exhibiting a mosaic angle of $(0.4 \pm 0.1)^\circ$ from Structure Probe, Inc. (West Chester, USA). Clean and oriented HOPG surfaces were prepared by cleaving an HOPG substrate at a pressure of 10^{-6} mbar by using a carbon tape.

3 Metalloporphyrin molecules on surfaces

3.1 Introduction

Porphyrins are a class of organic molecules. They are built up by a heterocyclic macrocycle, containing nitrogen and carbon atoms. In figs. 22 (a) and (b) the two different chemical components, which contribute to the macrocycle, are displayed. Four pyrrol subunits (a) are connected by four methine groups (b) and compose together the so called porphine. Its substituted compounds are named porphyrins. The *p*-orbitals within the macrocycle form a conjugated system and thus the corresponding electrons are delocalized. In the periphery of the porphyrin molecule different kind of chemical groups can coordinate to the macrocycle. These functional groups primarily determine the interaction of the porphyrins with each other and with the chemical environment in general. In the center of the porphyrins an available position can be occupied by a metal atom, forming a coordination bond with the four nitrogen atoms of the pyrrol subunits. Thus planar organic metal complexes are formed, where a twice negatively charged ligand of tetradentate nature acts on the metal ions. These chemical compounds are called metalloporphyrins (MP). Thereby the nature of the metal atom in the core position defines in particular the electronic and magnetic properties of the molecule.

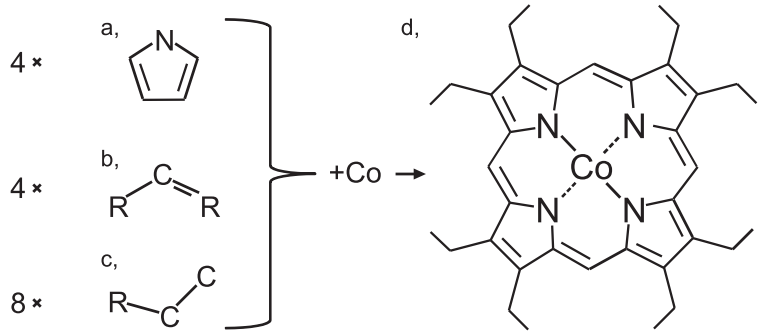

Figure 22: Diagrammatic elevation of the composition of Co octaethylporphyrin. Schematic top view of pyrrole (a), methine group (b), ethyl group (c), and CoOEP molecule (d). Hydrogen atoms are omitted and R stands for a generic unspecified group.

Porphyrin molecules have already accompanied the scientific community for quite a long time. So for the first time a porphyrin and in that case the hematoporphyrin was produced in 1867 by Thudichum [103]. Two other chemical compounds chlorophyll [104] and cobalamin [105], which possess a derivated porphyrin macrocycle, play a key role in biological systems and also have been studied for decades. Chlorophyll, which contains manganese as central metal ion, enables plants to produce energy by adsorbing light. Cobalamin features a cobalt ion at its center, and is important among other things for the cell division and the haematopoiesis in the human body. Further hemoglobin, which acts in the blood of mammals as oxygen carrier, contains heme, an iron-based porphyrin, which has been therefore subject to a large amount of investigations.

At the begining of the 1970s, finally X-ray spectroscopy was first used to explore the

electronic structure of porphyrin bulk samples. XPS studies focused on the impact of the presence of a coordinated metal ion on the electronic structure of the nitrogen atoms [106] and on the influence of different chemical groups, being attached to the macrocycle, on the electronic properties of the center of the molecules [107]. Later on the study of MP molecules by means of XAS started [108]. Investigations of MP molecules in recent years are not just motivated by biological aspects but also by the idea to use them as molecular building blocks for an architecture of solar cells [109]. In this context an easily tunable electronic structure, which porphyrins do provide by an exchange of the end groups or the central metal ions, is desired. Here, XAS presents an ideal tool to study the influence of these changes on the electronic structure of porphyrins [110].

In the framework of this doctoral thesis, FeOEP and CoOEP molecules are studied by XAS and XMCD measurements. The full chemical names of these molecular compounds are Fe(II)-2,3,7,8,12,13,17,18-octaethylporphyrin and Co(II)-2,3,7,8,12,13,17, 18-octaethylporphyrin, respectively. FeOEP is introduced to the readership in section 3.5.3, while CoOEP is schematically shown in Fig. 22 (d). In the periphery of CoOEP eight ethyl groups, displayed in Fig. 22 (c), are coordinated to the macrocycle, and in its center a Co +2 ion is located. The unsaturated coordination sites of this MP molecule permits an interaction of additional axial ligands with its metal ion. This general feature of many porphyrins, which also leads to their biological importance, will serve in this work to influence and specifically control the electronic and magnetic properties of CoOEP and FeOEP molecules. For this purpose the two available axial coordination sites will be occupied not only by different surfaces but also by the small molecules NO and CO. This bio-inspired use of MP molecules in different circumstances and with new objectives will be motivated at the beginning of the respective sections.

3.2 XAS measurements of Co porphyrin bulk-samples

Before discussing within the next sections the interaction of porphyrins with surfaces, in the following XA spectra at the Co $L_{2,3}$, the N K, and the C K edges of CoOEP bulk material are displayed. They are discussed in the context of the electronic properties of the molecule, while the angular dependence of the absorption can be ignored due to the polycrystalline nature of the sample. The XA spectra at the N K and C K edges are compared to corresponding theoretical XA spectra of a free CoOEP molecule, published in our recent work [111]. The experimental spectra will serve as reference for the ones of CoOEP molecules adsorbed in the submonolayer regime on different solid surfaces in the subsequent sections, in order to analyse the porphyrin-substrate intercation.[2]

For an investigation of the electronic structure of the active center of the Co porphyrins, Fig. 23 shows Co $L_{2,3}$ XA spectra of CoOEP bulk material. The physical process behind such a spectrum is the excitation of $2p$ core electrons into empty $3d$ orbitals. Thereby the L_3 and the L_2 edges correspond to the creation of a hole in the Co $2p_{3/2}$ or $2p_{1/2}$ levels, respectively. The line shape of the Co L_3 XA spectrum reveals a detailed fine structure. Many different transitions contribute to the spectrum, while their respective photon energy depends, amongst other things, on the energetic separation between the available states within the $3d$ shell. Various physical interactions influence the amount of available states and their separation in energy like the multiplet splitting, caused by the coulomb and exchange interaction between the probed $3d$ states and revealing a characteristic energy of $0-2$ eV, the spin$-$orbit splitting, provoked by the spin$-$orbit coupling and being here around 66 meV [53], and the crystal field splitting, induced by the electrostatic potential of nearest-neighbor atoms. The latter can amount up to around 0.1 eV for the first-row transition metals in bulk, but for systems with lower symmetry, as it is here the case, also values of $1-2$ eV are possible [53]. The Co L_3 edge shows three features: one maximum at 779.2 eV and two local maxima at 777.5 and 780.4 eV. Almost identical results for CoOEP and CoPc bulk samples can be found in literature [110], which underlines the similar chemical environment of the Co ions, within CoPc with its very similar equitorial ligand compared to CoOEP. Theoretical Co $L_{2,3}$ XA spectra of CoPc [53, 112], obtained from atomic multiplet calculations including a ligand field, show that the fine structure at the Co L_3 edge with its triple-peak structure is a fingerprint for a +2 valency and a low-spin d^7 configuration of the Co ions. Thereby the four different d orbitals created by crystal field splitting (introduced in section 1.7), carry two holes in the b_{1g} ($d_{x^2-y^2}$) state, while the e_g ($d_{yz,xz}$) and a_{1g} (d_{z^2}) states carry together one hole. Density functional theory (DFT) calculations for a CoOEP molecule in gas phase additionally revealed that the three holes within the $3d$ shell lead to a fully unoccupied b_{1g} ($d_{x^2-y^2}$) and half filled a_{1g} (d_{z^2}) state, yielding a nonzero magnetic moment [113].

The Co bonding partners are the four N atoms of the porphyrin macrocycle. For the purpose of studying their electronic sructure, Fig. 24 shows the XA spectrum of the N K egde of CoOEP bulk material. By means of a comparison to a theoretical N K edge XA spectrum of an isolated CoOEP molecule, obtained from StoBe cluster calculations [114], an assignment of the different resonances to excitations is possible

[2]The written elaboration of this chapter is partly based on a recently published manuscript [111].

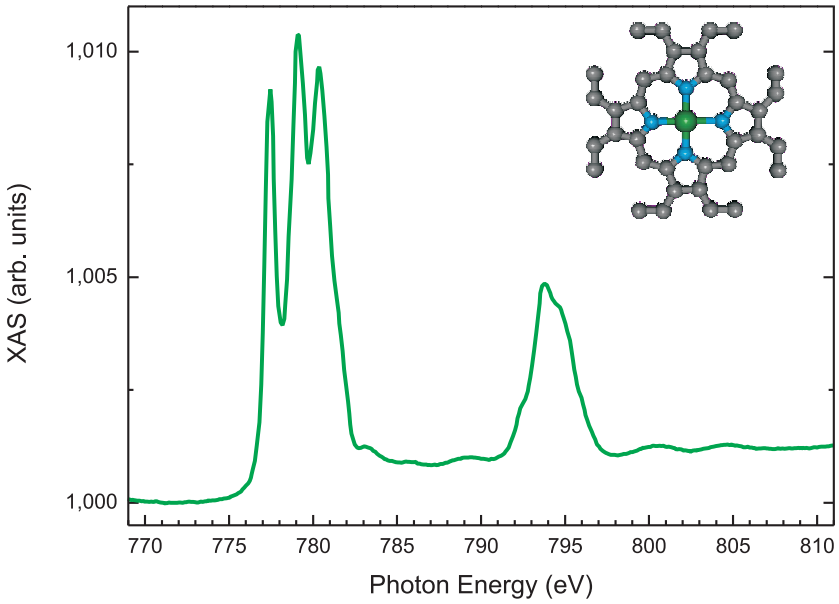

Figure 23: XA spectrum at the Co $L_{2,3}$ edges of a CoOEP bulk sample. Inset: Schematic top view of the CoOEP molecule, where green, blue, and grey balls represent cobalt, nitrogen, and carbon atoms, respectively, and hydrogen atoms are omitted.

[111]. The experimental spectrum is taken at RT and with lineraly polarized light under normal incidence. It represents excitations from the N 1s level of the nitrogen atoms which are part of the macrocycle and thus equivalent due to symmetry. The probed final states within the excitation are antibonding molecular orbitals either of σ^* or π^* character with respect to the porphyrin plane.

The spectrum exhibits two sharp resonances in the region of lower photon energies with maxima at 399.2 and 402.2 eV, while the latter reveals a shoulder at the energetically lower lying flank. The final-state orbitals which are involved in the process of creating the resulting double-peak structure are mainly three different ones. Two of them are π^* type orbitals, which result from a hybridisation of N and C 2p states and do not show any contribution of Co states. The other one originates from Co 3d and N 2p states, while only a small fraction is added from the molecular periphery. This yields an altogether σ^*- type orbital which belongs to the energetically lower excitation peak with a maximum at 399.2 eV. This spectral feature is further related to an excitation into one of the two π^*- type orbitals, being just 0.25 eV separated in energy from the σ^*- type orbital. The energetically higher lying sharp resonance with a maximum at 402.2 eV is predominantly caused by an excitation into the other one of the two π^* type orbitals. At higher energies a pure σ^* region builds up the spectrum with a broad resonance having a local maximum at 416.4 eV and a main maxima at 406.9 eV with a shoulder at the energetically higher lying flank. These resonances originate from excitations of electrons into antibonding σ^* orbitals of the porphyrin macrocycle. By a comparison to literature, a good agreement between the here presented N K XA spectrum and experimental ones of other MP molecules, which do not contain more nitrogen atoms within their endgroups in the periphery, is found, independently of the nature of the central metal ion [35, 108, 110]. For the

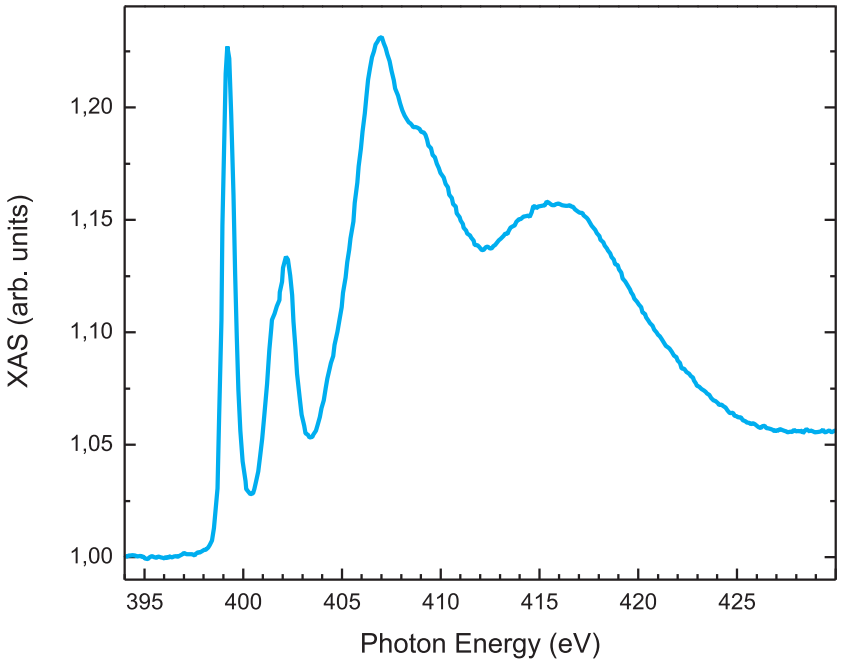

Figure 24: XA spectrum at the N K edge obtained from a bulk sample of CoOEP.

sake of completeness, it has to be mentioned that the spectrum shown here resembles to a certain extent another available theoretical N K XA spectrum of a Zn porphyrin molecule obtained by static-exchange calculations [115].

In order to complement the study of the electronic structure of the porphyrin macrocycyle and to investigate further the electronic properties of the periphery of the molecules, Fig. 25 displays XA measurements of the C K egde of CoOEP bulk material. The spectrum is measured at RT and with linearly polarized light under normal incidence, too. Also in this case, comparing the experimental result to a theroretical XA spectrum of the C K edge of CoOEP bulk material allows its deeper analysis [111]. In particular, an assignment of the different resonances detected to excitations from C 1s levels of specific carbon atoms is possible.

The spectrum possesses four sharp resonances at photon energies of 284.2, 285.0, 285.7, and 287.8 eV, while the latter one presents the main maximum and the other three form a triple peak structure at lower energies. All of them stem exclusively from excitations into π^*- type orbitals originating from carbon atoms of the inner part of the CoOEP molecule, the macrocycle. Only excitations at the carbon atoms closest to the nitrogen atoms cause the central peak of the triple structure and to a big extent the main maximum of the spectrum. Almost all the other contributions to the carbon spectrum in the energy region of the four π^* peaks originate from excitations at the other carbon atoms inside the macrocycle. Spectral features above a photon energy of 289 eV belong only to final state orbitals of σ^* character, and all carbon atoms contribute to the spectrum. While C K XA spectra of metalloporphyrins have already been discussed in literature, for MP molecules adsorbed on a substrate [34] and of a bulk sample [88], here to the best knowledge for the first time a detailed physical interpretation of the line shape is provided with the help of computations [111].

Summarising the above, it can be said that the experimentally obtained XA spectra

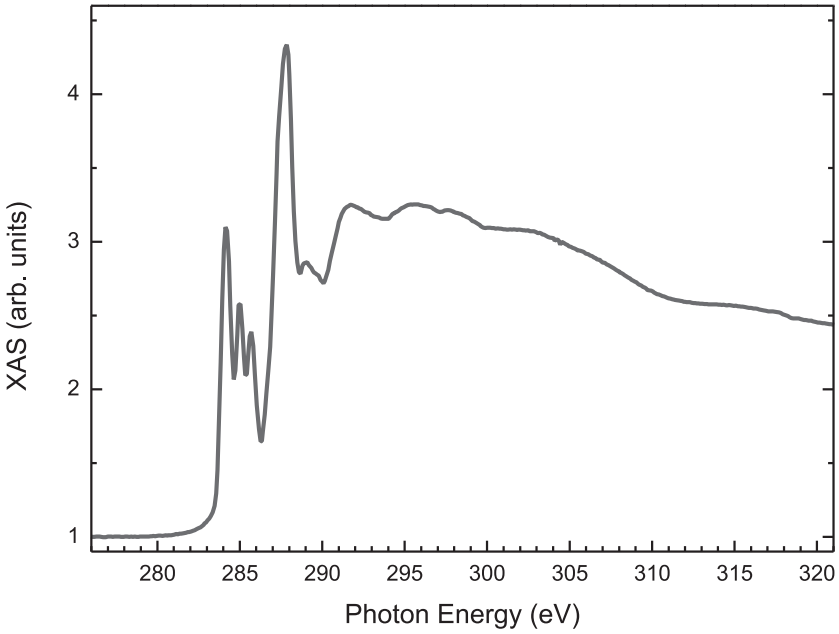

Figure 25: XA spectrum at the C K edge of CoOEP bulk material.

at the Co $L_{2,3}$, the N K, and the C K edges of CoOEP bulk material are consistent with earlier investigations of the same or similar physical systems. The final state orbital character and the excitation center that belong to the different spectral features of the N as well as the C K XA spectra, can be assigned with the help of respective theoretical XA spectra, which were computated by the collaborating group of Prof. Hermann.

3.3 Interactions between Co porphyrins and surfaces and their influence on electronic and magnetic properties

Passing from CoOEP bulk material to Co porphyrin molecules adsorbed in the submonolayer regime on a crystalline surface, electronic and magnetic properties of the molecules, which arrange in a two-dimensional fashion, may change significantly. Further by placing them on top of a solid substrate, the molecules get immobile at least against motions in the third dimension, as desired for their use as building blocks for a molecular architecture. For planar π conjugated organic compounds, as MP or chemically similar MPc molecules, the substrate–molecule interactions prevail over the intermolecular ones within the first layer of molecules on clean metal surfaces [116]. Accordingly, MP and MPc molecules adsorb flat on these substrates, as substantiated by STM studies [117], while one of their axial coordination sites remains free as active center for chemical reactions. The potential catalytic activity of such systems has been subject to many studies and it has only recently been shown that manganese porphyrins at a liquid–solid interface catalyse O_2 molecules before incorporating them into an alkene substrate [118]. In particular, CoTPP molecules on TiO, for instance, catalyse the reduction of NO with H or CO molecules, whereas unsupported CoTPP or TiO on its own remains inert [119]. This raises the interest in the molecule–substrate interaction enabling such a behaviour. In addition, the first layer of MP molecules on a surface may be used as a template for the further growth of a thin film, which is desired for the architecture of organic electronic devices. The ability to create tailor-made films depends on the kind of formation of the first molecular layer, which among other things influences the physical properties of such films.

Hence a better understanding of the molecule–substrate and the molecule–molecule interaction within the first layer is mandatory. The latter is normally attractive. However, it has also been found to be repulsive for tin Pc molecules on Ag(111) [120]. In that context substrate-induced modifications of molecular electronic properties are of interest, too. Bonds between the adsorbate and the substrate may have van der Waals nature, leaving the adsorbate properties unchanged. This state is designated as phy-sisorption. Alternatively, the surface may modify the ligand field of the metal ions and hence induce a redistribution of charge in the $3d$ orbitals by a covalent bond formation. Further a charge transfer from and to the active centre or macrocycle may occur. Thus the oxidation and/or the spin state can be changed. Such a stronger adsorbate–substrate interaction is labeled as chemisorption, while also a geometrical deformation of the porphyrin macrocycle may arise.

Exemplary for some physical incidences, some results for different systems can be mentioned. Representatively, FePc on HOPG stands for a system with a weak molecular surface interaction. HOPG represents a rather inert substrate. Thus, the interplay between molecules of the first layer and the surface is characterised by van der Waals forces as it is also the case between layers inside a thin film of FePc on HOPG. By making use of the angular dependence of NEXAFS spectra, which provides an excellent tool for the study of the molecular orientation [47], the porphyrin planes are found to be parallel oriented to the surface for both monolayers and thin multilayers [121, 122]. On the other hand, the axial ligation of CoPc with Ag(111) induces a charge transfer from the surface to the molecule which quenches the spin moment [112] and for MnPc on Bi(110) the spin state is reduced from S=3/2 to S=1 [123].

For CoTPP adsorbed on Ag(111), for instance, the geometry of the molecules changes and the molecular macrocycle exhibits a pronounced saddle-shaped form [124], while for NiPc and CuPc on Ag(100) one electron is added to the π orbitals of the macrocycle [19]. Both, nickel-phthalocyanine and CuPc, do not have empty d-orbitals on the central ion whose probability distribution lies outside the phtalocyanine plane and so no charge transfer from the substrate to the Ni or Cu ions occurs.

Angle-dependent XMCD measurements with their high surface sensitivity present an ideal tool to study the magnetic and spin dipole moments of the central metal site in such systems. As SOC is relatively weak compared to the ligand field effects for MP and MPc molecules containing first-row transition metals, the atomic spin density nearly represents the related atomic charge density [46, 52]. In the case of a system with S=1/2, it can be therefore distinguished whether the unpaired electron is localized inside or outside the molecular plane. So for CuPc on Ag(100), an XMCD study revealed that the spin state S=1/2 survives upon adsorption and that the spatial distribution of the spin density and hence of the unpaired hole within the $3d$ shell lies parallel to the surface [125].

The interaction of MP and MPc molecules with a bare ferromagnetic substrate also presents an appealing subject, in particular regarding the architecture of a molecular spin electronics, as outlined in the introduction. XMCD studies revealed that for MnTPPCl on Co films as well as for FeOEP on Co and Ni films, the central metal ions are ferromagnetically coupled to the substrate magnetization [33, 34]. This was possible to find out, as the element-selective probe of the magnetization by means of XMCD in the absorption of soft X-rays allows to study the adsorbate and substrate magnetism independently. Respective DFT+U calculations for manganese and iron porphine molecules on Co films showed that an indirect magnetic coupling is responsible for the observed results. A 90°-ferromagnetic superexchange interaction, mediated via N atoms of the macrocycle, between the magnetization of the films and the central metal spins stabilizes the latter against their thermal fluctuations [34, 126]. Additionally, temperature-dependent XMCD investigations revealed that the coupling strength is weaker for FeOEP adsorbed on a Ni surface compared to an adsorption on a Co substrate [127]. Also for CoPc in contact with a thin iron film it is known that a substrate-induced order of the Co spins occurs [128], while the molecule–substrate interaction significantly changes the Co electronic structure. Finally, DFT+U calculations of manganese porphine molecules on a thin Co film, which are aimed to represent a prototypical case of metalloporphyrins magnetically coupled to the magnetization of a substrate, addressed the question to the adsorption strengths of the molecules on bare ferromagnetic surfaces [129]. Two minima of the total energy versus the molecule–surface layer distance exist. One of them corresponds to a chemisorption and the other to a physisorption of the porphines, which shows the possibility of an adsorption in two distinct configurations.

The MP molecule of choice for the investigations presented here is the CoOEP. For this porphyrin in contact with surfaces it is known that a partial reduction of the Co ions takes place in the case of its adsorption on Ag(110) [113] and Ag(111) [130], whereas just a small modification of the Co electronic structure occurs for its adsorption on an oxygen-covered Cu(100) surface [88]. Here CoOEP molecules in direct contact with a HOPG and a Cu(100) surface as well as with a Ni film, grown on Cu(100), are investigated. The molecular macrocycle possesses a near-in-

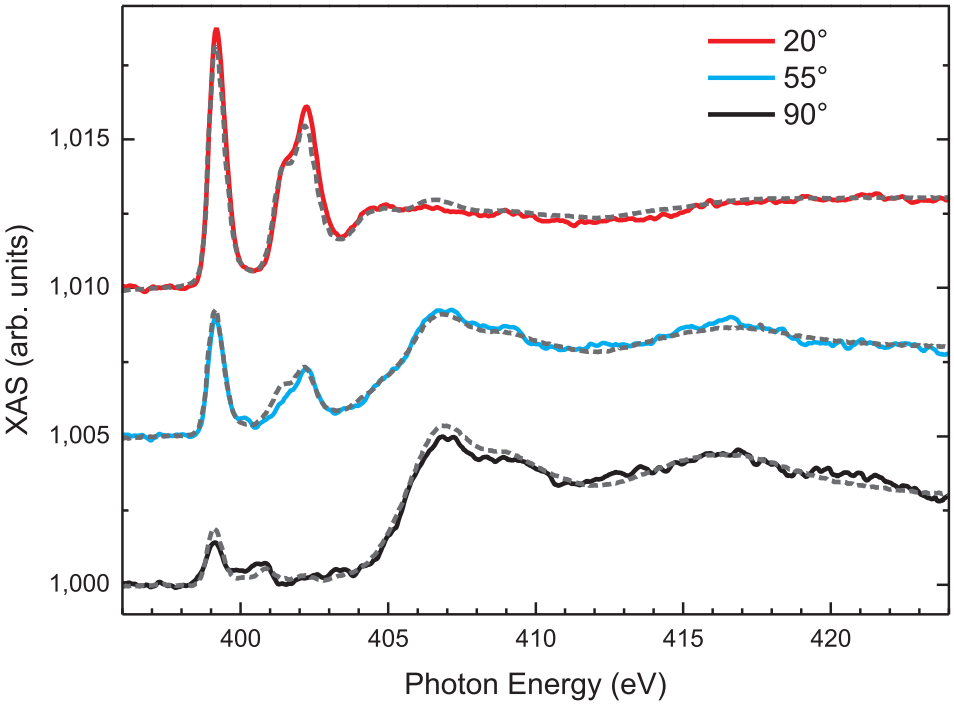

Figure 26: N K XA spectra of 0.2 (solid lines) and approximately 3 (grey dashed lines) ML of CoOEP adsorbed on HOPG, measured at 300 K. Spectra taken with linearly polarized light and an angle of 20° (red line), 55° (blue line), and 90° (black line) between the surface and the wavevector of the X rays are presented. The spectra of the multilayer are scaled to the ones of the submonolayer for each measurement geometry for comparison. Additionally, the spectra are vertically offset for different detection angles.

plane orientation for all systems under study. For Co porphyrins in direct contact with HOPG, mainly van der Waals forces interact between the molecules and the substrate, which leaves the molecular properties unchanged upon adsorption. The adsorption of the molecules on Cu(100), in contrast, induces a modification of the N and Co electronic properties. Thereby the spin state $S = 1/2$ survives, but the unpaired electron is now located inside and not outside of the molecular plane, as it is the case for bulk CoOEP. On Ni/Cu(100) the Co spins of the porphyrins, which are paramagnetic before adsorption, are stabilized against their thermal fluctuations, which leads to a detected Co magnetization even at RT.

3.3.1 Conservation of molecular properties upon absorption

This section deals with the electronic properties of CoOEP molecules, adsorbed in the submonolayer and multilayer regime on bare HOPG single crystales. An angle-dependent study of N K and Co $L_{2,3}$ XA spectra provides an insight into the adsorption geometry of the molecules with respect to the substrate. The type of interaction between the molecules and the substrate is discussed by comparing absorption signals for different coverages.

Figure 26 and 27 display XA spectra of the N K and the Co $L_{2,3}$ edges of 0.2 and around 3 ML of CoOEP adsorbed on HOPG (different coloured and grey dashed lines,

respectively). The spectra are measured at 90° normal and at 55° and 20° grazing incidence with p-linearly polarized light at room temperature. The spectra of the multilayer are scaled to the ones of the submonolayer for each detection angle for comparison, while spectra taken at a different measurement geometry are vertically offset. For the XA signal of the two elements for both the submonolayer and multilayer of CoOEP, significant differences are detected for the three detection angles.

XA spectra of the N K as well as of the Co $L_{2,3}$ edges of the CoOEP multilayer, recorded at 55° grazing incidence, closely resemble the ones of the CoOEP bulk sample, which are shown in the previous section 3.2. This is related to the fact that they are recorded under the so-called magic angle, for which the orientation of the molecular orbitals is canceled out and the isotropic spectrum is obtained. The N K spectrum reveals two sharp resonances at 399.2 eV and 402.2 eV, while the latter exhibits a shoulder at the low-energy flank. At higher photon energies only broad resonances contribute to the spectrum. Contrasting the isotropic XA spectra at the N K and the Co $L_{2,3}$ edges of the submonolayer and the multilayer of CoOEP, their similarity is obvious. Just a small deviation between them at the N K edge around an energy of 401.3 eV is detected, however being in its dimension close to the noise level of the spectrum of the submonolayer. The Co $L_{2,3}$ XA spectra, exhibiting at the L_3 edge a triple-peak structure with maxima at 777.5, 779.2, and 780.4 eV, even resemble each other completely. On this account it is concluded that, on the one hand, the $3d$ orbitals of the Co ions do not hybridize with electronic states of the substrate and, on the other hand, that the equatorial ligand of the Co ions, the porphyrin macrocycle, is not significantly modified upon adsorption. Further it is a finger print for the presence of intact molecules on the substrate. From the high sensitivity of the fine structure at the N K and the Co $L_{2,3}$ edges on the chemical environment paired with their almost unchanged signal upon adsorption follows that the Co porphyrins physisorb on the substrate. A partial formation of a second layer of CoOEP can not be excluded for a coverage of 0.2 ML. Nevertheless, molecules in direct contact with the HOPG surface are also present in this case.

The detection of N K spectra with linearly polarized light under different incident angles, corresponding to a different orientation between the $\vec{E}$ vector and the surface, allows to test for a preferential spatial orientation of the probed molecular orbitals. The strength of the dipole transition matrix element of the excitation is maximum for an $\vec{E}$ vector parallel to the axis of the probed orbital. At normal incidence the $\vec{E}$ vector is parallel to the surface, hence in-plane lying orbitals are probed, while at 20° grazing incidence a bigger component of the $\vec{E}$ vector is vertical to the surface and consequently more out-of-plane oriented orbitals are tested. The presence of an angular dependence, which is designated as X-ray natural linear dichroism, reveals a spatial order of probed orbitals. This is the case for CoOEP on top of HOPG. As the spatial distribution of molecular orbitals is correlated with the geometrical arrangement of a molecule, information about the adsorption geometry can be obtained from such measurements.

The N K XA spectrum for 0.2 ML CoOEP on HOPG resembles almost the one of CoOEP bulk material, for which the final state character of spectral features was discussed in section 3.2. The sharp peak at 399.2 eV belongs to two excitations, where one probed orbital has σ^* character and the other one π^* character. The spectral feature with a maximum at 402.2 eV and a shoulder at lower photon energies belongs

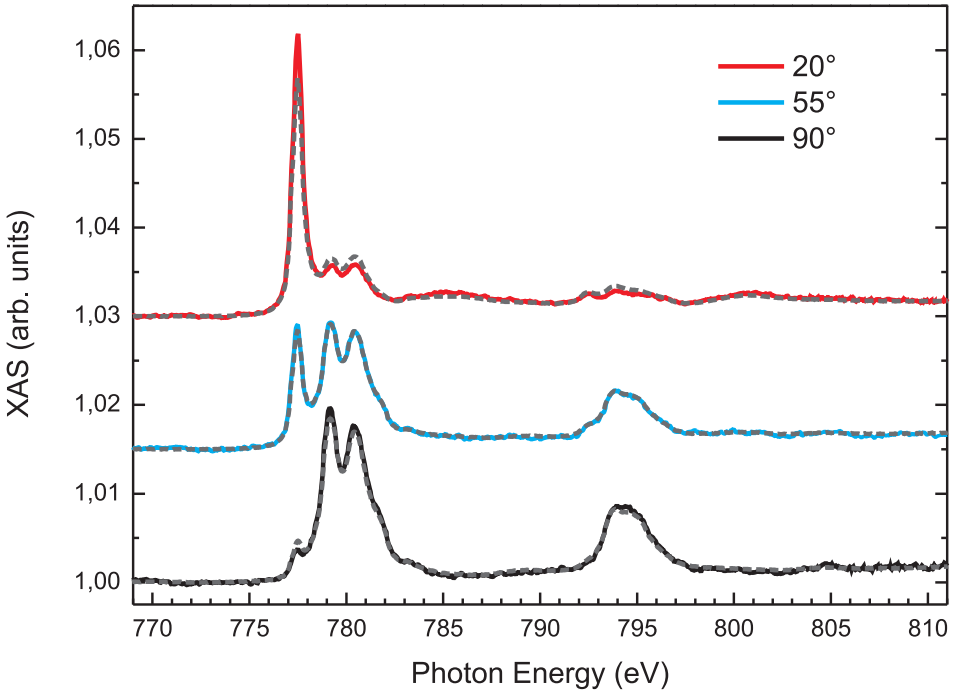

Figure 27: Co $L_{2,3}$ XA spectra of 0.2 (solid lines) and around 3 (grey dashed lines) ML of CoOEP adsorbed on HOPG, recorded at 300 K. Spectra taken with p-linearly polarized light and an angle of 20° (red line), 55° (blue line), and 90° (black line) between the surface and the wavevector of the X rays are shown. The spectra of the multilayer are scaled to the ones of the submonolayer for each detection angle for comparison. The spectra are vertically offset for different measurement geometries.

to an excitation into an orbital with π symmetry and at higher energies a pure σ^* region builds up the spectrum. For excitations into final state orbitals with σ^* and π^* symmetry an opposite angle dependence is expected in the case of ordered molecules on the substrate. At 20° grazing and at 90° normal incidence the features belonging to π^* and σ^* regions of the N K XA spectra, respectively, are much more pronounced, for both the submonolayer and multilayer. This fits to a rather perpendicular and parallel orientation of the π and σ orbitals to the surface, respectively, and hence to a near-flat adsorption of the molecules.

There is a non-equal shape of the spectral features in the photon energy region below 401.5 eV for 20° grazing and normal incidence. This is in agreement with a contribution to the spectra of excitations into orbitals with σ^* and π^* character in this energy region, as the mentioned calculations suggest. The slightly different line shape of the N K XA spectra recorded at normal incidence for the two chosen coverages points towards a weak contribution of electronic states originating from N orbitals to the electronic interaction between the molecules and the substrate. In comparison to substrate-induced modifications for other MP molecules adsorbed on ferromagnetic substrates, the detected changes here at the N K XA edge are almost negligible [34].

Applying the formular 11 deduced in section 1.4.2 to the absorption intensities recorded at an energy of 402.2 eV, an average tilt angle of (14 ± 8)° for the sub-

monolayer and of (18 ± 8)° for the multilayer between the surface normal and the molecular π^* orbitals is calculated. The noise level of the spectra determines the error in the obtained values. This non-zero result in the case of the submonolayer might be either interpreted as an average tilt angle of 14° between the surface normal and planar porphyrin macrocycles or as a distortion of the macrocycle due to the interaction with the substrate, which has been reported for Co-tetraphenylporphyrins on Ag(111) [124]. Also the presence of more than one CoOEP species which are in direct contact with the surface may explain this result. In such a scenario one part of the molecules, being for instance located closely at step edges, may interact with the substrate to such an extent that N π orbitals hybridize with electronic states of the surface [34]. For CoOEP in direct contact with a Ag(110) surface, for comparison, each molecular macrocycle is tilted with respect to the metal surface by about 15° [113].

An almost identical line shape of the N K XA spectra for a coverage in the submonolayer and multilayer regime at 20° grazing incidence strongly supports the picture of physisorbed molecules in direct contact with the surface. The slightly less pronounced angular dependence for the multilayer reveals a lower degree of molecular order within the approximatly 3 ML thick CoOEP film compared to the submonolayer.

The strength of excitations of electrons from $2p$ levels into unoccupied $3d$ states at the Co site also depends on the orientation of the $\vec{E}$ vector of the X rays regarding the spatial orientation of the probed $3d$ states. The fine structure at the L_3 absorption edge results from multiplet splitting of the individual multi-electron $3d$ orbitals and is related to core-hole interactions, too. Such different peaks represent different many body multiplet states. In order to interpret conveniently and illustratively the differences of the fine structure at the L_3 absorption edges, which occur at changing measurement geometries, the angular dependence for an excitation into individual $3d$ one-electron orbitals is helpful [46, 52]. Such an approach presents on the one hand a simplification of the absorption process, but on the other hand allows an assignement of the empty orbitals accessed by the excitations in a qualitative manner, without going beyond the scope of this work. Being aware that spectral features never belong to an excitation into a particular d-state hole, this comparison nicely shows that there are in-plane and out-of-plane orbitals, which can be viewed by varying the detection angle.

Figure 28 displays the calculated relative XA resonance intensity for the excitation into the individual $3d$ one-electron orbitals as a function of incidence angle, according to eq. 10. Thereby a tetragonal symmetry of the ligand field which constrains the Co ions is assumed. Further a flat adsorption of the porphyrin molecules on the surface is implied, which leads to a quantization axis z that is parallel to the surface normal. The equivalent x and y axes define the surface plane. The $3d$ orbitals transform as $d_{x^2-y^2}$, d_{xy}, d_{xz}, d_{yz}, and d_{z^2}, as dicussed in section 1.7. The spatial anisotropy of the charge density among the orbitals causes the angular dependence of the XA intensity. The two in-plane orbitals $d_{x^2-y^2}$ and d_{xy} show the same evolution of the intensity, exhibiting a maximum for measurements at 90° normal incidence. The transition intensity is lower at gradually more grazing detection angles, as the $\vec{E}$ vector possesses thereby less and less an in-plane-projected component. The three out-of-plane orbitals d_{xz}, d_{yz}, and d_{z^2} exhibit accordingly an opposite behavior for the XAS intensity as a function of angle. For the latter orbital this effect is more pronounced than for the two others, as its charge density is mainly located along the z axis. At an incidence angle

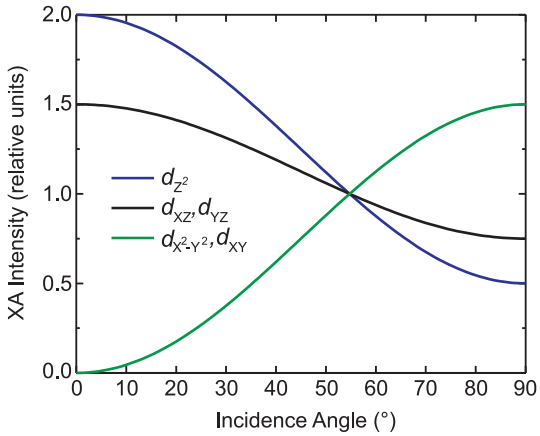

Figure 28: Angle-dependent XA intensities for excitations with linearly polarized X rays of electrons from $2p$ into individual $3d$ orbitals. The quantization axis z of the orbitals coincidences with the surface normal.

of 54.7° the XA intensity for all orbitals is the same, and the angular dependence cancels out. A measurement at this angle, earlier defined as the magic angle, yields the isotropic spectrum. Within the technical metering precision XA measurements at 55°, as performed in the framework of this thesis, agree with that.

For isolated CoOEP, as mentioned in section 3.2, the $d_{x^2-y^2}$ orbital is the highest in energy and carries two holes. Another hole is located either inside the d_{z^2} orbital or carried by all the out-of-plane orbitals together. Now the earlier-mentioned fine structure at the Co L_3 XA edge, shown in Fig. 27, can be discussed in the context of the Co electronic structure. The narrow peak at 777.5 eV is more apparent at 20° grazing incidence, where excitations into out-of-plane orbitals dominate, as shown in Fig. 28. Conversely, the energetically higher-lying peaks are more pronounced at normal incidence. At this measurement geometry excitations into in-plane orbitals, like the $d_{x^2-y^2}$, contribute more to the spectrum as out-of-plane ones, like the d_{z^2}. Consequently the orbital occupation of the Co atom theoretically found is consistent with the angular dependence and the energetic position between the components building up the L_3 edge. The degree of angular dependence is slightly lower for the multilayer than for the submonolayer. This is in line with the results found at the N K edge and supports the picture of less molecular order within the thin film than for porphyrins in direct contact with the substrate.

In conclusion, CoOEP adsorbs almost flat in the submonolayer regime on HOPG and a 3 ML thick film of porphyrins only reveals slightly less molecular order. The $3d$ states of the Co ions do not contribute to the molecule–substrate interaction; electronic states originating from the N atoms only to a very limited extent. The Co electronic structure does not change upon adsorption. Moreover, the interaction between the porphyrins and the HOPG surfaces is weak, and the molecules physisorb on the substrate. It shows the possibility to place porphyrin molecules on top of a surface without changing their physical properties. This is interesting regarding the design of prospective porphyrin-based molecular devices with well-defined characteristics, independently of adsorbate–substrate interactions.

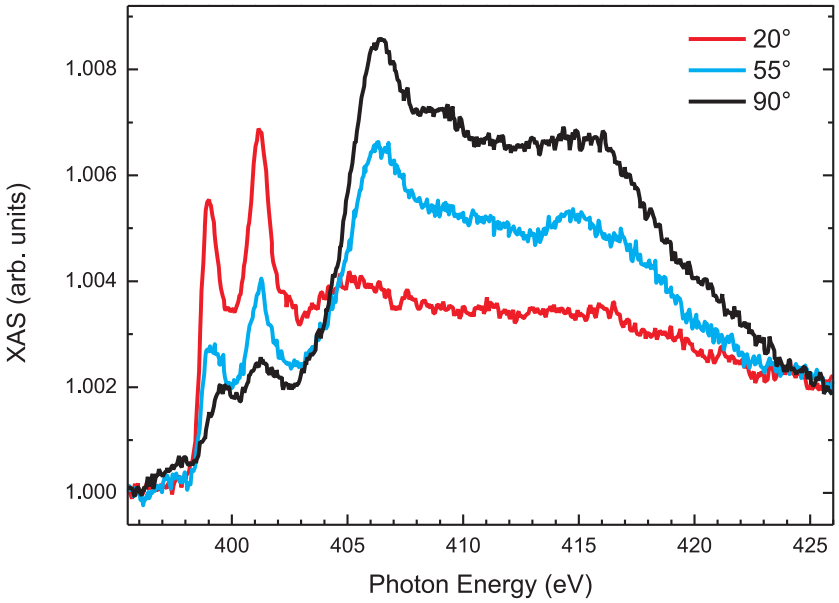

Figure 29: N K XA spectra of 0.4 ML CoOEP adsorbed on Cu(100). The measurements were performed at RT and with p-linearly polarized light and an angle of 20° (red line), 55° (blue line), and 90° (black line) between the surface and the wavevector of the X rays.

3.3.2 Spatial spin density distribution of a hybrid molecule/metal system

This section deals with the electronic and magnetic properties of CoOEP in direct contact with bare Cu(100) single crystal surfaces. The adsorption geometry of the molecules and the modification of the Co electronic structure upon adsorption are analysed by means of angle-dependent XA measurements at the N K and the Co $L_{3,2}$ edges. Additionally, temperature-, angle-, and field-dependent XMCD measurements at the Co $L_{2,3}$ edges provide insight into the spin state of the Co ions and the spatial distribution of the spin density at their site.

Figure 29 shows N K XA spectra of 0.4 ML CoOEP adsorbed on a bare Cu(100) surface taken at RT. The spectra are recorded at 90° normal (black line) and at 20° (red line) and 55° (blue line) grazing incidence. They reveal a pronounced angular dependence with a double peak structure, possessing two maxima at lower photon energies of 399.0 and 401.2 eV, and broad resonances above 404 eV. The line shape of the isotropic spectrum, measured at 55° grazing incidence, at which the angular dependence of the molecular orbitals cancels out, features clear differences compared to the spectrum of CoOEP bulk material (see Fig. 24) and to the one of CoOEP adsorbed on HOPG (see Fig. 26). The most prominent is the stronger appearance of the peak at higher photon energies for CoOEP on Cu(100) compared to the other systems. This reveals a substrate-induced modification of the probed final state orbitals within the absorption process. Accordingly, it is very likely that electronic states which originate from the N $2p$ states contribute to a relatively strong electronic interaction between the molecules and the surface.

In order to enlighten the modification of the N K spectrum upon adsorption, some results from literature are helpful. So it is known for octaethylporphyrin molecules in

bulk that the exchange of the coordinated transition metal does not influence the N K XA spectrum significantly [88, 110]. On the other hand, N K XA spectra of different kind of metallotetraphenylporphyrin (MTPP) molecules in thin films [131, 132] reveal similarities to the isotropic spectrum for CoOEP on Cu(100) shown here. In the low photon energy range also two sharp peaks characterize the spectra. Moreover, the energetically higher-lying feature is more pronounced, just as for CoOEP on Cu(100). MTPP molecules are known to possess a slight saddle-shape conformation of the macrocycle, which is therefore not planar [133]. These comparisons may indicate that CoOEP on Cu(100) also exhibits a saddle-shape conformation.

For a similar system as the one studied here, FeOEP molecules adsorbed on Cu(100), it is known from STM studies that the porphyrins lie in a flat manner on the substrate [88]. Accordingly, it is reasonable to assume that this is also the case for CoOEP on Cu(100). Here, for measurements at the N K XA edge recorded at 20° grazing incidence, spectral features below 404 eV are more pronounced. On the contrary, above 404 eV spectral contributions are more distinctive at normal incidence. This angular dependence is similar as for CoOEP adsorbed on HOPG (see Fig. 27). However, at lower photon energies it is comparatively less pronounced. Hence, the final state orbitals probed at low photon energies have rather π^* character and the ones at higher photon energies σ^* character, as it is the case for CoOEP on HOPG.

Referring again to the comparison between the system studied here and MTPP molecules, CuTPP molecules adsorbed on Cu(111) and FeTPP molecules on Ag(111) show a similar angular dependence for measurements at the N K edge as the one detected here [132, 133]. The remaining spectral intensity observed for CoOEP on Cu(100) at normal incidence would therefore be consistent with a slightly buckled shape of the porphyrin macrocycles as already suggested. Additionally, it is most likely the case that in the low photon energy range also an excitation into an orbital with σ symmetry contributes to the spectrum, just as for CoOEP bulk material. Under the assumption of a flat adsorption of CoOEP, such a contribution should be more prominent at normal incidence. Alternatively, new formed orbitals may be probed in the absorption process, which leads to the detected spectral intensity for measurements at normal incidence.

The impact of the mentioned interaction between the molecules and the substrate on the electronic properties of the Co ions is dicussed in the following by means of angle-dependent XA spectra of the Co $L_{2,3}$ edges of 0.4 ML CoOEP on Cu(100). The spectra are shown in Fig. 30 and belong to the same sample preparation as the ones presented in Fig. 29. Measurements are also performed at RT and at 20° (red line), 55° (blue line), and 90° (black line) between the surface and the wavevector of the X rays. The isotropic Co spectrum shows striking differences as opposed to the Co $L_{2,3}$ XA spectrum of CoOEP bulk material (see Fig. 23) and of CoOEP on HOPG (see Fig. 27). The multiplet structure at the L_3 edge is much less pronounced, so there is only one peak with a maximum at 778.9 eV and a small shoulder at the low energy flank. The contraction of the multiplett structure uncovers unambiguously a change of the Co electronic structure upon adsorption of the porphyrins. The substrate-induced modification of the N atoms, which form a coordination bond with the Co ions, is in agreement with this result. Furthermore Co states may hybridize with electronic states of the copper substrate.

The fine structure at the Co L_3 edge reveals an angular dependence, as it is the

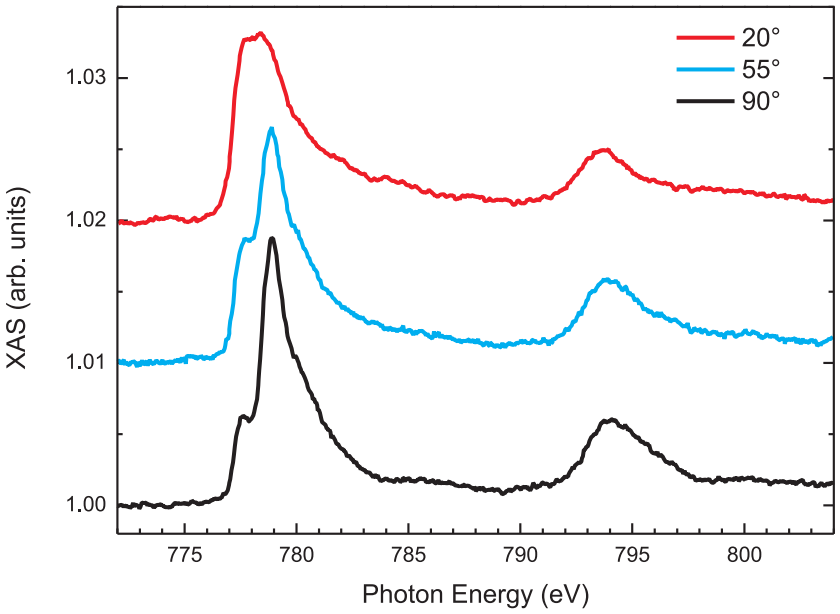

Figure 30: Co $L_{2,3}$ XA spectra of 0.4 ML CoOEP on Cu(100) recorded at RT and with p-linearly polarized light and an angle of 20° (red line), 55° (blue line), and 90° (black line) between the surface and the wavevector of the X rays.

case for CoOEP on HOPG, too. At a detection angle of 20° grazing incidence, at which final states with more out-of-plane hole density are probed, the shoulder at 777.6 eV is more distinctive and the main peak reduces in intensity. On the contrary, for measurements at normal incidence, at which only final states with in-plane hole density are probed, the main peak is more apparent and the shoulder at the low energy flank is clearly diminished. Therefore, at lower photon energies the spectral features at the Co L_3 edge can be qualitatively assigned to excitations into out-of-plane orbitals like the $d_{xz,yz}$ or the d_{z^2} orbitals. Accordingly, the contributions to the fine structure at the Co L_3 edge at higher photon energies belong to excitations into in-plane orbitals like the $d_{x^2-y^2}$ or d_{xy} orbitals.

With regard to the study of the magnetic properties of CoOEP adsorbed on Cu(100), the XMCD effect is used in the following. It is based on the different absorption for left and right circularly polarized X rays, as outlined in section 1.5. Since CoOEP on Cu(100) represents a paramagnetic system, this effect is only observable at high externally applied magnetic fields and at sufficiently low temperatures.

Fig. 31 displays helicity-averaged Co $L_{2,3}$ XA (upper panel) and corresponding XMCD (lower panel) spectra of 0.4 ML CoOEP on Cu(100). Helicity-averaged X-ray absorption spectra present an average over the signals detected for positive and negative helicity of the circularly polarized light while XMCD spectra represent the according differences of the two signals. The spectra are recorded at 4.5 K and in an external magnetic field of 5.9 T applied along the incident direction of the X rays. The chosen measurement geometries are 90 ° normal incidence (black lines) and 35° grazing incidence (blue lines). In analogy to spectra recorded with linearly polarized X rays, also helicity averaged spectra are sensitive to the unoccupied density of states. The angle-dependent variance is less pronounced, though. Circularly polarized light can be viewed as a combination of two sources of linearly polarized light with $\vec{E}$

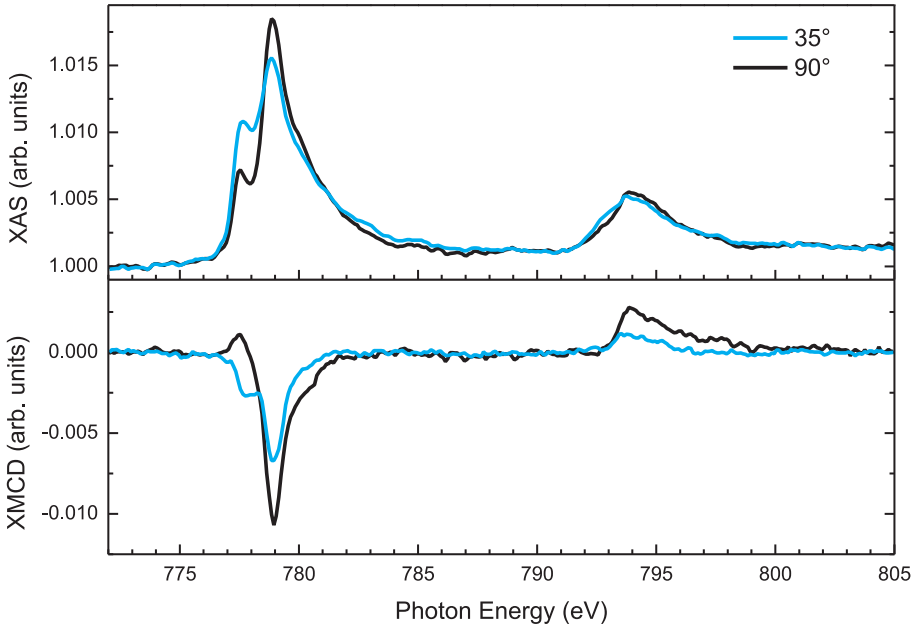

Figure 31: Helicity-averaged Co $L_{2,3}$ XA (a) and corresponding XMCD (b) spectra of 0.4 ML CoOEP adsorbed on Cu(100). The measurements are carried out at a temperature of 4.5 K and an external magnetic field of 5.9 T, which is applied parallel to the wave vector of the circularly polarized light. Spectra taken at 90° normal (black line) and at 35° grazing (blue line) incidence are displayed.

vectors being rotated to each other by 90°. Thus for all incidence angles always one component of the $\vec{E}$ vector is parallel oriented to the surface plane.

The Co $L_{2,3}$ edge XA spectra displayed in Fig. 31 are qualitatively in agreement with the Co spectra presented in Fig. 30. Also here the spectrum recorded at normal incidence reveals a main maximum at 778.9 eV and at the lower photon energies a second spectral feature at 777.6 eV. For measurements at 35° grazing incidence, the main peak is reduced and the intensity at lower photon energy increases. This is also the case for measurements with p-lineraly polarized light under grazing incidence. For both measurement geometries a considerable XMCD signal is detected. Their existence proves the presence of a magnetic moment on the Co side. The features which build up the Co L_3 XMCD signal lie at the same photon energies of 778.9 and 777.6 eV as the ones of the Co L_3 XA edge. Contributions to the Co L_3 XMCD spectrum measured at normal incidence have a positive and negative sign below and above 777.9 eV, respectively. In contrast, the Co L_3 XMCD spectrum recorded at 35° grazing incidence does not possess a zero crossing. The main contribution to the spectra for both detection angles is the peak at 778.9 eV. The feature at lower photon energies appears at 35° grazing incidence as shoulder of this main peak, and as small peak with an inversed sign at normal incidence. Furthermore the Co L_2 XMCD edge is significantly smaller at grazing detection angles.

Fig. 32 shows the calculated XA intensity for excitations of $2p$ electrons into individual $3d$ orbitals with helicity-averaged circularly polarized X rays as a function of incidence angle (left panel), according to eq. 10. The corresponding expected XMCD

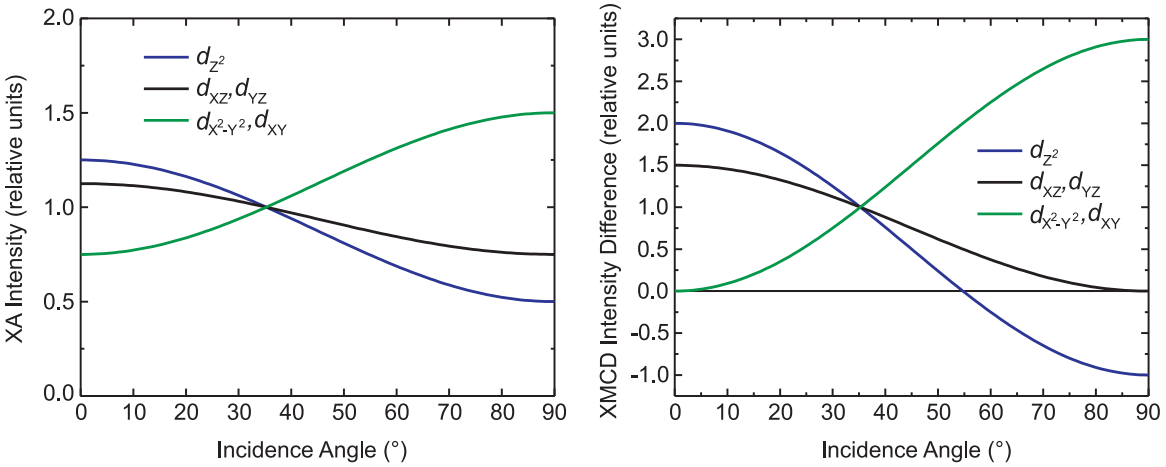

Figure 32: Expected intensity of the XA (left panel) and XMCD (right panel) resonances as a function of the incidence angle for excitations from $2p$ into individual $3d$ orbitals with the quantization axis along the surface normal. A magnetic field is applied in parallel to the $\underline{k}$ vector of the circularly polarized X rays. Zero magnetic anisotropy and magnetic saturation are assumed.

intensity differences (right panel) are presented as well, according to table 2. Besides the assumptions stated earlier, also zero anisotropy of the spin and orbital moment, magnetic saturation, and a magnetic field applied along the wavevector of the X rays are assumed for these XMCD intensity differences. For both, XAS and XMCD measurements, the detection angle at which the isotropic spectrum is obtained amounts to 35.3° grazing incidence. This is the so called magic angle for circularly polarized light, which is different compared to the one for p-linearly polarized light of 54.7°. The functional evolution of the XA intensity for the individual $3d$ orbitals is the same for p-linearly and for circularly polarized light. However, it is less pronounced in the latter case. On the other hand, the XMCD contrast by changing the measurement geometry is much higher. Thus, for measurements at normal incidence, the XMCD intensity difference of the $d_{xz,yz}$ orbitals vanishes completely and the one of the $d_{x^2-y^2}$ and d_{xy} orbitals increases in intensity by 200% compared to measurements at the magic angle. For excitations into the d_{z^2} orbital the sign of the XMCD signal is even inversed at normal incidence. For measurements performed at gradually more grazing incidence than the magic angle, the in-plane orbitals $d_{x^2-y^2}$ and d_{xy} reveal a diminishing dichroism and the out-of-plane orbitals $d_{xz,yz}$ and d_{z^2} an increasing one. For the experimentally not feasible case of a grazing detection angle of 0°, the XMCD intensity difference is consequently maximum for the out-of-plane orbitals and zero for the in-plane orbitals. The physical picture behind these drastic variations of the expected XMCD intensity is based on the strongly anisotropic charge density of the individual d orbitals, which leads to an inhomogeneous spatial distribution of the spin density. This in turn can be viewed as a non-vanishing intra-atomic spin dipole moment that influences the XMCD intensity angle-dependently. According to this, the application of the spin sum rule only yields the magnetic spin moment by averaging over the results of three separate measurements along orthogonal directions. Alternatively, the evaluation of the spin sum rule for a single XMCD spectrum recorded

	$n_h = 3$		$n_h = 2$	
α	$m_S^{\text{eff}}(\alpha)/\mu_B$	$m_L(\alpha)/\mu_B$	$m_S^{\text{eff}}(\alpha)/\mu_B$	$m_L(\alpha)/\mu_B$
35°	(0.75 ± 0.05)	(0.29 ± 0.03)	(0.50 ± 0.03)	(0.19 ± 0.02)
90°	(1.47 ± 0.05)	(0.19 ± 0.02)	(0.98 ± 0.03)	(0.13 ± 0.01)

Table 4: Experimental expectation values as a function of angle α of the orbital magnetic moment and the effective spin moment derived from sum-rule analysis for 0.4 ML CoOEP on Cu(100), assuming $n_h = 3$ or 2.

at the magic angle, provides the magnetic moment, considering magnetic saturation and symmetries of $D_{2\text{h}}$, $C_{4\text{v}}$, as assumed here, or higher [46].

Referring again to the experimental results presented in Fig. 31, the Co $L_{2,3}$ edge XA and XMCD spectra, measured at 35° grazing incidence, represent in the technical metering precision the isotropic Co XA and XMCD spectra, respectively. The Co XA and XMCD spectra, recorded at normal incidence, carry additional information about the in-plane hole and spin density.

A sum-rule analysis can determine the spin and orbital magnetic moments at the chosen measurement conditions. In this context, it is necessary to know the number of holes within the $3d$ shell in order to determine the magnetic moments, according to eqs. 16 and 17. For CoOEP in bulk, the Co ions are in a +2 oxidation state and hence there are 3 d holes. However, the molecule–substrate interaction for CoOEP on Cu(100) may modify this and induces for instance a charge transfer from the surface or the porphine ligand to the Co atoms. Here, a comparison of the energetic position of the Co L_3 XA edge for CoOEP bulk material (see Fig. 23) and for the isotropic spectrum of CoEOP/Cu(100) is helpful. This is because the Co L_3 peak position is to some extent related to the amount of charge at the Co site [134]. There is a small shift of spectral weight in energy at the Co L_3 edge to lower photon energies for the adsorbed porphyrins as opposed to CoOEP in bulk. This may indicate a reduction of the Co ions.

The physical quantity which is obtained by applying the spin sum rule to XMCD spectra which are not recorded at the magic angle, is the so called effective magnetic spin moment. By assuming flat adsorbed molecules and an angle of incidence α between the surface plane and the $\vec{k}$ vector of the X rays, it is mathematically described as [135]:

$$m_S^{eff}(\alpha) = m_S - 7\underbrace{\left(m_T^z \sin^2(\alpha) + m_T^{xy}\cos^2(\alpha)\right)}_{m_T(\alpha)}. \tag{29}$$

Thereby m_S is the spin moment and the term $7m_T(\alpha)$ stands for the intra-atomic spin dipole moment. A fourfold rotational symmetry of the molecules, leading to a uniaxial anisotropy along the surface normal, is assumed, which implies $(m_T^z + 2m_T^{xy}) = 0$. The results of the sum-rule analysis of the experimental spectra for $m_S^{\text{eff}}(35°)$ are $(0.75 \pm 0.05)\ \mu_B$ or $(0.50 \pm 0.03)\ \mu_B$ assuming either three or two d holes, respectively. These values are displayed in table 4 together with results for $m_S^{\text{eff}}(90°)$, which are $(1.47 \pm 0.05)\ \mu_B$ in the case of $n_h = 3$ and $(0.98 \pm 0.03)\ \mu_B$ for $n_h = 2$. The integrated helicity-averaged Co XA spectrum, recorded at the magic angle, is used as isotropic intensity.

A second contribution to the magnetic moment of the Co ions is the angle-dependent

orbital moment $m_L(\alpha)$. The orbital sum rule enables to determine $m_L(35°)$ to $(0.29 \pm 0.03)\ \mu_B$ or $(0.19 \pm 0.02)\ \mu_B$, and $m_L(90°)$ to $(0.19 \pm 0.03)\ \mu_B$ or $(0.13 \pm 0.02)\ \mu_B$, assuming three or two d holes, respectively. Hence, the orbital moment is anisotropic. The reason for this is the recreation of orbital moment by SOC. The crystal field, which constrains the Co atoms, quenches the orbital moment at a first stage, and only an additional mixing of eigenstates by SOC induces new states with anisotropic orbital moments unequal zero [52], as dicussed in section 1.8.

For the XMCD measurements at 35° grazing incidence, the calculated effective spin moments present within the measurement accuracy the Co spin moments. In the case of three d holes, the Co ions may occupy the spin states $S = 1/2$ or $S = 3/2$. In the former the spin moment per atom is one Bohr magnetons, and in the latter it amounts to three Bohr magnetons. Under the assumption of two holes within the $3d$ shell, the possible spin states are $S = 0$ and $S = 1$, with a spin moment per Co atom of zero and two Bohr magnetons, respectively. The values of the spin moment experimentally obtained are smaller than the ones listed above. Only for the spin state $S = 0$ this is not the case, which can be, however, excluded from the detection of a XMCD signal. Hence, the externally applied magnetic field at the selected temperature is not sufficient to fully align the magnetic moments at the Co site. The XMCD measurement technique detects a projection of the magnetic moments onto the direction of the applied magnetic field and the $\underline{k}$ vector of the X rays. Therefore the here obtained values present lower limits of the magnetic moments.

For the purpose of figuring out the saturated values of m_S and $m_S^{\text{eff}}(90°)$, field- and temperature-dependent XMCD measurements at the Co L_3 edge for 35° grazing and normal incidence are performed. By varying the external field at 4.5 K and changing the temperature at 5.9 T during the XMCD measurements, the Co L_3 XMCD resonance changes in height. The size of the integrated Co L_3 XMCD signals can be scaled to the ones of the spectra in Fig. 31. By doing so the behavior of m_S and $m_S^{\text{eff}}(90°)$ versus the external magnetic field at 4.5 K and versus the temperature at 5.9 T is found. Figs. 33 and 34 present the obtained experimental values for m_S (●) and $m_S^{\text{eff}}(90°)$ (●). They are shown together with theoretically modeled field or temperature dependences of the respective magnetic moments (black line for $m_S^{\text{eff}}(90°)$ and blue line for m_S).

In quantum mechanics the ground state of a paramagnet, with the total electronic angular momentum J, within an externally applied magnetic field B_{ext} is split into $(2J + 1)$ energy levels. This energetic contribution is called Zeemann energy. A population of the energy levels follows the Boltzmann statistics, favoring an equal population of the levels at elevated temperatures. The resulting relation between the average magnetization $M(T, B_{ext})$ and the saturation magnetization M_0 can be expressed with the help of the Brillouin function $B_J(\alpha)$:

$$M(T, B_{ext}) = M_0 B_J(\alpha), \tag{30}$$

$$B_J(\alpha) = \frac{2J+1}{2J}\coth\left(\frac{2J+1}{2J}\alpha\right) - \frac{1}{2J}\coth\left(\frac{1}{2J}\alpha\right). \tag{31}$$

Thereby the argument α is $g\mu_B J B_{ext}/k_B T$, where g is the Landé factor and k_B is the Boltzmann constant. However, the relationship between $M(T, B_{ext})$ and M_0 in equation 30 does not take into account magnetic anisotropy.

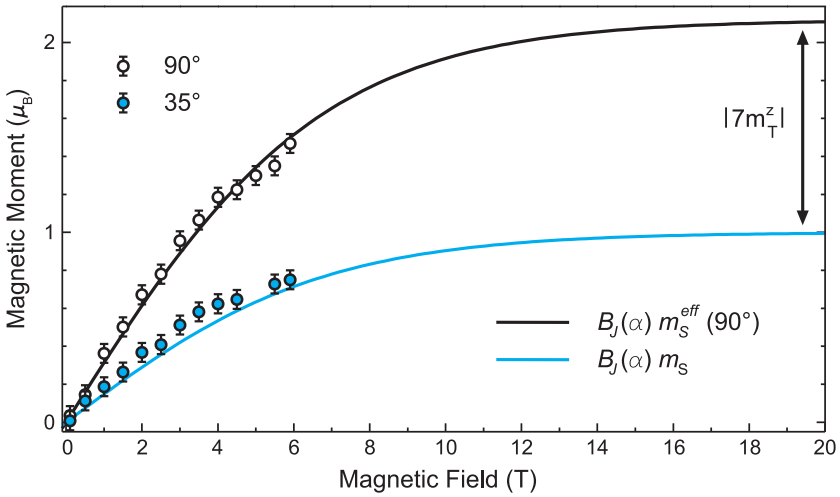

Figure 33: Experimental expectation values of $m_S^{\text{eff}}(90°)$ and m_S as a function of the applied magnetic field, determined from the sum-rule analysis of the magnetic field dependence of the XMCD at the Co L_3 edge. The temperature was 4.5 K and the magnetic field was always parallel to the X-ray beam. The blue and black continuous lines show the functional behavior of m_S and $m_S^{\text{eff}}(90°)$ versus magnetic field according to equation 30 for $S = 1/2$ and $M_0 = 1\ \mu_B$ per Co ion, where the latter is obtained by multiplying the former with a scaling factor received from a fit.

With the help of this physical model, the expected magnetic spin moment can be calculated at a temperature of 4.5 K and an applied magnetic field of 5.9 T. Here, the contribution of the orbital moment to the magnetic moment is neglected. Thus the spin moment is equal to the total electron magnetic moment, $S = J$, and a Landé factor of g = 2 is assumed. For spin systems with $S = 1/2$ the magnetic spin moment amounts to 0.71 μ_B, for $S = 1$ to 1.62 μ_B, and for $S = 3/2$ to 2.59 μ_B. A comparison between those values and the experimental values of $(0.50 \pm 0.03)\ \mu_B$ for $n_h = 2$ and $(0.75 \pm 0.05)\ \mu_B$ for $n_h = 3$ shows that there is an agreement within the error only for $S = 1/2$. 1.62 μ_B in the case of $S = 1$ and 2.59 μ_B for $S = 3/2$ are by far bigger than $(0.50 \pm 0.03)\ \mu_B$ or $(0.75 \pm 0.05)\ \mu_B$. Contributions of the intra-atomic spin dipole moment can not explain such findings, as they are zero for the measurement geometry used for a determination of m_S. This points strongly towards an $S = 1/2$ spin state of the Co ions.

However, the total energy of a magnetic system may also depend on the direction of the magnetization with respect to its geometry, as discussed in section 1.8. The presence of a so called MCA, i.e., an energy required to alter the magnetic orientation from the so-called easy axis to the so called hard axis, also leads to contributions to the total energy besides the Zeemann interaction. In this context, an out-of-plane anisotropy may lead to detections of lower m_S values for XMCD measurements recorded at the magic angle, where the external magnetic field has a bigger component lying inside the surface plane. The physical phenomenom out-of-plane anisotropy describes the fact that it is easier to align magnetic moments parallel to the surface normal than perpendicular to it.

It is appropriate to assume a uniaxial anisotropy for CoOEP on Cu(100). This

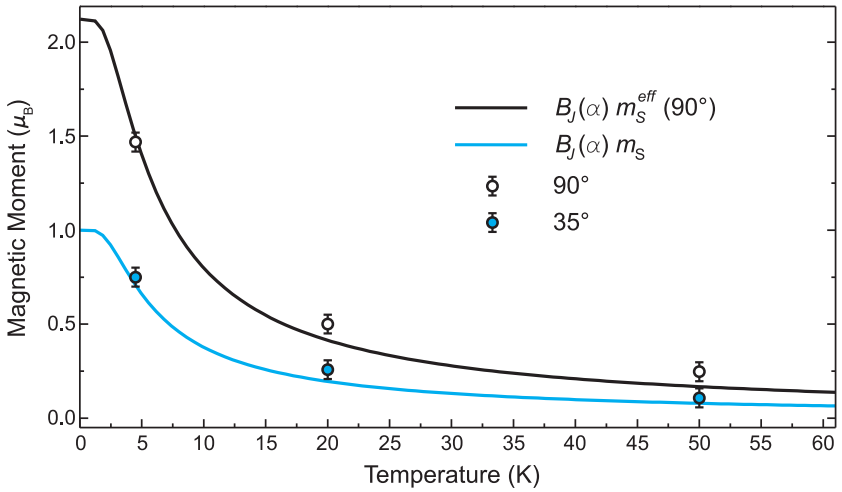

Figure 34: Experimental expectation values of $m_S^{eff}(90°)$ and m_S as a function of temperature, determined from the sum-rule analysis of the temperature dependence of the XMCD at the Co L_3 edge. The magnetic field was 5.9 T and always parallel to the X-ray beam. The blue and black continuous lines show the functional behavior of m_S and $m_S^{\text{eff}}(90°)$ versus temperature according to equation 30 for $S = 1/2$ and $M_0 = 1\ \mu_B$ per Co ion, where the latter is obtained by multiplying the former with a scaling factor received received from a fit.

means that the x and y axes are equal and there is no preferential magnetization direction inside the surface plane. The so-called Bruno model states that the MCA is proportional to the difference between the orbital moments along the easy and hard magnetization directions [67]. This implies also that the orbital moment is larger along the easy magnetization axis. For the system under study here, $m_L(35°)$, which has a bigger in-plane than out-of-plane component, is found to be higher than $m_L(90°)$. This is independent of the number of d holes. Hence, the in-plane orbital moment is bigger than the out-of-plane one. Consequently an in-plane anisotropy is expected for CoOEP on Cu(100). This in turn would lead to the detection of a magnetic spin moment at the magic angle higher than predicted by eq. 30. Therefore it is unlikely that the smaller magnetic spin moments experimentally found in the case of the spin states $S = 1$ and $S = 3/2$ can be explained by an anisotropy effect. For the sake of completeness it has to be mentioned that the Bruno model presumes a large exchange splitting. Furthermore, it assumes a negligible magnetic dipole term, the presence of which may either strengthen or weaken the statement of Bruno [136]. To the best of my knowledge there is no physical system for which the Bruno model is not valid, even in cases where the magnetic dipole term can not be ignored [135].

Solid blue lines in Figures 33 and 34 display the magnetic spin moment versus the magnetic field and the temperature for $S = 1/2$ according to equation 31 with $M_0 = 1\ \mu_B$ per Co ion. Slightly higher Co spin moments in the experiment compared to the functional behavior of the theoretical model could be explained by an in-plane anisotropy of the Co ions. This would be consistent with the higher in-plane orbital moment of the Co ions.

The experimental data of $m_S^{\text{eff}}(90°)$ versus the applied magnetic field at 4.5 K and

versus the temperature in an applied magnetic field of 5.9 T can now be fitted simultaneously to the functional behaviour of eq. 30. For that matter a potential minor in-plane anisotropy of the Co ions is neglected. Furthermore, $S = 1/2$ enters as an input parameter in addition to the assumptions stated earlier and again the contribution of the orbital moment to the magnetic moment is neglected. M_0 in eq. 30 is multiplied by an additional scaling factor in order to account for the intra-atomic spin dipole moment. $m_S^{\text{eff}}(90°)$ can than be obtained from the fit. It yields $(2.12 \pm 0.00)\ \mu_B$ for $m_S^{\text{eff}}(90°)$ and accordingly $(1.12 \pm 0.00)\ \mu_B$ for $-7m_T(90°)$. Hence, m_T^z is $-(0.16 \pm 0.00)\ \mu_B$ and m_T^{xy} amounts to $+(0.08 \pm 0.00)\ \mu_B$. The non-zero intra-atomic spin dipole moment shows that there is an inhomogeneous spatial distribution of the spin density. The detection of a bigger value for $m_S^{\text{eff}}(90°)$ than for m_S reveals that there is more spin density accumulated in-plane than out-of-plane. As the SOC is relatively small for Co, the atomic charge density follows closely the spin density. Therefore the unpaired electron occupies an orbital whose projected charge distribution lies more in-plane than out-of-plane.

For reasons of comparison the value of $-7m_T(90°)$ for CuPc adsorbed on Ag(100) has to be mentioned [125]. In this system the Cu ions are also in an $S = 1/2$ spin state and the unpaired hole density lies parallel to the surface plane in the $d_{x^2-y^2}$ orbital. $-7m_T(90°)$ amounts in this case to 1.88 μ_B, which is a bigger value than for CoOEP on Cu(100). For the XMCD intensity of an individual in-plane $3d$ orbital even a value of 2 μ_B is expected, as shown in Fig. 32. An explanation for a lower value of $-7m_T(90°)$ for CoOEP on Cu(100) could be that the unpaired hole density does not lie exactly inside the surface plane.

For isolated CoOEP molecules and for CoOEP in bulk it is know from literature [53, 112, 113] that the out-of-plane orbitals d_{xz}, d_{yz}, and d_{z^2} carry either together one unpaired hole or only the d_{z^2} does so. In contrast, the energetically highest lying d orbital, the $d_{x^2-y^2}$ one, is completely unoccupied and the d_{xy} orbital totally filled. In the case of such an electronic structure of the Co ions, the value of $-7m_T(90°)$ has an inversed sign compared to m_S, as shown in section 3.4.2. Hence the interaction between CoOEP and the Cu(100) leads to a redistribution of the electrons within the $3d$ shell.

Discussing the physical scenario in the framework of individual $3d$ orbitals could be as follows: The coordination of the Co ions to a surface raises the d_{z^2} orbital in energy. Additionally, a saddle-shape conformation of the porphyrin macrocycle lowers the in-plane crystal field, as the metal ions are no longer constrained by four N atoms which lie in a plane. Thus, the $d_{x^2-y^2}$ and the d_{xy} orbitals lie energetically lower and the unpaired electron may occupy the $d_{x^2-y^2}$ orbital.

In conclusion, the adsorption of CoOEP on Cu(100) induces a rather strong modification of the N and Co electronic structure. The porphyrins adsorb flat on the surface and the oxidation state of the Co atoms does not change. Furthermore the metal ions remain in an $S = 1/2$ spin state, but there is a redistribution of the electrons within the $3d$ shell. Upon adsorption the unpaired electron occupies an orbital whose charge distribution lies primarily in-plane and not out-of-plane, as for isolated CoOEP. This shows that the molecule–substrate interaction is important for the use of porphyrins as molecular building blocks on surfaces. It affects the target-oriented architecture of porphyrin-based devices on substrates concerning their electronic properties.

3.3.3 Substrate-induced magnetic ordering

The electronic interaction between porphyrin molecules and surfaces can either be weak or strong, as described in the last two sections. Thereby a substrate-induced modification of the molecular electronic and magnetic properties may occur. Also magnetic interactions between porphyrins and substrates are certainly of interest. A feasible strategy to align the magnetic moments of paramagnetic molecules without applying an external magnetic field is their adsorption on a ferromagnetic substrate. Within this section, Co $L_{2,3}$ XMCD spectra of CoOEP adsorbed on Ni films, grown on Cu(100), are presented. The spectra were measured in remanence of the ferromagnetic film. The focus of interest addresses a potential magnetic exchange coupling between the Co and Ni spins. Also angle-dependent XA measurements recorded at the N K edge of CoOEP on Ni/Cu(100) are shown, which provide information about the adsorption geometry of the porphyrins. Additionally, these spectra are compared to theoretically calculated ones of a Ni_4-(CoOEP) cluster, as published in our recent work [111]. This allows to gain insight into the formation of bonds at the molecule substrate-interface.

First a potential magnetic interaction between the porphyrin molecules and the Ni substrate is of interest. Therefore, Fig. 35 shows a helicity-averaged Co $L_{2,3}$ XA spectrum (a) and the corresponding XMCD spectrum (b) of 0.6 ML CoOEP adsorbed on 12 ML Ni/Cu(100). The spectra are taken at normal incidence and at RT. A Ni film on Cu(100) with such a thickness has an out-of-plane easy axis [137]. The spectra are measured in remanence of the ferromagnetic film. The Co L_3 XA edge possesses a rather featureless line shape with a main maximum at a photon energy of 778.9 eV and a pre-peak at the lower energy flank at 777.6 eV. The Co XMCD spectrum at the L_3 edge shows a main peak with a negative sign at the same energy as the XA spectrum. At lower photon energies, a much smaller peak contributes to the spectrum, which displays opposite XMCD contrast. The overall appearance of the Co $L_{2,3}$ XA and XMCD spectra resembles to a large extent the one of Co $L_{2,3}$ XA and XMCD spectra for CoOEP on Cu(100) also recorded at normal incidence (see Fig. 31). This points towards a similar electronic structure of the Co ions for CoOEP adsorbed on these two substrates.

The presence of a Co XMCD signal proves not only a $3d$ magnetic moment at the Co site, but also a magnetic exchange coupling between the Ni magnetization and the Co spins, since no external magnetic field is applied. The Ni $L_{2,3}$ XMCD spectrum of the ferromagnetic film underneath the porphyrins is shown in the inset of Fig. 35 (a). As the Ni L_3 XMCD signal has the same sign as the one of the Co L_3 XMCD signal, the magnetic moments situated at these two elements point into the same direction. Hence, it can be stated that the Co magnetic moments couple in a ferromagnetic fashion to the magnetization of the Ni film. The magnetic exchange coupling acts similarly to an external magnetic field on the Co spins. So, it stabilizes the Co magnetic moments against their thermal fluctuations. The detection of an XMCD signal even at RT reveals that the strength of the exchange coupling must be relatively big. For CoOEP adsorbed on graphene- and oxygen-covered Ni films a reasonable XMCD signal is detected only at temperatures lower than 125 K and 30 K [138, 139], respectively, as will be discussed in section 3.4.1 and 3.5.2. In contrast, for MnTPPCl and FeOEP on bare ferromagnetic substrates significant XMCD signals

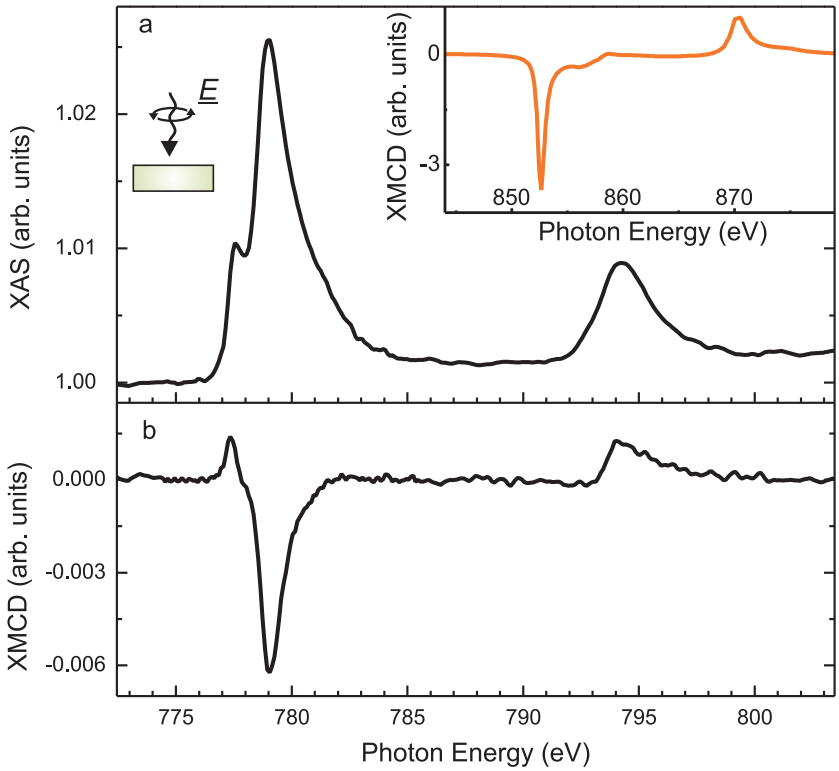

Figure 35: Co $L_{2,3}$ XA helicity-averaged spectrum (a) of 0.6 ML CoOEP on 12 ML Ni/Cu(100) and the corresponding XMCD spectrum (b), measured at normal incidence and 300 K. Inset: XMCD spectrum at the Ni $L_{2,3}$ edges.

are found even at RT [33, 34, 127].

The out-of plane magnetization of the Ni film aligns the Co magnetic moments accordingly. Thus, the isotropic Co XMCD spectrum is not detected which would be only possible by pulling the Ni film magnetization away from its easy axis. This in turn would require a high magnetic field. Hence, by making use of the XMCD sum rules [49, 50], values of $(0.52 \pm 0.05)\ \mu_B$ for the effective spin moment $m_S^{\text{eff}}(90°)$ and of $(0.11 \pm 0.04)\ \mu_B$ for the out-of-plane orbital moment $m_L(90°)$ can be given. It is reasonable to assume here that the Co magnetic moments are not in saturation at RT, although it can not be ruled out. Correspondingly, the application of the sum rules only yields lower limits of the Co orbital and effective spin moments. For the evaluation of $m_S^{\text{eff}}(90°)$ and $m_L(90°)$ using the sum rules, three d holes are assumed. It is reasonable to do so, as $n_h = 3$ for CoOEP on Cu(100).

In the following the electronic interaction between the CoOEP molecules and the bare Ni surface is deeper analysed. To do so, Fig. 36 displays N K XA spectra of 0.8 ML of CoOEP on Ni/Cu(100). The measurements are performed at 90° (black line) normal and at 20° (red line) and 55° (blue line) grazing incidence at RT. The isotropic XA spectrum of the N K edge is obtained for the latter detection angle. It reveals two local maxima at photon energies of 399.3 and 401.4 eV. This leads to a double-peak structure similar as for CoOEP in bulk (see Fig. 24), while the energetic separation between the peaks is 0.9 eV smaller for CoOEP on Ni. A comparison of this experimental spectrum with a theoretically calculated one of a Ni_4-(CoOEP)

cluster allows to assign spectral features to particular probed final state orbitals [111]. The Ni_4-(CoOEP) cluster simulates the adsorption of CoOEP on Ni/Cu(100) in the submonolayer regime. The calculated spectra are generated by means of StoBe cluster and DFT calculations [114]. According to the computations, mainly five excitations contribute to the spectrum below a photon energy of 402.5 eV. So the energetically lowest peak with a maximum at 399.3 eV belongs to three excitations that are very close in energy. One of the final state orbitals being involved in these transitions is of σ^* type symmetry. It contains contributions of Co 3*d*, N 2*p*, and Ni 3*d* states. Within the Ni_4-(CoOEP) cluster the four nitrogen atoms sit on top of the four Ni atoms, such that Ni 3*d* orbitals hybridize with the N 2*p* ones. The electronic interaction between the Co ion and the nitrogen atoms is similar as for isolated CoOEP, and Co 3*d* orbitals form a bond with N 2*p* ones. The final state orbitals of the other two excitations which contribute to the energetically lowest peak are of π^* type symmetry. 2*p* states of carbon atoms of the macrocycle which are binding partners of the nitrogen atoms form these orbitals with their 2*p* states, while only minor Ni 3*d* contributions are present. Another final-state orbital of an excitation at the N *K* XA edge stems from such an electronic interaction between these elements. The energetically higher excitation peak at 401.4 eV is dominated by this transition. Furthermore, the molecule–substrate interaction causes the increased spectral intensity between the two local maxima at 399.3 and 401.4 eV as opposed to the N *K* XA spectrum of CoOEP bulk material. An excitation into a π^* type orbital which possesses large Ni 3*d* and 4*s* contributions with some N 2*p* admixture induces this additional spectral intensity. At higher photon energies than 404.5 eV exclusively excitations into final state orbitals with σ^* character contribute to the spectrum. These orbitals are located at the core of the adsorbate as well as at the periphery of the molecules according to the calculations. The spectrum features in this energy region a main maximum at 406.6 eV.

Only antibonding orbitals are probed within the absorption process. The corresponding occupied orbitals describe the physical bonding. Hence, knowledge about the nature of the peaks which contribute to the N *K* XA spectrum allows to analyze the electronic coupling between the Ni atoms and the CoOEP molecule. It can be stated from the above assignment of the peaks that a bond between Ni 3*d* and N 2*p* orbitals contributes to the electronic intercation between the Ni surface and the porphyrins.

As for CoOEP on HOPG (see Fig. 26) and Cu(100) (see Fig. 29), different contributions of the spectra reveal a different angular dependence. At photon energies lower than 404.5 eV the spectral features are more apparent at 20° grazing incidence. In contrast, above an energy of 404.5 eV contributions to the spectra are more apparent at normal incidence. This experimental observation is in agreement with the differently assigned symmetry of final state orbitals being involved in the absorption process. The angular dependence of theoretical N *K* edge XA spectra, which are computed for flatly adsorbed porphyrins, reveals this behavior, too [111]. Hence, the molecules adsorb flat on the surface. Below 404.5 eV the shape of the spectral features at 20° grazing and at normal incidence is not fully identical. This goes well with excitations into final state orbitals with π- and σ- type symmetry in this energy range. Nevertheless, the contributions of excitations into π^*- type orbitals are predominant with respect to the ones into σ^*- type orbitals. Further there is a remaining intensity at around 401.4 eV under normal incidence. This hints at adsorbate–substrate

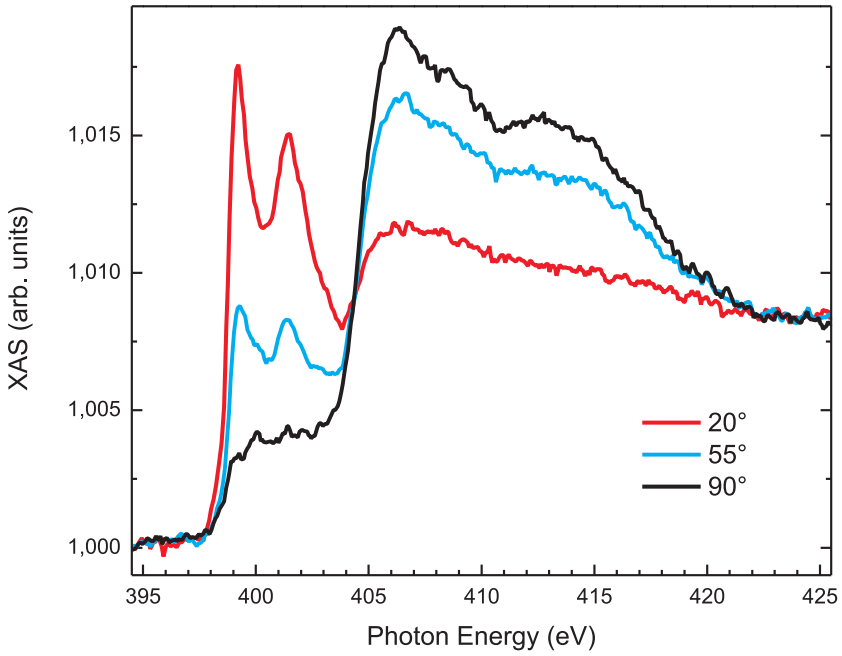

Figure 36: N K XA spectra of 0.8 ML of CoOEP adsorbed on 12 ML Ni/Cu(100). The spectra are recorded at RT and 20° (red line), 55° (blue line), and 90° (black line) between the k-vector of the p-linearly polarized X rays and the surface plane.

hybridization effects which cause transitions into final state orbitals with σ type symmetry at these energies. These interactions are not included in the theoretical cluster model, with the help of which spectral features are assigned to particular probed final state orbitals.

The results presented here are very similar to the ones of angle-dependent measurements at the N K edge for FeOEP adsorbed on thin Co and Ni films on Cu(100) from literature [88]. This points towards a similar electronic interaction between the nitrogen atoms of the porphyrin macrocycle for CoOEP and FeOEP on Ni substrates.

Now, with a deeper knowledge about the electronic adsorbate–substrate coupling, the magnetic exchange coupling mechanism between the Co spins and the Ni magnetization can be discussed. The basics about magnetic coupling can be found in section 1.9. A direct magnetic interaction between the Co ions and the substrate might be an explanation for the experimental results. This would imply that there is a direct electronic wavefunction overlap in space of Co and Ni orbitals which induces a direct exchange coupling between the magnetic moments of these elements. However, also an indirect coupling mechanism via the nitrogen atoms as reported for FeOEP on Co and Ni thin films [34] may be possible. The similarity of angle-dependent N K edge XA spectra for CoOEP and FeOEP adsorbed on a Ni surface supports this. The characterisation of the electronic interaction between the CoOEP molecules and the surface by means of a comparison between experimental and theoretical N K edge XA spectra is helpful. It points towards an indirect coupling mechanism, as there is an electronic coupling between Ni $3d$ and N $2p$ states and an additional electronic coupling of the latter with Co $3d$ states. However, the exact exchange mechanism can not be clarified without further calculations.

Recapitulating, it is possible to align the Co magnetic moments of CoOEP molecules by adsorbing them on top of a thin Ni film. A magnetic exchange coupling between the substrate magnetization and the Co spins stabilizes them against their thermal fluctuations. This allows, even at RT and zero external magnetic field, to gain control over the Co magnetization. Regarding the design of porphyrin-based spintronic devices, these results are interesting. The molecule–surface interaction modifies the Co electronic structure, and N $2p$ orbitals hybridize with Ni $3d$ orbitals of the substrate. The porphyrin molecules adsorb flat on the surface.

3.4 Magnetic coupling across graphene

Graphene, a material with unique properties [140], is expected to complement todays Si-based information technology with new and more efficient functions [15, 141–143]. It features desirable characteristics for spin electronic applications such as low intrinsic spin-orbit interaction, high charge carrier mobility, as well as low hyperfine interaction [14, 144], as outlined in the introduction. Of special interest is the interaction of magnetic molecules with graphene, as such a system presents a promising attempt towards organic spin electronics due to the reduced conductivity mismatch at the interface. The laterally extended π electron system of graphene exhibits molecule-like properties perpendicular to the plane, and metal-like electronic properties along the plane. This makes graphene highly relevant for the design of hybrid metal-organic spintronic materials. In such a system a bit is represented by a single molecular magnetic moment, which must be stabilized against thermal fluctuations [145]. Molecules interact with graphene primarily by van der Waals forces, whereby the molecular properties of the adsorbate, like its reactivity, are conserved. This permits a molecular design of the adsorbate independent of its interaction with the substrate. Organic molecules akin to the ones investigated here, FePc, in contact with a graphene-covered nonmagnetic metal surface, have been observed to decouple electronically from the substrate and to preserve their molecular electronic properties [146]. The ability to generate a magnetic exchange coupling for a graphene-covered magnetic metal substrate has not been shown yet.

In this section it is demonstrated that the magnetic moments of CoOEP molecules adsorbed on graphene can be aligned by a remarkable antiferromagnetic coupling to a Ni substrate underneath the graphene. This coupling is mediated via the π electronic system of graphene, while no covalent bonds between the molecule and the substrate are established.

In addition, the contribution of the orbital as well as the spin moment to the Co magnetization is analysed in detail. Free transition metal atoms possess the highest possible multiplicity and the largest orbital moment regarding Hund's rules. Isolated from each other, they still preserve these physical properties on alkali films due to the localization of the $3d$ states [147]. But hybridization, a requirement for spin alignment and magnetic coupling, as well as crystal field effects quench the orbital moment [148] and can also affect the spin state. Not only the spin moment but also the orbital moment decreases as the atomic coordination is increased passing from adsorbed single atoms [149] to magnetically coupled transition metal atoms inside free [150, 151] and adsorbed clusters [149], monoatomic chains [152], two-dimensional films [85], and bulk. Thereby generally $m_S > m_L$ is valid, as the orbital moment is more sensitive to modifications of the crystal field [150]. Nonetheless, SOC can recreate an anisotropic orbital moment [69], as explained in section 1.8. So values of $m_L/m_S < 0.08$ for transition metals in bulk [153] have been reported. In planar organometallic complexes even absolut values of m_L as high as 0.20 μ_B on metal surfaces [125] and 0.53 μ_B for molecular bulk material [135] have been observed. Further, the anisotropic m_L destines the alignment direction of magnetic moments of nanostructures at interfaces [42], akin to metallic films [154] via the SOC.

The adsorption of metalloporphyrins which contain fourfold coordinated transition metal ions on reactive ferromagnetic substrates can cause a substrate-induced mag-

netic ordering of their unpaired spins due to an exchange coupling to the substrate, as shown in section 3.3.3. The hybridization of the transition metal orbitals, enabling the spin polarization, hampers the contribution to the magnetization of the orbital moment, which is linked via the SOC to m_s [33]. No particular interest has been paid to the orbital moment within such systems so far, as its contribution to the central ion magnetization was marginally.

Here, it is demonstrated that the Co ions of CoOEP on graphene/Ni reveal an extraordinary huge in-plane orbital moment, despite their fourfold coordination, even comparable in size to the spin moment. Such an equal distribution of orbital and spin moment to the entire magnetic moment has so far not been reported for $3d$ transition metals, whose orbitals are hybridized with the ones of neighbour atoms, enabling the establishment of a magnetic exchange coupling. The orbital moment, which is recreated by spin-orbit coupling, reveals a giant anisotropy in size of 489%.[3]

3.4.1 Physisorption versus substrate-induced spin polarization

In the previous sections it was demonstrated that porphyrin molecules may both physisorb or chemisorb on single cristalline surfaces, depending on their reactivity. It was even shown that it is possible to align the magnetic moments of CoOEP by an adsorption of the molecules on bare ferromagnetic films, as an exchange interaction is established between the substrate and the adsorbate. However, the electronic structure of the Co ions is thereby modified due to the interaction between the porphyrins and the reactive magnetic surface. A strategy to achieve on the one hand a substrate-induced magnetic ordering of the Co magnetic moments, without the need of an externally applied magnetic field, and on the other hand to preserve the electronic properties of the CoOEP molecules, is their adsorption on a graphene-covered Ni film. With the purpose of studying the adsorption geometry and the character of CoOEP on a graphene-protected Ni surface, angle-resolved N and C K edge and Co $L_{2,3}$ XA spectra are shown in the following. Also temperature-dependent Co and Ni XMCD measurements taken in remanence of the ferromagnetic film are presented in order to gain insight into the magnetic properties of the porphyrin molecules and to evaluate the coupling strength between them and the substrate. All experimental results are discussed in the context of DFT+U calculations performed for the same system by the collaborating group of Prof. Oppeneer. The combined experimental and theoretical work is published in our recent work [139].

Figure 37 displays C K edge XA spectra of 0.7 ML CoOEP molecules on graphene/Ni/W(110) recorded at 25° (red line) grazing and 90° normal incidence (black line). In the photon energy range up to 289 eV, four π^* resonances are present. The first three with maxima at energies of 284.2, 285.0, and 285.7 eV are separately resolved only in the spectrum recorded at grazing incidence (red line). The fourth at an energy of 287.8 eV is also more apparent at grazing incidence. Above 289 eV, σ^* resonances contribute to the spectra. Up to 296.8 eV, the absorption intensity is higher for grazing incidence with a maximum at 292.4 eV, while between 296.8 eV and 306.1 eV it is higher for normal incidence. The isotropic XA spectrum at the C K edge of CoOEP bulk material (see Fig. 25) possesses very similar spectral features. The C K

[3]The written elaboration of this chapter is based on a publication [139] and one unpublished manuscript [155] as well as respective supplementary informations.

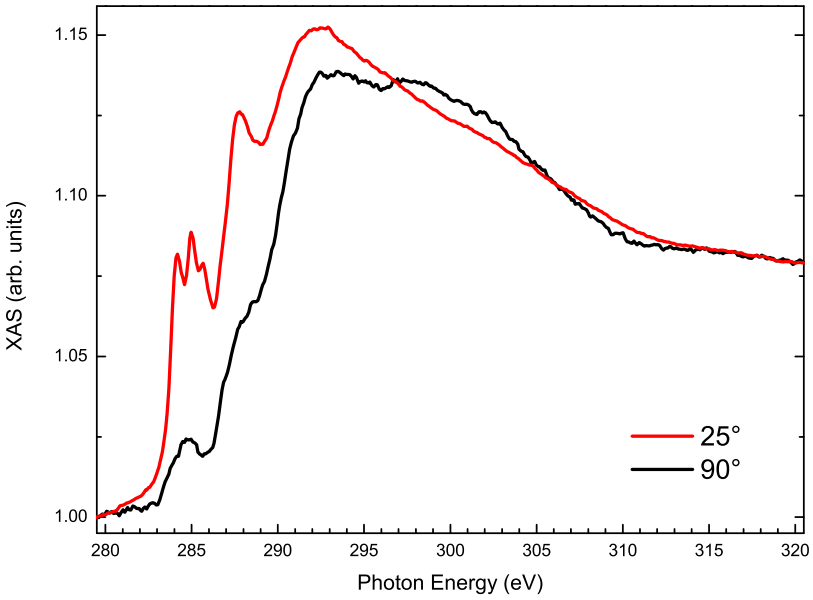

Figure 37: C K XA spectra of 0.7 ML CoOEP on graphene/Ni/W(110) measured at 300 K with p-linearly polarized light and an angle of 25° (red line) and 90° (black line) between the X-ray wave vector and the surface.

edge XA spectra of CoOEP on graphene/Ni/W(110) and a theoretical C K edge XA spectrum of a free CoOEP molecule, calculated by StoBe cluster calculations by the collaborating group of Prof. Hermann [111], also have an overall similarity to a great extent. All this points towards a weak interaction between the CoOEP molecules and the substrate. Following the last comparison, it is feasible to assign the π^* resonances to excitations from C 1s levels from carbon atoms within the porphyrin macrocycle. On the contrary, the σ^* resonance with a maximum at 292.4 eV is primarily caused by excitations from C 1s levels from carbon atoms being part of the ethyl groups, which are directly bonded to the macrocycle. The angular dependence of the π^* resonances, still visible for measurements at normal incidence, matches to a near-out-of-plane orientation of the C π^* orbitals. The angular dependence of the σ^* resonance with a maximum at 292.4 eV is an indication that the ethyl end groups are not aligned in the molecular plane.

Angle-dependent N K edge XA measurements of 0.7 ML CoOEP on graphene/Ni, presented in Fig. 38, were recorded at angles of 20° (red line), 55° (blue line), and 90° (black line) between the surface and the incoming X-ray wave vector. The spectra feature a broad σ^* resonance with a maximum at 407.0 eV, which is more dominant at normal incidence, and two sharp resonances with maxima at 399.2 eV and 402.2 eV, being more visible at 20° grazing incidence. In the photon energy range up to 404.8 eV the shape of the spectral features is not fully identical for normal and 20° grazing incidence, similar as for CoOEP adsorbed on HOPG (see Fig. 26). Hence, the spectral contributions do not belong to the same probed molecular orbitals at these energies. Most likely, excitations at these energies into final state orbitals with π^* and σ^* like shape as for CoOEP in bulk are one explanation for this phenomenon.

The dependence of the measurement geometry on the N K edge spectra as well as

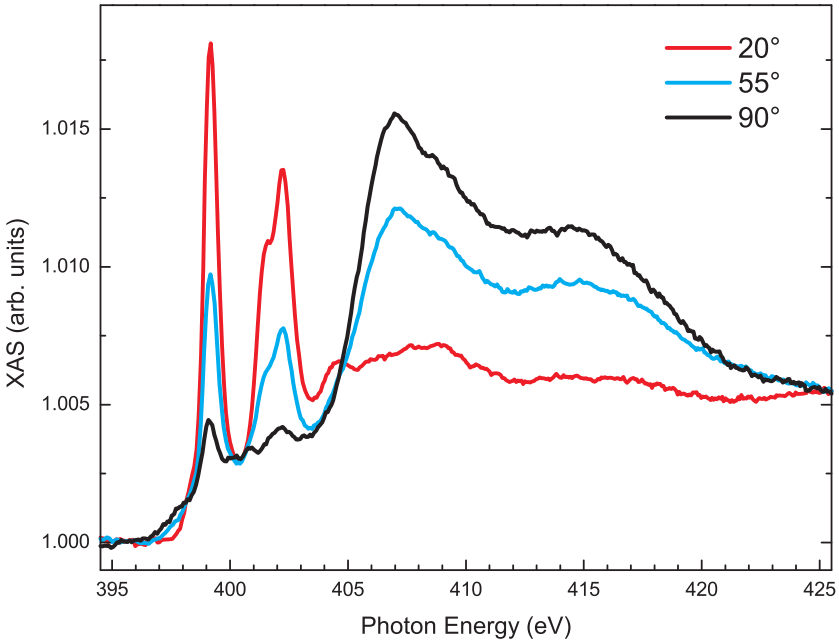

Figure 38: N K XA spectra of 0.7 ML CoOEP on graphene/26 ML Ni/W(110) measured at 300 K with p-linearly polarized light and an angle of 20° (red line), 55° (blue line), and 90° (black line) between the X-ray wave vector and the surface.

the above-mentioned angular dependence of the C K edge intensity fit to a flat adsorption of CoOEP. The intensity in the lower photon energy range for measurements under normal incidence at the N as well as at the C K edges can be explained, for instance, by a slightly buckled shape of the porphyrin macrocycle. The N K edge XA spectrum taken at the magic angle of incidence for p-linearly polarized X rays (55°, blue line), for which the dependence on the orientations of the molecular orbitals cancels out, closely resembles the N K XA spectrum of a polycrystalline bulk sample shown in Fig. 24. This indicates again a weak interaction between the CoOEP molecules and the substrate.

In our recent work [139], DFT+U calculations, including VdW corrections, of a Co porphyin molecule on a graphene-covered Ni stack with a tickness of 3 ML, have been carried out by the collaborating group of Prof. Oppeneer to shed light on the adsorption geometry and characteristics of the adsorbate. The molecule is computed to adsorb in planar geometry, with a slight bending of the macrocyclic rings towards the surface. This is consistent with the presented results of angle-dependent XA measurements. Further the Ni-graphene distance is 2.03 Å, while the graphene-metal ion distance amounts to 3.26 Å. This last distance fits to a physisorption of the molecules, conversely to a value of slightly more than 2 Å for chemisorbed metalloporphyrin on a metallic substrate [129]. This theoretical result is in agreement with the experimental findings.

For a study of the electronic and, in particular, the magnetic properties of the active center of the molecules, a helicity-averaged Co $L_{2,3}$ XA spectrum, taken with circularly polarized light, is shown in Fig. 39 (a) together with the corresponding Co $L_{2,3}$ XMCD spectrum (b). The spectra are taken at 20° grazing incidence in

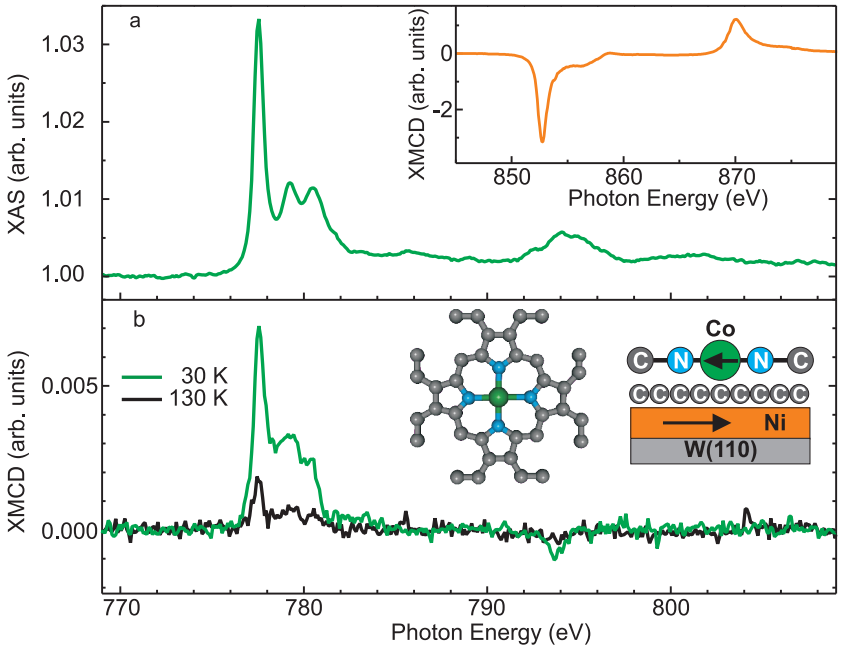

Figure 39: Co $L_{2,3}$ XAS (a) and XMCD (b) spectra of 0.7 ML CoOEP on graphene/26 ML Ni/W(110) measured at 70° grazing incidence at 30 K (green lines) and 130 K (black line). Insets: (a) XMCD spectrum at the Ni $L_{2,3}$ edges (orange line) at 130 K showing opposite sign at the L_3 and the L_2 edges compared to the Co XMCD spectrum. (b) Schematic top view of CoOEP molecule and side view of the sample, where green, blue, and grey balls represent cobalt, nitrogen, and carbon atoms, respectively, and hydrogen atoms are omitted.

remanence of the Ni film with a thickness of 26 ML, possessing an in-plane easy magnetization axis along the Ni [$\bar{1}$10] direction [156]. The unexpected detection of a finite Co XMCD signal demonstrates on the one hand a net 3d magnetic moment localized on the Co ions and on the other hand an unsuspected magnetic coupling between the magnetization of the Ni layer and these Co moments, stabilizing them against thermal fluctuations. The Co XA as well as the XMCD spectra exhibit a particular finestructure at the Co L_3 edge, which features a maximum at 777.5 eV for both the XA and the XMCD spectra. A comparison to angle-dependent Co XA spectra of thin ordered CoOEP layers, shown in section 3.2, and to angle-dependent Co XMCD measurements of thin ordered CoPc molecules [112], which contain Co ions in a very similar chemical environment as CoOEP, reveals a d^7 low-spin state of Co ions. The Co XMCD spectrum in Fig. 39 exhibits a positive excursion at the Co L_3 edge between about 777 and 781 eV, while its integrated signal is approximately by a factor of 4.1 larger at 30 K than at 130 K. At the Co L_2 edge at around 793.5 eV just a tiny negative XMCD signal is detected at the lower temperature. The Ni XMCD signal of the ferromagnetic film underneath the graphene, which is displayed in the inset of Fig. 39 (a), has an opposite sign compared to the Co XMCD signal. This reveals an antiparallel alignment of the Ni and the Co magnetization.

By applying the XMCD orbital and spin sum rules [49, 50] to the Co XMCD spectrum recorded at 30 K, orbital $m_L(0°)$ and effective spin $m_S^{eff}(0°)$ moments of

$-(0.51\pm0.05)\ \mu_B$ and $-(0.87\pm0.05)\ \mu_B$, respectively, are detected. These values represent lower limits, since the Co magnetic moments are subject to thermal fluctuations at finite temperatures. The in-plane magnetization direction of the thin ferromagnetic film aligns the Co magnetic moments accordingly. Thus the Co magnetization lies in-plane and is 20° off the wavevector of the X rays. This is considered when applying the sum rules. Usually, in local low-symmetry environments, a crystal field quenches the angular momentum [148], which, however, can be recreated by spin-orbit interaction [69], as discussed in section 1.8. The contribution of the orbital to the entire Co magnetic moment, which is here exceptionally large, is analysed in detail in section 3.4.2, where a more elaborate explanation is provided. The effective spin magnetic moment matches to a low-spin S=1/2 configuration of the Co ions.

Next, the coupling energy E_{ex} between the Co magnetic spin moment and the substrate magnetic moments is evaluated. The theoretical model used for its determination is based on the temperature dependence of the Ni and the Co magnetization and has been applied to similar systems before [35, 127]. Fig. 40 displays Co and Ni L_3 XMCD signals (squares and cycles), respectively, normalized to their extrapolated saturation values and plotted vs. the temperature. It is obvious that the temperature progression of these relative Co and Ni magnetizations ($M_r^{\mathrm{Co}}(T), M_r^{\mathrm{Ni}}(T)$) differs. Not only the experimental data are presented, but also a theoretically modeled temperature dependence of the respective magnetizations (green and orange lines). The progression of the relative Co magnetization $M_r^{\mathrm{Co}}(T) = M^{\mathrm{Co}}(T)/M_0^{\mathrm{Co}}$ with temperature has been modeled by treating its behavior like the one of a paramagnetic moment within an external field, where the latter simulates the magnetic coupling to the substrate.

The relation between the average and saturation magnetization of a paramagnet is given by the Brillouin function $B_J(\alpha)$ as explained in section 3.3.2. Within the scope of a mean field approach [157] the magnetic coupling of the adsorbate to the substrate is incorporated as an effective magnetic field B_{eff}, acting on the Co magnetic moments. The correlation of the thermal fluctuations of the substrate and adsorbate magnetic moments determines how the temperature dependence of the substrate is taken into account. Under the assumption that the fluctuations are strongly correlated, the magnetic moments of the film and the molecules are pinned to each other regarding their movement. In that case, the effective field B_{eff} is proportional to the substrate magnetization, since it is always experienced by the Co ions and can be written as $\gamma\mu_0 M_0^{\mathrm{sub}}$. Thereby γ presents the molecular field constant. A lower substrate magnetization at higher temperatures enters as a prefactor into the formula, while $g\mu_B J$ stands for the adsorbate magnetic moment μ_{ad}:

$$M^{\mathrm{ad}}(T) = M_0^{\mathrm{ad}}\frac{M^{\mathrm{sub}}(T)}{M_0^{\mathrm{sub}}}B_J(\frac{\gamma\mu_0\mu_{\mathrm{ad}}M_0^{\mathrm{sub}}}{k_BT}) \rightarrow M_r^{\mathrm{ad}}(T) = M_r^{\mathrm{sub}}(T)B_J(\frac{E_{ex}}{k_BT}). \quad (32)$$

Thereby $\gamma\mu_0\mu_{ad}M_0^{\mathrm{sub}}$ can be interpreted as the coupling energy E_{ex}. Assuming that the fluctuations of the substrate and the adsorbate magnetic moments are not correlated, only a time-averaged magnetic moment of the substrate acts on the adsorbate magnetic moment. Under this assumption, the effective field B_{eff} enters as $\gamma\mu_0 M^{sub}(T)$ into the model:

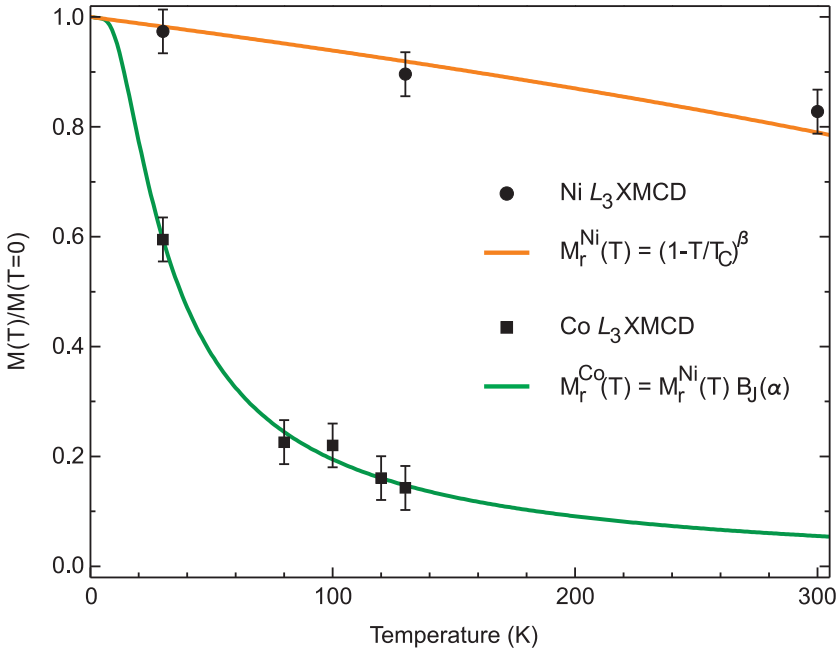

Figure 40: Temperature dependence of Co XMCD (squares: experimental data; green full line: fit of Brillouin-type model) and Ni XMCD (cycles: experimental data; orange full line: $(1-T/T_C)^{\beta}$ with $T_C = 630$ K and β =0.365) for 0.7 ML CoOEP on graphene/Ni/W(110).

$$M^{\mathrm{ad}}(T) = M_0^{\mathrm{ad}} B_J\left(\frac{\gamma\mu_0\mu_{ad} M_0^{\mathrm{sub}} \frac{M^{\mathrm{sub}}(T)}{M_0^{\mathrm{sub}}}}{k_B T}\right) \rightarrow M_r^{\mathrm{ad}}(T) = B_J\left(\frac{E_{ex} M_r^{\mathrm{sub}}(T)}{k_B T}\right) \qquad (33)$$

Coming back to the system under study, the Co magnetization experimentally obtained as a function of temperature can be fitted to both models. The Co saturation magnetization and the coupling energy E_{ex}, which is assumed to be temperature-independent, are used as fitting parameters. Thereby the Ni magnetization is approximated by a $(1 - T/T_C)^{\beta}$ law, with a Curie temperature of $T_C = 630$ and a critical exponent $\beta = 0.365$ [158]. The latter two values fit in fact to a description of a Ni bulk sample and reveal, regarding these parameters, a rather three-dimensional magnetic behavior of the Ni film with a thickness of about 26 ML. In any case, a completely correct theoretical simulation of the substrate magnetization at temperatures much lower than T_C would require to take into account, among other things, spin waves [157]. However, for a phenomenological discription the chosen model is accurate enough and reproduces the experimental results.

As an exchange field acts only directly on the spin, $J = 1/2$ and a Landé factor of g = 2 are assumed in the following. The detection of an orbital moment is a result of spin-orbit coupling which indirectly aligns the orbital magnetic moment [159]. The fit yields $E_{ex} = (1.8 \pm 0.5)$ meV for data acquired at temperatures between 30 and 130 K in the case of strongly correlated fluctuations of the adsorbate and substrate magnetization. For un-correlated fluctuations a value of E_{ex} is obtained which differs just by 1%. Also a non distinguishable functional behavior of the Co magnetization is observed. Hence, it can not be stated from the experimental data

which model is more suitable. Nevertheless, it can be expected that the adsorbate–substrate magnetizations are pinned to each other, implying a coupling that works on a faster time scale than the respective fluctuations. This corresponds to the first mentioned model, for which the relative Co magnetization is shown in Fig. 40. As opposed to metalloporphyrins adsorbed directly on reactive ferromagnetic substrates, the strength of the magnetic coupling across the graphene layer is comparatively small [35, 127].

Hereafter, the electronic interaction between the Co $3d$ orbitals and the graphene-protected Ni surface is investigated in more detail. To do so, Fig. 41 displays isotropic Co L_3 XA spectra, measured with p-linearly polarized light, of a CoOEP polycrystalline bulk sample (green line) and of 0.6 ML and 0.7 ML of CoOEP molecules adsorbed on graphene/Ni/W(110) (blue line) and Ni/Cu(100) (brown line), respectively. The samples of adsorbed CoOEP in the submonolayer regime are measured at 55° grazing incidence, while the one of the bulk material is recorded at normal incidence. The spectra are vertically offset and the main maximum of each spectrum is scaled on each other, in order to simplify a direct comparison. Three peaks at photon energies of 777.5, 779.2, and 780.4 eV are building up the fine structure of the Co L_3 edge for the bulk sample as well as for CoOEP on graphene/Ni/W(110). By means of this line shape, a +2 valency and a d^7 low-spin state of the Co ions is revealed by comparison to literature [110]. The conspicuous similarity of the two XA spectra evidences a negligible interaction of the Co $3d$ electronic states and the graphene-protected Ni surface. Conversely, CoOEP molecules adsorbed on a bare Ni surface exhibit a thoroughly changed Co L_3 XA spectrum in comparison to the one of the bulk sample. Here, the fine structure at the Co L_3 edge features a main peak at 779.7 eV and a shoulder at 777.6 eV. The multiplet structure is contracted compared to the polycrystaliine bulk sample, which unambiguously reveals a change of the Co electronic structure [113] upon the adsorption of the molecules on the bare Ni substrate. Electronic states of the reactive ferromagnetic substrate hybridize with molecular states for CoOEP on Ni/Cu(100), as shown in section 3.3.3. On the contrary, no covalent bonds between the surface and the adsorbate are formed on the graphene-protected Ni films. Nevertheless, in the latter case an antiferromagnetic coupling between the Ni substrate and the Co ions is established.

By means of DFT+U calculations performed by the collaborating group of Prof. Oppeneer and published in our lately work [139], insight can be obtained into the mechanism and the path of the unexpected exchange coupling from the Ni top layer to the Co metal center. The computation revealed also an antiparallel alignment between the substrate magnetization and the Co spins, as well as a d^7 low spin state of the metal ions, which is consistent with the experimental findings. Lately, investigations about graphene on Ni(111) have discussed six possible arrangements of the graphene atoms on a Ni(111) surface [97–101]. The four most prominent ones are named as the bridge-top, fcc-hcp, top-hcp, and top-fcc configurations, and are introduced in section 2.6. For these four configurations, among which the bridge-top one had been favored by DFT calculations [98, 102], geometrical optimizations and ab initio calculations of the molecule–substrate exchange interaction were performed.

It turned out that only the hcp-fcc and bridge-top adsorption geometry reproduce the antiferromagnetic coupling between the Co spins and the Ni magnetization, while the other two lead to a coupling of ferromagnetic nature. Moreover, the bridge-top

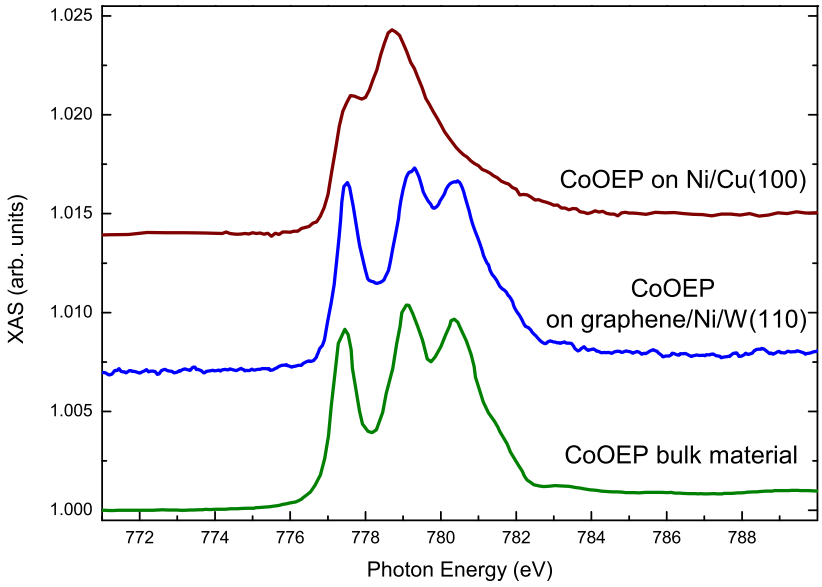

Figure 41: Co L_3 XA spectra of CoOEP bulk material (green line), of 0.7 ML CoOEP on graphene/Ni/W(110) (blue line), both measured at 300 K, and of 0.6 ML CoOEP on Ni/Cu(100) (brown line), recorded at 100 K. The spectra are taken with p-linearly polarized light at normal incidence for the bulk material, and at 55° grazing incidence for CoOEP on graphene/Ni/W(110) as well as on Ni/Cu(100). The main maximum of the spectra of the bulk and CoOEP/Ni sample are scaled to the one of the spectrum of the CoOEP/graphene/Ni sample, respectively, for comparison. The spectra are vertically offset for clarity.

configuration reveals the smallest computed total energy. Therefore the bridge-top geometry can be assumed to be the right one for CoOEP on graphene/Ni and its results are further analyzed in the following. A small negative net spin density on graphene of $-0.001\ \mu_B$ per carbon atom was found, antiparallel to that of the Ni, which is induced through hybridization of spin-minority Ni d with graphene p orbitals. The π-bond between two carbon neighbor atoms is just directly located above an atom of the first Ni layer. The upper and lower π-bond lobe show a negative and positive magnetization density, respectively. Additionally, a small spin polarization sits on the pyrrolic nitrogen atoms of $+0.015\ \mu_B$, being parallel to the Ni magnetization. On the Co center of the molecules a negative magnetization density with a d_{z^2}-type shape is found.

Being interested now in the exchange path, also the electronic interaction of the porphyrin molecules with the substrate and in particular the amount of spatial overlap of the short-ranged Co $3d$ and the macrocyclic π with the graphene p_z orbitals is of relevance. It turned out that the latter is small and the former even negligible, which fits to the experimental finding of an identical isotropic Co L_3 XA spectrum for CoOEP on graphene/Ni and in a polycrystalline bulk sample within the measurement precision. This excludes a magnetic exchange interaction between the Ni film and the Co ions mediated directly via the graphene. Much more, the calculations uncover a

weak superexchange interaction between the spin polarization of the Ni top layer and the pyrrolic nitrogen atoms conveyed by the graphene. The second component of the exchange path is a direct antiferromagnetic coupling between the spins on Co ions and the N atoms inside the macrocycle.

DFT calculations concerning the magnetism of organometallic complexes on a graphene sheet have been carried out [145], but without a stabilization mechanism for the magnetic moments, leading to a paramagnetic behaviour of the system [160]. For a graphene sheet sandwiched by pure metal layers magnetism was predicted, too, while an experimental validation has not been reported yet [161]. For the system studied within this section, the graphene layer hinders the formation of covalent bonds between the molecules and the reactive Ni film, passivating the ferromagnetic surface [162]. The advantage of an adsorbate electronically decoupled from the surface allows to obtain a molecular design independently of the interaction between the substrate and the molecules. Nevertheless, a coupling mechanism via the carbon atoms of the graphene layer is established between the molecules and the substrate. This is an essential ingredient for the use of paramagnetic molecules as building blocks of a molecular spin electronics. On the contrary, for metalloporphyrins in contact with bare and oxygen-covered magnetic substrates, a formation of covalent bonds is necessary for generating a magnetic exchange coupling [34, 35, 126]. Our result encourages the pursuit of spin-electronic devices such as spin qubits or spin field-effect transistors by assembling planar para- magnetic molecules wired by graphene on a surface. Electronic transport through the molecules or switching their magnetic properties, for example, could be accomplished by taking advantage of the empty sixth coordination place.

Recapitulating, a magnetic coupling across graphene, between the Co ions of CoOEP and a Ni film, is for the first time observed, in spite of the physisorption of the molecules on the substrate. The molecules adsorb flat on the graphene with a slightly buckled shape of their macrocycle. The π systemes of the graphene sheet and the porphyrin macrocycle mediate an antiferromagnetic coupling between the half-filled d_{z^2}-like orbital of the Co ions and the Ni surface. The perspective of joining a substrate-induced spin polarization and a weak electronic interaction opens a new toolbox for organic spin-electronic applications allowing the design of molecular functionalities without the necessity of considering substrate interactions.

3.4.2 Huge and highly anisotropic orbital moments

In the previous section it was shown that the adsorption of CoOEP on graphene-protected Ni films leads to a substrate-induced spin-polatization of the Co magnetization. Thereby a lower limit of the in-plane Co orbital moment of $(0.51 \pm 0.05)\mu_B$ was found. In order to determine more precisely the contribution of the orbital moment to the Co magnetization, angle- and field-dependent XMCD measurements of CoOEP adsorbed on graphene/Ni/W are presented in this section.

Fig. 42 displays Co $L_{2,3}$ helicity-averaged XA spectra (a) and the corresponding XMCD spectra (b) of 0.8 ML of CoOEP on graphene/25 ML Ni/W(110), taken at 4.5 K in an external magnetic field applied along the corresponding X-ray incidence direction. Spectra recorded at 25° and 35° grazing and at 90° normal incidence are presented. The Co XA and XMCD spectra feature a line shape qualitatively identical

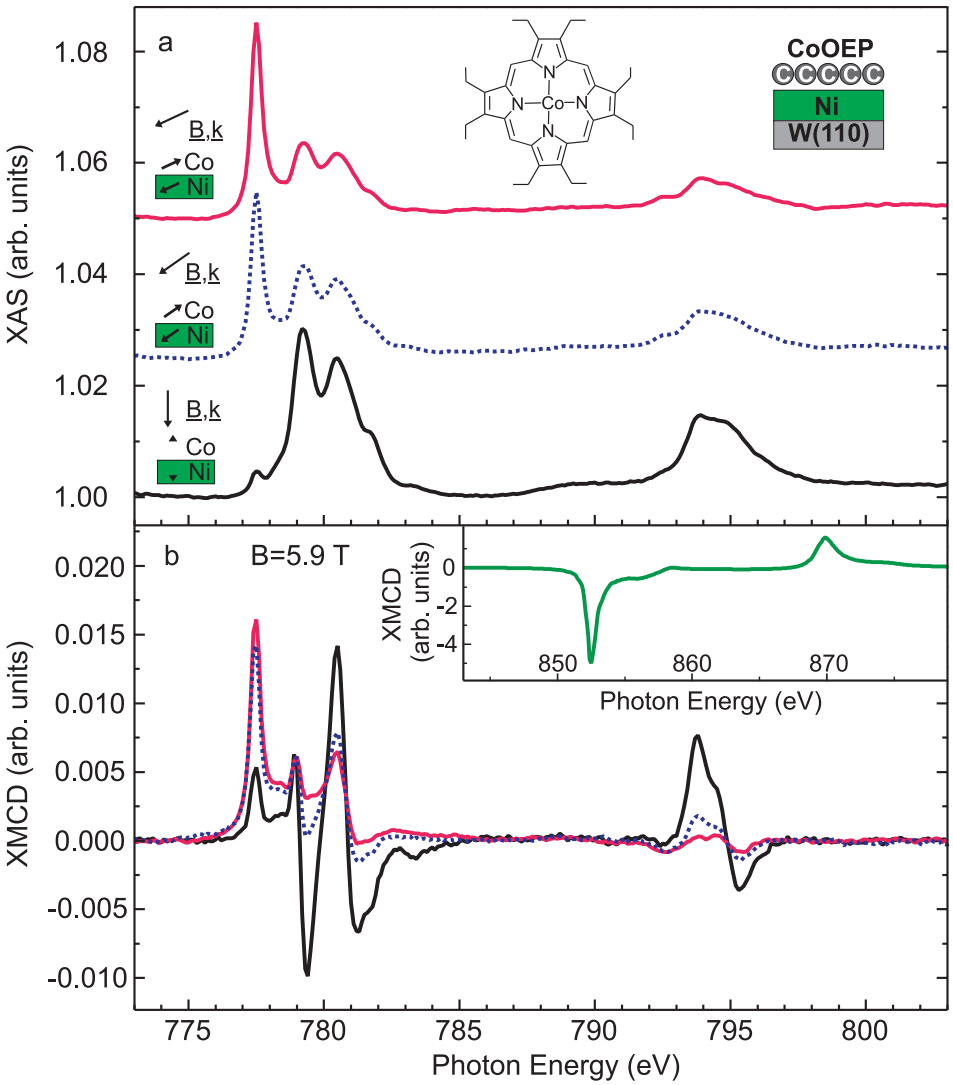

Figure 42: Co $L_{2,3}$ helicity-averaged XA spectra (a) and corresponding XMCD spectra (b) of 0.8 ML CoOEP on graphene/25 ML Ni/W(110) measured with circularly polarized light at 4.5 K in a magnetic field of B = 5.9 T applied along the X-ray incidence direction. Spectra taken at 25° (pink lines) and 35° (blue dashed lines) grazing and at normal (dark lines) incidence are shown. The Co XA spectra are shifted vertically for clarity. Insets: (a) Schematic top view of CoOEP molecule and side view of the sample. (b) XMCD spectrum at the Ni $L_{2,3}$ edges recorded at 35° grazing incidence.

to the ones presented in section 3.4.1. The XA spectra exhibit a detailed fine structure at the L_3 edge, which possesses a pronounced angular dependence. A narrow sharp peak at a photon energy of 775.5 eV is more prominent at 25° grazing incidence and thus belongs to excitations into out-of-plane orbitals. The other, energetically higher-lying peaks, are more apparent in the spectrum taken at normal incidence and originate therefore from excitations into states with in-plane hole density. DFT+U calculations revealed three holes within the 3d orbitals for the adsorbed CoOEP [139], with the energetically highest b_{1g} ($d_{x^2-y^2}$) orbital being empty and an a_{1g} (d_{z^2}) like orbital half filled. Such, the energetic position between the components building up the L_3 edge and their angular dependence are in agreement with the orbital occupation as obtained from computations. The Co $L_{2,3}$ XA spectrum, measured under the magic angle of 35° grazing incidence for circularly polarized X rays, at which the dependence on the orientation of the molecular orbitals cancels out, represents thus the isotropic spectrum.

The corresponding isotropic Co L_3 XMCD spectrum features a main positive peak at 777.5 eV and two local positive maxima at higher photon energies of 779.0 and 780.5 eV. Its signal obtained by integrating over the whole L_3 edge has the opposite sign than the one of the isotropic Ni L_3 XMCD spectrum of the ferromagnetic film underneath the graphene, shown in the inset of Fig. 42 (b). This reveals an antiferromagnetic coupling between the magnetization of the substrate and the magnetic moments at the Co site stronger than the Zeeman interaction. The Co L_3 XMCD possesses an angle-dependent line shape, too, which is characteristic for a cobalt d^7 low-spin system with such a crystal field as for CoOEP on graphene/Ni [88, 112, 138]. At 25° grazing incidence, the energetically lowest-lying peak at 775.5 eV is most pronounced, and at normal incidence the feature at 780.5 eV is the most prominent, while zero-crossings lead in this case to a fine structure with a double dip shape. The integrated Co L_2 edge XMCD signal reveals even a sign change as a function of angle. The distribution of the spin density, being correlated to the distribution of the unpaired electron density, explains the exceptional Co XMCD signal and, in particular, the one measured at normal incidence. The presence of the Co XMCD signal stems from density of unpaired 3d holes, which has mainly an out-of-plane distribution, while, to the contrary, the in-plane unoccupied density of states is probed by the measurement under normal incidence.

In order to gain insight into the alignment direction of the Co magnetic moments within the exchange-coupled system, the effect of the external magnetic field applied along different directions on the magnetization of the ferromagnetic film has to be considered as well. Regarding this, Fig. 43 displays helicity-averaged Ni $L_{2,3}$ XA (a and b) and corresponding XMCD (c and d) spectra of the Ni film underneath the graphene, recorded at 4.5 K with circulary polarized light at normal and 35° grazing incidence, respectively. The spectra are from the same sample as the ones in Fig. 42 and are recorded in an external magnetic field of 2 T (full cyan and dashed orange lines) and 5.9 T (dashed blue and full black lines) applied along the wavevector of the incoming X rays. The existence of a Ni XMCD at both measurement geometries reveals an alignment of the Ni magnetization into the direction of the applied magnetic field.

The Ni XA spectra exhibit a minor difference in their line shape at the two detection angles, which reflects an anisotropic hole density due to the reduced symmetry at the

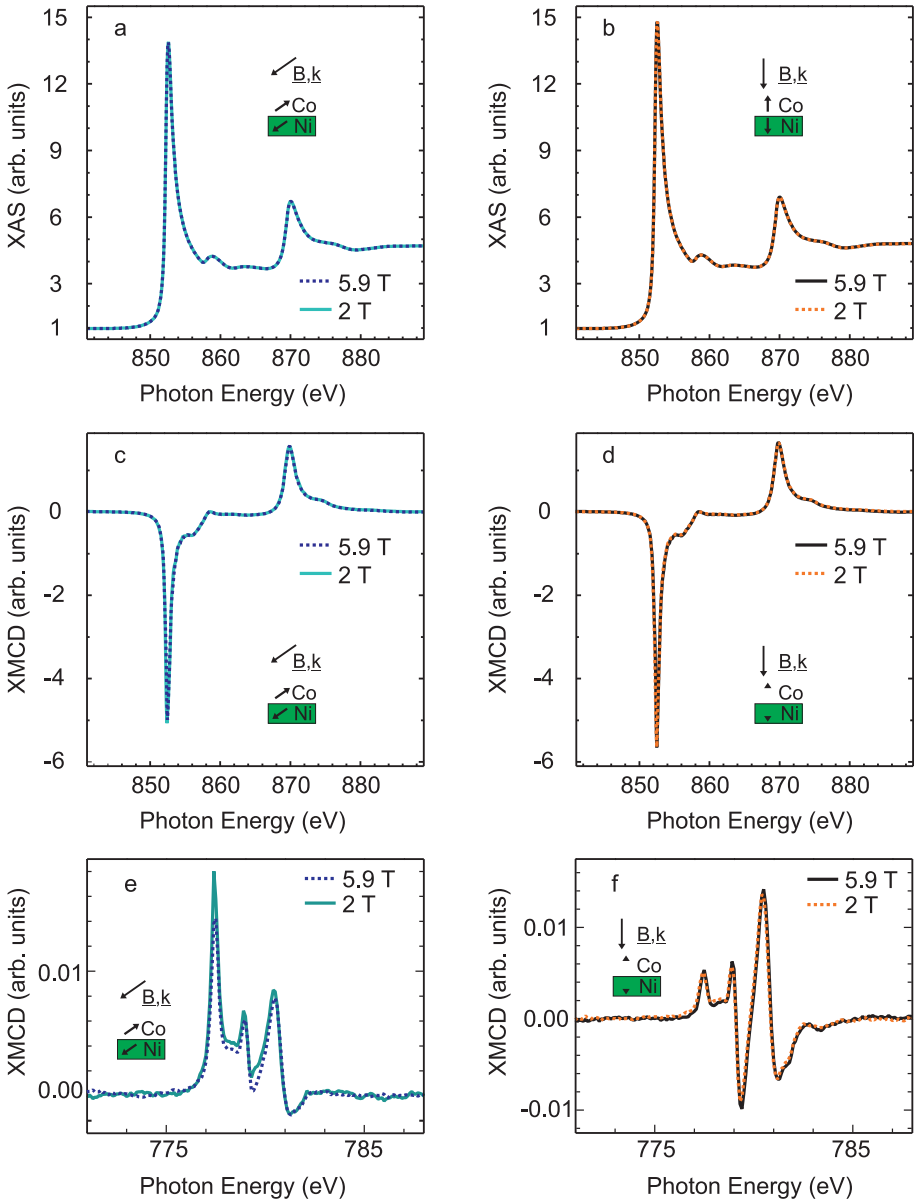

Figure 43: Ni $L_{2,3}$ XAS (a and b) and corresponding XMCD (c and d) spectra as well as Co L_3 XMCD spectra (e and f) of 0.8 ML CoOEP on graphene/25 ML Ni/W(110), recorded at 35° grazing (a, c, and e) and normal (b, d, and f) incidence, respectively. The spectra are taken at 4.5 K in an external magnetic field of 2 T (cyan and dashed orange lines) and 5.9 T (dashed blue and dark lines) applied along the wavevector of the incoming X rays.

Ni-graphene interface. A strain-induced change of the crystal field within the thin film opposed to bulk might play a role, too, but the in-plane film stress is already small for a 2 ML thick Ni film deposited on W(110) [163]. The line shape of the Ni XMCD spectra recorded at different incident angles are not exactly the same. An explanation might come from an anisotropic orbital moment as well as the anisotropically occupied Ni 3*d* states generating an anisotropic spin density at the Ni site [46]. At both detection angles, the size of the Ni XMCD is identical for the two different sizes of the external magnetic field. This proves a virtually fully aligned substrate magnetization at all chosen measurement conditions. The rotation of the Ni magnetization into the direction of the applied magnetic field modifies correspondingly the alignment of the antiferromagnetically coupled Co magnetization.

For the purpose of working out the competition between the Zeemann interaction of CoOEP and the antiferromagnetic exchange to the substrate, Fig. 43 displays also Co L_3 XMCD spectra, which were measured at 35° grazing (e) and normal (f) incidence, respectively, in an external magnetic field of 2 T (cyano and dashed orange lines) and 5.9 T applied along the wavevector of the incoming X rays at 4.5 K. Evidently the Co XMCD signals do not coincide in size at grazing, but at normal incidence. This reveals that in the latter case the Co magnetization is equally aligned at the two field strengths. On the contrary, at grazing incidence the counteraction of the applied magnetic field against the antiferromagnetic coupling between the Co spins and the magnetization of the Ni films is sufficiently large at 5.9 T to diminish the Co magnetization by $(17 \pm 2)\%$.

Referring to the line shape of the angle-dependent Co XAS and XMCD spectra, a comparison to results from Co phthalocyanine bulk measurements [112] allows to conclude that the spin-orbit coupling mixes the ground state and the first excited state of the electronic structure of the Co ions. This results in a non-vanishing hole density at the e_g orbital and a more than half filled a_{1g} orbital, and thus creates an in-plane orbital moment [69], as discussed in section 1.8.

An evaluation of the orbital and the spin moment can be carried out by applying the XMCD sum rules to the angle-dependent Co XMCD spectra shown in Fig. 42 (b). To this end, the integrated helicity-averaged Co XA spectrum taken at 35° grazing incidence is used as isotropic intensity, the decrease of the Co magnetization by the applied magnetic field is taken into account, as shown in Fig. 43 (e), and three holes within the Co 3*d* orbitals are presumed. For flatly adsorbed molecules and an angle of incidence α between the wave vector of the X rays and the surface plane, the orbital moment experimentally measured is composed of two angle-dependent components. To do so, a fourfold rotational symmetry of the molecules is assumed, which leads to a uniaxial anisotropy along the surface normal [52]:

$$m_L(\alpha) = m_L^z \sin^2(\alpha) + m_L^{xy} \cos^2(\alpha), \tag{34}$$

where m_L^z is the orbital moment in the direction of the z axis and m_L^{xy} the average in the x-y plane, respectively. The effective spin moment contains two contributions [135]. They are the intra-atomic spin dipole moment -7$m_T(\alpha)$ and the spin moment m_S (see Eqs. 29). The former comes from an anisotropic spatial distribution of the spin density, as discussed in section 3.3.2. The sample geometry implies that $(m_T^z + 2m_T^{xy}) = 0$.

The magnetic moments evaluated from the sum rules are presented in table 5 as a function of α. For measurements recorded at the magic angle, $m_S^{\text{eff}}(35°) =$

α	$m_L(\alpha)/\mu_B$	$m_S^{\text{eff}}(\alpha)/\mu_B$
25°	$-(0.80 \pm 0.07)$	$-(1.37 \pm 0.10)$
35°	$-(0.69 \pm 0.06)$	$-(1.00 \pm 0.07)$
90°	$-(0.19 \pm 0.05)$	$+(0.34 \pm 0.05)$

Table 5: Experimental expectation values of the orbital magnetic moment and the effective spin moment derived from sum-rule analysis for 0.8 ML CoOEP on graphene/25 ML Ni/W(110) as a function of angle α.

$-(1.00 \pm 0.07)$ μ_B is found, as expected for an $S = 1/2$ system in saturation. A value of $m_S^{\text{eff}}(25°) = -(1.37 \pm 0.10)$ μ_B and an even opposite sign for $m_S^{\text{eff}}(90°) = +(0.34 \pm 0.05)$ μ_B are obtained. Also the orbital moment exhibits a pronounced angular dependence. The moment experimetally determined at normal incidence of $m_L(90°) = -(0.19 \pm 0.05)\mu_B$ is much smaller than the ones measured at grazing incidence: $m_L(35°) = -(0.69 \pm 0.06)$ μ_B and $m_L(25°) = -(0.80 \pm 0.07)$ μ_B. All the magnetic moments experimentally obtained are shown in Fig. 44 as a function of α , combined with fits to these results following Eqs. 29 and 34.

The free parameters of the fits are m_L^z, m_L^{xy}, m_S, and $m_T(90°)$. The results are summarized together with the orbital to spin moment ratio m_L^{xy}/m_S for an in-plane magnetization in table 6. The value of $-(0.19 \pm 0.05)\mu_B$ for the out-of-plane orbital moment m_L^z is much smaller than the in-plane orbital moment $m_L^{xy} = -(0.93 \pm 0.07)\mu_B$, which means an exceptionally large orbital moment anisotropy of 489%. Orbital magnetism of metallophthalocyanines on surfaces has already been studied, while an anisotropy of m_L in size of 500% was observed, but just for MPc molecules on non-magnetic substrates and with much lower absolute values of up to 0.20 μ_B for m_L. Moreover, as a result of the fits, a spin moment of $-(1.03 \pm 0.07)$ comes out, which is in agreement with the $S = 1/2$ spin state of the Co ions. Thus, the highest ever found ratio $m_L^{xy}/m_S = 0.90$ in $3d$ complexes and compounds is observed, despite the hybridization of Co $3d$ with molecular orbitals, which is necessary for the magnetic coupling between the Co orbital moments and the Ni magnetization. In literature, a value of $m_L^{xy}/m_S = 0.83$ was reported for an ordered FePc bulk sample [135], but with lower values of 0.64 μ_B for the spin moment and 0.53 μ_B for the in-plane orbital moment. The explanation for the huge in-plane orbital moment for the CoOEP molecules adsorbed on graphene/Ni is provided by the almost degenerate e_{g} and $a_{1\text{g}}$ states. Spin-orbit coupling admixes them and creates a new state with an anisotropic orbital momentum and a huge in-plane orbital moment [69]. Treating the spin-orbit coupling as a second order perturbation effect, the in-plane orbital moment thereby recreated is inversely proportinal to the energetic separation between the two states, as discussed in section 1.8.

m_L^z/μ_B	m_L^{xy}/μ_B	m_S/μ_B	$m_T(90°)/\mu_B$	m_L^{xy}/m_S
$-(0.19 \pm 0.05)$	$-(0.93 \pm 0.07)$	$-(1.03 \pm 0.07)$	(0.20 ± 0.05)	0.90

Table 6: Values of m_L^z, m_L^{xy}, m_S, and $m_T(90°)$ received from the fit of the XMCD sum rule results to Eqs. 29 and 34, and the calculated orbital to spin moment ratio for a Co in-plane magnetization.

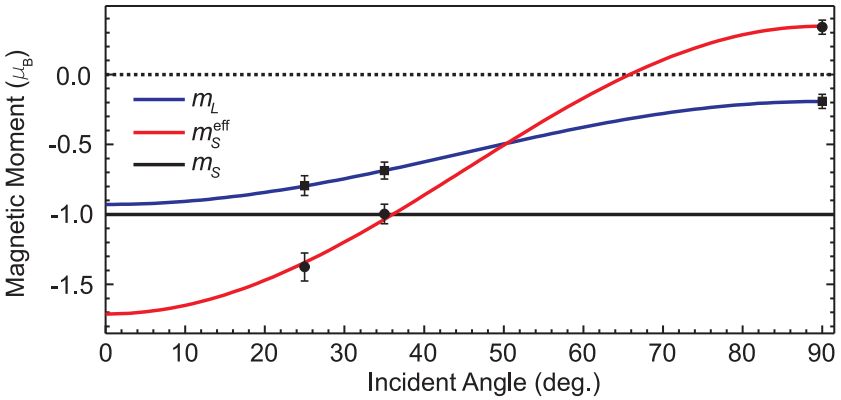

Figure 44: Angle dependence of the experimental expectation values of the orbital magnetic moment m_L (squares) and the effective spin moment m_S^{eff} (circles), shown together with fits to these results following Eqs. 34 (blue line) and 29 (red line). Also m_S is displayed (black line).

The fit further yields a value of $(0.20 \pm 0.05)\ \mu_B$ for $m_T(90°)$, which is an unusually big value. This extraordinarily large anisotropy of the intra-atomic dipole contribution within this low-symmetry system elucidates the sign change of the effective spin moment as a function of angle. Theoretically it has been predicted that this occurs for an unpaired hole in the d_{z^2} orbital [46], which fits to the DFT+U calculations of the group of Prof. Oppeneer, published in our recent work [139]. Nevertheless, experimental verification of such a sign change does not exist in literature so far.

An even higher absolute value of 0.26 μ_B was found for $m_T(90°)$ in the case of 1 ML CuPc adsorbed on Ag(100) [125] and an absolute value of $(0.16 \pm 0.00)\ \mu_B$ for CoOEP in contact with a Cu(100) surface, as shown in section 3.3.2. However, in both cases the intra-atomic spin dipole moment leads to a bigger absolute value of $m_S^{\text{eff}}(90°)$ than m_S, as in these cases the unpaired holes are located in in-plane orbitals. Then $m_T(0°)$ is too small to inverse the sign of $m_S^{\text{eff}}(0°)$ as opposed to m_S. For that reason no sign change as a function of angle of the effective spin moment was observed in these systems.

A non-zero value of $m_T(\alpha)$ is based on an anisotropic spin density. Generally, this effect is quite weak in the bulk, but in low-symmetry environments directional bonds or crystal fields can produce an inhomogeneous spatial distribution of the spin density from unpaired $3d$ electrons over the atomic unit cell [46]. It may be even present in systems with O_h symmetry such as it is the case for first row transition metals in bulk [164]. This is because an interplay between spin-orbit coupling and crystal field effects can induce an atomic spin density which does not follow exactly the atomic charge density.

On the basis of the results from the sum rule analysis, the reduction of the Co magnetization at grazing incidence by applying an external magnetic field of 5.9 T instead of 2 T can be further analysed. An in-plane easy axis, as suggested by the anisotropy in size of the Co m_L, a result of the sum rules, and also reported for isolated CoPc, which presents a similar system [165], would lead to the opposite behavior. Assuming a lack of saturation in this case, the alignement of Co magnetic moments versus magnetic fields is always higher for an in-plane than for an out-of-plane pointing

Co magnetization. The same applies for different Zeemann energies in magnetic fields applied along different directions due to the anisotropy of the orbital moment. Such different Zeemann energies can not provide an explanation neither. The finding has to be explained by an orbitally-dependent exchange interaction between the Co and Ni spin moments that is magnetically anisotropic [166, 167]. This has already been reported for single molecular spins of Cu-tetraazaporphyrin molecules with 8 4-tert-butylphenyl substituents adsorbed on $Fe_3O_4(100)$ [168] and of $TbPc_2$ in direct contact with thin Ni films [38].

The unusual emergence of significant orbital magnetism in the context of molecular magnetism on surfaces, as found here for CoOEP on graphene/Ni/W(110) has so far not been reported in literature and expands the research field of magnetic molecules on substrates. The intrinsic source of magnetism in the case of an electron is its spin magnetic moment m_S, while its motion around the atomic nucleus is associated to the orbital magnetic moment m_L. While nature tries to maximizes m_S as well as m_L for free transition metals, crystal field effects and hybridization, a requirement for magnetic coupling, quench to a great extent m_L and may also reduce m_S due to the formation of low-spin states. In magnetic materials of $3d$ transition metals the main microscopic origin of the magnetization of an element are the spin moments, which order by an exchange interaction, and the microscopic origin of magnetic anisotopy is related to the anisotopy in size of the orbital moment. Interestingly, for the here presented system, m_L^{xy} and m_S are of the same order of magnitude for the Co ions. Since the CoOEP molecules are physisorbed on the graphene/Ni surface and the Co electronic structure is not changed upon adsorption, the large value of the m_L^{xy} for the Co ions presents an intrinsic property of CoOEP. This result motivates further studies regarding the magnetic anisotropy of pure CoOEP molecules or sytems containing weakly interacting CoOEP molecules.

Recapitulating, it has been demonstrated that the magnetism of CoOEP molecules adsorbed on a graphene-covered Ni surface features apparent anomalies. On the one hand the Co magnetic moments are stabilized against their thermal fluctuations by an antiferromagnetic exchange interaction between the Co spins and the substrate magnetization, which necessitates a hybridization of the Co $3d$ states with molecular orbitals. Generally such an interaction diminishes the contribution of m_L to the entire magnetic moment. Here, however, values of the same order of magnitude of $-(1.03 \pm 0.07)\ \mu_B$ and $-(0.93 \pm 0.05)\ \mu_B$ are found for the spin and orbital angular moments, respectively, for an in-plane-aligned Co magnetization. The Co orbital moment is recreated by SOC and reveals a giant anisotropy in size of 489%. Further, the indirect exchange interaction between the molecules and the ferromagnetic film is magnetically anisotropic. The almost out-of-plane density of unpaired holes at the Co site causes an extremely anisotropic spin density. This leads to an intra-atomic spin dipole moment, which surpasses the spin moment by a factor of 1.4 and induces a sign change of the effective spin moment as a function of angle.

3.5 Controlling the magnetization of adsorbed metalloporphyrins by small adsorbates

Metalloporphyrins and metallophthalocyanines consist of a metal ion surrounded by a planar tetradentate dianionic ligand, and two axial coordination sites being opposed situated to each other. Generally, the metal center behaves as a local reactive site due to its coordinatively unsaturated nature, which enables the control of its electronic and magnetic properties by external chemical stimuli. The interaction of MP molecules, and here in particular CoOEP molecules, with surfaces has been up to now the issue of the presented work. Among other things, this approach was inspired by the functionality of MP molecules in biological systems. In nature, for instance the protein hemoglobin, which contains as active group an Fe porphyrin, acts as carrier of oxygen in the bloodstream by adsorbing it within the lungs and desorbing it to tissues. XA studies about different metalloproteins in physiological solution have been already reported [169]. Also the application of phthalocyanines and porphyrins in gas sensors is based on the coordination of the corresponding molecule as axial ligand to the active centre inducing measurable changes of electronic properties [170, 171]. In the case that an axial ligand has already formed a coordination bond to the metal ion, a second one can still do so, while a competition between the ligands starts. The latter one withdraws electron density from the bond to the ligand in the opposite coordination site. Such a phenomenon is called trans effect in organic chemistry [172, 173].

By placing the molecules on top of a solid surface, they get immobilized as required for their use as molecular building blocks. By doing so, one of the axial coordination sites gets occupied by the substrate, while an electronic interaction between the surface and the adsorbate can modify the molecular properties, as discussed in general in section 3.3 and shown in detail for CoOEP adsorbed on HOPG, Cu(100), and Ni/Cu(100). Thereby the second axial coordination site of MPs and MPcs still remains free for additional ligands like, for instance, small molecules as carbon monoxide (CO), nitrogen monoxide (NO), oxygen molecules (O_2), or ammonia (NH_3). Taking advantage of that, these different chemical stimuli were used in order to coordinate to FePc adsorbed on a Au(111) surface [174–176]. While doing so, the FePc molecules get electronically decoupled from the substrate and the choice of the small adsorbate allows for tuning the extension of this effect. A change of the hybridization of molecular and substrate states is accompanied by an adsorbate-dependent spin state change. Such a process is called surface trans effect, where the surface–metal interaction is affected by another ligand, in analogous way to the trans effect. Even a reversible switching of the interaction with the substrate has been achieved by a subsequent thermal desorption of NO from Co, Fe, and Zn tetraphenylporphyrins (TTP) on Ag(111) [177, 178] and of CO from Mn phthalocyanines on Bi(110) [123].

The adsorption of paramagnetic metalorganic molecules on ferromagnetic surfaces is of special interest as shown in section 3.3.3 since thereby a magnetic exchange interaction between the adsorbate and the substrate can align the unpaired spin moments of metalloporphyrins, stabilizing them against thermal fluctuations. Regarding this, it was also demonstrated that by putting atomic oxygen as an intermediate layer between metalloporphyrins and ferromagnetic substrates, an antiferromagnetic coupling between the molecules and the surface can be established [35] and this even for

self-assembled molecules [179]. Only very recently, and correspondigly later than in refs. [138, 180], it has been observed by means of XMCD that such a spin polarization of central metal ions of MP and MPc molecules provoked by an interaction with ferromagnetic surfaces can be influenced by the gaseous ligands NH_3 and NO. So the coordination of NO to CoTPP/Ni, iron-tetraphenylporphyrin/Ni, and manganese-tetraphenylporphyrin/Co reduces the spin moments at the central metal site without destroying the magnetic order and reverses in the latter case even the sign of the exchange interaction. On the contrary, the adsorption of NH_3 on MnPc/Co sizeably increases the aligned magnetic spin moments of the Mn ions [59]. Apparently, also a tuning of such substrate-induced magnetic ordering in a reversible manner is desirable. It has been demonstrated that an attachment of NH_3 to nickel-tetraphenylporphyrin on Co films [181] and of NO to CoTTP on Ni films [40] together with a subsequent detachment of the small adsorbates leads to a reversible on-off and off-on switching of the molecular spins, respectively. Following the labeling above, these observations were called spin trans effect. However, within the last mentioned study, neither the issue of NO-induced modifications on the Co $L_{2,3}$ X-ray absorption (XA) spectra nor their reversibility have been unequivocally addressed.

This section presents new strategies to control at finite temperatures the magnetization of metalloporphyrins magnetically coupled to magnetic films by an attachment and a subsequent thermal detachment of small adsorbates. Three different systems, CoOEP adsorbed on graphene/Ni/W(110) as well as on oxygen-covered Ni films, grown on Cu(100), and FeOEP adsorbed on O/Co/Cu(100) are used as starting point in order to form nitrosyl and carbonyl complexes on the surface by dosing with NO and CO, respectively. Then thermal energy is brought to the system in order to remove the small adsorbates. The measurements were carried out at zero externally applied magnetic fields in remanence of the thin ferromagnetic films. They have an easy magnetization axis in-plane along the $[1\bar{1}0]$ and [110] direction for graphene/Ni/W(110) and O/Co/Cu(100), respectively, as well as an easy magnetization axis out-of-plane for O/Ni/Cu(100) for the chosen Ni thickness of 8 ML. A substrate-induced ordering for CoOEP adsorbed on graphene/Ni as well as for FeOEP on O/Co is already know from studies presented in section 3.4 and from literature [35], respectively. Here, it is shown for CoOEP on a ferromagnetic Ni film covered with an ordered c(2×2) layer of atomic oxygen that the magnetization of the substrate and the spins of Co ions are parallel aligned. This is the first report on a ferromagnetic coupling between paramagnetic metalloporphyrins and a ferromagnetic substrate across an intermediate layer of oxygen.

The uptake of NO and CO provokes different effects on the electronic properties and the magnetism of the respective system. After dosing with CO on top of CoOEP/graphene/Ni, the Co orbital moment is reduced. The coordination of NO to the Co ions of CoOEP on O/Ni/Cu(100), in contrast, partially oxidizes the Co atoms compared to the pristine state and the Co magnetization at 30 K is smaller than before dosing. The adsorption of NO on FeOEP/O/Co neither changes the Fe spin state nor the Fe orbital moment, but the strength of the magnetic coupling between the Co and Fe spins.[4]

[4]The written elaboration of this section is based on three publications [111, 138, 180] and one unpublished manuscript [155] as well as respective supplementary informations.

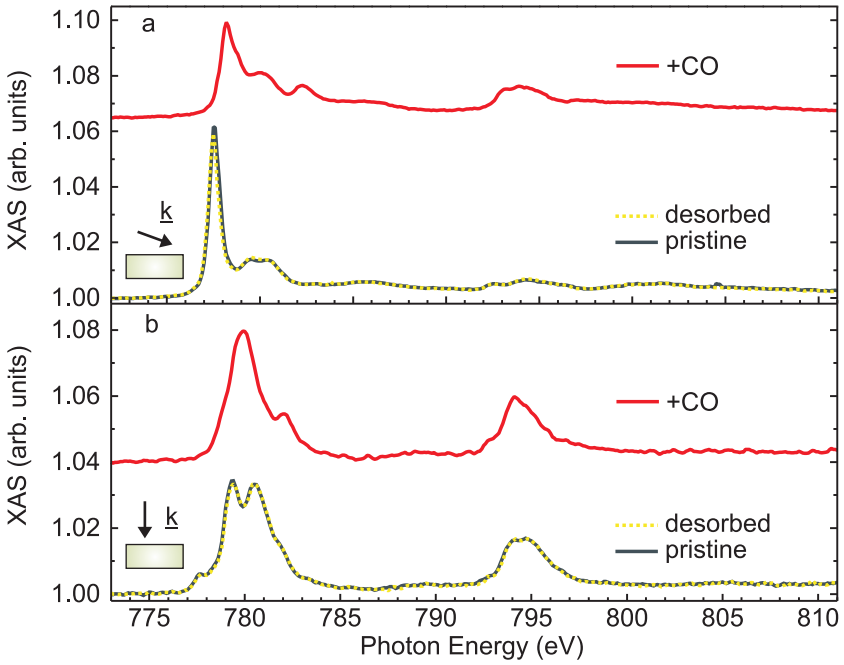

Figure 45: Co $L_{2,3}$ XA spectra of 0.9 ML CoOEP on graphene/21 ML Ni/W(110) measured with p-linearly polarized light and an angle of 20° (a) and 90° (b) between the X-ray wavevector and the surface. In both subfigures, the spectra are shown for the pristine state of the sample (dark green line), recorded at 165 K, after dosing with 90 L of CO (red line), measured at 35 K, and after the desorption of CO (yellow dashed lines), recorded again at 165 K. The spectra after dosing are vertically offset for clarity.

3.5.1 Controlling hugh orbital moments by the chemical stimulus CO

In chapter 3.4 it is shown that the adsorption of CoOEP on a graphene-covered Ni films leads to a substrate-induced order of the Co spins, which is of antiferromagnetic type with respect to the Ni magnetization. At zero external magnetic fields, the in-plane easy axis of the Ni film, along the [$\bar{1}$10] direction [156], enables an in-plane Co magnetization. In this case, a huge orbital moment of $-(0.93\pm0.05)\mu_B$ resulting from spin-orbit coupling, contributes to the Co magnetic moment, as discused in section 3.4.2. In order to manipulate the crystal field, which together with the spin-orbit coupling determines the recreated orbital moment, and thus the Co magnetization, the influence of an additional ligand to the Co ions of CoOEP on graphene/Ni is investigated. This presents a new attempt for the manipulation of exchange-coupled magnetic moments of organometallic molecules on surfaces. To this aim XAS measurements at the Co $L_{2,3}$ are presented in this section after dosing with CO on CoOEP on graphene/Ni, which leads to the formation of CO-CoOEP carbonyl complexes on the surface. For the purpose of testing the reversibility of CO-induced modifications of the Co XAS signal, thermal energy is brought to the system to desorb the CO molecules. A Co XMCD study is presented in order to figure out the impact of the CO attachment on the in-plane aligned Co magnetic moments.

In Fig. 45, Co $L_{2,3}$ XA spectra of 0.9 ML CoOEP on graphene/21 ML Ni/W(110) taken with p-linearly polarized light are shown, which were recorded at 165 K (black

lines), after dosing with 90 L of CO, recorded at 40 K (red lines), and after thermal desorption of CO by a subsequent annealing of the sample to 165 K, measured again at 165 K (yellow dashed lines). XA spectra measured at 20° grazing incidence (a) and at normal incidence (b) are presented, where those of the pristine sample exhibit a qualitatively identical lineshape to the helicity-averaged XA spectra taken with circular polarization and presented in Fig. 42. Unequivocally, lineshape modifications are detected at both detection angles after dosing CO, which exhibits a formation of CO-CoOEP carbonyl complexes on the surface. After CO uptake, the respective spectra taken at normal and grazing incidence reveal at the Co L_3 edge a main maximum at a photon energy of 779.9 and 778.2 eV, respectively, both with local maxima at the high energy flank. The restoration of the original lineshape at the two detection angles after annealing the sample to 165 K reveals a subsequent thermal desorption of the CO from the Co ions, proving the full reversibility of the process. A comparison of the spectral intensity at around 777.5 eV of the Co L_3 XA spectra recorded at 20° grazing incidence before and after dosing with CO reveals that a dosage of 90 L CO is sufficient to at least coordinate to 90% of the Co ions a CO molecule, if not to all.

By making use of the charge sum rule [46] and opposing the results before and after dosing with CO, a rise of the integrated intensity of the white line of $(6 \pm 3)\%$ for grazing incidence and a reduction of $(5\pm3)\%$ for normal incidence are obtained, respectively. This demonstrates that after CO uptake, electron density is withdrawn from out-of-plane orbitals and augmented at in-plane orbitals. These results are consistent with CO acting as an additional axial σ-acceptor and π-donor ligand. In addition, a shift to higher photon energies of the Co L_3 XAS edge after CO attachement and thus of spectral weight is detected for measurements at grazing incidence, while no significant influence on the energetic position is observed at normal incidence. As a consequence, the linear dichroism for the CO-CoOEP complexes is diminished. This is in accordance with a coordination of CO to the Co ions, which modifies the rather square planar shape of the crystal field (D_{4h} symmetry) to a more tetragonally acentrically distorted one (C_{4v} symmetry) [55]. Such a change pushes the Co 3d states with out-of-plane charge distribution e_g and $a_{1\mathrm{g}}$ to higher energies. A fourfold coordination of the Co atoms before dosing with CO can be assumed due to the negligible spatial overlap of the Co 3d with the graphene p_z orbitals, as discussed in section 3.4.1.

The branching ratio, defined as the ratio between the integrated XA white line intensity of the L_3 edge and the sum of the L_3 and L_2 edges, gets reduced for the carbonyl complexes at grazing incidence from 0.80 ± 0.03 to 0.69 ± 0.03, but remains equal for normal incidence (0.68 ± 0.03 vs. 0.67 ± 0.03). Under the assumption of a negligible electrostatic interaction between valence electrons and the core hole, the deviation of the branching ratio from the statistic value of 2/3 is proportional to the angle-dependent part of the spin-orbit operator [182]. The anisotropic branching ratio before dosing with CO is consistent with the large and anisotropic orbital moment, as mentioned in section 3.4.2 and caused by an angle-dependent spin-orbit interaction [183]. On the contrary, the rather isotropic branching ratio of the CO-CoOEP carbonyl complexes indicates a smaller influence of the spin-orbit coupling on the ground state of the electronic structure of the Co ions.

In order to work out the influence of the CO on the magnetic properties of the Co ions, Fig. 46 shows Co $L_{2,3}$ XA helicity-averaged spectra (a) of 0.9 ML CoOEP (dark lines) and CO-CoOEP (red lines) on graphene/21 ML Ni/W(110) and the correspond-

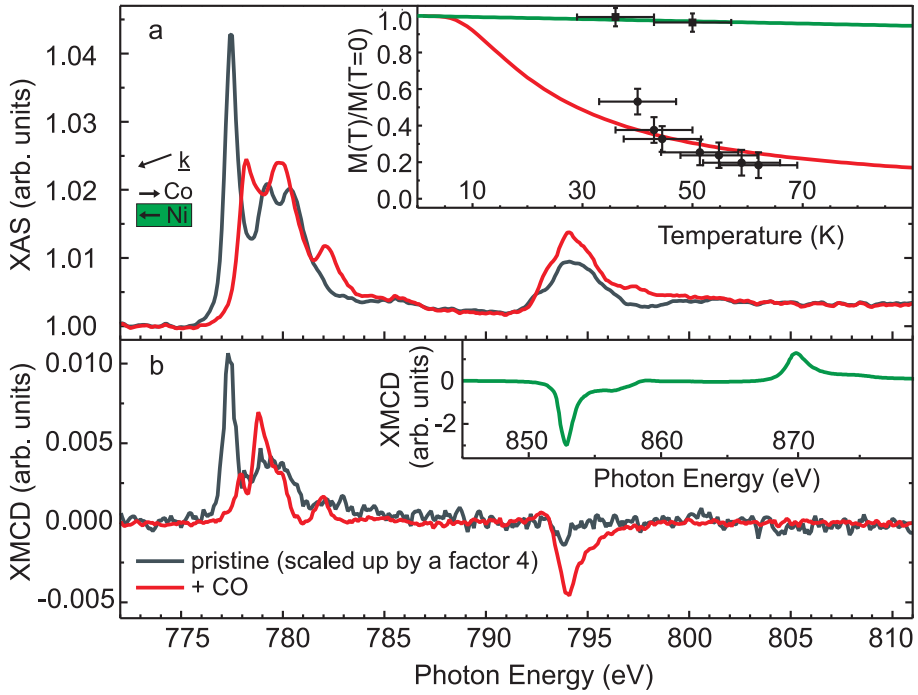

Figure 46: Co $L_{2,3}$ XA helicity-averaged spectra (a) of 0.9 ML CoOEP (dark green lines), taken at 125 K, and CO-CoOEP (red lines), measured at 40 K, on graphene/21 ML Ni/W(110) and the corresponding XMCD spectra (b) recorded at 20° grazing incidence and in remanence of the Ni film. Insets: (a) $M_r^{Co}(T)$ and $M_r^{Ni}(T)$ derived from integrated XMCD signals of CO-CoOEP/graphene/Ni (circles and squares, respectively) and presented together with the respective calculated progression (red line for Co: $M_r^{Ni}(T)B_J(\alpha)$; green line for Ni: $(1 - T/T_C)^\beta$ with $\beta = 0.365$ and $T_C = 630$K). (b) Ni $L_{2,3}$ XMCD spectra taken at 125 K and before dosing CO.

ing XMCD spectra (b) recorded at 20° grazing incidence. The spectra belong to the same sample preparation as the ones diplayed in Fig. 45 and are taken at 125 and 40 K before and after CO attachement, respectively. While the measurement results regarding the line shape of the Co XA and XMCD spectra of the pristine sample are in qualitative agreement with the respective ones presented in Fig. 39, the Co XMCD signal is scaled up by a factor of 4 for reasons of comparability following the temperature dependence of the system presented in Fig. 40. The Ni XMCD signal of the ferromagnetic film, shown in the inset of Fig. 46 (b), possesses an opposite sign compared to the Co XMCD signal, which again reveals an antiferromagnetic coupling between the Co and Ni spins. Consistent to the CO-provoked modifications of the Co L_3 XA spectra taken with linearly polarized light, spectral weight is shifted to higher photon energies in the helicity-averaged XA spectrum of the Co L_3 edge, which possesses, after dosing CO, three local maxima at photon energies of 778.2, 779.8, and 782.1 eV. The integration the two Co XA spectra, which are measured 15° off the magic angle, reveals a CO-induced increase by $(2 \pm 3)\%$ of the white line intensity. Taking into account this small raise, which is zero within the error bar, as well as the CO influence on the white line intensity for different measurement conditions (see

Fig. 45), it can be concluded from the charge sum rule [46] that CO adsorption does not modify the oxidation state of the Co ions.

The nearly disappearing Co XMCD at the L_2 edge before CO attachment, opposed to the huge intensity at the L_3 edge, manifests the large Co in-plane orbital moment of the adsorbed CoOEP molecules. A non-vanishing Co XMCD signal for the carbonyl complexes proves the presence of a magnetic moment at the Co site of the prophyrins, and concurrently a magnetic coupling between these magnetic moments and the substrate magnetization. The most salient alteration of the Co XMCD spectrum after CO adsorption is a shift of spectral weight to higher photon energies at both the L_2 and the L_3 edges. This is accompanied by a change of the line shape of the latter, which now exhibits a main maximum at 778.9 eV and two local maxima at 778.0 and 782.1 eV. Furthermore, a striking raise of the XMCD at the Co L_2 edge after dosing CO indicates a strongly diminished orbital moment. An application of the sum rules [49, 50] yields lower limits of the Co magnetic moments, as they are subject to thermal fluctuations. Correspondingly, the orbital and effective spin moments amount to -(0.11 ± 0.02) μ_B and -(0.75 ± 0.05) μ_B, respectively, in the case of the CO-CoOEP complexes. The latter result is consistent with a low-spin S=1/2 configuration of the Co ions, considering the incomplete alignment of the Co moments due to thermal fluctuations and being aware of the potential presence of an intra-atomic spin dipol moment.

In order to extrapolate the absolute magnetic moments upon CO uptake, the temperature progression of the Co and Ni L_3 edge XMCD signals is investigated. In the inset of Fig. 46 (a) the deduced relative Co and Ni magnetizations ($M_r^{Co}(T), M_r^{Ni}(T)$) are displayed versus temperature together with their theoretical temperature progression. $M_r^{Co}(T)$ is reproduced by the product of a Brillouin function and $M_r^{Ni}(T)$ following equation 32 with $J = 0.5$ and an exchange energy E_{ex} of (1.4 ± 0.5) meV. $M_r^{Ni}(T)$ is again, as in section 3.4, represented by a $(1 - T/T_C)^{\beta}$ law, with a Curie temperature of $T_C = 630$ K and a critical exponent $\beta = 0.365$ [158]. The experimental and the theoretically modeled relative Co magnetizations agree to a good extent. The extrapolated effective spin moment after the attachment of CO amounts to $-(1.43 \pm 0.10)$ μ_B. Co porphyrins have a distinctive preference just to access low-spin states, also in the case of a coordination of axial ligands to the Co ions, due to the size of ligand fields of the porphyrin ligand. High-spin states have been reported in literature only in the case of a weak in-plane ligand field as a result of additional coordination of peripheral substituents to the macrocycle consisting of fluorine [184, 185]. Thereby a smaller spacing between the cobalt d-orbital energies allows the full complement of spin states. The encountered deviation of $-(0.43 \pm 0.04)$ μ_B to the expected spin moment of one Bohr magneton for a S=1/2 system, the difference between $-(1.43 \pm 0.10)$ μ_B and -1 μ_B, can be interpreted as an intra-atomic spin dipole moment. Further an extrapolated orbital moment of $-(0.21 \pm 0.05)$ μ_B is found, compared to $-(0.93 \pm 0.07)$ μ_B without CO, which means a reduction upon CO uptake by (77 ± 6)% and hence a decrease of the total Co magnetic moment by (37 ± 3)%.

The explanation for the reduced Co in-plane orbital moment after adsorption of CO derives from the altered Co electronic structure. The crystal field of the Co ions gets modified, whereas both the spin as well as the oxidation state remain unchanged. For CoOEP on graphene/Ni/W(110) a nearly energetic degeneration of the e_g and a_{1g} states admixes them. Thereby a new state with an anisotropic orbital moment is

formed and a huge in-plane orbital moment is created [69]. In the event of the carbonyl complexes, the CO molecules coordinate as an additional axial ligand to the Co ions, so that they push up the a_{1g} state more efficiently in energy than the e_g state [42, 55]. Treating the recreated in-plane orbital moment as a second-order perturbation effect, it is inversely proportional to the energetic separation between the two states, which is bigger for the CO-CoOEP complexes. Consequently, the Co in-plane orbital moment decreases after dosing with CO. A CO-provoked reorganization of the Co $3d$ orbital occupation, leading to a totally filled e_g orbital, may also play a role, though.

To sum up, the electronic structure of the Co ions within CoOEP molecules adsorbed on graphene/Ni can be controlled in a reversible manner by adsorbing CO to the molecules and its subsequent thermal desorption. CO acts here as a chemical stimulus. Thereby neither the oxidation state nor the substrate-induced magnetic order are modified. The coordination of CO as additional axial ligand to the central metal ions changes their crystal field, which, together with the spin–orbit coupling, specifies the size of the IP orbital moment. CO adsorption lowers the Co orbital moment by $(77 \pm 6)\%$, and, under the reasonable assumption that the spin state does not change, the total Co magnetization by $(37 \pm 3)\%$, for measurements taken in zero external magnetic fields. These results show that it is possible to modify the magnetic moments by a chemical approach in an exchange-coupled system of metalloporphyrins adsorbed on surfaces not only by a variation of the spin moments but also by a change of the orbital moments.

3.5.2 Switching the electronic properties of Co porphyrins by NO adsorption

Besides a control of the magnetization of paramagnetic porphyrin molecules magnetically coupled to a ferromagnetic thin film by changing the size of the orbital moment due to adsorption of small molecules, also a modification of the spin moments at finite temperatures by external means within such a magnetically coupled system presents an auspicious approach for tuning the molecular magnetization. To this end, it is shown within this section by means of an angle-dependent XA study of the Co $L_{3,2}$ edges that the electronic properties of Co ions of CoOEP adsorbed on an oxygen-covered Ni film, grown on Cu(100), can be reversibly manipulated by the chemical stimulus NO. Further, by means of an XMCD study at the Co and Ni $L_{2,3}$ edges at zero magnetic fields, a potential magnetic coupling between the Co spins and the substrate magnetization before and after NO attachement is investigated with a special focus on the NO-induced modifications on these physical characteristics. Additionally, an angle-resolved XA study at the C and N K edges provides insight into the adsorption characteristics and geometry of both the CoOEP and the NO molecules on the surface. These experimental data are physically interpreted with the help of DFT calculations of a Ni_4O-(CoOEP) cluster used to simulate theoretical angle-dependent C and N K edge XA spectra for a comparison.

First the investigation of the interaction between the oxygen-covered Ni film and the CoOEP molecules and in particular the Co electronic structure is of interest. Also the influence of dosing with NO on the physical properties of the system is studied. For these reasons, Fig. 47 displays Co $L_{2,3}$ XA spectra of 0.7 ML CoOEP on O/8 ML Ni/Cu(100) before dosing NO, after dosing with 28 L of NO, after a subsequent thermal desorption of NO at 350 K, and after dosing once more with 14 L of NO,

taken with p-linearly polarized light and an angle of 20°, 55°, and 90° between the incoming X-ray wavevector and the surface. All spectra are recorded at 130 K.

Also the NO was dosed at this temperature in order to prevent its dissociation on the surface. The temporal order of the data acquisition is specified by vertical arrows. Once NO is adsorbed to CoOEP, spectral changes appear for each measurement geometry. At the L_3 as well as at the L_2 edges spectral weight is pushed to higher photon energies. This is apparent for measurements at 90° normal incidence and even more distinctive for the ones at 20° grazing incidence. Further, a reduction of the linear dichroism, i.e., the difference between the absorption spectra for different incidence angles, as explained in section 1.4.2, is detected after NO uptake and a smaller occurrence of the multiplet fine structure. In order to test the reversibilty of the NO-induced changes, the system was heated up to 350 K. Then the temperature was once more reduced for taking angle-dependent Co $L_{2,3}$ XA spectra. As evidenced by Fig. 47, the original lineshapes are restored at all detection angles, demonstrating the complete reversibility of the process. Actually, by dosing once more with 14 L of NO, it is possible to obtain the same spectral modifications of the lineshape and so to carry out again the manipulation of the electronic properties, as shown by the topmost curves in Fig. 47 (a)-(c). Angle-resolved XAS spectra recorded with linearly polarized light at the C K edge reveal that CoOEP molecules adsorbs flat on the oxygen-covered Ni surface as will be discussed later in this section. With the help of this knowledge the Co $L_{2,3}$ edge XA spectra are analysed.

The Co XA spectra of the pristine sample features two salient components forming the fine structure of the L_3 edge. One of them, a rather broad peak with a maximum at 779.5 eV and two shoulders at 780.3 eV and 781.6 eV, is more pronounced in the case of the spectrum recoded at normal incidence and therefore stems from excitations into states with in-plane hole density. The other component is a narrow peak at 777.7 eV, appearing more strongly in the spectra recorded at grazing incidence and, for this reason, originating from excitations into states with out-of-plane hole density. The spectrum recorded at the magic angle of incidence of 55° for p-linearly polarized light, and thus representing the isotropic spectrum, shows correspondingly features of both the spectra recorded at normal and 20° grazing incidence, but less pronounced. In the case of the pristine sample, the spectra recorded at the three different angles of incidence resemble to a good extent those of a thin ordered film of CoOEP, shown in Fig. 27. Also a comparison of the results presented here to the ones of thin films of CoPc, revealing for bulk material a similar Co $L_{2,3}$ XA spectrum as for CoOEP [110], and to the corresponding multiplet calculations of the Co $L_{2,3}$ edges [53, 112] show similarities. For that reason it can be concluded that the crystal field which constrains the Co atoms is not strongly modified upon adsorption. Further, the Co ions retain their oxidation state which they have in isolated CoOEP, despite the interaction with the substrate. For an isolated CoOEP molecule, DFT calculations yielded a low-spin state and a 2+ valency of the Co ions [113]. Following this comparison and considering the angular dependence and the energetic position between the fine-structure components of the Co L_3 edge, an assignment of the empty orbitals accessed by excitations of the 2p core-level electrons can be qualitatively made. Corresponding to crystal field theory, the $3d$ orbitals of the Co ions transform as a_{1g} (d_{z^2}), b_{1g} ($d_{x^2-y^2}$), b_{2g} (d_{xy}), and e_g ($d_{yz,xz}$), which is expected for flatly adsorbed CoOEP molecules, too. The energetically highest lying state b_{1g} ($d_{x^2-y^2}$) is empty and the a_{1g} (d_{z^2}) one carries

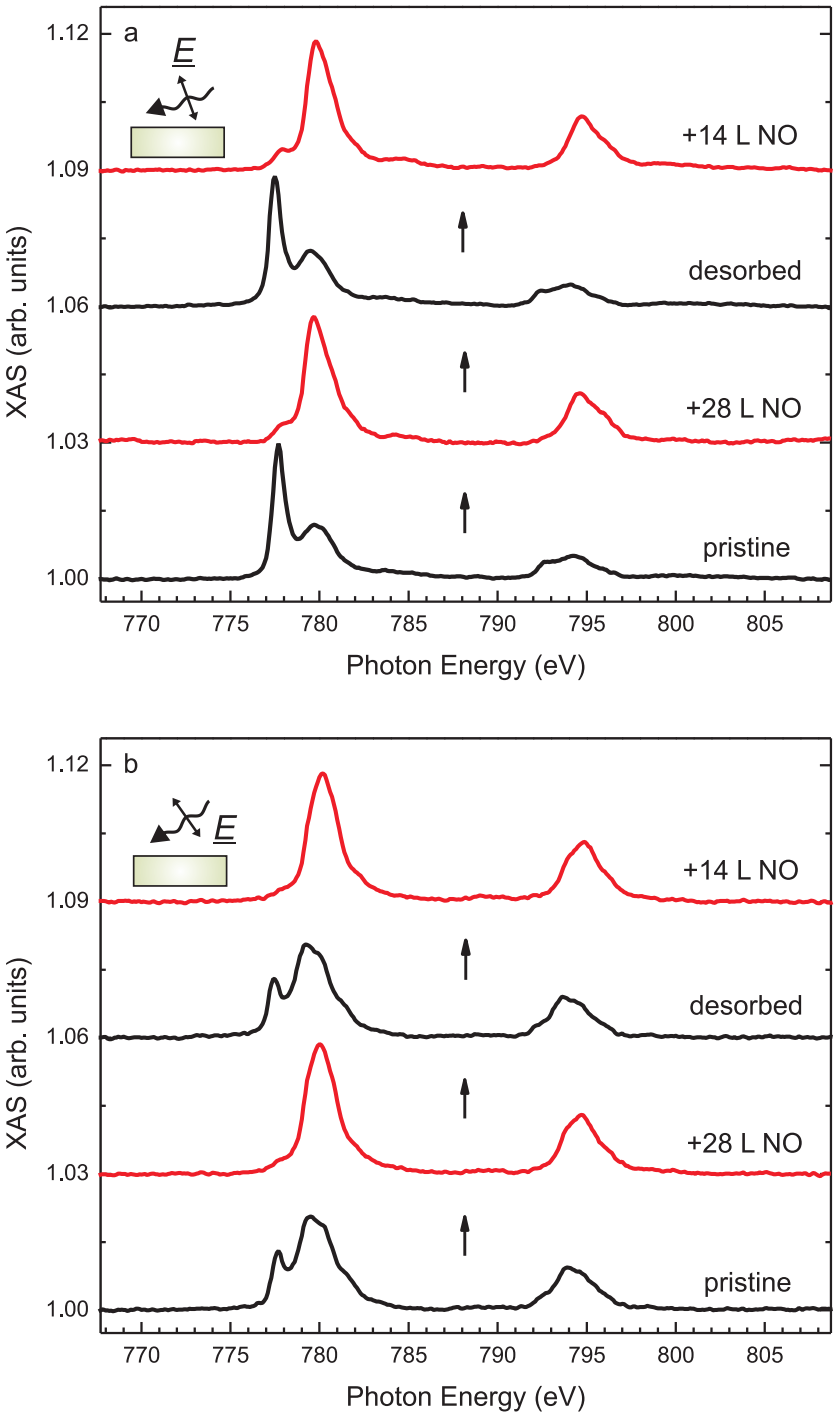
a
E
+14 L NO
desorbed
+28 L NO
pristine
XAS (arb. units)
1.12
1.09
1.06
1.03
1.00
770
775
780
785
790
795
800
805
Photon Energy (eV)
b
E
+14 L NO
desorbed
+28 L NO
pristine
XAS (arb. units)
1.12
1.09
1.06
1.03
1.00
770
775
780
785
790
795
800
805
Photon Energy (eV)

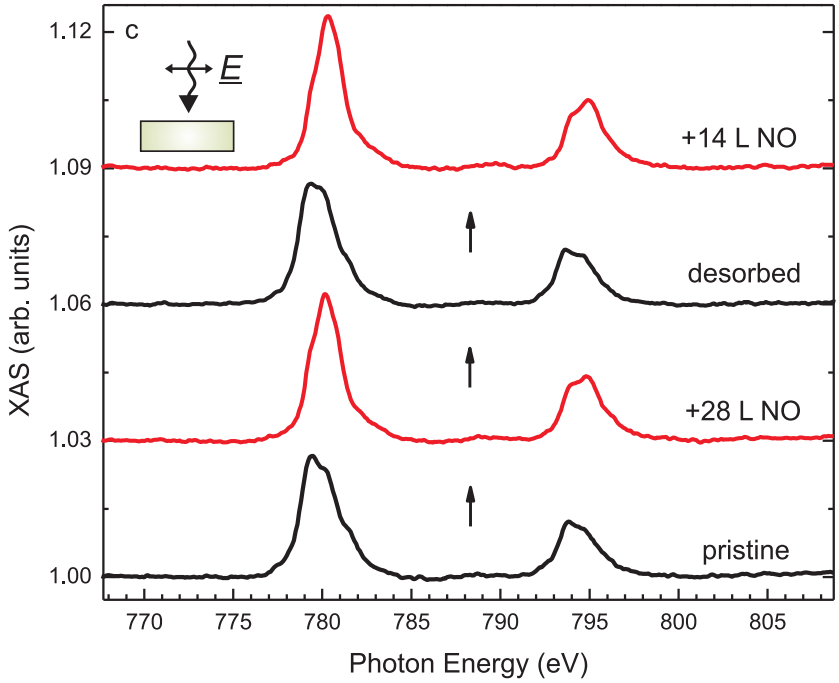

Figure 47: Co $L_{2,3}$ XA spectra of 0.7 ML CoOEP on O/Ni measured with p-linearly polarized light and an angle of 20° (a), 55° (b) and 90° (c) between the X-ray wavevector and the surface at 130 K for each NO dosage step. From the bottom to the top the spectra are shown for the sample in the pristine state, after dosing with 28 L of NO, after ensuing desorption of NO by heating to 350 K, and after dosing again 14 L of NO. The spectra are shifted vertically for clarity.

an unpaired hole. Hence, the former can be associated with the energetically higher-lying broad peak with a maximum at 779.5 eV, and, on the other hand, the latter with the narrow peak at 777.7 eV. Yet the a_{1g} (d_{z^2}) and e_g ($d_{yz,xz}$) states could also together carry one hole according to the mentioned multiplet calculations. Supposing this, excitations into the $d_{yz,xz}$ orbital would also contribute to the spectra taken at an incidence angle of 55° and 20°. An angle-dependent XA study at the Co $L_{2,3}$ edges of CoOEP adsorbed on an oxygen-covered Cu(100) surface revealed an almost identical lineshape as for the system studied here, indicating in both cases a small electronic coupling between the Co ions and the substrate [88]. By contrast, for CoOEP on a Ag(110) and Ag(111) surface [113, 130], a direct electronic interaction was observed, which partially reduces the Co^{2+} ions.

By integrating the white line intensities of the isotropic Co $L_{2,3}$ XA spectra, before and after dosing with NO, and making use of the charge sum rule [46], a reduced electron density at the Co site is discovered after the NO attachement. The intensity raises by (10±2)% and hence the number of holes of the Co ions within the 3d shell. Carrying out the same integration for the Co $L_{2,3}$ XA spectra taken at normal and 20° grazing incidence reveals a respective increase of the white-line intensity by (8.5±2)% and (12±2)%. This demonstrates that, due to the coordination of NO, more electron density is extracted from out-of-plane than from in-plane Co orbitals. The offset of spectral weight to higher photon energies of the Co XA spectra after the formation of

the nitrosyl complexes is in accordance with a lower electron density at the Co site.

The removal of a non-integer charge away from the Co ions can be comprehended within the charge transfer multiplet model, in which the ground state is constructed by mixing Co ions with a different valency and the according electrons or holes in the ligands. Within such a concept, the contraction of the multiplet structures after the coordination of NO can be understood as a consequence of such charge transfer effects, which are induced by charge fluctuations in the initial and final states participating in the absorption process [186]. Thus a NO-provoked reduction of charge at the site of the Co ion causes a minor pronounced multiplet structure. In conformity with crystal field theory [55], the observed reduction of linear dichroism after the formation of the nitrosyl complexes indicates a change of the crystal field acting on the Co ions, which exhibits then a less tetragonally acentric distorted shape (C_{4v} symmetry), but rather approaches a more octahedral one (O_h symmetry). This alteration of the symmetry is consistent with the detected redistribution of spectral weight, the shift to higher photon energies of the Co $L_{2,3}$ XA edges, in particular for measurements at grazing incidence compared to the ones at normal incidence. NO, which acts here as additional axial ligand to the Co ions, causes a shift to higher energies of $3d$ states with an out-of-plane charge distribution e_{g} and $a_{1\mathrm{g}}$, whereas it has just a minor influence on states with an in-plane charge distribution $b_{1\mathrm{g}}$ and $b_{2\mathrm{g}}$.

A potential magnetic interaction between the porphyrin molecules and the Ni film could couple the Co spins to the substrate magnetization before and after NO attachment. For the purpose of testing this, Fig. 48 shows Co L_3 (a) and Co L_2 (b) XA spectra recorded with circularly polarized light at zero external magnetic fields. They are taken at normal incidence and 30 K and are part of the same measurement series as the ones of Fig. 47. Co L_3 (a) and Co L_2 (b) XA spectra with different line shapes are discovered for magnetizations of the sample being parallel and antiparallel to the direction of the photon angular momentum of the incoming X rays. This applies to results for the pristine sample (dark and dotted blue lines) as well as to the ones after dosing with 28 L of NO (orange and dotted magenta lines). Additionally, Fig. 48 (d) diplays the corresponding XMCD difference spectra, whose presence for the CoOEP molecules as well as for the NO-CoOEP nitrosyl complexes proves a magnetic moment on the cobalt ions and a magnetic coupling between these moments and the ferromagnetic Ni film. The energetic positions of the Co $L_{2,3}$ XMCD signals before (black line) and after (red line) dosing with NO are nearly the same, whereas the Co XMCD signal after dosing is about a factor of two smaller than before dosing.

The zero crossings of the XMCD signal of the pristine sample at both the L_3 edge and the L_2 edge leads to a rather atypical line shape of the XMCD spectrum, taken under normal incidence. This is known to appear in other Co d^7 low-spin systems in an environment with C_{4v} or D_{4h} symmetry [88, 112, 139]. As the spectrum displayed does not represent the isotropic XMCD, it carries additional information about the distribution of the spin density, being correlated to the distribution of the unpaired electron density. Hence, the characteristics of its line shape can be better comprehended by the circumstances that the XMCD signal stems from the density of unpaired 3d holes, which features mainly an out-of-plane distribution, while on the other hand the in-plane unoccupied density of states is probed by the measurement under normal incidence. Due to the small Co XMCD signal, a sum rule analysis can not be performed within reasonable accuracy.

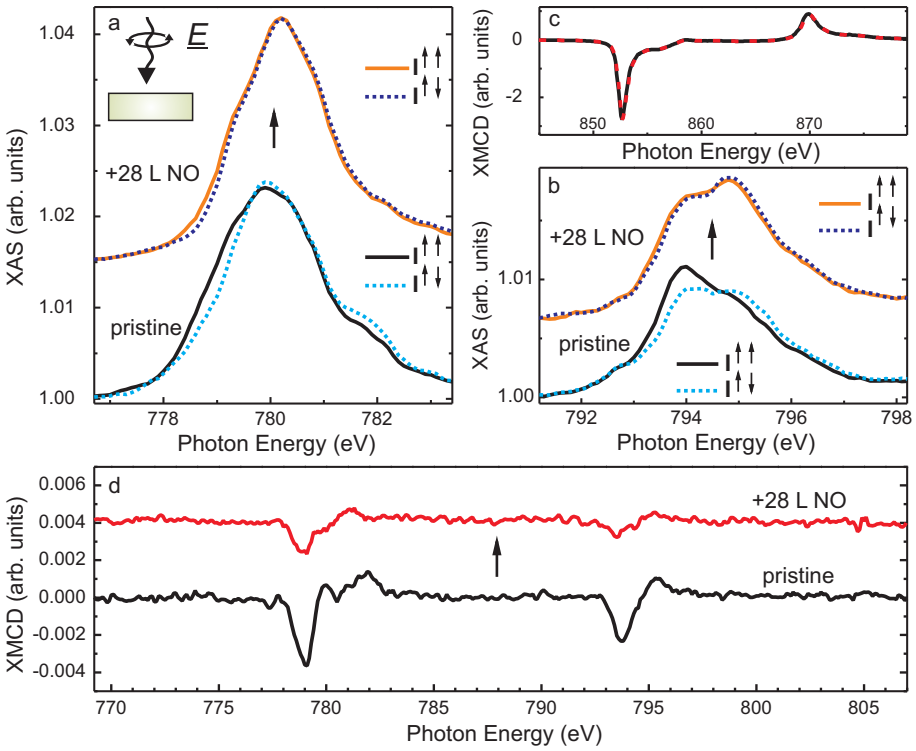

Figure 48: Co L_3 (a) and Co L_2 XA spectra (b), which are recorded at 30 K at normal incidence with circularly polarized light and a magnetization of the sample being parallel and antiparallel to the direction of the photon angular momentum of the incoming X-rays before (continuous dark and dotted blue lines) and after dosing 28 L of NO (continuous orange and dotted magenta lines), and corresponding XMCD spectra (d) before (black line) and after (red line) dosing with 28 L NO of 0.7 ML CoOEP on O/Ni. Spectra are shifted vertically for clarity. (c) XMCD spectra at the Ni $L_{2,3}$ edges before (full black line) and after (dashed red line) dosing NO.

Figure 48 (c) shows the XMCD spectrum of the Ni film before dosing with NO (black line), which possesses a negative signal at the L_3 edge. Interestingly, the cobalt XMCD signal also presents predominantly a negative signal at the L_3 edge. This observation verifies a ferromagnetic coupling of the molecules to the ferromagnetic film through the intermediate layer of atomic oxygen. The fact that the Co XMCD signal at the L_2 edge exhibits in overall terms the same sign as the one at the L_3 edge is not in contradiction with this conclusion, having in mind the results of the XMCD study about CoOEP on graphene/Ni (see section 3.4.2). By way of comparison, the coupling strength must be small, as at temperatures higher than 30 K no significant XMCD signal could be detected, in contrast to, for instance, Fe-octaethylporphyrin molecules (FeOEP) on ferromagnetic substrates [34, 127].

Pondering about the mechanism behind this exchange coupling, the intermediate layer of atomic oxygen casts into doubt a direct magnetic interaction between the Co ions and the substrate. On the contrary, an indirect magnetic coupling mediated via the oxygen atoms appears to be very likely, and has already been found for manganese tetraphenylporphyrin chloride (MnTPPCl) and FeOEP on oxygen-covered

ferromagnetic metal surfaces. Along such an exchange path, a 180° superexchange interaction can establish an antiferromagnetic coupling between the paramagnetic metalloporphyrins and the spins of the substrate [35, 179]. However, a ferromagnetic double exchange interaction across an oxygen layer has been theoretically predicted, too [187]. The latter could provide an explanation for the ferromagnetic coupling between the spins of the Ni substrate and the ones of the Co ions of the porphyrin molecules. Basics about the double exchange mechanism are presented in section 1.9. Certainly, also a magnetic exchange mechanism mediating the coupling between the magnetization of the substrate and the magnetic moment of the Co ions across the atomic oxygen by the π system of the porphyrins can not be ruled out.

For the purpose of testing the implication on the magnetic properties of the Co ions after dosing with NO, the influence of the NO adsorption on the magnetization of the Ni substrate has to be considered as well. Therefore Fig. 48 (c) displays the Ni XMCD spectrum after dosing with 28 L of NO (red dotted line). From virtually identical Ni XMCD spectra for the pristine sample and after dosing with NO follows a negligible impact of NO on the magnetism of the Ni film, which appears to be protected by the oxygen adatoms, whereas upon the attachment of NO the Co XMCD signal, as remarked before, is lowered by about a factor of 2. Hence, the spin of the Co ions can not be zero as the XMCD signal does not disappear, similar as for NO coordinated to CoTPP on Ni [59]. The decrease of the XMCD is in qualitative accord with the partial oxidation of the Co ions described above. Due to the fact that the XMCD tests the local spin polarization at the site of the Co core, the net transfer of non-integer charge away from the metal ion induced by the coordination of NO could lead to a smaller XMCD signal if the low-spin state is maintained, since then the a_{1g} (d_{z^2}) state would be less than half filled. The distinctive preference of Co porphyrins not to access high spin-states [184, 185], as mentioned in the previous section 3.5.1, strongly supports this idea. Following this argumentation, the partial oxidation of the Co ions leads to a reduced Co spin moment. Unfortunatly, due to the small Co XMCD signal, a sum-rule analysis can not be performed within reasonable accuracy. Further, an NO-induced modification of the XMCD line shape at the high-energy flank of the L_3 peak points towards an electronic change of the in-plane orbitals provoked by the coordination of NO. An additional contribution to the reduction in XMCD signal might come from the influence of the small adsorbate on the strength of the magnetic coupling between the Co ions and the Ni film. The latter might be reduced in size after the formation of the nitrosyl complexes, which would cause a lower XMCD signal at finite temperatures, too.

In order to rule out that the remaining Co XMCD signal upon NO exposure is just due to uncovered Co sites, Fig. 49 presents Co $L_{2,3}$ XA spectra of different dosage steps, which belong to the same preparation as the ones of Fig. 47. They are measured at 130 K under normal incidence before dosing NO (black line), after dosing 14 L NO on the pristine sample (blue dashed line) and after dosing another 14 L NO (red line). The data definitely reveal that a dosage of NO higher than 14 L does not induce further spectral changes of the Co $L_{2,3}$ absorption spectra, and that the sticking coefficient of NO for an adsorption on CoOEP is high enough to ensure that all CoOEP molecules are coordinated by NO. A higher dosage of 28 L has been used for the first NO adsorption in the presented study in order to make sure that the NO adsorption to the Co ions is saturated.

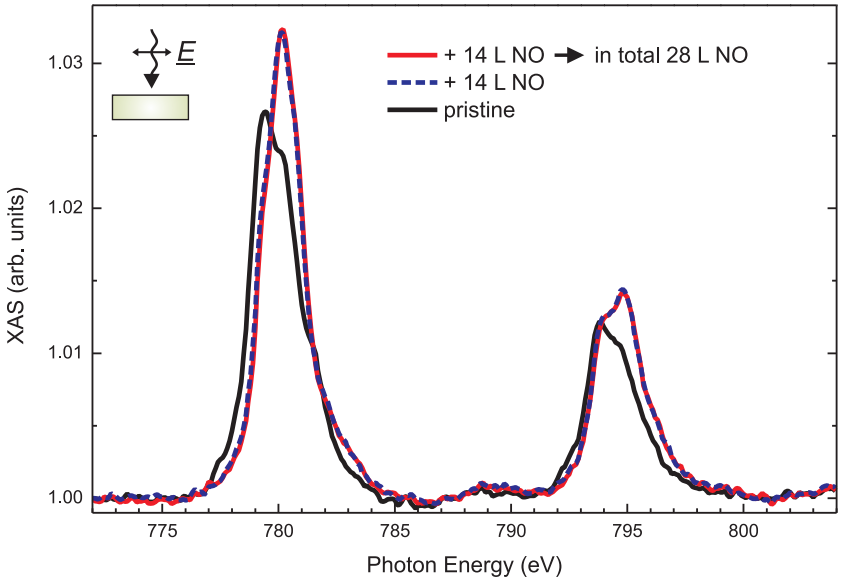

Figure 49: Co $L_{2,3}$ XA spectra of 0.7 ML CoOEP on O/Ni recorded under normal incidence with linearly polarized light at 130 K for in the pristine state, after dosing with 14 L of NO, and after dosing another 14 L of NO.

Next, insight into the adsorption geometry and the electronic structure of 0.7 ML CoOEP on O/Ni/Cu(100) is gained with the help of C K XA spectra presented in Fig. 50 and taken at a temperature of 140 K at 90° normal (dark line) and at 20° (red line) and 55° (blue line) grazing incidence. The spectra show four π^* resonances with maxima at photon energies of 284.1, 285.0, 285.7, and 287.7 eV as well as contributions in the σ^* region above 289 eV with a maximum at 292.5 eV and a broader peak at higher energies. In the π^* region, spectral features are much more pronounced at grazing incidence, while at normal incidence not all details are energetically resolved. On the contrary, at normal incidence, the peak lying above 294 eV is more prominent than at grazing incidence. The C K spectrum measured at 55° grazing incidence presents the isotropic spectrum for which the dependence on the orientation of the molecular orbitals cancels out. Thus it can be compared to the corresponding spectrum of CoOEP bulk material shown in section 3.2. Its line shape resembles to some extent the one of the polycrystalline bulk sample, also exhibiting a triple-peak structure in the energy range between 284.0 eV and 286.0 eV, which points towards a rather unperturbed electronic structure upon adsorption. By means of a comparison of experimental spectra to theoretically calculated angle-dependent C K XA spectra of a Ni_4O-(CoOEP) cluster used to simulate the electronic coupling of CoOEP with an oxygen-covered Ni(100) surface, more information about the electronic interaction between the adsorbate and the substrate can be obtained. The theoretical spectra are calculated by the collaborating group of Prof. Hermann and published in our recent work [111]. Regarding the computation, the oxygen of the Ni_4O subunit can be thought as a spacer atom weakening the electronic coupling of the CoOEP molecule with the Ni_4 cluster. A good agreement between results from experiment and theory supports the picture of a weak bonding between the substrate and the molecules, the electronic properties of which are similar to isolated CoOEP according to the calculations. The angular dependence of the C K XA spectra experimentally observed fits

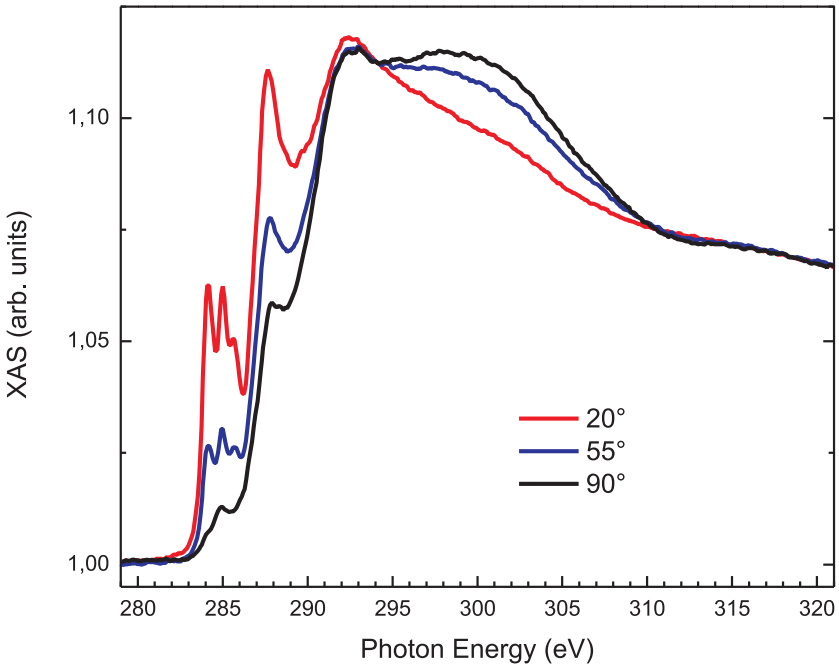

Figure 50: C K XA spectra of CoOEP on O/Ni/Cu(100) taken at 140 K with p-linearly polarized light and an angle of 20° (red line), 55° (blue line), and 90° (black line) between the X-ray wave vector and the surface.

to an almost out-of-plane (in-plane) oriented π^* (σ^*) orbital of the macrocyclic ring of the porphyrin molecules. It is reproduced assuming flat adsorbed CoOEP molecules. However, within the spectra obtained from theory for normal incidence, no spectral contribution at all is present in the π^* region. The absence of signals in the calculation may be due to several reasons. Either the cluster calculation is not accurate enough to model the physical system, as just four Ni atoms are used to model the Ni(100) surface, or a small amount of molecules, adsorbed at step edges, reveal a different electronic structure in the experiment, which is not taken into account for the calculations. For instance, a slight buckling of the CoOEP adsorbate resulting in a non-planar π^* orbital, or the formation of an additional bond between adsorbate and molecule, in particular having involved the ethyl groups, could explain the remaining intensity at normal incidence in the experimental spectrum. The peak at 292.5 eV originates mainly from excitations into σ^* orbitals of carbon atoms within the eight ethyl groups. Therefor its slightly stronger appearance at normal incidence indicates that these groups, being at the periphery of the molecules, are not exactly in the same plane as the macrocycle.

For the purpose of providing a better comprehension about the adsorption geometry and character of the CoOEP as well as the NO molecules, Figs. 51 and 52 present N K edge XA spectra, recorded with p-linearly polarized light at 55° and 90° between the incoming X-ray wavevector and the surface, respectively. They belong to the same sample preparation as the Co $L_{2,3}$ XA spectra earlier shown (Figs. 47 and 48). The results for the pristine sample, after dosing with 28 L of NO, after subsequent warming up to 350 K, and after dosing once more with 14 L of NO are displayed in panels (a). For the sake of clarity, the spectra of the last three steps, after substracting the spectra before the first dosing with NO, are displayed in panels (b).

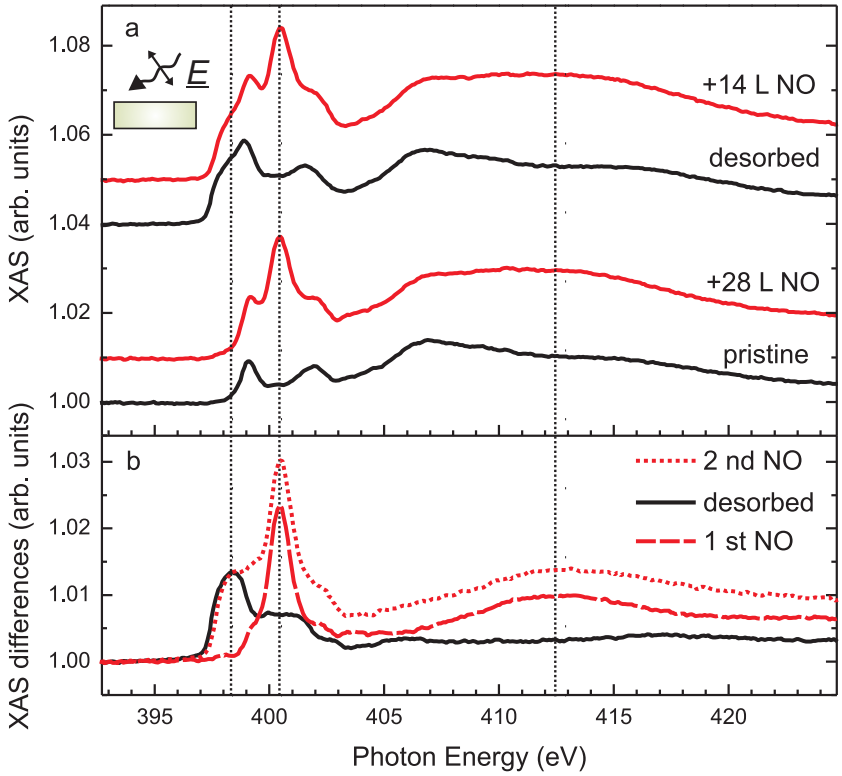

Figure 51: (a) N K XA spectra of 0.7 ML CoOEP on O/Ni measured at 130 K with p-linearly polarized light and an angle of 55° between the X-ray wavevector and the surface at each NO dosage step. The spectra are shifted vertically for clarity. (b) Difference spectra between the spectra corresponding to the three dosage steps and the spectrum of the pristine sample in (a).

The isotropic spectrum of the CoOEP molecules (bottommost curve in Fig. 51 (a)) reveals two maxima at photon energies of 399.1 and 402.0 eV leading to a double-peak structure, similar as for CoOEP bulk material (see Fig. 24) and CoOEP adsorbed on a bare Ni film on Cu(100) (see Fig. 36). By comparing the experimental CoOEP spectra to theoretically calculated angle-resolved N K XA spectra of a Ni_4O-(CoOEP) cluster from the collaborating group of Prof. Hermann, also used to simulate the C K XA spectra and just recently published [111], the data experimentally obtained can be further interpreted regarding their physical content. The computation is based on StoBe cluster and DFT calculations. According to this, at photon energies below 402.5 eV, the spectral features originate mainly from two excitations involving π^*-type final state orbitals, but also from one with a σ^*-type final state orbital. The latter follows from the electronic coupling between Co 3d and N 2p states, similar as for non-adsorbed CoOEP molecules and discussed in section 3.2, while here, in contrast, a minor Ni 3d admixture is added like in the case of CoOEP on a bare Ni/Cu(100) sample. Further, the presence of the metal surface leads to additional excitations compared to free CoOEP, which contribute to the spectrum within this energy range. However, these are just of minor importance regarding their intensity as opposed to the excitations above mentioned. The excitation into orbitals with π^* typ character contributes to both of the features of the double-peak structure with maxima at 399.1 and 402.0 eV, while the excitation into the orbital with σ^* typ character contributes

only to the energetically lower-lying peak.

At higher photon energies, the spectrum is characterized by a broad σ^* resonance with a maximum at 406.8 eV originating from excitations in orbitals with σ^* symmetry, which are located at the periphery as well as at the core of the adsorbate, according to the calculations. The different symmetries of final state orbitals, being involved in the absorption process, affect the angular dependence of the N K XA signal. The experimental observation that at normal incidence the spectral features at lower photon energies are more dominant, while the ones above 404 eV are stronger pronounced at a more grazing detection angle, is in accordance with the discussed symmetry of the final state orbitals of the absorption process. Also the angle dependence of the theroretical N K edge XA spectra, which are calculated for flatly adsorbed molecules, shows this behaviour [111]. In the energy range below 404 eV, the small remaining intensity clarifies that final state orbitals are of dominant π^* type symmetry with σ^* type orbitals being much less important. Lastly, the electronic coupling between the substrate and the adsorbate is much lower than for CoOEP on a bare Ni surface, regarding the calculations. This is due to the atomic oxygen, which acts as spacer between the reactive Ni surface and the porphyrin molecules.

Upon dosing with 28 L of NO, an additional σ^* resonance with a maximum at 412.4 eV and a new π^* resonance at 400.5 eV arise. This furnishes evidence for the existence of intact NO molecules on the sample by a comparison to XAS studies of gas phase NO from literature [188]. Further, it has been reported that NO chemisorbs on oxygen-covered Ni surfaces [189]. On this account it is adequate to assume that NO molecules are both situated on top of the CoOEP molecules and sitting between the porphyrins directly on the substrate, while all of them contribute to the N K XA spectra. On the other hand, only one additional peak in the π^* region is detected. This indicates an almost identical electronic structure of these two kinds of NO molecules and hence chemisorption of the NO on the CoOEP molecules, being in agreement with the partial oxidation of the Co^{+2} ions.

The delivery of thermal energy to the system by warming up the sample to 350 K results in vanishing of the intensity at 400.5 eV. This is consistent with the detachment of bonded NO molecules, while a new peak at 398.3 eV arises. Presumably, the latter can be ascribed to a chemisorbed atomic N species resulting from the dissociation of NO on the sample [190]. The second dosage of NO does not affect this feature, and the signals at around 400.5 and 412.3 eV show up again. Considering the surface reactivity, NO dosage, or temperature, the surface chemistry of nitric monoxide in all its particulars can be quite complex on transition metal substrates and may be found elsewhere in literature [190, 191].

At normal incidence, the π^* peak arising after dosing with NO is more pronounced (Fig. 52(b)), whereas the additional broad peak with a maximum at 412.3 eV is more strongly developed at more grazing detection angles (Fig. 51). This signifies a rather upright average orientation of the NO molecules on the surface. The average zenithal angle between the surface normal and the NO bond axis calculated from the peak intensity at 400.5 eV amounts to $(24 \pm 3)^\circ$. Since the reported angle for NO on oxygen-covered films was approxiamtely 50° with respect to the surface normal [192], this points towards a more upright attachment of the NO molecules to CoOEP.

In conclusion, this section deals with the electronic and magnetic properties of CoOEP molecules and NO-CoOEP nitrosyl complexes adsorbed on an oxygen-covered

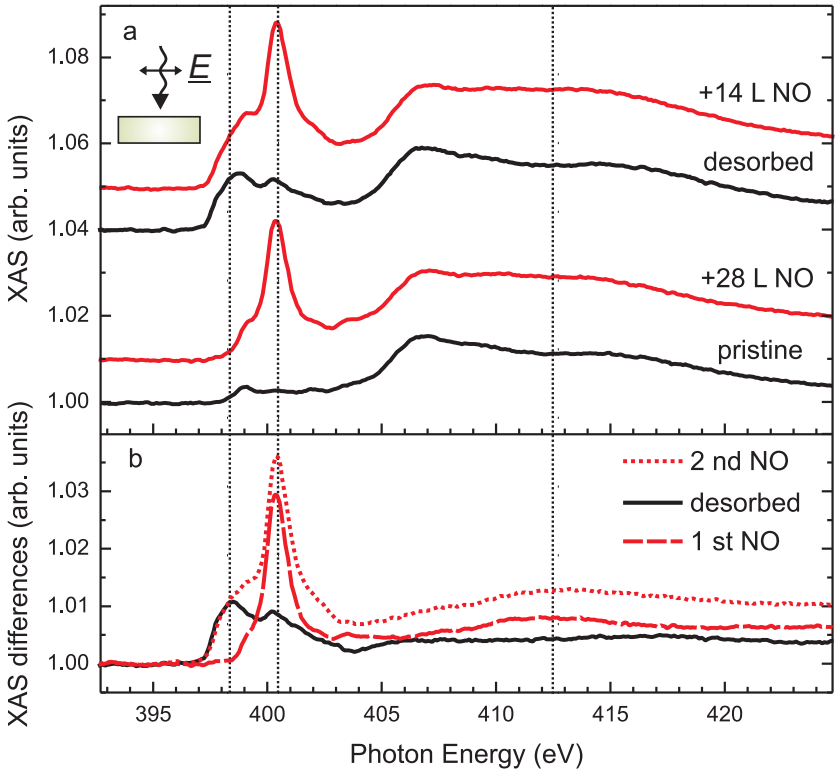

Figure 52: (a) N K XA spectra of 0.7 ML CoOEP on O/Ni measured with linearly polarized light under normal incidence (angle of 90° between the X-ray wavevector and the surface) at 130 K at each NO dosage step. The spectra are shifted vertically for clarity. (b) Difference spectra between the spectra corresponding to the three dosage steps and the spectrum of the pristine sample in (a).

Ni film, grown on Cu(100). The porphyrin molecules adsorb flat on the surface, while their Co ions have a valency of 2+, just as it is the case for isolated CoOEP. Further, the atomic oxygen on top of the Ni surface acts as a spacer layer to increase the distance between the CoOEP molecules and the Ni film, thus weakening their electronic interaction compared to CoOEP adsorbed on a bare Ni film. Nevertheless, the magnetic moment of the Co ions in the centre of the porphyrins couple in a ferromagnetic fashion to the magnetization of the substrate. Up to now, just antiferromagnetic coupling between paramagnetic metalloporphyrins and a ferromagnetic substrate across adsorbed oxygen atoms has been reported. To judge whether, for instance, the suggested ferromagnetic double exchange mechanism could provide an explanation for the findings, future theoretical studies are mandatory.

It is shown that the attachment of the small molecule NO to the Co ions and its subsequent thermal desorption allow to tune the electronic properties of CoOEP molecules in a reversible manner. The uptake of NO leads to the partial oxidation of the Co ions and thus provides the possibility to control the amount of charge localized on the Co ions. The 3d states of the Co ions which have an out-of-plane charge distribution are pushed up in energy. The flow of a non-integer amount of charge away form the Co ions after the coordination of NO changes the Co spin moment. This together with a potentially lower magnetic coupling strength between

the Co ions and the Ni magnetization leads to an NO-induced lowering of the Co magnetization by about a factor of two at 30 K. This demonstrates the possibilty to control the magnetization by the chemical stimulus NO at finite temperatures.

3.5.3 Reversible manipulation of the magnetic coupling strength

The coordination of an additional axial ligand to central metal atoms of metalloporphyrins, adsorbed on ferromagnetic surfaces, can modify both the orbital as well as the spin moment of the central metal ions, as shown in preceding sections. Thereby the magnetic moments, which are aligned by an exchange coupling to the substrate, are changed in absolute values. Within such systems it is tempting to tailor the magnetic coupling strength, as this presents a different approach for a magnetization control of the molecules at finite temperatures. Regarding this, the chemical nature of the central metal atom of MP molecules magnetically coupled to a substrate is of importance. The studies presented in sections 3.5.1 and 3.5.2 deal with CoOEP molecules adsorbed on magnetic surfaces containing Co ions with a +2 valency before dosing with CO or NO. In contrast, for FeOEP on O/Co/Cu(100) the Fe atoms are in a +3 oxidation state. It is already known from literature for this system that the Fe spins couple antiferromagnetically to the magnetization of the thin transition metal film and that the orbital moments of the Fe ions are completely quenched [35]. It is most likely the case, that a coordination of an additional axial ligand to the Fe atoms of this system should not lead to a transfer of charge away from the central metal ions, as a +4 oxidation state of porphyrinato iron derivatives is very unusual [193]. Here, in order to test this, FeOEP molecules are adsorbed on oxygen-covered Co films, grown on Cu(100), and by dosing with NO the Fe electronic properties and the adsorbate–substrate interaction are tried to be influenced.

Angle-dependent XA measurements at the Fe $L_{2,3}$ edges as well as an XMCD study at the Co and Fe $L_{2,3}$ edges in remanence of the thin Co film are presented, before and after dosing with NO. The data of the pristine state are compared with an isotropic XA spectrum at the Fe $L_{2,3}$ edges of FeOEP-Cl bulk material. This together with an angle-dependent XA study at the N K edge has the aim to ensure a preparation of the system as known from literature. Then the focus of interest is on the impact of the small molecules on both the electronic and magnetic properties of the Fe ions as well as on their exchange interaction with the Co spins. For the purpose of restoring the pristine state after dosing, the system is annealed in order to remove the NO molecules. Also the influence of a second dosage of NO on the physical properties of the system is discussed. Further, the adsorption behavior of NO on FeOEP/O/Co and the impact of thermal energy, brought to the system to desorb NO molecules, is investigated by means of N K XA spectra and N 1s XPS spectra. Finally, the role of the Cl atoms, which are attached to the Fe ions within the molecular powder of FeOEP-Cl used for the preparation of FeOEP/O/Co/Cu(100), is analysed in the context of the presented study by Cl 2p XPS spectra.

FeOEP molecules contain an Fe ion, which is constrained by the crystal field of a planar porphinato ligand, instead of a Co ion like it is the case for CoOEP. The coordinatively unsaturated nature of the Fe ions causes a high reactivity of this chemical compound. However, the axial coordination of a Cl atom to the central metal ion stabilizes them chemically and leads to the formation of FeOEP-Cl molecules (see

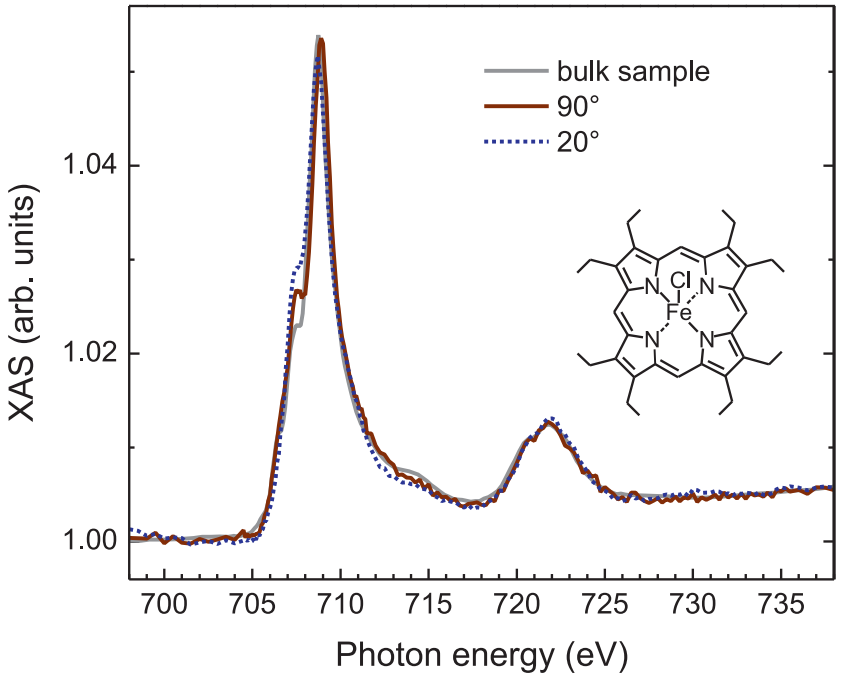

Figure 53: Fe $L_{2,3}$ XAS spectra of 0.6 ML FeOEP on O/Co measured at 120 K at 90° normal incidence (brown line) and 20° grazing incidence (blue dashed line), compared to the spectrum of an FeOEP-Cl powder reference sample (grey line). Inset: sketch of the FeOEP-Cl molecule.

sketch in Fig. 53).

In order to study the electronic properties of the Fe ions situated in the centre of FeOEP-Cl molecules evaporated on O/Co/Cu(100), Fig. 53 shows angle-resolved Fe $L_{2,3}$ edge XA spectra, which correspond to a molecular coverage of 0.6 ML, together with the one of a bulk FeOEP-Cl reference sample (grey line). The latter is acquired at RT from a powder sample pressed into indium foil, while the spectra of the adsorbed molecules are recorded at 20° grazing (blue dotted line) and 90° normal (brown line) incidence, both at 120 K. The main differences for the spectra measured in the submonolayer regime under different measurement geometries are a small shift in the L_3 energy position and the intensity of the shoulder at lower photon energies. The line shape of the spectrum of the bulk material agrees well with results from literature [110], for which a +3 oxidation state is known. It also bears a close resemblance to the ones of the adsorbed porphyrin molecules concerning the shape of spectral features. Also it possesses an almost identical energetic position of both the Fe L_3 and L_2 edges. The absorption energy is related to the amount of charge at the Fe site [134]. These two facts are strong indicators for a +3 oxidation state of the Fe ions for the adsorbed molecules and an exchange of the Cl ligand by the surface, acting instead as a new coordination partner. This agrees well with the theoretically discussed +3 oxidation state of the Fe ions after the adsorption of the porphyrin molecules, where also a detachment of the axial Cl ligand from the FeOEP-Cl molecules is the case [35]. The presence of intact FeOEP-Cl molecules on the oxygen-covered Co film and Fe atoms which only weakly interact with the substrate could also explain the almost identical line shape of the Fe $L_{2,3}$ XA spectra shown in Fig. 53. However, this is unlikely, since

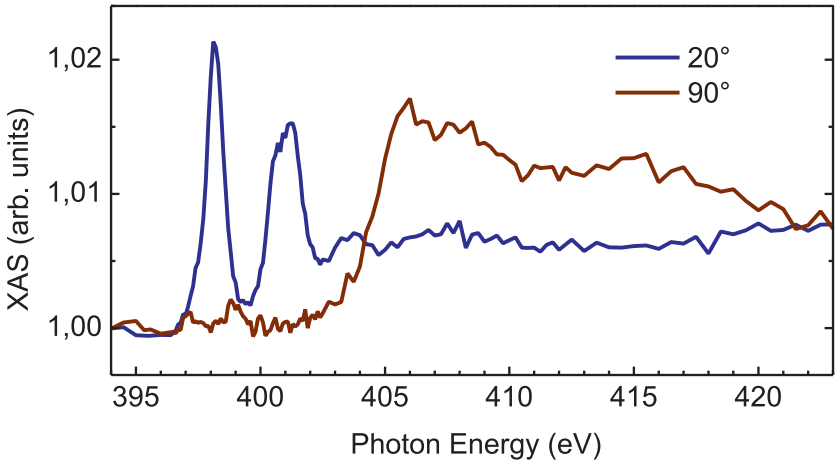

Figure 54: Angle-dependent N K edge XA spectra of 0.6 ML FeOEP/O/Co taken with p-linearly polarized X rays. The blue and brown lines display the absorption spectrum for 20° grazing and 90° normal incidence of the incoming beam with respect to the sample plane.

there is a magnetic coupling between the Fe and Co spins mediated by the O atoms [35], which requires an electronic interaction between the Fe atoms and the substrate.

A flat adsorption of FeOEP on O/Co/Cu(100) was revealed by the angular dependence of the N K XA signal and DFT+U calculations [35]. With the intention to check the earlier published results on that system for consistency, Fig. 54 presents N K edge XA spectra of 0.6 ML FeOEP/O/Co recorded with p-linearly polarized X rays. The spectra are taken at 120 K and at 90° normal (brown line) and 20° grazing incidence (blue line). At lower photon energies spectral features are much more pronounced at grazing incidence and two sharp resonances are detected, while at higher photon energies the spectrum is more appearant under normal incidence and a broad resonance is visible. There is a clear and close overall similarty of the angle resolved N K edge XA spectra with the ones published earlier for the same system [35] and with the ones for CoOEP molecules adsorbed on an oxygen-covered Ni film on Cu(100), shown in the previous section (Figs. 51 and 52). This demonstrates that there are intact FeOEP molecules on the surface and that the porphyrins adsorb flat on the substrate.

For the purpose of studying also the magnetic properties of the exchange coupled system Fig. 55 displays helicity-averaged XA spectra of the Fe $L_{2,3}$ edges (a) and the XMCD spectrum (b) of 0.6 ML FeOEP on O/5 ML Co/Cu(100) (black curves). Also the XMCD spectrum of the Co $L_{2,3}$ edges of the ferromagnetic film underneath the molecules is presented in the inset of Fig. 55 (b). Magnetic measurements were carried out in remanence of the Co film with a thickness of five monolayers. Further, the data were recorded at 120 K and at 20° grazing incidence, since the ferromagnetic Co film possesses an in-plane easy axis along the [110] direction [93, 194]. The Fe XA spectrum of the L_3 edge of the pristine sample with a maximum at a photon energy of 708.7 eV and a shoulder at the low energy flank (black line) fits to the ones measured with p-linearly polarized light. The corresponding Fe XMCD signal at the L_3 edge has a main maximum at 708.6 eV and a local maximum at 707.2 eV, while it even changes sign towards higher photon energies due to a zero crossing at 709.9 eV. A

comparison of the totally integrated Co and Fe L_3 XMCD signals reveals that they are of opposite sign and that the Co and Fe spins are antiparallel coupled to each other. Hence, the resulting Fe magnetization lies in-plane. By applying the sum rules [49, 50] to the Fe XMCD spectrum and assuming five holes within the $3d$ shell, a value of -(2.74 ± 0.20) μ_B is obtained for the effective spin moment $m_S^{\text{eff}}(0°)$ per Fe atom, while the orbital moment is zero within the error bar. Thereby an angle of 20° between the $\vec{k}$ vector of the X rays and the Fe magnetization is taken into account. A temperature-dependent XMCD study of this system revealed a saturated effective spin moment of -(3.46 ± 0.35) μ_B [88], which is compatible with the value here found at 120 K considering that the Fe spins are subject to thermal fluctuations at finite temperatures. In this context it has to be mentioned that the applicability of the spin sum rule to Fe +3 ions is questionable owing to the mixing of intensities at the $L_{2,3}$ edges provoked by multiplet effects and the $3d$ SOC [164, 195, 196]. In that particular case the spin sum rule can underestimate the effective spin moments by more than 30%. Being also aware of the presence of the intra-atomic spin dipole moment, which can be significant in low-symmetry systems, as shown in sections 3.3.2 and 3.4.2, either an intermediate spin state with $S = 3/2$ or a high-spin state with S=5/2 of the Fe ions can be deduced on the basis of the spin sum rule results [197]. Consequently, for the former a spin moment of -3 μ_B and for the latter of -5 μ_B is expected, which would be both consistent with the experimental findings. However, the Fe ions might be also in an admixed $S = 3/2, 5/2$ spin state. A low spin state with $S = 1/2$ of the Fe ions can be ruled out with a high probability from the experimental results, while DFT+U calculations for the system studied here revealed for both, the high and intermediate spin state, an antiparallel alignment of the Co and Fe magnetic moments [88].

Having so far reproduced known results for FeOEP adsorbed on O/Co/Cu(100), in the following the influence of dosing with NO on the magnetic characteristics of the system is investigated. In Fig. 55 the helicity-averaged Fe $L_{2,3}$ XA and the corresponding XMCD spectrum of 0.6 ML FeOEP on O/Co/Cu(100) are shown after dosing with 24 L of NO (red curves), which is done at 120 K in order to avoid a dissociation of the NO on the surface [191]. The most prominent modifications of the Fe XA line shape, provoked by the NO, are the reduction of the shoulder in the low-energy flank of the L_3 peak at an energy of 707.5 eV and the augmentation in intensity of the L_2 peak at around 722 eV. Additionally, the similarity of the Fe XA $L_{2,3}$ edges regarding their energy positions before and after dosing with NO is obvious. The branching ratio, defined as the proportion of the Fe L_3 to the entire Fe $L_{2,3}$ XAS intensity, as already introduced in section 3.5.1, reduces from 0.77 ± 0.03 to 0.70 ± 0.03 upon NO adsorption. This quantity has been used in literature to obtain information about the spin state of the element under study [198]. So in the presence of a weak ligand field and no charge transfer from or to any ligand, a lower branching ratio would suggest a lower spin state of the Fe atoms. Unfortunately, the system under study does not have these characteristics and there might be a lack of correlation between the spin state and the branching ratio. The discussed NO-induced changes of the Fe $L_{2,3}$ XA spectrum reveal that NO interacts with the Fe ions. The almost unchanged absorption energy after NO uptake indicates that the Fe atoms preserve their oxidation state [199, 200], since otherwise mostly a shift of spectral weight would be observed.

To work out the influence of the NO on magnetic properties of the Fe ions within the

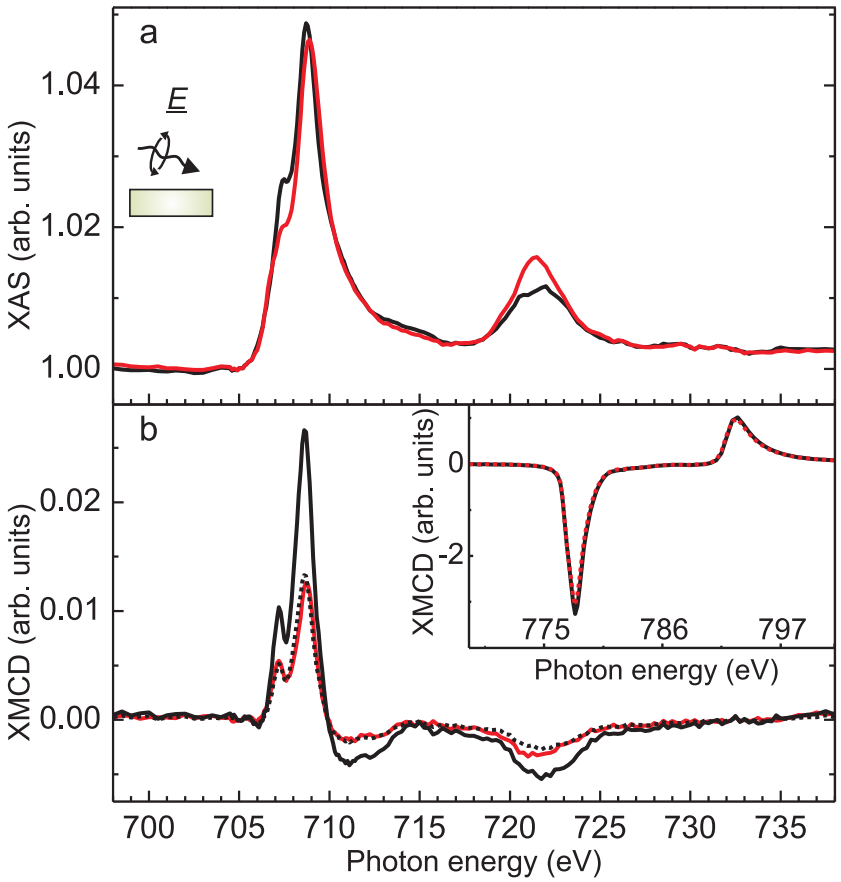

Figure 55: Fe $L_{2,3}$ XAS (a) and corresponding XMCD (b) spectra of 0.6 ML FeOEP on O/5 ML Co/Cu(100) recorded at 120 K and at 20° grazing incidence before (black lines) as well as after (red lines) dosing with 24 L of NO. In (b) the black dotted line also presents the spectrum before NO dosage, but scaled by a factor of 0.5. Inset: XMCD spectra at the Co $L_{2,3}$ edges before (black line) and after (red dotted line) dosing with NO.

exchange-coupled system, it is essential to clarify the alteration of the Co magnetic properties upon dosing with NO. To do so, in the inset of Fig. 55 (b) also the Co $L_{2,3}$ XMCD spectrum (red dotted line) after NO adsorption is displayed. Only a tiny variation of the strength of the Co XMCD signal is detected compared to the pristine state of the sample. Hence, the oxygen layer practically protects the substrate magnetic properties from being influenced by NO adsorption [189], similar as for CoOEP/O/Ni/Cu(100) shown in section 3.5.2. This is opposite to other uncovered ferromagnetic films like thin Co films grown on a stepped Cu surface for which a change of the easy magnetization axis by NO attachment has been reported [201].

The NO attachment to the Fe atoms modifies neither the spectral line shape of the Fe $L_{2,3}$ XMCD spectrum nor its energetic position compared to the pristine state, but reduces its signal by around a factor of 2. For reason of comparability and clearness the Fe $L_{2,3}$ XMCD spectrum before dosing is scaled by a factor of 0.5 and shown as well (black dotted curve) in Fig. 55 (b). It reveals a minor mismatch in the relative height of the XMCD peaks at the Fe L_3 edge as opposed to the Fe spectrum after

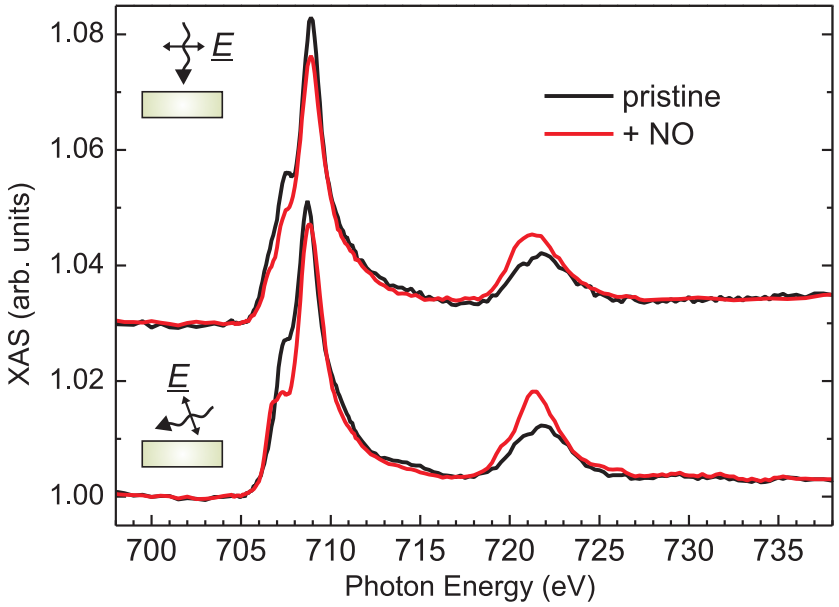

Figure 56: Fe $L_{2,3}$ XAS spectra of 0.6 ML FeOEP on O/Co measured at 120 K at 90° normal incidence (top pair of curves)and at 20° grazing incidence (bottom pair of curves) before (black lines) and after (red lines) dosing with 4 and 24 L of NO, respectively.

dosing with NO and a marginally lower XMCD signal at the L_2 edge. Clearly, the negligible modification of the line shape evidences an unchanged spin state of the Fe atoms after NO uptake.

Fe $L_{2,3}$ absorption spectra, taken with p-linearly polarized light, provide further insight on the interaction between the small adsorbate and the metal centers of the porphyrin molecules. Fig. 56 presents such spectra before (black lines) and after (red lines) NO adsorption, where the ones of the pristine sample are the same as the spectra shown in Fig. 53. The bottom pair of curves is recorded at 20° grazing incidence and the top pair at 90° normal incidence, shifted vertically for the sake of clearness. Measurements are performed after a dosage of 24 and 4 L of NO, for 20° grazing and normal incidence, respectively. The NO-induced modifications of the lineshape are qualitatively identical to the ones detected in measurements with circularly polarized light and averaged over the signals for positive and negative helicity. They are more pronounced at grazing incidence, where unoccupied orbitals with rather out-of-plane distribution are probed. This reflects the axial attachment of the NO molecules to the Fe atoms. By applying the charge sum rule [46] before and after NO uptake, an unchanged white line intensity is found for 20° grazing incidence and a reduction by $(1 \pm 3)\%$, which is zero within the error margin, for normal incidence. Hence, there is no net charge transfer between the Fe ions and the NO molecules and thus the Fe atoms remain in an oxidation state of +3. As discussed later in this section in the context of Fig. 61, the different NO dosage for measurements at the different detection angles, 4 vs. 24 L, is not the reason for the more apparent effect at grazing incidence compared to normal incidence.

In order to work out the influence of the NO adsorption on the magnetism of the Fe ions, the sum rules [49, 50] are applied to the Fe XMCD spectrum after dosing with

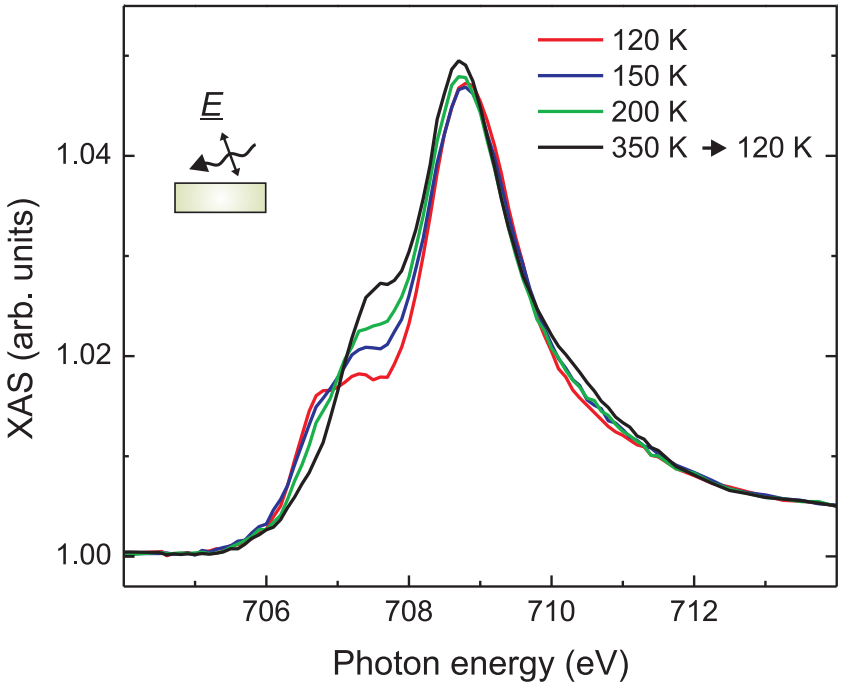

Figure 57: Fe L_3 XAS spectra of 0.6 ML FeOEP on O/Co after dosing with 24 L NO at 120 K, recorded at 20° grazing incidence. Red, blue, and green lines belong to spectra taken at 120, 150, and 200 K, respectively, while the black line was recorded at 120 K after heating the sample to 350 K.

NO. This yields a value of -(1.42 ± 0.20) μ_B for $m_S^{\text{eff}}(0°)$ per Fe ion and an orbital moment $m_L(0°)$, which is 0 within the error. Thereby again 5 holes within the Fe 3d shell are assumed. The conspicuous resemblance of the lineshape of the Fe XMCD signal at the $L_{2,3}$ edges reveals that the spin-pairing energy of Fe^{3+} hinders a spin crossover transition. The similarity of the Fe XMCD signals also strongly suggests that the intra-atomic spin dipole moment is of similar size before and after dosing as the ligand field, the orbital occupation, and the symmetry are mainly conserved. Also the extent of mixing of the L_3 and L_2 edges in their respective $2p_{3/2}$ and $2p_{1/2}$ characters has an influence on the sum rule analysis as discussed above [164, 195, 196]. Since the valency of the Fe atoms stays constant after NO exposure, this influence on the sum rule analysis, which dependes basically on the oxidation state, does not change. Thus, the reduced effective spin moment has to be rather explained by a lower magnetic coupling strength between the Fe spins and the Co magnetization. It has been found that the mechanism establishing the magnetic ordering inside FeOEP before dosing with NO is a 180° superexchange coupling between the Fe and Co spins mediated via O atoms [88]. The corresponding magnetic coupling energy has been estimated as 37 meV [88], which leads to an alignment of the Fe magnetic moment at 120 K of about 93% of the saturation value. The thereby used model is the same as the one introduced in section 3.4.1. A reduction of this coupling energy by the NO uptake to 10 meV would induce an Fe magnetization of 48% at 120 K, as evaluated with this model, and would alone explain the experimentally found lowering of the XMCD signal after NO attachment. The physisorption of NO onto FeOEP is

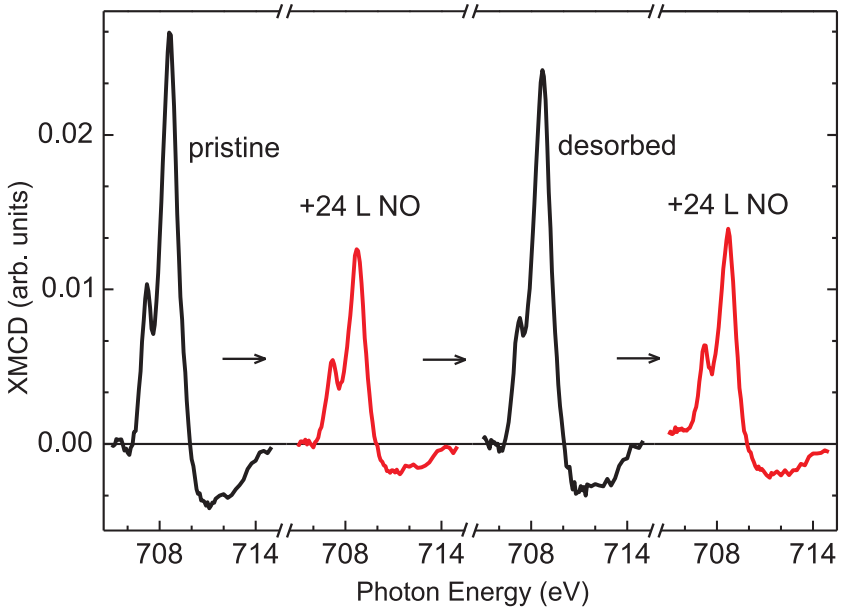

Figure 58: Fe L_3 XMCD signals measured at 120 K at each NO dosage step. From left to right, the spectra correspond to the sample in the pristine state, after dosing with 24 L of NO, after subsequent desorption of NO by warming up to 350 K, and after dosing with 24 L of NO once more.

obviously inducing this reduction. A potential mechanism could be the modification of the bond length between the O and Fe atoms due to the presence of the NO. Only lately, also a reduction of the magnetic coupling strength of an exchange interaction between Mn ions of MnPc molecules and the magnetization of Co films caused by the adsorption of ammonia was reported. However, the attachement of NH_3 to the Mn atoms significantly modifies their electronic and magnetic properties in contrast to the system studied here, where the Fe ions preserve their physical characteristics [59].

In order to desorb the NO from the porphyrins and thus to control the electronic properties of the Fe ions in a reversible manner, thermal energy is brought to the system. Fig. 57 displays Fe L_3 XA spectra of 0.6 ML FeOEP on O/Co after dosing with 24 L NO at 120 K (red line), measured at 20° grazing incidence. The evolution of the Fe L_3 XA spectrum with temperature during the annealing of the sample is revealed by displaying spectra taken at 150 (blue line) and 200 K (green line) as well as at 120 K after heating the sample to 350 K (black line). Unambiguously, the NO-reduced reduction of the shoulder at the low-energy flank at 707.5 eV is stepwise reversed. This proves the possibility to reversibly switch the Fe electronic structure. Further the gradual transition between two spectra, resembling the ones shown in Fig. 55 (a), reveals that there is no transition from a weakly to a strongly interacting NO on top of FeOEP before desorption.

For the purpose of revealing a reversible modification of the magnetic interactions between the porphyrins and the substrate provoked by the NO also XMCD measurements at the Fe L_3 edge are performed after annealing the sample to 350 K and subsequent cooling to 120 K. Figure 58 contrasts the XMCD signals at the Fe L_3 edge of the pristine sample, of the sample after dosing with 24 L of NO, after bringing the system to 350 K, and after dosing once more with 24 L of NO, all measured at 120

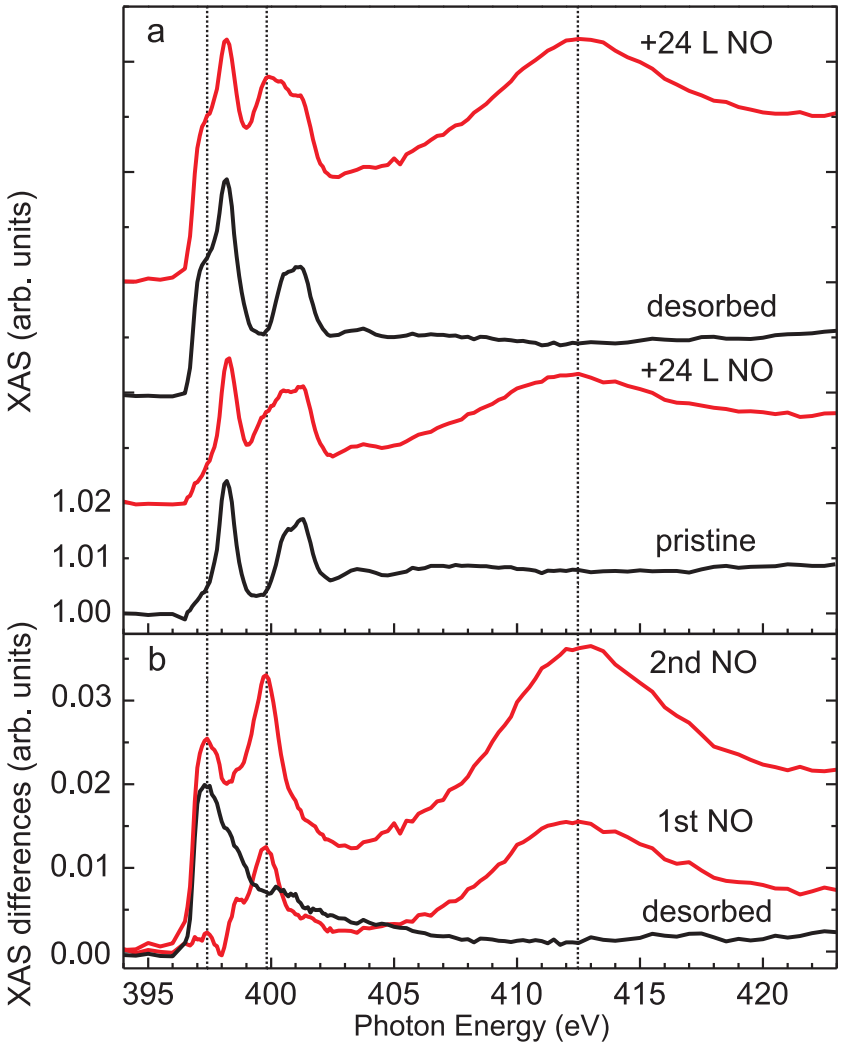

Figure 59: (a) From bottom to top, N K edge XA spectra of the sample in the pristine state, after dosing with 24 L of NO, after subsequent desorption of NO by warming up to 350 K, and after dosing with 24 L of NO once more. Spectra are taken at 20° grazing incidence with p-lineraly polarized light and are shifted vertically for clarity. (b) Difference between the top three XA spectra of panel (a) and the XA spectrum of the pristine sample.

K. It is apparent that after the detachment of NO from the Fe ions the original Fe XMCD intensity is nearly totally regained and that a dosage of NO induces again a reduction by almost a factor of 2. This reveals that it is possible to reversibly control the Fe magnetization at a finite temperature of 120 K.

Measurements at the N K edge can be used to gain insight into the adsorption characteristics of NO on FeOEP/O/Co. Fig. 59 (a) displays from bottom to top such spectra recorded at 120 K, at 20° grazing incidence, and at each step of the measurement series shown in Fig. 58. Thus, results are shown of the pristine sample, after dosing with 24 L of NO, after annealing, and after dosing once more with 24 L of NO. In panel (b), for reasons of clarity, the spectra of the last three steps after subtracting the spectrum of the pristine sample are presented. The N K edge spectrum before dosing with NO possesses the same lineshape as the one shown in Fig.

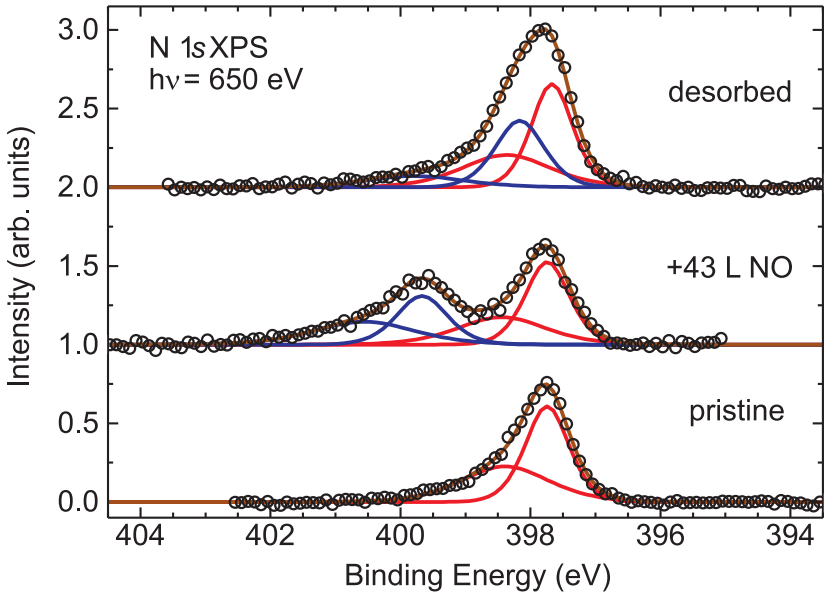

Figure 60: N 1*s* XP spectra of 0.6 ML FeOEP on O/Co before exposure of NO (bottom), after a dosage of 43 L of NO (middle), and after annealing the system to 350 K (top).

54. After the first NO dosage further spectral intensity in the lower photon energy range is found at 399.9 and 398.7 eV. At higher photon energies a broad peak with a maximum around 412.5 eV eV shows up. The same energetic position as for the new resonance at 399.9 eV has been found for NO in the gas-phase [188]. This suggests the presence of NO molecules that only weakly interact with the porphyrins, as already discussed in the context of the NO-induced changes of Fe $L_{2,3}$ XMCD spectra. The peak in the low-energy flank at 398.7 eV may be ascribed to some NO chemisorbed on the oxygen-covered Co film. After heating the system, the new intensity at 399.9 eV vanishes. This is consistent with the detachment of the weakly bonded NO species. At the same time a new resonance arises at 397.4 eV. The latter is most likely related to a chemisorbed atomic N species, which results from the dissociation of NO on the surface [190]. Dosing once more with NO does not affect this peak but restores the peaks at around 399.9 and 412.5 eV. In general, surface chemistry of NO molecules on transition-metal substrates can be quite versatile, as discussed in literature [190, 191]. Parameters such as temperature, surface reactivity, or amount of NO are of importance.

For an even deeper understanding of the interaction of NO with FeOEP/O/Co, Fig. 60 shows N 1*s* XP spectra recorded before (bottom), after dosing with 43 L of NO (middle), and after desorbing the NO molecules by annealing the system up to 350 K (top). The spectra are recorded with an excitation energy of 650 eV. The binding energy is calibrated relative to the energy of the Co $3p_{3/2}$ peak, which is set to 75.1 eV. The XPS signal of the pristine sample is fitted with two peaks, which have to be attributed to the four nitrogen atoms inside the porphyrin macrocycle. Their energetic positions of 397.8 and 398.4 eV coincide with the absorption energy of the first sharp resonance in the N K edge spectrum (see Fig. 54). After dosing with 43 L of NO new spectral features appear, which can be fitted by two peaks with maxima

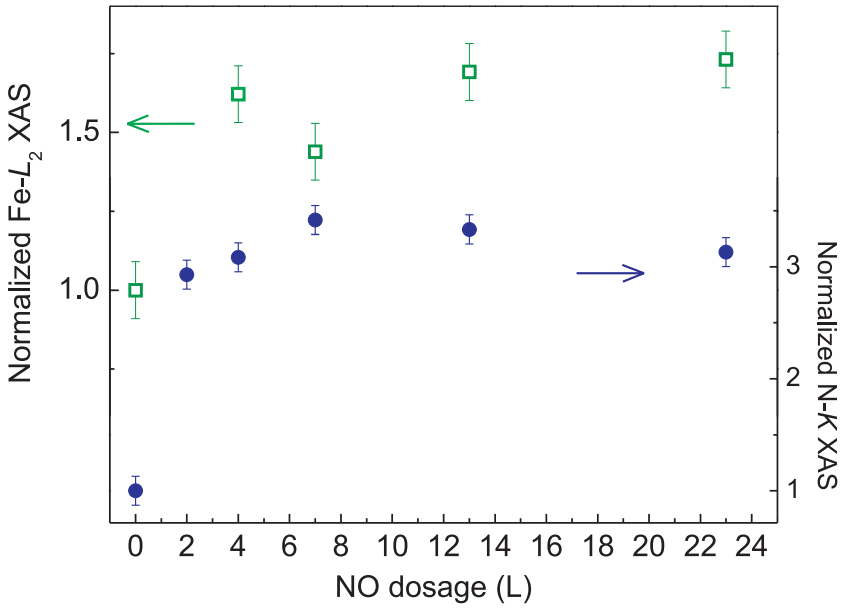

Figure 61: NO dosage dependence of the Fe L_2 and N K XAS signals at photon energies of 721.4 (squares) and 412.5 eV (circles), respectively, relative to the corresponding intensities of the pristine sample. Each y-axis has an individual labeling.

at 399.7 and 400.6 eV. In literature a peak position of 403 eV has been reported for free NO molecules [202] and of 399 eV for NO in contact with a Co surface [203]. In line with the interpretation of the N K edge XA spectra, the peak at 399.7 eV is such ascribed to NO molecules situated on the oxygen-covered Co substrate, and the one at 400.6 eV to a NO species interacting with Fe porphyrin molecules. The peak areas reveal a ratio of 1:3 between the amount of porphyrin and NO molecules on the surface. Further, the two new peaks, arising after the NO uptake, possess a ratio between their areas of 1:1. This reveals that the probability for an NO adsorption directly on the oxygen-covered Co surface or onto FeOEP is equally 50%. After having brought thermal energy to the system, the peak at 400.6 eV vanishes and the one at 399.7 eV survives, but loses significantly in intensity. Additionally, a peak arises at 398.2 eV, which is ascribed to atomic nitrogen bonded to O/Co, following the results of the N K XA spectra (see Fig. 59). With the help of the peak areas it can be concluded that 13% of the initially existing NO molecules on the surface are desorbed and approximately three quarters of the remaining NO molecules dissociate, which leads to the presence of atomic nitrogen on the O/Co substrate.

With the intention to reveal how the NO attachment is linked to the modification of the magnetization of the Fe ions, Fig. 61 displays the NO-induced changes at the N K (●) and the Fe $L_{2,3}$ (□) edges as a function of NO dosage. The evolution of the absorption signals at 412.5 and 721.4 eV is shown, respectively, which are normalized to their values prior to NO exposure. A distinct rise of these two intensities at low dosages, which saturates approximately after 4 L of NO, is found. Following the results of the N 1s XPS study, this corresponds about to 3 NO molecules per FeOEP molecule on the substrate. On the basis of the similar behavior of the nitrogen and iron signals as a function of NO dosage it can be concluded that the changes of the

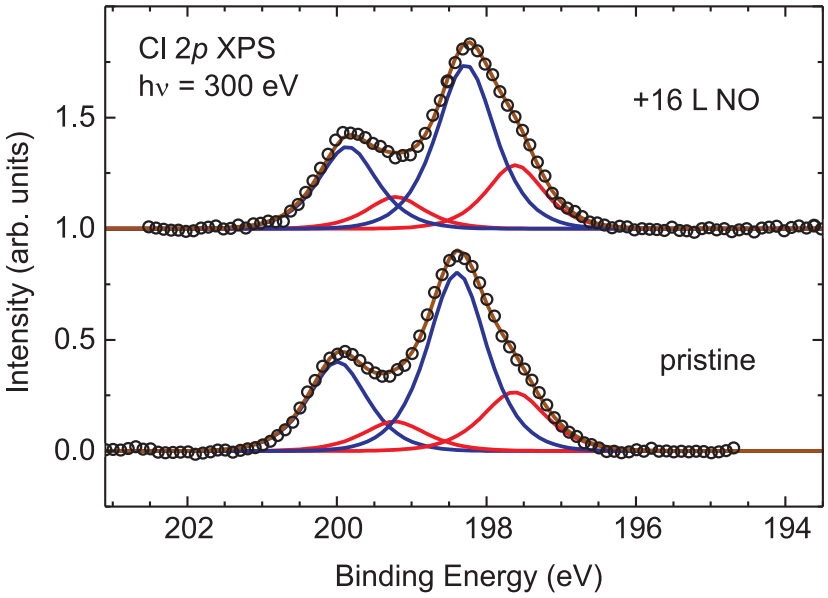

Figure 62: Cl 2*p* XP spectra of 0.6 ML FeOEP on O/Co before (bottom) and after dosing with 16 L of NO (top).

Fe electronic structure and magnetization are in fact caused by the adsorption of the NO in the vicinity of the Fe atoms.

For the sake of completeness, Cl 2*p* XP spectra of 0.6 ML FeOEP on O/Co are shown in Fig. 62, measured with an excitation energy of 300 eV before (bottom) and after (top) dosing with 16 L of NO. They help to analyse in which form Cl is present on the surface after sublimating FeOEP-Cl on O/Co/Cu(100). The influence of the sublimation of Cl-containing trivalent transition-metal porphyrin molecules on their chemical entity is crucial for a desired controlled sample preparation. Obtaining a straight evidence for a Cl-porphyrin dissociation by a XPS study is almost impossible as the binding energies of 198.5 eV for atomic Cl coordinated to the Fe atoms or adsorbed on the substrate are virtually the same [204, 205]. In the pristine state of the sample, the Cl 2*p* XP spectrum possesses two peak doublets. The energy splitting between the Cl $2p_{3/2}$ and the Cl $2p_{1/2}$ peaks is 1.6 eV. The respective $2p_{3/2}$ binding energies of the main and minor doublet are 198.4 (blue curves) and around 197.7 eV (red curves). A relative calibration of the binding energy is done by means of the Co $3p_{3/2}$ peak position set to 75.1 eV. The main doublet of the Cl XPS signal could be assigned to atomic Cl bonded to the Fe ion as well as to the Co thin film. The smaller doublet has to be of different physical origin. For MnTPPCl molecules on Co(001), for instance, an additional Cl $2p_{3/2}$ XP peak was observed at a slightly higher binding energy than 200 eV [179]. It was ascribed to a Cl species which remained bound to the substrate after the partial molecular decomposition.

Nevertheless, from a comparison of Fe $L_{2,3}$ XA spectra of FeOEP-Cl bulk material and FeOEP adsorbed in the submonolayer regime on O/Co (see Fig. 53), it was already concluded that the axial Cl ligand dissociates from the Fe ions and is exchanged by the oxygen-covered Co surface. Then, by dosing with NO, a lineshape modification of the Fe $L_{2,3}$ XA spectra was induced, revealing the existence of an axially uncoordinated site at the Fe atoms. By comparing the Cl 2*p* XP spectra before and after NO uptake,

which are identical, no influence of the NO on the electronic properties of the chlorine is found. This supports the idea of a detachment of the axial Cl ligand from the FeOEP-Cl molecules already before NO exposure.

The modification of the magnetization of central metal ions of MP molecules magnetically coupled to ferromagnetic films has been the subject of the previous sections of this thesis. Also results within cited literature deal with this issue. All these studies have in common that the electronic and magnetic properties of the central metal ions of the adsorbed MP and MPc molecules are changed upon the attachment of small molecules from the gas phase. In contrast, here the adsorption of NO on FeOEP/O/Co leaves the electronic structure and the magnetic properties of the Fe ions unaffected while at the same time inducing a sizeable change of the Fe magnetization at finite temperatures. The virtue of a weakly interacting small ligand allows to design the electronic and magnetic properties of the formed complex by only considering porphyrin–substrate interactions. On the other hand the axial coordination enables to control the degree of alignment of single molecular spins on magnetic surfaces at finite temperatures, which presents new prospects in the context of molecular spin electronics.

In conclusion, it has been demonstrated that the magnetization of Fe ions within FeOEP molecules magnetically coupled to the magnetization of a thin Co film can be controlled in a reversible manner by adsorbing and thermally removing NO molecules. The NO physisorbs on top of FeOEP adsorbed on O/CO. Thus, the electronic and magnetic properties of the Fe atoms are unchanged upon NO uptake. However, the strength of the magnetic exchange coupling between the Fe and Co spins is sizeably lowered and so the Fe magnetization is reduced by about 50% at 120 K. After the detachment of NO the original Fe magnetization at 120 K is restored and dosing once more with NO reduces again the strength of the magnetic exchange coupling. This proves the reversibility of the process.

Conclusions

Comprehensive investigations of cobalt-octaethylporphyrin (CoOEP) and iron-octaethylporphyrin (FeOEP) molecules as well as of CO-CoOEP carbonyl, NO-CoOEP and NO-FeOEP nitrosyl complexes on surfaces have been presented. By in-situ sublimation, monomolecular layers of metalloporphyrin (MP) molecules on non-magnetic as well as on bare, oxygen-, and graphene-covered ferromagnetic substrates were prepared. Their electronic properties were characterized by means of angle-dependent X-ray absorption spectrosopy (XAS). This technique was also used to reveal the formation of nitrosyl and carbonyl complexes after dosing with carbon monoxide (CO) and nitric oxide (NO), to monitor the thermal desorption of the small gas molecules as well as to study their influence on the electronic structure of the central Fe and Co ions. By means of field-, temperature-, and angle-dependent X-ray magnetic circular dichroism (XMCD) studies, both the magnetic properties of adsorbed MP molecules and magnetic adsorbate–substrate interactions before and after dosing with CO or NO were analysed. Some of the experimental results are interpreted with the help of theoretically calculated X-ray absorption (XA) spectra from the group of Prof. Hermann obtained from density functional theory (DFT) and StoBe cluster calculations. The magnetic coupling mechanism of one of the experimentally studied exchange-coupled systems is explained by means of DFT+U calculations from the group of Prof. Oppeneer.

This work can be attributed to chemical surface physics and deals especially with molecular compounds with uncompensated spin moments. These are the mentioned metalloporphyrin molecules, which contain a metal ion being surrounded by a planar porphinato ligand and two axial coordination sites. The latter can be occupied by additional ligands like metal surfaces or small molecules, as shown. By putting the molecules on top of a solid surface, they get immobilized at least against motions in the third dimension as desired for their use as molecular building blocks, while a second axial coordination site remains available, e.g., for small molecules. The choice of the two axial ligands enables the tuning of the electronic and magnetic properties of the MP molecules in a desired manner. The adsorption of MP molecules on magnetic surfaces is of special interest for the architecture of a molecular spintronics, since the spins of the central metal ions can get stabilized against thermal fluctuations by a magnetic exchange coupling. In the framework of this thesis, all these properties of MP molecules are picked up to design hybrid metal-organic systems from adsorbates with desired physical characteristics. The aim is to design magnetic structures on the nanoscale that can be used as building blocks for a prospective molecular spintronics.

First the electronic properties of pure CoOEP are discussed in the context of XA measurements of CoOEP bulk material and an associated theoretical work of the collaborating group of Prof. Hermann. The Co ions have a valency of +2 and are in a d^7 low-spin state. These experimental results serve as reference for the analysis of experimental data of CoOEP molecules in direct contact with surfaces and help to figure out the impact of the adsorption on the molecular electronic structure. The coordination of CoOEP with two non-magnetic surfaces, highly ordered pyrolytic graphite (HOPG) and Cu(100), is studied in detail. The two systems represent examples for a weak and strong molecule-surface interaction, respectively. The molecules adsorb almost flat on HOPG. Further, the Co 3d states do not contribute to the

molecule–substrate interaction at all, and the electronic states originating from the nitrogen atoms only to a negligible extent. Thus, the Co electronic structure does not change upon adsorption on HOPG and the porphyrins physisorb on the surface. In contrast, the adsorption of CoOEP on Cu(100) strongly modifies the electronic structure of the central Co ions and the N atoms of the porphyrin macrocycle. The Co ions neither change their oxidation state of +2 nor their spin state of $S = 1/2$ upon adsorption. However, as found out by determining the distribution of the spin density located at the Co site in space, a redistribution of the electrons within the Co 3*d* shell occurs. Upon adsorption, the unpaired electron occupies an orbital whose charge distribution lies primarily in the plane of the macrocycle and not perpendicular to this plane as for isolated CoOEP. The observed physisorption of CoOEP on HOPG, on the one hand, and the detected chemisorption of CoOEP on Cu(100), on the other hand, reflect the respective reactivity of these surfaces. The results expand the already broad knowledge about the electronic structure of MP molecules adsorbed on surfaces. They reveal that the porphyrin–surface interaction plays an important role for the target-oriented engineering of future molecular devices concerning their electronic properties.

For the purpose of achieving an alignement of the Co magnetic moments without the need of applying an external magnetic field, CoOEP molecules are placed on bare and oxygen-covered thin Ni films. The porphyrins are found to adsorb flat on the two substrates. On both surfaces, a ferromagnetic (FM) exchange interaction between the Ni magnetization and the Co spins is observed. This stabilizes the latter against their thermal fluctuations. For CoOEP on Ni the substrate-induced magnetic ordering leads to a Co magnetization even at room temperature (RT). In contrast, for CoOEP on O/Ni the magnetic exchange coupling is much weaker and only at temperatures lower than 30 K the Co magnetic moments get significantly aligned. The modification of the Co electronic structure upon adsorption on the Ni film is much more pronounced than on the oxygen-covered Ni film, where the Co ions have a valency of +2. The oxygen layer between the Ni surface and the CoOEP molecules acts as a spacer layer, which weakens the adsorbate–substrate electronic interaction. In the context of other studies about magnetic interactions of MP molecules with ferromagnetic substrates, the results presented here show a new physical phenomenon. So far only an antiferromagnetic coupling across adsorbed oxygen atoms between paramagnetic metalloporphyrins and a ferromagnetic substrate has been observed. Knowledge about the electronic interaction between molecular states originating from C as well as N atoms and substrate states is experimentally obtained and complemented by the theoretical work of the collaborating group of Prof. Hermann. For CoOEP on Ni it is found that there is electronic N–Ni coupling by orbital hybridization, whereas for CoOEP on O/Ni this can be almost neglected. On the basis of this, potential magnetic coupling mechanisms can be discussed for both systems. For CoOEP on O/Ni a direct magnetic interaction between the Co and Ni spins is unlikely due to the intermediate layer of atomic oxygen, but an indirect one mediated via the O atoms is likely. In contrast, for CoOEP on bare Ni a direct as well as an indirect magnetic coupling between the Ni magnetization and the Co magnetic moments may be present, where for the latter the exchange path includes the N atoms of the porphyrins. Future theoretical studies may identify the nature of the magnetic interaction between the molecules and the surface for both systems. Combining the magnetism of thin

ferromagnetic films and MP molecules is interesting in terms of designing spintronic devices such as molecular spin valves on the basis of porphyrins, since it provides the possibility to gain control over their molecular magnetization.

The magnetic interactions observed between CoOEP and bare as well as oxygen-covered Ni films are accompanied by a modification of the Co electronic structure. A possibilty to preserve the Co electronic properties of CoOEP and to achieve at the same time a substrate-provoked spin polarization is presented in this work by putting the molecules on top of a graphene-passivated Ni surface. This leads to a Co magnetization at 130 K and lower temperatures which is antiparallel aligned to the one of the ferromagnetic film. Experimentally a magnetic coupling energy (E_{ex}) of (1.8 ± 0.5) meV between in-plane aligned Co and Ni spins is found. The corresponding exchange interaction is magnetically anisotopic, as for out-of-plane aligned spins E_{ex} is found to be higher. Interestingly, the electronic overlap in space of the Co $3d$ and the electronic states of the substrate is in this case negligible. An indirect magnetic interaction between the Co and Ni spins as revealed by the theoretical work of the collaborating group of Prof. Oppeneer can explain the experimental findings. The coupling mechanism is based on an electronic interaction between macrocyclic π and graphene p_z orbitals. However, the electronic molecule–substrate coupling is very weak, similar as for CoOEP on HOPG, and leads to a physisorption of CoOEP on graphene/Ni. The nitrogen atoms of CoOEP and the carbon atoms of the graphene possess a spin polarization which is antiparallel and parallel aligned to the one of the Co ions, respectively. The total exchange path is as follows: Ni *sp* states hybridize with graphene p_z orbitals, which thus mediate a weak superexchange between the spin polarization of Ni and the pyrrolic N atoms. The spin densities of the latter couples directly to the ones situated at the Co site in an antiferromagnetic (AFM) fashion. From a theoretical point of view, such a coupling mechanism mediated via the π electronic system of graphene is intriguing and has not been observed before. It allows the design of molecular functionalities independent of the weak electronic adsorbate–substrate interaction, while at the same time a magnetic interaction is establised via the carbon atoms. The latter is an essential ingredient for the use of paramagnetic molecules as building blocks of a molecular spin electronics. The results also show the possibility to incorporate magnetic functionalities into graphene and the potential to combine molecular magnetism with concepts from graphene-based electronics.

Special interest is paid to the contribution of the orbital as well as the spin moment to the Co magnetization. At zero external magnetic fields, the in-plane magnetization of the Ni film correspondingly aligns the Co magnetic moments. Thereby the spin m_S and orbital m_L^{xy} magnetic moments contribute with values of $-(1.03 \pm 0.07)\ \mu_B$ and $-(0.93 \pm 0.05)\ \mu_B$ to the entire Co magnetization, respectively. Despite the hybridization of the Co $3d$ with molecular states, which makes the alignment of the Co magnetic moments by the magnetic exchange interaction possible, m_S and m_L^{xy} are of similar size. The emergence of significant orbital magnetism within the exchanged-coupled system is unusual. For free transition metal atoms, nature maximizes m_S as well as m_L, but hybridization and the presence of a crystal field (CF) strongly quench m_L and may also reduce m_S due to the formation of low-spin states. For CoOEP on graphene/Ni, the influence of the spin–orbit coupling (SOC) on the electronic properties of the Co ions explains the large orbital moment m_L^{xy} as compared to m_S. SOC mixes the ground state and the first excited state of the electronic structure

of the Co atoms. This leads to the formation of a state with finite in-plane orbital moment. The anisotropy in size of the orbital moment of 489% reflects its much lower contribution to the Co magnetization by aligning it perpendicular to the surface. Further the spin and charge distribution of the unpaired electron at the Co site is highly anisotropic, too. Both lie perpendicular to the plane of the macrocycle, as expected for pure CoOEP molecules being consistent with an electronically weak interaction between CoOEP and graphene/Ni. The study of the orbital moment and in particular its anisotropy of nanostructures at interfaces is interesting given its importance for the orientation of the magnetic moments via the SOC. Here, it is shown that also the orbital moment can provide a sizeable contribution to the entire magnetization of an element within an exchange-coupled system of magnetic nanostructures possessing interesting characteristics for potential spintronic devices.

After the adsorption of MP molecules on surfaces, the second axial coordination site of their central metal ion still can be occupied by a further ligand. This enables coordination chemistry of MP molecules on ferromagnetic substrates. This possibility is used in the framework of this thesis in order to manipulate the electronic and magnetic properties of Fe and Co atoms inside FeOEP and CoOEP molecules, which are magnetically coupled to the magnetization of a thin magnetic film. So by dosing with CO on CoOEP/graphene/Ni and with NO on CoOEP/O/Ni the total size of the magnetization of the central metal ion is modified. An attachment of NO to FeOEP on O/Co allows to tune the magnetic coupling strength between the Co magnetization and the Fe spins and thus to control the Fe magnetization at finite temperatures. A subsequent thermal desorption of the chemical stimuli restores the original electronic structure of the metal atoms in all systems and shows the possibility to control the electronic properties of the central metal ions in a reversible manner.

After dosing with CO on CoOEP/graphene/Ni/W(110), the successful formation of carbonyl complexes modifies the CF which constrains the Co atoms compared to the pristine state. As the SOC together with the CF determines the size of the in-plane orbital moment, the CO uptake changes m_L^{xy}. The latter is reduced by (77±6)%, while the Co oxidation state of +2 is unchanged. Also the substrate-induced magnetic order of the Co magnetic moments caused by the indirect exchange interaction between the Co and Ni spins is not diversified. Under the reasonable assumption that the spin state does not change, the CO adsorption induces in total a decrease of the in-plane aligned Co magnetic moments by (37±3)%. These findings show that it is possible to modify the magnetic moments by a chemical approach in an exchange-coupled system of MP molecules on magnetic substrates not only by changing the spin moments but also by altering the orbital moments. This presents an interesting approach since usually m_L is almost completely quenched in such systems due to the hybridization of the $3d$ central metal ion orbitals with electronic states of the substrate and other molecular orbitals of the macrocycle.

In contrast, the coordination of NO as axial ligand to the Co ions of CoOEP molecules adsorbed on oxygen-covered Ni films partially oxidizes the transition metal atoms. So the NO attachment provides the possibility to control the amount of charge localized on the Co site while in particular more electron density is withdrawn from out-of-plane than from in-plane $3d$ orbitals after the NO uptake. Out-of-plane Co $3d$ orbitals are shifted up in energy, while in-plane ones are less affected by the NO attachment regarding their energies. This reflects the axial coordination of NO to the

Co ions of CoOEP. Before and after NO uptake, an exchange interaction couples the Co and Ni spins in a ferromagnetic fashion. The NO-induced flow of a non-integer charge away from the Co atoms changes the Co spin moment. This together with a potentially weaker magnetic coupling between the magnetic moments of the substrate and the Co ions provokes a Co magnetization for the NO-CoOEP complexes that is about a factor of two smaller than the one of CoOEP at 30 K. This shows the possibility to control the Co magnetization by the chemical stimulus NO at finite temperatures.

Unlike the strong interaction between NO and CoOEP on O/Ni, the interaction between NO and FeOEP molecules adsorbed on an oxygen-covered Co film is weak. Here, instead of changing the spin or orbital moments, the presence of the NO modifies the antiferromagnetic superexchange coupling between the Fe spins of the molecules and the magnetization of the substrate. This is caused by physisorbed NO molecules. As a result the Fe magnetization is reduced by approximately 50% at 120 K. After the detachment of NO, the original Fe magnetization at 120 K is restored and dosing again with NO lowers once more the strength of the magnetic exchange coupling. The physisorption of NO allows to control the degree of alignment of the exchange-coupled single molecular spins, while simultaneously the magnetic properties of the Fe ions are not changed. The virtue of a weakly interacting small ligand allows to design the magnetic properties of the formed complex by only considering porphyrin–substrate interactions, which presents a new prospect in the context of molecular spin electronics.

All in all, advantage is taken of the empty sixth coordination place of MP molecules, which are magnetically coupled to the magnetization of substrates. It is shown that the magnetization of the central metal ions of the metalloporphyrins can be switched at finite temperatures. To do so, a chemical switch is used. It is interesting to achieve such a control of molecular magnetization at organic-ferromagnetic interfaces that present model systems for a future molecular spin electronics. It is demonstrated that this can be obtained by changing the size of the spin and the orbital moment at the site of the central metal atoms as well as by modifiying the magnetic coupling strength between the molecular spins and the ones of the substrate.

Bibliography

[1] S. Deshang and L. Guodong: *History of Electromagnetism: Observation and Utilization of Electrical and Magnetic Phenomena*. Popular Press Publishers, Guang Xi (1987).

[2] J. Stöhr and H. C. Siegmann: *Magnetism*. Springer-Verlag Berlin Heidelberg (2006).

[3] S. A. Wolf, D. D. Awschalom, R. A. Buhrman, J. M. Daughton, S. v. Molnár, M. L. Roukes, A. Y. Chtchelkanova, and D. M. Treger: *Spintronics: A Spin-Based Electronics Vision for the Future*. Science **294**, 1488 (2001), DOI: 10.1126/science.1065389.

[4] M. N. Baibich, J. M. Broto, A. Fert, F. N. Van Dau, F. Petroff, P. Etienne, G. Creuzet, A. Friederich, and J. Chazelas: *Giant Magnetoresistance of (001)Fe/(001)Cr Magnetic Superlattices*. Phys. Rev. Lett. **61**, 2472 (1988), DOI: 10.1103/PhysRevLett.61.2472.

[5] G. Binasch, P. Grünberg, F. Saurenbach, and W. Zinn: *Enhanced magnetoresistance in layered magnetic structures with antiferromagnetic interlayer exchange*. Phys. Rev. B **39**, 4828 (1989), DOI: 10.1103/PhysRevB.39.4828.

[6] J. K. Gimzewski and C. Joachim: *Nanoscale Science of Single Molecules Using Local Probes*. Science **283**, 1683 (1999), DOI: 10.1126/science.283.5408.1683.

[7] J. M. Tour, W. A. Reinerth, L. Jones, T. P. Burgin, C.-W. Zhou, C. J. Muller, M. R. Deshpande, and M. A. Reed: *Recent Advances in Molecular Scale Electronics*. Ann. N.Y. Acad. Sci. **852**, 197204 (1998), DOI: 10.1111/j.1749-6632.1998.tb09873.x.

[8] G. Schmidt, D. Ferrand, L. W. Molenkamp, A. T. Filip, and B. J. van Wees: *Fundamental obstacle for electrical spin injection from a ferromagnetic metal into a diffusive semiconductor*. Phys. Rev. B **62**, R4790 (2000), DOI: 10.1103/PhysRevB.62.R4790.

[9] M. Cinchetti, K. Heimer, J.-P. Wüstenberg, O. Andreyev, M. Bauer, S. Lach, C. Ziegler, Y. Gao, and M. Aeschlimann: *Determination of spin injection and transport in a ferromagnet/organic semiconductor heterojunction by two-photon photoemission*. Nature Mater. **8**, 115 (2009), DOI: 10.1038/nmat2334.

[10] Z. H. Xiong, D. Wu, Z. V. Vardeny, and J. Shi: *Giant magnetoresistance in organic spin-valves*. Nature **427**, 821 (2004), DOI: 10.1038/nature02325.

[11] S. Sanvito and A. Rocha: *Molecular-Spintronics: The Art of Driving Spin Through Molecules*. J. Comput. Theor. Nanosci. **3**, 624 (2006), DOI: 10.1166/jctn.2006.003.

[12] S. Sanvito: *Molecular spintronics*. Chem. Soc. Rev. **40**, 3336 (2011), DOI: 10.1039/C1CS15047B.

[13] O. V. Yazyev: *Hyperfine Interactions in Graphene and Related Carbon Nanostructures*. Nano Lett. **8**, 1011 (2008), DOI: 10.1021/nl072667q.

[14] D. Huertas-Hernando, F. Guinea, and A. Brataas: *Spin-orbit coupling in curved graphene, fullerenes, nanotubes, and nanotube caps*. Phys. Rev. B **74**, 155426 (2006), DOI: 10.1103/PhysRevB.74.155426.

[15] N. Tombros, C. Jozsa, M. Popinciuc, H. T. Jonkman, and B. J. van Wees: *Electronic spin transport and spin precession in single graphene layers at room temperature*. Nature **448**, 571 (2007), DOI: 10.1038/nature06037.

[16] L. Cambi and L. Szegö: *Über die magnetische Susceptibilität der komplexen Verbindungen*. Ber. Dtsch. Phys. Ges. **64**, 25912598 (1931), DOI: 10.1002/cber.19310641002.

[17] S. Venkataramani, U. Jana, M. Dommaschk, F. D. Sönnichsen, F. Tuczek, and R. Herges: *Magnetic Bistability of Molecules in Homogeneous Solution at Room Temperature*. Science **331**, 445 (2011), DOI: 10.1126/science.1201180.

[18] A. Mugarza, R. Robles, C. Krull, R. Korytár, N. Lorente, and P. Gambardella: *Electronic and magnetic properties of molecule-metal interfaces: Transition-metal phthalocyanines adsorbed on Ag(100)*. Phys. Rev. B **85**, 155437 (2012), DOI: 10.1103/PhysRevB.85.155437.

[19] A. Mugarza, C. Krull, R. Robles, S. Stepanow, G. Ceballos, and P. Gambardella: *Spin coupling and relaxation inside molecule-metal contacts*. Nature Commun. **2**, 490 (2011), DOI: 10.1038/ncomms1497.

[20] N. Tsukahara, K.-i. Noto, M. Ohara, S. Shiraki, N. Takagi, Y. Takata, J. Miyawaki, M. Taguchi, A. Chainani, S. Shin, and M. Kawai: *Adsorption-Induced Switching of Magnetic Anisotropy in a Single Iron(II) Phthalocyanine Molecule on an Oxidized Cu(110) Surface*. Phys. Rev. Lett. **102**, 167203 (2009), DOI: 10.1103/PhysRevLett.102.167203.

[21] Y.-S. Fu, S.-H. Ji, X. Chen, X.-C. Ma, R. Wu, C.-C. Wang, W.-H. Duan, X.-H. Qiu, B. Sun, P. Zhang, J.-F. Jia, and Q.-K. Xue: *Manipulating the Kondo Resonance through Quantum Size Effects*. Phys. Rev. Lett. **99**, 256601 (2007), DOI: 10.1103/PhysRevLett.99.256601.

[22] K. J. Franke, G. Schulze, and J. I. Pascual: *Competition of Superconducting Phenomena and Kondo Screening at the Nanoscale*. Science **332**, 940 (2011), DOI: 10.1126/science.1202204.

[23] J. Brede, N. Atodiresei, S. Kuck, P. Lazić, V. Caciuc, Y. Morikawa, G. Hoffmann, S. Blügel, and R. Wiesendanger: *Spin- and Energy-Dependent Tunneling through a Single Molecule with Intramolecular Spatial Resolution*. Phys. Rev. Lett. **105**, 047204 (2010), DOI: 10.1103/PhysRevLett.105.047204.

[24] N. Atodiresei, J. Brede, P. Lazić, V. Caciuc, G. Hoffmann, R. Wiesendanger, and S. Blügel: *Design of the Local Spin Polarization at the Organic-Ferromagnetic Interface*. Phys. Rev. Lett. **105**, 066601 (2010), DOI: 10.1103/PhysRevLett.105.066601.

[25] C. Iacovita, M. V. Rastei, B. W. Heinrich, T. Brumme, J. Kortus, L. Limot, and J. P. Bucher: *Visualizing the Spin of Individual Cobalt-Phthalocyanine Molecules*. Phys. Rev. Lett. **101**, 116602 (2008), DOI: 10.1103/PhysRevLett.101.116602.

[26] Y.-S. Fu, Q.-K. Xue, and R. Wiesendanger: *Spin-Resolved Splitting of Kondo Resonances in the Presence of RKKY-Type Coupling*. Phys. Rev. Lett. **108**, 087203 (2012), DOI: 10.1103/PhysRevLett.108.087203.

[27] Y. Zhan and M. Fahlman: *The study of organic semiconductor/ferromagnet interfaces in organic spintronics: A short review of recent progress*. J. Polym. Sci., Part B: Polym. Phys. **50**, 14531462 (2012), DOI: 10.1002/polb.23157.

[28] T. Methfessel, S. Steil, N. Baadji, N. Gromann, K. Koffler, S. Sanvito, M. Aeschlimann, M. Cinchetti, and H. J. Elmers: *Spin scattering and spin-polarized hybrid interface states at a metal-organic interface*. Phys. Rev. B **84**, 224403 (2011), DOI: 10.1103/PhysRevB.84.224403.

[29] S. Steil, K. Goedel, A. Ruffing, I. Sarkar, M. Cinchetti, and M. Aeschlimann: *Investigation of the spin-dependent properties of electron doped cobalt–CuPc interfaces*. Synth. Met. **161**, 570 (2011), DOI: 10.1016/j.synthmet.2010.11.031.

[30] S. Lach, A. Altenhof, K. Tarafder, F. Schmitt, M. E. Ali, M. Vogel, J. Sauther, P. M. Oppeneer, and C. Ziegler: *Metal-Organic Hybrid Interface States of A Ferromagnet/Organic Semiconductor Hybrid Junction as Basis For Engineering Spin Injection in Organic Spintronics*. Adv. Funct. Mater. **22**, 989997 (2012), DOI: 10.1002/adfm.201102297.

[31] T. Suzuki, M. Kurahashi, and Y. Yamauchi: *Spin Polarization in Molecular Orbitals of Copper-Phthalocyanine Deposited on a Magnetized Fe(100) Substrate*. J. Phys. Chem. B **106**, 7643 (2002), DOI: 10.1021/jp0204760.

[32] T. Suzuki, M. Kurahashi, X. Ju, and Y. Yamauchi: *Spin Polarization of Metal (Mn, Fe, Cu, and Mg) and Metal-Free Phthalocyanines on an Fe(100) Substrate*. J. Phys. Chem. B **106**, 11553 (2002), DOI: 10.1021/jp021524j.

[33] A. Scheybal, T. Ramsvik, R. Bertschinger, M. Putero, F. Nolting, and T. Jung: *Induced magnetic ordering in a molecular monolayer*. Chem. Phys. Lett. **411**, 214 (2005), DOI: 10.1016/j.cplett.2005.06.017.

[34] H. Wende, M. Bernien, J. Luo, C. Sorg, N. Ponpandian, J. Kurde, J. Miguel, M. Piantek, X. Xu, P. Eckhold, W. Kuch, K. Baberschke, P. M. Panchmatia, B. Sanyal, P. M. Oppeneer, and O. Eriksson: *Substrate-induced magnetic ordering and switching of iron porphyrin molecules*. Nature Mater. **6**, 516 (2007), DOI: 10.1038/nmat1932.

[35] M. Bernien, J. Miguel, C. Weis, M. E. Ali, J. Kurde, B. Krumme, P. M. Panchmatia, B. Sanyal, M. Piantek, P. Srivastava, K. Baberschke, P. M. Oppeneer, O. Eriksson, W. Kuch, and H. Wende: *Tailoring the Nature of Magnetic Coupling of Fe-Porphyrin Molecules to Ferromagnetic Substrates*. Phys. Rev. Lett. **102**, 047202 (2009), DOI: 10.1103/PhysRevLett.102.047202.

[36] Y. Zhan, E. Holmström, R. Lizárraga, O. Eriksson, X. Liu, F. Li, E. Carlegrim, S. Stafström, and M. Fahlman: *Efficient Spin Injection Through Exchange Coupling at Organic Semiconductor/Ferromagnet Heterojunctions*. Adv. Mater. **22**, 16261630 (2010), DOI: 10.1002/adma.200903556.

[37] T. L. A. Tran, P. K. J. Wong, M. P. de Jong, W. G. van der Wiel, Y. Q. Zhan, and M. Fahlman: *Hybridization-induced oscillatory magnetic polarization of C_{60} orbitals at the C_{60}/Fe(001) interface*. Appl. Phys. Lett. **98**, 222505 (2011), DOI: doi:10.1063/1.3595269.

[38] A. Lodi Rizzini, C. Krull, T. Balashov, J. J. Kavich, A. Mugarza, P. S. Miedema, P. K. Thakur, V. Sessi, S. Klyatskaya, M. Ruben, S. Stepanow, and P. Gambardella: *Coupling Single Molecule Magnets to Ferromagnetic Substrates*. Phys. Rev. Lett. **107**, 177205 (2011), DOI: 10.1103/PhysRevLett.107.177205.

[39] J. Schwöbel, Y. Fu, J. Brede, A. Dilullo, G. Hoffmann, S. Klyatskaya, M. Ruben, and R. Wiesendanger: *Real-space observation of spin-split molecular orbitals of adsorbed single-molecule magnets*. Nature Commun. **3**, 953 (2012), DOI: 10.1038/ncomms1953.

[40] C. Wäckerlin, D. Chylarecka, A. Kleibert, K. Müller, C. Iacovita, F. Nolting, T. A. Jung, and N. Ballav: *Controlling spins in adsorbed molecules by a chemical switch*. Nature Commun. **1**, 61 (2010), DOI: 10.1038/ncomms1057.

[41] C. Wäckerlin, J. Nowakowski, S.-X. Liu, M. Jaggi, D. Siewert, J. Girovsky, A. Shchyrba, T. Hählen, A. Kleibert, P. M. Oppeneer, F. Nolting, S. Decurtins, T. A. Jung, and N. Ballav: *Two-Dimensional Supramolecular Electron Spin Arrays*. Adv. Mater. **25**, 24042408 (2013), DOI: 10.1002/adma.201204274.

[42] P. Gambardella, S. Stepanow, A. Dmitriev, J. Honolka, F. M. F. d. Groot, M. Lingenfelder, S. S. Gupta, D. D. Sarma, P. Bencok, S. Stanescu, S. Clair, S. Pons, N. Lin, A. P. Seitsonen, H. Brune, J. V. Barth, and K. Kern: *Supramolecular control of the magnetic anisotropy in two-dimensional high-spin Fe arrays at a metal interface*. Nature Mater. **8**, 189 (2009), DOI: 10.1038/nmat2376.

[43] T. Miyamachi, M. Gruber, V. Davesne, M. Bowen, S. Boukari, L. Joly, F. Scheurer, G. Rogez, T. K. Yamada, P. Ohresser, E. Beaurepaire, and W. Wulfhekel: *Robust spin crossover and memristance across a single molecule*. Nature Commun. **3**, 938 (2012), DOI: 10.1038/ncomms1940.

[44] J. H. Hubbell: *Photon cross section compilation activity in the U. S. in the range 1 keV to 100 GeV*. J. Phys. Colloques **32**, C4 (1971), DOI: 10.1051/jphyscol:1971403.

[45] H. Ebert, J. Stöhr, S. S. P. Parkin, M. Samant, and A. Nilsson: *L-edge x-ray absorption in fcc and bcc Cu metal: Comparison of experimental and first-principles theoretical results*. Phys. Rev. B **53**, 16067 (1996), DOI: 10.1103/PhysRevB.53.16067.

[46] J. Stöhr and H. König: *Determination of Spin- and Orbital-Moment Anisotropies in Transition Metals by Angle-Dependent X-Ray Magnetic Circular Dichroism*. Phys. Rev. Lett. **75**, 3748 (1995), DOI: 10.1103/PhysRevLett.75.3748.

[47] J. Stöhr and D. A. Outka: *Determination of molecular orientations on surfaces from the angular dependence of near-edge x-ray-absorption fine-structure spectra*. Phys. Rev. B **36**, 7891 (1987), DOI: 10.1103/PhysRevB.36.7891.

[48] W. Kuch: *Abbildende magnetische Mikrospektroskopie*. Habilitation treatise, Martin-Luther-Universiät Halle-Wittenberg (2002), http://sundoc.bibliothek.uni-halle.de/habil-online/02/03H047/habil.pdf.

[49] P. Carra, B. T. Thole, M. Altarelli, and X. Wang: *X-ray circular dichroism and local magnetic fields*. Phys. Rev. Lett. **70**, 694 (1993), DOI: 10.1103/PhysRevLett.70.694.

[50] B. T. Thole, P. Carra, F. Sette, and G. van der Laan: *X-ray circular dichroism as a probe of orbital magnetization*. Phys. Rev. Lett. **68**, 1943 (1992), DOI: 10.1103/PhysRevLett.68.1943.

[51] C. T. Chen, Y. U. Idzerda, H.-J. Lin, N. V. Smith, G. Meigs, E. Chaban, G. H. Ho, E. Pellegrin, and F. Sette: *Experimental Confirmation of the X-Ray Magnetic Circular Dichroism Sum Rules for Iron and Cobalt*. Phys. Rev. Lett. **75**, 152 (1995), DOI: 10.1103/PhysRevLett.75.152.

[52] J. Stöhr: *X-ray magnetic circular dichroism spectroscopy of transition metal thin films*. J. Electron. Spectrosc. Relat. Phenom. **75**, 253 (1995), DOI: 10.1016/0368-2048(95)02537-5.

[53] T. Kroll, V. Y. Aristov, O. V. Molodtsova, Y. A. Ossipyan, D. V. Vyalikh, B. Büchner, and M. Knupfer: *Spin and Orbital Ground State of Co in Cobalt Phthalocyanine*. J. Phys. Chem. A **113**, 8917 (2009), DOI: 10.1021/jp903001v.

[54] J. Becquerel: *Theory of magneto-optical phenomena in crystals*. Z. Physik **58**, 205 (1929).

[55] H. Bethe: *Termaufspaltung in Kristallen*. Ann. Phys. **395**, 133208 (1929), DOI: 10.1002/andp.19293950202.

[56] C. J. Ballhausen: *Introduction to ligand field theory*. McGraw-Hill (1962).

[57] J. C. Donini, B. R. Hollebone, G. London, A. B. P. Lever, and J. C. Hempel: *Application of the normalized spherical harmonic (NSH) Hamiltonian and of ground-state energy space diagrams to the tetragonal field*. Inorg. Chem. **14**, 455 (1975), DOI: 10.1021/ic50145a001.

[58] M.-S. Liao and S. Scheiner: *Electronic structure and bonding in metal porphyrins, metal=Fe, Co, Ni, Cu, Zn*. J. Chem. Phys. **117**, 205 (2002), DOI: doi:10.1063/1.1480872.

[59] C. Wäckerlin, K. Tarafder, D. Siewert, J. Girovsky, T. Hählen, C. Iacovita, A. Kleibert, F. Nolting, T. A. Jung, P. M. Oppeneer, and N. Ballav: *On-surface coordination chemistry of planar molecular spin systems: novel magnetochemical effects induced by axial ligands*. Chem. Sci. **3**, 3154 (2012), DOI: 10.1039/C2SC20828H.

[60] B. B. Wayland, J. V. Minkiewixz, and M. E. Abd-Elmageed: *Spectroscopic studies for tetraphenylporphyrincobalt(II) complexes of carbon monoxide, nitrogen oxide, molecular oxygen, methylisonitrile, and trimethyl phosphite, and a bonding model for complexes of carbon monoxide, nitrogen oxide, and molecular oxygen with cobalt(II) and iron(II) porphrins*. J. Am. Chem. Soc. **96**, 2795 (1974), DOI: 10.1021/ja00816a022.

[61] M. Kozuka and K. Nakamoto: *Vibrational studies of (tetraphenylporphyrinato)cobalt(II) and its adducts with carbon monoxide, nitric oxide, and oxygen in gas matrixes*. J. Am. Chem. Soc. **103**, 2162 (1981), DOI: 10.1021/ja00399a004.

[62] M. Hoshino, L. Laverman, and P. C. Ford: *Nitric oxide complexes of metalloporphyrins: an overview of some mechanistic studies*. Coord. Chem. Rev. **187**, 75 (1999), DOI: 10.1016/S0010-8545(98)00228-8.

[63] J. Enemark and R. Feltham: *Principles of structure, bonding, and reactivity for metal nitrosyl complexes*. Coord. Chem. Rev. **13**, 339 (1974), DOI: 10.1016/S0010-8545(00)80259-3.

[64] E. Schrödinger: *Quantisierung als Eigenwertproblem*. Ann. Phys. **385**, 437490 (1926), DOI: 10.1002/andp.19263851302.

[65] C. J. Ballhausen: *Molecular electronic structures of transition metal complexes*. McGraw-Hill International Book Co. (1979).

[66] G. Filoti, M. D. Kuz'min, and J. Bartolomé: *Mössbauer study of the hyperfine interactions and spin dynamics in α-iron(II) phthalocyanine*. Phys. Rev. B **74**, 134420 (2006), DOI: 10.1103/PhysRevB.74.134420.

[67] P. Bruno: *Tight-binding approach to the orbital magnetic moment and magnetocrystalline anisotropy of transition-metal monolayers*. Phys. Rev. B **39**, 865 (1989), DOI: 10.1103/PhysRevB.39.865.

[68] D. Weller, J. Stöhr, R. Nakajima, A. Carl, M. G. Samant, C. Chappert, R. Mégy, P. Beauvillain, P. Veillet, and G. A. Held: *Microscopic Origin of Magnetic Anisotropy in Au/Co/Au Probed with X-Ray Magnetic Circular Dichroism*. Phys. Rev. Lett. **75**, 3752 (1995), DOI: 10.1103/PhysRevLett.75.3752.

[69] J. Stöhr: *Exploring the microscopic origin of magnetic anisotropies with X-ray magnetic circular dichroism (XMCD) spectroscopy*. J. Magn. Magn. Mater. **200**, 470 (1999), DOI: 10.1016/S0304-8853(99)00407-2.

[70] W. Heitler and F. London: *Wechselwirkung neutraler Atome und homöpolare Bin- dung nach der Quantenmechanik*. Z. Physik **44**, 455 (1927).

[71] W. Heisenberg: *Zur Theorie des Ferromagnetismus*. Z. Physik **49**, 619 (1928).

[72] Peter Fulde: *Electron Correlations in Molecules and Solids*. Springer Series in Solid-State Science Vol. 100 (1995).

[73] J. B. Goodenough: *Theory of the Role of Covalence in the Perovskite-Type Manganites [La,M(II)]MnO_3*. Phys. Rev. **100**, 564 (1955), DOI: 10.1103/PhysRev.100.564.

[74] J. Kanamori: *Superexchange interaction and symmetry properties of electron orbitals*. J. Phys. Chem. Solids **10**, 87 (1959), DOI: 10.1016/0022-3697(59)90061-7.

[75] J. B. Goodenough: *Magnetism and the Chemical Bond*. Wiley (1963).

[76] C. Zener: *Interaction between the d-Shells in the Transition Metals. II. Ferromagnetic Compounds of Manganese with Perovskite Structure*. Phys. Rev. **82**, 403 (1951), DOI: 10.1103/PhysRev.82.403.

[77] J. Als-Nielsen and D. McMorrow: *Elements of Modern X-ray Physics*. Wiley (2011).

[78] E. M. McMillan: *The Synchrotron-A Proposed High Energy Particle Accelerator*. Phys. Rev. **68**, 143 (1945), DOI: 10.1103/PhysRev.68.143.

[79] K. Wille: *Physik der Teilchenbeschleuniger und Synchrotronstrahlungsquellen: Eine Einführung*. Teubner Verlag (1996).

[80] F. R. Elder, A. M. Gurewitsch, R. V. Langmuir, and H. C. Pollock: *Radiation from Electrons in a Synchrotron*. Phys. Rev. **71**, 829 (1947), DOI: 10.1103/PhysRev.71.829.5.

[81] A. Liénard: *L'Eclairage Elect.* **16**, 5 (1898).

[82] J. Schwinger: *On the Classical Radiation of Accelerated Electrons*. Phys. Rev. **75**, 1912 (1949), DOI: 10.1103/PhysRev.75.1912.

[83] F. Schaefers, M. Mertin, and M. Gorgoi: *KMC-1: A high resolution and high flux soft x-ray beamline at BESSY*. Rev. Sci. Instrum. **78**, 123102 (2007), DOI: doi:10.1063/1.2808334.

[84] S. Sasaki: *Analyses for a planar variably-polarizing undulator*. Nucl. Instr. and Meth. A in Phys. Res. A **347**, 83 (1994), DOI: 10.1016/0168-9002(94)91859-7.

[85] M. Tischer, O. Hjortstam, D. Arvanitis, J. Hunter Dunn, F. May, K. Baberschke, J. Trygg, J. M. Wills, B. Johansson, and O. Eriksson: *Enhancement of Orbital Magnetism at Surfaces: Co on Cu(100)*. Phys. Rev. Lett. **75**, 1602 (1995), DOI: 10.1103/PhysRevLett.75.1602.

[86] H. A. Dürr, G. van der Laan, J. Vogel, G. Panaccione, N. B. Brookes, E. Dudzik, and R. McGrath: *Enhanced orbital magnetism at the nanostructured Co/Cu (1 1 13) surface*. Phys. Rev. B **58**, R11853 (1998), DOI: 10.1103/PhysRevB.58.R11853.

[87] R. N. Sodhi and C. Brion: *Reference energies for inner shell electron energy-loss spectroscopy*. J. Electron. Spectrosc. Relat. Phenom. **34**, 363 (1984), DOI: 10.1016/0368-2048(84)80050-X.

[88] M. Bernien: *X-Ray absorption spectroscopy of Fe complexes on surfaces*. Doctoral thesis, Freie Universität Berlin (2010), http://www.diss.fu-berlin.de/diss_receive/FUDISS_thesis_000000019678.

[89] M. Piantek, G. Schulze, M. Koch, K. J. Franke, F. Leyssner, A. Krüger, C. Navio, J. Miguel, M. Bernien, M. Wolf, W. Kuch, P. Tegeder, and J. I. Pascual: *Reversing the Thermal Stability of a Molecular Switch on a Gold Surface: Ring-Opening Reaction of Nitrospiropyran*. J. Am. Chem. Soc. **131**, 12729 (2009), DOI: 10.1021/ja901238p.

[90] H. C. Herper, M. Bernien, S. Bhandary, C. F. Hermanns, A. Krüger, J. Miguel, C. Weis, C. Schmitz-Antoniak, B. Krumme, D. Bovenschen, C. Tieg, B. Sanyal, E. Weschke, C. Czekelius, W. Kuch, H. Wende, and O. Eriksson: *Iron porphyrin molecules on Cu(001): Influence of adlayers and ligands on the magnetic properties*. Phys. Rev. B **87**, 174425 (2013), DOI: 10.1103/PhysRevB.87.174425.

[91] F. de Groot and A. Kotani: *Core Level Spectroscopy of Solids*. CRC Press (2008).

[92] R. Nakajima, J. Stöhr, and Y. U. Idzerda: *Electron-yield saturation effects in L-edge x-ray magnetic circular dichroism spectra of Fe, Co, and Ni*. Phys. Rev. B **59**, 6421 (1999), DOI: 10.1103/PhysRevB.59.6421.

[93] C. Sorg, N. Ponpandian, M. Bernien, K. Baberschke, H. Wende, and R. Q. Wu: *Induced magnetism of oxygen in surfactant-grown Fe, Co, and Ni monolayers*. Phys. Rev. B **73**, 064409 (2006), DOI: 10.1103/PhysRevB.73.064409.

[94] R. Nünthel, T. Gleitsmann, P. Poulopoulos, A. Scherz, J. Lindner, E. Kosubek, C. Litwinski, Z. Li, H. Wende, K. Baberschke, S. Stolbov, and T. Rahman: *Epitaxial growth of Ni on Cu(001) with the assistance of O-surfactant and its magnetism compared to Ni/Cu(001)*. Surf. Sci. **531**, 53 (2003), DOI: 10.1016/S0039-6028(03)00438-2.

[95] Y. S. Dedkov, M. Fonin, U. Rüdiger, and C. Laubschat: *Rashba Effect in the Graphene/Ni(111) System*. Phys. Rev. Lett. **100**, 107602 (2008), DOI: 10.1103/PhysRevLett.100.107602.

[96] A. Varykhalov, J. Sánchez-Barriga, A. M. Shikin, C. Biswas, E. Vescovo, A. Rybkin, D. Marchenko, and O. Rader: *Electronic and Magnetic Properties of Quasifreestanding Graphene on Ni*. Phys. Rev. Lett. **101**, 157601 (2008), DOI: 10.1103/PhysRevLett.101.157601.

[97] Y. S. Dedkov and M Fonin: *Electronic and magnetic properties of the graphene-ferromagnet interface*. New J. Phys. **12**, 125004 (2010), DOI: 10.1088/1367-2630/12/12/125004.

[98] W. Zhao, S. M. Kozlov, O. Höfert, K. Gotterbarm, M. P. A. Lorenz, F. Viñes, C. Papp, A. Görling, and H.-P. Steinrück: *Graphene on Ni(111): Coexistence of Different Surface Structures*. J. Phys. Chem. Lett. **2**, 759 (2011), DOI: 10.1021/jz200043p.

[99] D. Usachov, A. M. Dobrotvorskii, A. Varykhalov, O. Rader, W. Gudat, A. M. Shikin, and V. K. Adamchuk: *Experimental and theoretical study of the morphology of commensurate and incommensurate graphene layers on Ni single-crystal surfaces*. Phys. Rev. B **78**, 085403 (2008), DOI: 10.1103/PhysRevB.78.085403.

[100] J. Lahiri, Y. Lin, P. Bozkurt, I. I. Oleynik, and M. Batzill: *An extended defect in graphene as a metallic wire*. Nature Nanotech. **5**, 326 (2010), DOI: 10.1038/nnano.2010.53.

[101] R Bäcker and G Hörz: *Scanning tunneling microscopy of carbon- and sulfur-induced modifications of Ni(111) and Ni(110) surfaces*. Vacuum **46**, 1101 (1995), DOI: 10.1016/0042-207X(95)00115-8.

[102] M. Fuentes-Cabrera, M. I. Baskes, A. V. Melechko, and M. L. Simpson: *Bridge structure for the graphene/Ni(111) system: A first principles study*. Phys. Rev. B **77**, 035405 (2008), DOI: 10.1103/PhysRevB.77.035405.

[103] J. L. W. Thudichum: *On cruentine*. Report Med. Off. Privy. Council **7-10**, 152 (1867).

[104] I. Fleming: *Absolute Configuration and the Structure of Chlorophyll*. Nature **216**, 151 (1967), DOI: 10.1038/216151a0.

[105] J. E. Johnson Jr, F. E. Reyes, J. T. Polaski, and R. T. Batey: *B12 cofactors directly stabilize an mRNA regulatory switch*. Nature **492**, 133 (2012), DOI: 10.1038/nature11607.

[106] M. V. Zeller and R. G. Hayes: *X-ray photoelectron spectroscopic studies on the electronic structures of porphyrin and phthalocyanine compounds*. J. Am. Chem. Soc. **95**, 3855 (1973), DOI: 10.1021/ja00793a006.

[107] D. Karweik, N. Winograd, D. G. Davis, and K. M. Kadish: *X-ray photoelectron spectroscopic studies of silver(III) octaethylporphyrin*. J. Am. Chem. Soc. **96**, 591 (1974), DOI: 10.1021/ja00809a050.

[108] S. Mitra-Kirtley, O. C. Mullins, J. Van Elp, S. J. George, J. Chen, and S. P. Cramer: *Determination of the nitrogen chemical structures in petroleum asphaltenes using XANES spectroscopy*. J. Am. Chem. Soc. **115**, 252 (1993), DOI: 10.1021/ja00054a036.

[109] A. Yella, H.-W. Lee, H. N. Tsao, C. Yi, A. K. Chandiran, M. K. Nazeeruddin, E. W.-G. Diau, C.-Y. Yeh, S. M. Zakeeruddin, and M. Grätzel: *Porphyrin-Sensitized Solar Cells with Cobalt (II/III)-Based Redox Electrolyte Exceed 12 Percent Efficiency*. Science **334**, 629 (2011), DOI: 10.1126/science.1209688.

[110] P. L. Cook, X. Liu, W. Yang, and F. J. Himpsel: *X-ray absorption spectroscopy of biomimetic dye molecules for solar cells*. J. Chem. Phys. **131**, 194701 (2009), DOI: doi:10.1063/1.3257621.

[111] C. S. Guo, L. Sun, K. Hermann, C. F. Hermanns, M. Bernien, and W. Kuch: *X-ray absorption from large molecules at metal surfaces: Theoretical and experimental results for Co-OEP on Ni(100)*. J. Chem. Phys. **137**, 194703 (2012), DOI: doi:10.1063/1.4765373.

[112] S. Stepanow, P. S. Miedema, A. Mugarza, G. Ceballos, P. Moras, J. C. Cezar, C. Carbone, F. M. F. de Groot, and P. Gambardella: *Mixed-valence behavior and strong correlation effects of metal phthalocyanines adsorbed on metals*. Phys. Rev. B **83**, 220401 (2011), DOI: 10.1103/PhysRevB.83.220401.

[113] M. Fanetti, A. Calzolari, P. Vilmercati, C. Castellarin-Cudia, P. Borghetti, G. Di Santo, L. Floreano, A. Verdini, A. Cossaro, I. Vobornik, E. Annese, F. Bondino, S. Fabris, and A. Goldoni: *Structure and Molecule-Substrate Interaction in a Co-octaethyl Porphyrin Monolayer on the Ag(110) Surface*. J. Phys. Chem. C **115**, 11560 (2011), DOI: 10.1021/jp2011233.

[114] K. Hermann and L. G. M. Pettersson: *StoBe software V. 3.1*, http://www.fhi-berlin.mpg.de/KHsoftware/StoBe/.

[115] G. Polzonetti, V. Carravetta, G. Iucci, A. Ferri, G. Paolucci, A. Goldoni, P. Parent, C. Laffon, and M. Russo: *Electronic structure of platinum complex/Zn-porphyrinato assembled macrosystems, related precursors and model molecules, as probed by X-ray absorption spectroscopy (NEXAFS): theory and experiment*. Chem. Phys. **296**, 87 (2004), DOI: 10.1016/j.chemphys.2003.09.036.

[116] F. Schreiber: *Organic molecular beam deposition: Growth studies beyond the first monolayer*. phys. stat. sol. (a) **201**, 10371054 (2004), DOI: 10.1002/pssa.200404334.

[117] S. Yoshimoto and K. Itaya: *Advances in supramolecularly assembled nanostructures of fullerenes and porphyrins at surfaces*. J. Porphyrins Phthalocyanines **11**, 313 (2007), DOI: 10.1142/S1088424607000369.

[118] B. Hulsken, R. Van Hameren, J. W. Gerritsen, T. Khoury, P. Thordarson, M. J. Crossley, A. E. Rowan, R. J. M. Nolte, J. A. A. W. Elemans, and S. Speller: *Real-time single-molecule imaging of oxidation catalysis at a liquid-solid interface*. Nature Nanotech. **2**, 285 (2007), DOI: 10.1038/nnano.2007.106.

[119] I. Mochida, K. Tsuji, K. Suetsugu, H. Fujitsu, and K. Takeshita: *Modified electronic structure and enhanced catalytic activity of cobalt tetraphenylporphyrin supported by titanium dioxide*. J. Phys. Chem. **84**, 3159 (1980), DOI: 10.1021/j100461a006.

[120] C. Stadler, S. Hansen, I. Kröger, C. Kumpf, and E. Umbach: *Tuning intermolecular interaction in long-range-ordered submonolayer organic films*. Nature Phys. **5**, 153 (2009), DOI: 10.1038/nphys1176.

[121] C. Isvoranu, J. Åhlund, B. Wang, E. Ataman, N. Mårtensson, C. Puglia, J. N. Andersen, M.-L. Bocquet, and J. Schnadt: *Electron spectroscopy study of the initial stages of iron phthalocyanine growth on highly oriented pyrolitic graphite*. J. Chem. Phys. **131**, 214709 (2009), DOI: doi:10.1063/1.3259699.

[122] J. Åhlund, J. Schnadt, K. Nilson, E. Göthelid, J. Schiessling, F. Besenbacher, N. Mårtensson, and C. Puglia: *The adsorption of iron phthalocyanine on graphite: A scanning tunnelling microscopy study*. Surf. Sci. **601**, 3661 (2007), DOI: 10.1016/j.susc.2007.06.008.

[123] A. Stróżecka, M. Soriano, J. I. Pascual, and J. J. Palacios: *Reversible Change of the Spin State in a Manganese Phthalocyanine by Coordination of CO Molecule*. Phys. Rev. Lett. **109**, 147202 (2012), DOI: 10.1103/PhysRevLett.109.147202.

[124] W. Auwärter, K. Seufert, F. Klappenberger, J. Reichert, A. Weber-Bargioni, A. Verdini, D. Cvetko, M. Dell'Angela, L. Floreano, A. Cossaro, G. Bavdek, A. Morgante, A. P. Seitsonen, and J. V. Barth: *Site-specific electronic and geometric interface structure of Co-tetraphenyl-porphyrin layers on Ag(111)*. Phys. Rev. B **81**, 245403 (2010), DOI: 10.1103/PhysRevB.81.245403.

[125] S. Stepanow, A. Mugarza, G. Ceballos, P. Moras, J. C. Cezar, C. Carbone, and P. Gambardella: *Giant spin and orbital moment anisotropies of a Cu-phthalocyanine monolayer*. Phys. Rev. B **82**, 014405 (2010), DOI: 10.1103/PhysRevB.82.014405.

[126] D. Chylarecka, T. K. Kim, K. Tarafder, K. Muller, K. Gödel, I. Czekaj, C. Wäckerlin, M. Cinchetti, M. E. Ali, C. Piamonteze, F. Schmitt, J.-P. Wüstenberg, C. Ziegler, F. Nolting, M. Aeschlimann, P. M. Oppeneer, N. Ballav, and T. A. Jung: *Indirect Magnetic Coupling of Manganese Porphyrin to a Ferromagnetic Cobalt Substrate*. J. Phys. Chem. C **115**, 1295 (2011), DOI: 10.1021/jp106822s.

[127] M. Bernien, X. Xu, J. Miguel, M. Piantek, P. Eckhold, J. Luo, J. Kurde, W. Kuch, K. Baberschke, H. Wende, and P. Srivastava: *Fe-porphyrin monolayers on ferromagnetic substrates: Electronic structure and magnetic coupling strength*. Phys. Rev. B **76**, 214406 (2007), DOI: 10.1103/PhysRevB.76.214406.

[128] E. Annese, J. Fujii, I. Vobornik, G. Panaccione, and G. Rossi: *Control of the magnetism of cobalt phthalocyanine by a ferromagnetic substrate*. Phys. Rev. B **84**, 174443 (2011), DOI: 10.1103/PhysRevB.84.174443.

[129] M. E. Ali, B. Sanyal, and P. M. Oppeneer: *Tuning the Magnetic Interaction between Manganese Porphyrins and Ferromagnetic Co Substrate through Dedicated Control of the Adsorption*. J. Phys. Chem. C **113**, 14381 (2009), DOI: 10.1021/jp902644q.

[130] Y. Bai, F. Buchner, I. Kellner, M. Schmid, F. Vollnhals, H.-P. Steinrück, H. Marbach, and J Michael Gottfried: *Adsorption of cobalt (II) octaethylporphyrin and 2H-octaethylporphyrin on Ag(111): new insight into the surface coordinative bond*. New J. Phys. **11**, 125004 (2009), DOI: 10.1088/1367-2630/11/12/125004.

[131] S. Narioka, H. Ishii, Y. Ouchi, T. Yokoyama, T. Ohta, and K. Seki: *XANES Spectroscopic Studies of Evaporated Porphyrin Films: Molecular Orientation and Electronic Structure*. J. Phys. Chem. **99**, 1332 (1995), DOI: 10.1021/j100004a038.

[132] G. Di Santo, C. Castellarin-Cudia, M. Fanetti, B. Taleatu, P. Borghetti, L. Sangaletti, L. Floreano, E. Magnano, F. Bondino, and A. Goldoni: *Conformational Adaptation and Electronic Structure of 2H-Tetraphenylporphyrin on Ag(111) during Fe Metalation*. J. Phys. Chem. C **115**, 4155 (2011), DOI: 10.1021/jp111151n.

[133] K. Diller, F. Klappenberger, M. Marschall, K. Hermann, A. Nefedov, C. Wöll, and J. V. Barth: *Self-metalation of 2H-tetraphenylporphyrin on Cu(111): An x-ray spectroscopy study*. J. Chem. Phys. **136**, 014705 (2012), DOI: doi:10.1063/1.3674165.

[134] A. S. Vinogradov, A. B. Preobrajenski, S. A. Krasnikov, T. Chassé, R. Szargan, A. Knop-Gericke, R. Schlögl, and P. Bressler: *X-ray absorption evidence for the back-donation in iron cyanide complexes*. Surf. Rev. Lett. **09**, 359 (2002), DOI: 10.1142/S0218625X02002270.

[135] J. Bartolomé, F. Bartolomé, L. M. Garca, G. Filoti, T. Gredig, C. N. Colesniuc, I. K. Schuller, and J. C. Cezar: *Highly unquenched orbital moment in textured Fe-phthalocyanine thin films*. Phys. Rev. B **81**, 195405 (2010), DOI: 10.1103/PhysRevB.81.195405.

[136] G. van der Laan: *Microscopic origin of magnetocrystalline anisotropy in transition metal thin films*. J. Phys.: Condens. Matter **10**, 3239 (1998), DOI: 10.1088/0953-8984/10/14/012.

[137] B. Schulz and K. Baberschke: *Crossover from in-plane to perpendicular magnetization in ultrathin Ni/Cu(001) films*. Phys. Rev. B **50**, 13467 (1994), DOI: 10.1103/PhysRevB.50.13467.

[138] C. F. Hermanns, M. Bernien, A. Krüger, J. Miguel, and W. Kuch: *Switching the electronic properties of Co-octaethylporphyrin molecules on oxygen-covered Ni films by NO adsorption*. J. Phys.: Condens. Matter **24**, 394008 (2012), DOI: 10.1088/0953-8984/24/39/394008.

[139] C. F. Hermanns, K. Tarafder, M. Bernien, A. Krüger, Y.-M. Chang, P. M. Oppeneer, and W. Kuch: *Magnetic coupling of porphyrin molecules through graphene*. Adv. Mater. (in print).

[140] A. K. Geim and K. S. Novoselov: *The rise of graphene*. Nature Mater. **6**, 183 (2007), DOI: 10.1038/nmat1849.

[141] K. V. Emtsev, A. Bostwick, K. Horn, J. Jobst, G. L. Kellogg, L. Ley, J. L. McChesney, T. Ohta, S. A. Reshanov, J. Röhrl, E. Rotenberg, A. K. Schmid, D. Waldmann, H. B. Weber, and T. Seyller: *Towards wafer-size graphene layers by atmospheric pressure graphitization of silicon carbide*. Nature Mater. **8**, 203 (2009), DOI: 10.1038/nmat2382.

[142] H. Yang, J. Heo, S. Park, H. J. Song, D. H. Seo, K.-E. Byun, P. Kim, I. Yoo, H.-J. Chung, and K. Kim: *Graphene Barristor, a Triode Device with a Gate-Controlled Schottky Barrier*. Science **336**, 1140 (2012), DOI: 10.1126/science.1220527.

[143] L. Britnell, R. V. Gorbachev, R. Jalil, B. D. Belle, F. Schedin, A. Mishchenko, T. Georgiou, M. I. Katsnelson, L. Eaves, S. V. Morozov, N. M. R. Peres, J. Leist, A. K. Geim, K. S. Novoselov, and L. A. Ponomarenko: *Field-Effect Tunneling Transistor Based on Vertical Graphene Heterostructures*. Science **335**, 947 (2012), DOI: 10.1126/science.1218461.

[144] B. Trauzettel, D. V. Bulaev, D. Loss, and G. Burkard: *Spin qubits in graphene quantum dots*. Nature Phys. **3**, 192 (2007), DOI: 10.1038/nphys544.

[145] S. M. Avdoshenko, I. N. Ioffe, G. Cuniberti, L. Dunsch, and A. A. Popov: *Organometallic Complexes of Graphene: Toward Atomic Spintronics Using a Graphene Web*. ACS Nano **5**, 9939 (2011), DOI: 10.1021/nn203719a.

[146] J. Mao, H. Zhang, Y. Jiang, Y. Pan, M. Gao, W. Xiao, and H.-J. Gao: *Tunability of Supramolecular Kagome Lattices of Magnetic Phthalocyanines Using Graphene-Based Moire Patterns as Templates*. J. Am. Chem. Soc. **131**, 14136 (2009), DOI: 10.1021/ja904907z.

[147] P. Gambardella, S. S. Dhesi, S. Gardonio, C. Grazioli, P. Ohresser, and C. Carbone: *Localized Magnetic States of Fe, Co, and Ni Impurities on Alkali Metal Films*. Phys. Rev. Lett. **88**, 047202 (2002), DOI: 10.1103/PhysRevLett.88.047202.

[148] van Vleck, J. H.: *The Theory of Electric and Magnetic Susceptibilities*. Clarendon Press (1932).

[149] P. Gambardella, S. Rusponi, M. Veronese, S. S. Dhesi, C. Grazioli, A. Dallmeyer, I. Cabria, R. Zeller, P. H. Dederichs, K. Kern, C. Carbone, and H. Brune: *Giant Magnetic Anisotropy of Single Cobalt Atoms and Nanoparticles*. Science **300**, 1130 (2003), DOI: 10.1126/science.1082857.

[150] M. Niemeyer, K. Hirsch, V. Zamudio-Bayer, A. Langenberg, M. Vogel, M. Kossick, C. Ebrecht, K. Egashira, A. Terasaki, T. Möller, B. v. Issendorff, and J. T. Lau: *Spin Coupling and Orbital Angular Momentum Quenching in Free Iron Clusters*. Phys. Rev. Lett. **108**, 057201 (2012), DOI: 10.1103/PhysRevLett.108.057201.

[151] S. Peredkov, M. Neeb, W. Eberhardt, J. Meyer, M. Tombers, H. Kampschulte, and G. Niedner-Schatteburg: *Spin and Orbital Magnetic Moments of Free Nanoparticles*. Phys. Rev. Lett. **107**, 233401 (2011), DOI: 10.1103/PhysRevLett.107.233401.

[152] P. Gambardella, A. Dallmeyer, K. Maiti, M. C. Malagoli, W. Eberhardt, K. Kern, and C. Carbone: *Ferromagnetism in one-dimensional monatomic metal chains*. Nature **416**, 301 (2002), DOI: 10.1038/416301a.

[153] O. Eriksson, A. M. Boring, R. C. Albers, G. W. Fernando, and B. R. Cooper: *Spin and orbital contributions to surface magnetism in 3d elements*. Phys. Rev. B **45**, 2868 (1992), DOI: 10.1103/PhysRevB.45.2868.

[154] S. I. Csiszar, M. W. Haverkort, Z. Hu, A. Tanaka, H. H. Hsieh, H.-J. Lin, C. T. Chen, T. Hibma, and L. H. Tjeng: *Controlling Orbital Moment and Spin Orientation in CoO Layers by Strain*. Phys. Rev. Lett. **95**, 187205 (2005), DOI: 10.1103/PhysRevLett.95.187205.

[155] C. F. Hermanns, M. Bernien, A. Krüger, W. Walter, Y.-M. Chang, E. Weschke, and W. Kuch: *Huge magnetically coupled orbital moments of Co porphyrin molecules and their control by CO adsorption*. Resubmitted to Phys. Rev. B(R).

[156] K. Baberschke: *The magnetism of nickel monolayers*. Appl. Phys. A **62**, 417 (1996), DOI: 10.1007/BF01567112.

[157] K. Kopitzki and P. Herzog: *Einführung in die Festkörperphysik*. Vieweg+Teubner Verlag (2007).

[158] Y. Li and K. Baberschke: *Dimensional crossover in ultrathin Ni(111) films on W(110)*. Phys. Rev. Lett. **68**, 1208 (1992), DOI: 10.1103/PhysRevLett.68.1208.

[159] F. de Groot and A. Kotani: *Core Level Spectroscopy of Solids*. CRC Press (2008).

[160] S. M. Avdoshenko, I. N. Ioffe, G. Cuniberti, L. Dunsch, and A. A. Popov: *Correction to Organometallic Complexes of Graphene: Toward Atomic Spintronics Using a Graphene Web*. ACS Nano **6**, 2860 (2012), DOI: 10.1021/nn300708n.

[161] B. Li, L. Chen, and X. Pan: *Spin-flip phenomena at the Co|graphene|Co interfaces*. Appl. Phys. Lett. **98**, 133111 (2011), DOI: 10.1063/1.3571553.

[162] Y. S. Dedkov, M. Fonin, and C. Laubschat: *A possible source of spin-polarized electrons: The inert graphene/Ni(111) system*. Appl. Phys. Lett. **92**, 052506 (2008), DOI: 10.1063/1.2841809.

[163] C. Schmidthals, D. Sander, A. Enders, and J. Kirschner: *Structure and morphology of Ni monolayers on W(110)*. Surf. Sci. **417**, 361 (1998), DOI: 10.1016/S0039-6028(98)00689-X.

[164] J. P. Crocombette, B. T. Thole, and F Jollet: *The importance of the magnetic dipole term in magneto-circular x-ray absorption dichroism for 3d transition metal compounds*. J. Phys.: Condens. Matter **8**, 4095 (1996), DOI: 10.1088/0953-8984/8/22/013.

[165] J. Wang, Y. Shi, J. Cao, and R. Wu: *Magnetization and magnetic anisotropy of metallophthalocyanine molecules from the first principles calculations*. Appl. Phys. Lett. **94**, 122502 (2009), DOI: doi:10.1063/1.3100783.

[166] J. M. Baker: *Interactions between ions with orbital angular momentum in insulators*. Rep. Prog. Phys. **34**, 109 (1971), DOI: 10.1088/0034-4885/34/1/303.

[167] A. Palii, B. Tsukerblat, S. Klokishner, K. R. Dunbar, J. M. Clemente-Juan, and E. Coronado: *Beyond the spin model: exchange coupling in molecular magnets with unquenched orbital angular momenta*. Chem. Soc. Rev. **40**, 3130 (2011), DOI: 10.1039/C0CS00175A.

[168] J. Klanke, E. Rentschler, K. Medjanik, D. Kutnyakhov, G. Schönhense, S. Krasnikov, I. V. Shvets, S. Schuppler, P. Nagel, M. Merz, and H. J. Elmers: *Beyond the Heisenberg Model: Anisotropic Exchange Interaction between a Cu-Tetraazaporphyrin Monolayer and $Fe_3O_4(100)$*. Phys. Rev. Lett. **110**, 137202 (2013), DOI: 10.1103/PhysRevLett.110.137202.

[169] E. F. Aziz, N. Ottosson, S. Bonhommeau, N. Bergmann, W. Eberhardt, and M. Chergui: *Probing the Electronic Structure of the Hemoglobin Active Center in Physiological Solutions*. Phys. Rev. Lett. **102**, 068103 (2009), DOI: 10.1103/PhysRevLett.102.068103.

[170] F. I. Bohrer, A. Sharoni, C. Colesniuc, J. Park, I. K. Schuller, A. C. Kummel, and W. C. Trogler: *Gas Sensing Mechanism in Chemiresistive Cobalt and Metal-Free Phthalocyanine Thin Films*. J. Am. Chem. Soc. **129**, 5640 (2007), DOI: 10.1021/ja0689379.

[171] G. Guillaud, J. Simon, and J. Germain: *Metallophthalocyanines: Gas sensors, resistors and field effect transistors*. Coord. Chem. Rev. **178-180**, 1433 (1998), DOI: 10.1016/S0010-8545(98)00177-5.

[172] F. Basolo and R. G. Pearson: *The Trans Effect in Metal Complexes*. Prog. Inorg. Chem. 381453, John Wiley & Sons, Inc. (2007), http://onlinelibrary.wiley.com/doi/10.1002/9780470166055.ch6/summary.

[173] J. W. Buchler, W. Kokisch, and P. D. Smith: *Cis, trans, and metal effects in transition metal porphyrins*. Novel Aspects 79, Springer Berlin Heidelberg. (1978), http://link.springer.com/chapter/10.1007/BFb0116542.

[174] C Isvoranu, B Wang, K Schulte, E Ataman, J Knudsen, J. N. Andersen, M. L. Bocquet, and J Schnadt: *Tuning the spin state of iron phthalocyanine by ligand adsorption*. J. Phys.: Condens. Matter **22**, 472002 (2010), DOI: 10.1088/0953-8984/22/47/472002.

[175] C. Isvoranu, B. Wang, E. Ataman, K. Schulte, J. Knudsen, J. N. Andersen, M.-L. Bocquet, and J. Schnadt: *Ammonia adsorption on iron phthalocyanine on Au(111): Influence on adsorbate-substrate coupling and molecular spin*. J. Chem. Phys. **134**, 114710 (2011), DOI: doi:10.1063/1.3563635.

[176] C. Isvoranu, B. Wang, E. Ataman, J. Knudsen, K. Schulte, J. N. Andersen, M.-L. Bocquet, and J. Schnadt: *Comparison of the Carbonyl and Nitrosyl Complexes Formed by Adsorption of CO and NO on Monolayers of Iron Phthalocyanine on Au(111)*. J. Phys. Chem. C **115**, 24718 (2011), DOI: 10.1021/jp204461k.

[177] K. Flechtner, A. Kretschmann, H.-P. Steinrück, and J. M. Gottfried: *NO-Induced Reversible Switching of the Electronic Interaction between a Porphyrin-Coordinated Cobalt Ion and a Silver Surface*. J. Am. Chem. Soc. **129**, 12110 (2007), DOI: 10.1021/ja0756725.

[178] W. Hieringer, K. Flechtner, A. Kretschmann, K. Seufert, W. Auwärter, J. V. Barth, A. Görling, H.-P. Steinrück, and J. M. Gottfried: *The Surface Trans Effect: Influence of Axial Ligands on the Surface Chemical Bonds of Adsorbed Metalloporphyrins*. J. Am. Chem. Soc. **133**, 6206 (2011), DOI: 10.1021/ja1093502.

[179] D. Chylarecka, C. Wäckerlin, T. K. Kim, K. Müller, F. Nolting, A. Kleibert, N. Ballav, and T. A. Jung: *Self-Assembly and Superexchange Coupling of Magnetic Molecules on Oxygen-Reconstructed Ferromagnetic Thin Film*. J. Phys. Chem. Lett. **1**, 1408 (2010), DOI: 10.1021/jz100253c.

[180] J. Miguel, C. F. Hermanns, M. Bernien, A. Krüger, and W. Kuch: *Reversible Manipulation of the Magnetic Coupling of Single Molecular Spins in Fe-Porphyrins to a Ferromagnetic Substrate*. J. Phys. Chem. Lett. **2**, 1455 (2011), DOI: 10.1021/jz200489y.

[181] C. Wäckerlin, K. Tarafder, J. Girovsky, J. Nowakowski, T. Hählen, A. Shchyrba, D. Siewert, A. Kleibert, F. Nolting, P. M. Oppeneer, T. A. Jung, and N. Ballav: *Ammonia Coordination Introducing a Magnetic Moment in an On-Surface Low-Spin Porphyrin*. Angew. Chem. **125**, 46664669 (2013), DOI: 10.1002/ange.201208028.

[182] G. van der Laan: *The X-ray absorption branching ratio of transition metal compounds*. Physica B **158**, 395 (1989), DOI: 10.1016/0921-4526(89)90322-0.

[183] G. van der Laan and B. Thole: *Anisotropic branching ratio in X-ray absorption spectra*. J. Electron. Spectrosc. Relat. Phenom. **86**, 57 (1997), DOI: 10.1016/S0368-2048(97)00049-2.

[184] H. Sun, V. V. Smirnov, and S. G. DiMagno: *Slow Electron Transfer Rates for Fluorinated Cobalt Porphyrins: Electronic and Conformational Factors Modulating Metalloporphyrin ET*. Inorg. Chem. **42**, 6032 (2003), DOI: 10.1021/ic034705o.

[185] M.-S. Liao, J. D. Watts, and M.-J. Huang: *Effects of Peripheral Substituents and Axial Ligands on the Electronic Structure and Properties of Cobalt Porphyrins*. J. Phys. Chem. A **109**, 11996 (2005), DOI: 10.1021/jp058212b.

[186] F. de Groot: *Multiplet effects in X-ray spectroscopy*. Coord. Chem. Rev. **249**, 31 (2005), DOI: 10.1016/j.ccr.2004.03.018.

[187] M. van Veenendaal: *Anomalous ground states at the interface between two transition-metal compounds*. Phys. Rev. B **78**, 165415 (2008), DOI: 10.1103/PhysRevB.78.165415.

[188] N. Saito and I. H. Suzuki: *Anisotropic dissociation of NO in K-shell excited states*. Phys. Rev. A **43**, 3662 (1991), DOI: 10.1103/PhysRevA.43.3662.

[189] G. Odörfer, R. Jaeger, G. Illing, H. Kuhlenbeck, and H.-J. Freund: *Adsorption of NO on an oxygen precovered Ni(100) surface*. Surf. Sci. **233**, 44 (1990), DOI: 10.1016/0039-6028(90)90174-7.

[190] T. Saito, M. Imamura, N. Matsubayashi, K. Furuya, T. Kikuchi, and H. Shimada: *Geometric and electronic structures of NO adsorbed on Ni, Rh and Pt studied by using near edge X-ray absorption fine structure (NEXAFS) and resonant photoemission spectroscopy*. J. Electron. Spectrosc. Relat. Phenom. **119**, 95 (2001), DOI: 10.1016/S0368-2048(01)00278-X.

[191] W. A. Brown and D. A. King: *NO Chemisorption and Reactions on Metal Surfaces: A New Perspective*. J. Phys. Chem. B **104**, 2578 (2000), DOI: 10.1021/jp9930907.

[192] H. Kuhlenbeck, G. Odörfer, R. Jaeger, G. Illing, M. Menges, T. Mull, H.-J. Freund, M. Pöhlchen, V. Staemmler, S. Witzel, C. Scharfschwerdt, K. Wennemann, T. Liedtke, and M. Neumann: *Molecular adsorption on oxide surfaces: Electronic structure and orientation of NO on NiO(100)/Ni(100) and on NiO(100) as determined from electron spectroscopies and ab initio cluster calculations*. Phys. Rev. B **43**, 1969 (1991), DOI: 10.1103/PhysRevB.43.1969.

[193] K. M. Kadish, K. M. Smith, and R. Guilard: *The porphyrin handbook: Inorganic, organometallic and coordination chemistry*. Elsevier (2003).

[194] C. Sorg: *Magnetic Properties of 3d and 4f Ferromagnets Studied by X-Ray Absorption Spectroscopy*. Doctoral thesis, Freie Universität Berlin (2005), http://www.physik.fu-berlin.de/∼bab/start_frame2/diss/CSdiss.pdf.

[195] Y. Teramura, A. Tanaka, and T. Jo: *Effect of Coulomb Interaction on the X-Ray Magnetic Circular Dichroism Spin Sum Rule in 3d Transition Elements*. J. Phys. Soc. Jpn. **65**, 1053 (1996), DOI: 10.1143/JPSJ.65.1053.

[196] C. Piamonteze, P. Miedema, and F. M. F. de Groot: *Accuracy of the spin sum rule in XMCD for the transition-metal L edges from manganese to copper*. Phys. Rev. B **80**, 184410 (2009), DOI: 10.1103/PhysRevB.80.184410.

[197] H. Masuda, T. Taga, K. Osaki, H. Sugimoto, Z. Yoshida, and H. Ogoshi: *Crystal and molecular structure of (octaethylporphinato)iron(III) perchlorate. Anomalous magnetic properties and structural aspects*. Inorg. Chem. **19**, 950 (1980), DOI: 10.1021/ic50206a031.

[198] B. T. Thole and G. van der Laan: *Branching ratio in x-ray absorption spectroscopy*. Phys. Rev. B **38**, 3158 (1988), DOI: 10.1103/PhysRevB.38.3158.

[199] W. M. Heijboer, A. A. Battiston, A. Knop-Gericke, M. Hävecker, R. Mayer, H. Bluhm, R. Schlögl, B. M. Weckhuysen, D. C. Koningsberger, and F. M. F. de Groot: *In-Situ Soft X-ray Absorption of Over-exchanged Fe/ZSM5*. J. Phys. Chem. B **107**, 13069 (2003), DOI: 10.1021/jp034125c.

[200] F. Zheng, V. Pérez-Dieste, J. McChesney, Y.-Y. Luk, N. L. Abbott, and F. Himpsel: *Detection and switching of the oxidation state of Fe in a self-assembled monolayer*. Surf. Sci. **587**, L191 (2005), DOI: 10.1016/j.susc.2005.05.014.

[201] T. Nakagawa, H. Watanabe, and T. Yokoyama: *Adatom-induced spin reorientation transitions and spin canting in Co films on a stepped Cu(001) surface*. Phys. Rev. B **74**, 134422 (2006), DOI: 10.1103/PhysRevB.74.134422.

[202] B. P. Tonner, C. M. Kao, E. W. Plummer, T. C. Caves, R. P. Messmer, and W. R. Salaneck: *Intermolecular Screening in Core-Level Photoemission from the Nitric-Oxide Dimer*. Phys. Rev. Lett. **51**, 1378 (1983), DOI: 10.1103/PhysRevLett.51.1378.

[203] Y. Fukuda: *Absence of the UPS 4 band for NO chemisorbed on cobalt*. Surf. Sci. **104**, L234 (1981), DOI: 10.1016/0039-6028(81)90062-5.

[204] K. C. Dash, B. Folkesson, R. Larsson, and M. Mohapatra: *An XPS investigation on a series of schiff base dioxime ligands and cobalt complexes*. J. Electron. Spectrosc. Relat. Phenom. **49**, 343 (1989), DOI: 10.1016/0368-2048(89)85022-4.

[205] T. Yoshida, K. Yamasaki, S. Sawada: *An X-ray Photoelectron Spectroscopy Study of Biuret Metal Complexes*. Bull. Chem. Soc. Jpn. **51**, 1561 (1978), DOI: 10.1246/bcsj.51.1561.

List of acronyms

Alq_3	8-hydroxy-quinoline aluminum
AFM	antiferromagnetic
bcc	body-centered cubic
CF	crystal field
CFT	crystal field theory
CoOEP	cobalt-octaethylporphyrin
CoPc	cobalt-phthalocyanine
CuPc	copper-phthalocyanine
CO	carbon monoxide
CoTPP	cobalt-tetraphenylporphyrin
DFT	density functional theory
fcc	face-centered cubic
FeOEP	iron-octaethylporphyrin
FeOEP-Cl	iron-octaethylporphyrin chloride
FePc	iron-phthalocyanine
FM	ferromagnetic
GMR	giant magnetoresistance
HIS	hybrid interface state
HOPG	highly ordered pyrolytic graphite
IP	in-plane
LEED	low energy electron diffraction
LFT	ligand field theory
M	metal
MCA	magnetocrystalline anisotropy
ML	monolayer
MnTPPCl	manganese-tetraphenylporphyrin chloride
MnPc	manganese-phthalocyanine

MP	metalloporphyrin
MPc	metallophthalocyanine
MTPP	metallotetraphenylporphyrin
NEXAFS	near-edge X-ray absorption fine-structure
NH_3	ammonia
NO	nitric oxide
Pc	phthalocyanine
RT	room temperature
SMM	single-molecule magnet
SOC	spin–orbit coupling
SCO	spin-crossover
SPUPS	spin-polarized ultraviolet photoelectron spectroscopy
SPSTM	spin-polarized scanning tunneling microscopy
SPMDS	spin-polarized metastable de-excitation spectroscopy
STM	scanning tunneling microscopy
$TbPc_2$	bis-phthalocyaninato-terbium
TEY	total electron yield
UHV	ultra-high vacuum
XA	X-ray absorption
XANES	X-ray absorption near-edge structure
XAS	X-ray absorption spectrosopy
XNLD	X-ray natural linear dichroism
XMCD	X-ray magnetic circular dichroism
XP	X-ray photoemisson
XPS	X-ray photoelectron spectroscopy

List of publications

Publications resulting from this thesis

C. F. Hermanns, M. Bernien, A. Krüger, W. Walter, Y.-M. Chang, E. Weschke, and W. Kuch: *Huge magnetically coupled orbital moments of Co porphyrin molecules and their control by CO adsorption.* Phys. Rev. B. **88**, 104420 (2013), DOI :10.1103/PhysRevB.88.104420.

C. F. Hermanns, K. Tarafder, M. Bernien, A. Krüger, Y.-M. Chang, P. M. Oppeneer, and W. Kuch: *Magnetic coupling of porphyrin molecules through graphene.* Adv. Mater. **25**, 3473 (2013), DOI :10.1002/adma.201205275.

C. S. Guo, L. Sun, K. Hermann, C. F. Hermanns, M. Bernien, and W. Kuch: *X-ray absorption from large molecules at metal surfaces: Theoretical and experimental results for Co-OEP on Ni(100).* J. Chem. Phys. **137**, 194703 (2012), DOI :10.1063/1.4765373.

C. F. Hermanns, M. Bernien, A. Krüger, J. Miguel and W. Kuch: *Switching the electronic properties of Co-octaethylporphyrin molecules on oxygen-covered Ni films by NO adsorption.* J. Phys.: Codens. Matter **24**, 394008 (2012), DOI :10.1088/0953-8984/24/39/394008.

J. Miguel, C. F. Hermanns, M. Bernien, A. Krüger, and W. Kuch: *Reversible Manipulation of the Magnetic Coupling of Single Molecular Spins in Fe-Porphyrins to a Ferromagnetic Substrate* J. Phys. Chem. Lett. **2**, 1455 (2011), DOI :10.1021/jz200489y.

Other publications

C. F. Hermanns, M. Bernien, A. Krüger, C. Schmidt, S. T. Waßerroth, G. Ahmadi, B. W. Heinrich, M. Schneider, P. Brouwer, K. J. Franke, E. Weschke, and W. Kuch: *Magnetic coupling of* $Gd_3N@C_{80}$ *endohedral fullerenes to a substrate.* Phys. Rev. Lett. **111**, 167203 (2013), DOI :10.1103/PhysRevLett.111.167203.

T. G. Gopakumar, M. Bernien, H. Naggert, F. Matino, C. F. Hermanns, A. Bannwarth, S. Mühlenberend, A. Krüger, D. Krüger, F. Nickel, W. Walter, R. Berndt, W. Kuch, F. Tuczek: *A spin crossover complex on Au(111): Structural and electronic differences between mono- and multilayers.* Accepted for publication in Chem. Eur. J.

H. C. Herper, M. Bernien, S. Bhandary, C. F. Hermanns, A. Krüger, E. Weschke, C. Czekelius, J. Miguel, C. Weis, C. Antoniak, B. Krumme, D. Bovenschen, B. Sanyal, W. Kuch, H. Wende, and O. Eriksson: *Iron porphyrin molecules on Cu(100): Influence of adlayers and ligands on the magnetic properties.* Phys. Rev. B. **87**, 174425 (2013), DOI :10.1103/PhysRevB.87.174425.

T. R. Umbach, M. Bernien, C. F. Hermanns, A. Krüger, V. Sessi, I. Fernández-Torrente, P. Stoll, J. I. Pascual, K. J. Franke, and W. Kuch: *Ferromagnetic Coupling of Mononuclear Fe Centers in a Self-Assembled Metal-Organic Network on Au(111).*

Phys. Rev. Lett. **109**, 267207 (2012), DOI :10.1103/PhysRevLett.109.267207.

M. Bernien, D. Wiedemann, C. F. Hermanns, A. Krüger, D. Rolf, W. Kroener, P. Müller, A. Grohmann, and W. Kuch: *Spin Crossover in a Vacuum-Deposited Submonolayer of a Molecular Iron(II) Complex.* J. Phys. Chem. Lett. **3**, 3431 (2012), DOI :10.1021/jz3011805.

Y. Luo, M. Bernien, A. Krüger, C. F. Hermanns, J. Miguel, Y.-M. Chang, S. Jaekel, W. Kuch, and R. Haag: *In Situ Hydrolysis of Imine Derivatives on Au(111) for the Formation of Aromatic Mixed Self-Assembled Monolayers: Multitechnique Analysis of This Tunable Surface Modification.* Langmuir **28**, 358 (2012), DOI :10.1021/la202696a.

J. I. Paez, V. Brunetti, M. C. Strumia, T. Becherer, T. Solomun, J. Miguel, C. F. Hermanns, M. Calderón, and R. Haag: *Dendritic polyglycerolamine as a functional antifouling coating of gold surfaces.* J. Mater. Chem. **22**, 19488 (2012), DOI :10.1039/c2jm32486e.

B. Borca, S. Barja, M. Garnica, D. Sánchez-Portal, V. M. Silkin, E. V. Chulkov, C. F. Hermanns, J. J. Hinarejos, A. L. Vázquez de Parga, A. Arnau, P. M. Echenique, and R. Miranda: *Comment on "Potential Energy Landscape for Hot Electrons in Periodically Nanostructured Graphene".* Phys. Rev. Lett. **105**, 219702 (2010), DOI : 10.1103/PhysRevLett.105.219702.

B. Borca, S. Barja, M. Garnica, D. Sánchez-Portal, V. M. Silkin, E. V. Chulkov, C. F. Hermanns, J. J. Hinarejos, A. L. Vázquez de Parga, A. Arnau, P. M. Echenique, and R. Miranda: *Potential Energy Landscape for Hot Electrons in Periodically Nanostructured Graphene.* Phys. Rev. Lett. **105**, 036804 (2010), DOI :10.1103/PhysRevLett.105.036804.

List of presentations

2013

C. F. Hermanns, K. Tarafder, M. Bernien, A. Krüger, W. Walter, Y.- M. Chang, E. Weschke, P. M. Oppeneer, and W. Kuch: *Huge magnetically coupled orbital moments of Co porphyrin molecules and their control by CO adsorption.* DPG Frühjahrstagung, Talk, 10.-15.03.2013, Regensburg, Germany.

2012

C. F. Hermanns, M. Bernien, A. Krüger, W. Walter, J. Miguel, Y.-M. Chang, and W. Kuch: *Tuning the electronic and magnetic properties of adsorbed Co porphyrin molecules by NO as an axial ligand.* Joint European Magnetic Symposia, Talk, 09.-14.09.2012, Parma, Italy.

C. F. Hermanns, M. Bernien, A. Krüger, J. Miguel, and W. Kuch: *Tuning the electronic and magnetic properties of adsorbed Co porphyrin molecules by NO as an axial ligand.* DPG Frühjahrstagung, Talk, 25.-30.03.2012, Berlin, Germany.

C. F. Hermanns, K. Tarafder, M. Bernien, A. Krüger, Y.- M. Chang, A. Bruch, P. M. Oppeneer, and W. Kuch: *Magnetic coupling between metalloporphyrins and Ni films across a graphene sheet.* DPG Frühjahrstagung, Talk, 25.-30.03.2012, Berlin, Germany.

2011

C. F. Hermanns, W. Walter, M. Bernien, A. Krüger, J. Miguel, and W. Kuch: *Switching the electronic properties of Co octaethyl-porphyrin molecules on oxygen-covered Ni films by NO adsorption.* BESSY II User Meeting, Poster, 30.11.-02.12.2011, Berlin, Germany.

C. F. Hermanns, J. Miguel, M. Bernien, A. Krüger, and W. Kuch: *Reversible chemical manipulation of the magnetic properties of Fe-Porphyrin molecules on a ferromagnetic substrate.* European Conference on Surface Science, Talk, 28.08-02.09.2011, Wroclaw, Poland.

C. F. Hermanns, J. Miguel, M. Bernien, A. Krüger, and W. Kuch: *Reversible chemical manipulation of the magnetic properties of Fe-Porphyrin molecules on a ferromagnetic substrate.* DPG Frühjahrstagung, Talk, 13.-18.03.2011, Dresden, Germany.

2010

C. F. Hermanns, A. Krüger, M. Bernien, J. Miguel, and W. Kuch: *Magnetic coupling of Co porphyrin molecules to ferromagnetic substrates.* BESSY II User Meeting, Poster, 09.-10.12.2010, Berlin, Germany.

C. F. Hermanns, A. Krüger, M. Bernien, J. Miguel, and W. Kuch: *Magnetic coupling of Co porphyrin molecules to ferromagnetic substrates.* DPG Frühjahrstagung, Poster, 21.-26.03.2010, Regensburg, Germany.

Acknowledgments

Zuerst möchte ich mich an dieser Stelle bei Herrn **Prof. Dr. Wolfgang Kuch** dafür bedanken, dass er mir die Möglichkeit gegeben hat in seiner Gruppe diese Doktorarbeit anzufertigen! Ich bin mir seinem entgegengebrachten Vertrauen bewusst und hoffe, dass ich mit meinen wissenschaftlichen Beiträgen und Ergebnissen seine Erwartungen erfüllen konnte. Ich möchte mich bei ihm dafür bedanken, dass ich so viele unterschiedliche Experimente durchführen konnte und dass er stets als Ansprechpartner zur Verfügung stand! Letzteres hat bei der Analyse von sehr tiefgründigen physikalischen Zusammenhängen entscheidende Impulse gegeben.

Muchas gracias a **Prof. Dr. José Ignacio Pascual** por haber accedido a ser el segundo evaluador de esta tesis doctoral. Además quiero mencionar la exitosa colaboración con su grupo y en concreto las medidas de STM que pude llevar a cabo.

Nun möchte ich auf Herrn **Dr. Matthias Bernien** zu sprechen kommen. Es ist wohl die Person, mit der ich am meisten Zeit in den letzten Jahren verbracht habe. Die Möglichkeit gehabt zu haben von ihm in jeglicher Hinsicht zu lernen, wie erfolgreiche Forschung gestaltet wird, hat entscheidend zur Verwirklichung dieser Arbeit beigetragen. Von der technischen Planung über theoretische Überlegungen bis hin zur experimentellen Umsetzung habe ich sehr viel von ihm lernen können. Ich werde auch nie unsere unendlichen Diskussionen über Physik vergessen.

Alex Krüger möchte ich für die gemeinsame Zeit bei BESSY Dank sagen. Unsere Messungen und das Lösen von technischen Problemen jeglicher Art im Team werde ich nicht vergessen.

Muchas gracias a **Dr. Jorge Miguel** por haberme introducido al mundo de los sincrotrones y por haberme asesorado al principio del doctorado, cuando todo era nuevo para mí.

I also want to say thanks to **Dr. Yin- Ming Chang** who contributed to measurements performed during my PhD work. In particular I wish him physical health and hope that he will recover as soon as possible.

Zudem möchte ich **Waldemar Walter**, der im Rahmen seiner Diplomarbeit mit mir gearbeitet hat, sowie **Fabian Nickel**, **Anton Bruch** und **Christian Schmidt**, die während der Anfertigung ihrer Bachelorarbeit zu Forschungsprojekten beigetragen haben, für ihre Zusammenarbeit und Anstrengungen loben.

I appreciate the effort of **Prof. Dr. Peter Oppeneer** and **Dr. Kartick Tarafder** on our common project about CoOEP on graphene/Ni. Thanks a lot for your calculations and physical explanations!

Die Zusammenarbeit mit **Prof. Dr. Katharina Franke** und **Tobias Umbach** im Rahmen von Kollaborationen möchte ich nicht missen, genauso wie die feuchtfröhlichen Diskussionen mit Tobi über die Arbeit im Allgemeinen und die Physik im Speziellen.

Bei **Dr. Eugen Weschke** vom Helmholtz-Zentrum Berlin möchte ich mich für die hervorragende Unterstützung während der Strahlzeiten am UE46-PGM1 bedanken.

Prof. Dr. Klaus Hermann and **Dr. C. S. Guo** vom Fritz-Haber-Institut möchte ich für die ertragreiche Zusammenarbeit und ihre Rechnungen über CoOEP auf Ni

und O/Ni danken.

También tengo que mencionar aquí a los miembros del grupo en cual hice mi tesina, y en particular, a **Prof. Dr. Amadeo L. Vázquez de Parga**. Durante mi tiempo en Madrid aprendí mucho sobre cómo trabajar en UAV, leer y analizar publicaciones críticamente, discutir sobre sus contenidos así como sobre la difusión de avances en física.

Vielen Dank an die gesamte **AG Kuch** für die hervorragende Atmosphäre in der Gruppe.

Zudem sollen hier auch die **zahlreichen Lehrer**, die mir im Verlaufe meiner Schulzeit die Physik nahegebracht haben, und insbesondere Herr **Anton Eisner** erwähnt werden. Vielen Dank für die Motivation zum Physikstudium!

Muchas gracias a **María José** por su amor, por vivir conmigo en Berlin y por haber aguantado los "beams" que no sólo afectaban a mi vida sino también a la de ella.

Zu guter Letzt möchte ich mich bei **meinen Eltern Prof. Dr. Arnold Hermanns** und **Heidi Hermanns-Klotz** dafür bedanken, dass sie es mir ermöglicht haben mein Abitur abzulegen, mich finanziell sehr unterstützt haben und immer während der Zeit meiner Ausbildung für mich da waren.

Erklärung

Hiermit versichere ich, dass ich die vorliegende Arbeit selbstständig verfasst und keine anderen als die angegebenen Quellen und Hilfsmittel genutzt habe.

Berlin, 28.06.2013